FEASIBILITY STUDY ON THE IMPLEMENTATION OF A BOILING CONDENSER IN A SOUTH AFRICAN FOSSIL FUEL POWER PLANT

by

Elmi Grové

Submitted in partial fulfilment of the requirements for the degree

MASTER OF ENGINEERING (Mechanical Engineering)

in the

Faculty of Engineering, Built Environment and Information Technology

University of Pretoria

2016

ABSTRACT

Title:	Feasibility study on the implementation of a boiling condenser in a South African fossil fuel power plant
Student:	Elmi Grové
Supervisor	Dr Mohsen Sharifpur and Prof Josua P Meyer
Department:	Mechanical and Aeronautical Engineering
University:	University of Pretoria
Degree:	Master of Engineering

The South African electricity mix is highly dependent on subcritical coal-fired power stations. The average thermal efficiency of these power plants is low. Traditional methods to increase the thermal efficiency of the cycle have been widely studied and implemented. However, utilising the waste heat at the condenser, which accounts for the biggest heat loss in the cycle, presents a large potential to increase the thermal efficiency of the cycle. Several methods can be implemented for the recovery and utilisation of low-grade waste heat.

This theoretical study focuses on replacing the traditional condenser in a fossil fuel power station with a boiling condenser (BC), which operates in a similar manner to the core of a boiling water reactor at a nuclear power plant (Sharifpur, 2007). The system was theoretically tested at the Komati Power Station, South Africa's oldest power station. The power station presented an average low-grade waste heat source. The BC cycle was theoretically tested with several working fluids and numerous different configurations. Several of the theoretical configurations indicated increased thermal efficiency of the cycle. The BC cycle configurations were also tested in two theoretical scenarios.

Thirty configurations and 103 working fluids were tested in these configurations. The configuration that indicated the highest increase in thermal efficiency was the BC cycle with regeneration (three regenerative heat exchangers) from the BC turbine. A 2.4% increase in thermal efficiency was obtained for the mentioned theoretical implementation of this configuration. The working fluid tested in this configuration was ethanol. This configuration also indicated a 7.6 MW generating capacity.

The increased thermal efficiency of the power station presents benefits not only in increasing the available capacity on South Africa's strained grid, but also environmental benefits. The mentioned reduction of 7.6 MW in heat released into the atmosphere also indicated a direct

environmental benefit. The increase in thermal efficiency could also reduce CO_2 emissions released annually in tons per MW by 5.74%.

The high-level economic analysis conducted, based on the theoretically implemented BC cycle with the highest increase in thermal efficiency, resulted in a possible saving of R46 million per annum. This translated to a saving of R19.2 million per annum for each percentage increase in thermal efficiency brought about by the BC cycle.

The theoretical implementation of the BC, with regeneration (three regenerative heat exchangers) from the BC turbine and ethanol as a working fluid, not only indicated an increase in thermal efficiency, but also significant economic and environmental benefits.

Keywords: Fossil fuel power plant; low-grade waste heat recovery; boiling condenser; thermal efficiency increase

Table of contents

List of figures

List of tables

Nomenclature

Acronyms

BC	Boiling condenser
BWR	Boiling water reactor
CHP	Combined heat and power
CO_2	Carbon dioxide
FGD	Flue gas desulphurisation
FWH	Feed water heater
HRSG	Heat recovery steam generator
ke	Kinetic energy
NERSA	National Energy Regulator of South Africa
T-s	Temperature-entropy
ORC	Organic Rankine cycle
pe	Potential energy
PS	Power station
TOU	Time of use
WH2P	Waste heat to power

Greek symbols

η	Efficiency
Σ	Sum of -
ν	Specific volume (m^3/kg)

Roman symbols

h	Enthalpy (kJ/kg)
$\dot{Q}$	Rate of heat transfer (kW)
s	Entropy (kJ/kgK)
T	Temperature (ºC)
$\dot{W}$	Rate of work (kW)

Subscripts

"number"	The node number
a	Actual
boil	Boiler
cond	Condenser
H	High or high-temperature source
L	Low or low-temperature source
P	Pump
s	Ideal properties for isentropic components
t	Turbine
th	Thermal

Superscript

g	Vapour
f	Liquid
fg	Mixture
sat -	Saturated – *g, f or fg*
c,f	Compressed liquid
sh,g	Superheated vapour

1. INTRODUCTION

1.1 Background

Energy is and will remain a vital resource for the developing world. With a growing awareness of sustainable energy supply and environmental concerns, the efficient manner in which energy is supplied has become an important field in research.

Fossil fuels, however, are projected to remain the main source of energy generation (Energy Information Administration, 2015). Concerns about fossil fuel availability and the environmental impact of fossil fuel energy generation demand attention to further research in this field.

In 2010, world energy consumption was 664.685 quadrillion ($x10^{15}$) kJ, and it is projected to increase to 865.145 ($x10^{15}$) kJ by 2040 (Energy Information Administration, 2015). Figure 1.1 indicates the projected increase in energy consumption between 1990 and 2040.

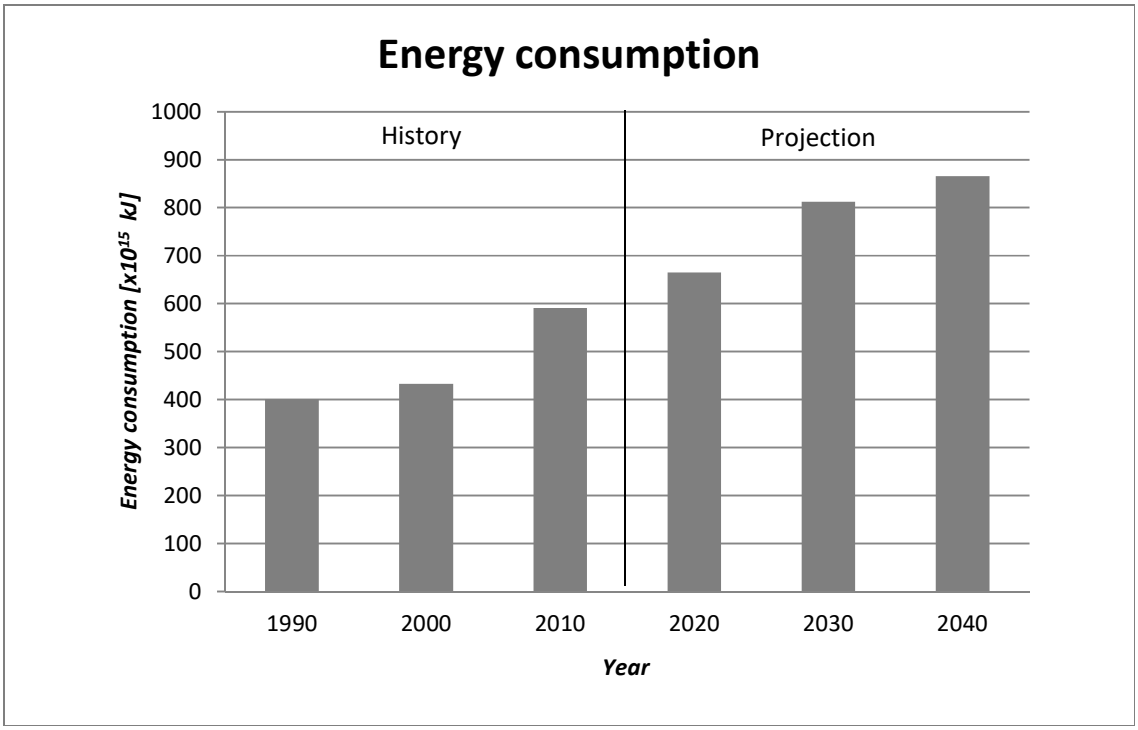

Figure 1.1: World energy consumption (Energy Information Administration, 2015)

Approximately 80% of the energy consumed is provided by means of fossil fuels. Coal is projected to be the largest source of fossil fuel energy production (Energy Information Administration, 2015). In 2012 alone, 41% of global electricity production was fuelled by coal (World Coal Association, 2012).

South Africa is among the top fossil fuel energy producers in the world where 72.1% of electricity is locally generated with coal (Eskom, 2013a).

Coal-fired power plants in South Africa generally operate with an overall thermal efficiency under 50% (Eskom, 2013a). This effectively implies that less than half of the heat supplied by the fuel is used to generate useful work, and more than half of the heat is released into the environment, (Elliott et al., 1997).

During the past four decades, several important concepts were implemented and studies conducted in an effort to improve the thermal efficiency of a power plant. Focusing on modifications made to the basic Rankine cycle to achieve higher thermal efficiencies will indicate several different configurations and combinations used in industry. Regenerative heating by means of open and closed feed water heaters (FWHs) proved to increase the thermal efficiency of the cycle. Super heating, along with reheating, also proved to be effective (Elliott et al., 1997).

Implementing the abovementioned modifications, although effective, does not change the fact that most of the heat provided by the fuel will still be released as waste heat. Combined cycles implement concepts where the waste heat is used to produce useful work, (Elliott et al., 1997). High-, medium- and low-temperature waste heat sources are present in fossil fuel power plants where high and medium temperature waste heat sources are frequently used for waste heat recovery applications, consequently increasing the thermal efficiency of a cycle (Thunmann, 1984).

Low-temperature waste heat sources, like the condenser, are important factors to consider when evaluating the thermal efficiency of a power plant. The efficiency of a cycle can increase significantly by reducing the heat rejected in the condenser (El-Wakil, 1985).

An increase in thermal efficiency can directly influence the amount of fuel used for energy generation and could have a significant effect on harmful emissions and unwanted by-products. Therefore, an increase in the thermal efficiency of a fossil fuel power plant could have a significant economic and environmental impact.

1.2 Justification and goal of the study

With rising energy demand and growing environmental concerns regarding fossil fuel power stations, increasing the thermal efficiency of a fossil fuel power plant has become a necessity. Current methods implemented to increase thermal efficiency are effective. However, there

seems to be a gap in the constructive use of waste heat in the condenser specifically. Implementing the waste heat at the condenser to produce useful work or reducing the amount of heat released into the atmosphere can increase the thermal efficiency of the cycle.

The study will concentrate on steam power in South Africa. This analysis is conducted on a system where the waste heat at the condenser is used to produce useful work, aiming to increase the thermal efficiency of the cycle. The analysis will also attempt to create a system where the heat released into the environment is reduced. The system is tested by implementing a boiling condenser (BC) (Sharifpur, 2007). The BC will replace a normal condenser in a steam power plant. The BC will act similarly to a boiling water reactor (BWR) in a nuclear reactor power plant. A separate cycle with a unique working fluid will run through the BC and generate useful work by implementing the waste heat from the steam cycle (Sharifpur, 2007). The cycle is tested with different configurations, along with suitable working fluids, to obtain the optimum thermal efficiency of the cycle.

The increase of the power plant's thermal efficiency will have far-reaching effects. Therefore, it is worthwhile to study the effect of increased thermal efficiency on the environmental impact of the power plant by implementing a BC. An increase in thermal efficiency will also have an effect on the economic facet of the power plant. Hence, a basic economic analysis is conducted on the cycle, including the BC.

1.3 Structure of the dissertation

The rest of this document will include a description of the work conducted on the topic from the beginning of the study. A study of available literature on the relevant topics is presented in Chapter 2. A description of the analyses conducted when implementing the BC is presented in Chapter 3. The results, along with a detailed discussion, are given in Chapter 4. Chapter 5 will present an environmental and economic analysis of the cycle with increased thermal efficiency by implementing a BC. The study is concluded in Chapter 6.

2. LITERATURE STUDY

2.1 Introduction

This chapter contains information regarding energy use and ways in which energy is generated. The effect of energy generation, specifically fossil fuel power generation, on the environment is discussed. Fossil fuel power station thermal efficiency, how and where the efficiency is lost and the methods used to increase thermal efficiency will also be discussed.

2.2 Energy consumption, electricity generation and the effect of energy production on the environment

Chapter 1 briefly mentioned that world energy consumption is projected to increase from 644.685 quadrillion ($x10^{15}$) kJ in 2010 to 856.145($x10^{15}$) kJ in 2040 (Energy Information Administration, 2015). Consequently, Figure 2.1 indicates energy consumption by fuel type and how the consumption per fuel type is projected to increase until 2040.

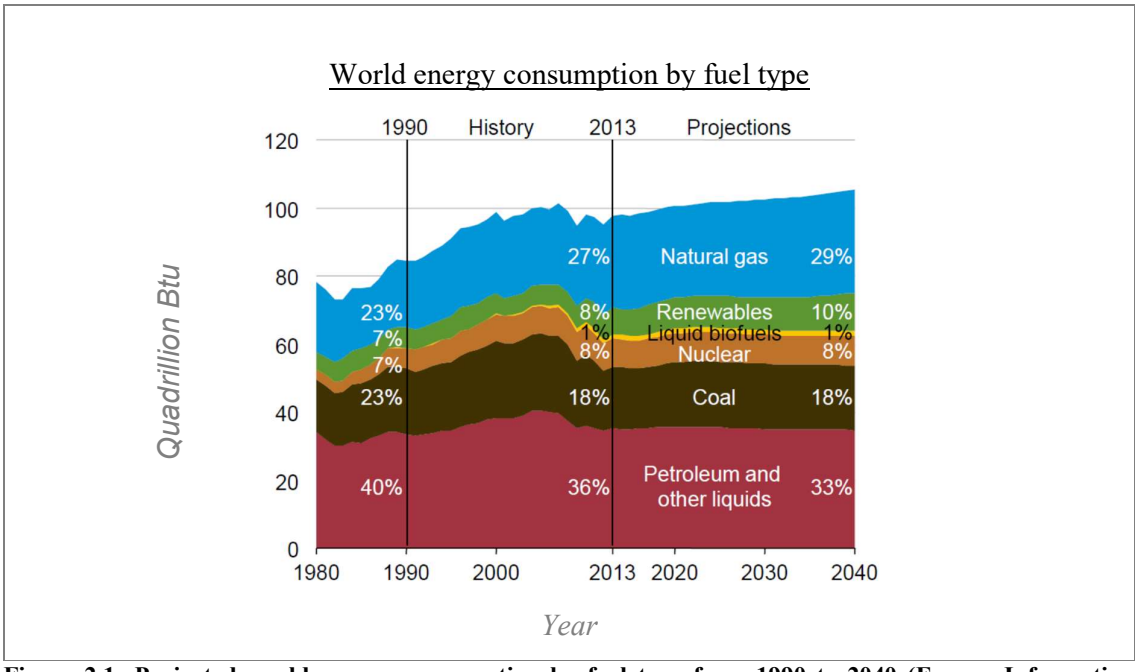

Figure 2.1: Projected world energy consumption by fuel type from 1990 to 2040 (Energy Information Administration, 2015)

It can be seen in Figure 2.1 that most of the energy consumption per fuel type is projected to be supplied by means of natural resources. Concerns regarding resource availability and greenhouse gas emissions have drawn attention to alternative energy supply, as well as the optimisation of existing electricity generation systems.

2.2.1 *Electricity generation and fuel used for generation*

Following Figure 2.1, it can be seen in Figure 2.2 that electricity generation is projected to increase from 20.2 trillion kWh in 2010 to 39.0 kWh in 2040 (Energy Information Administration, 2015).

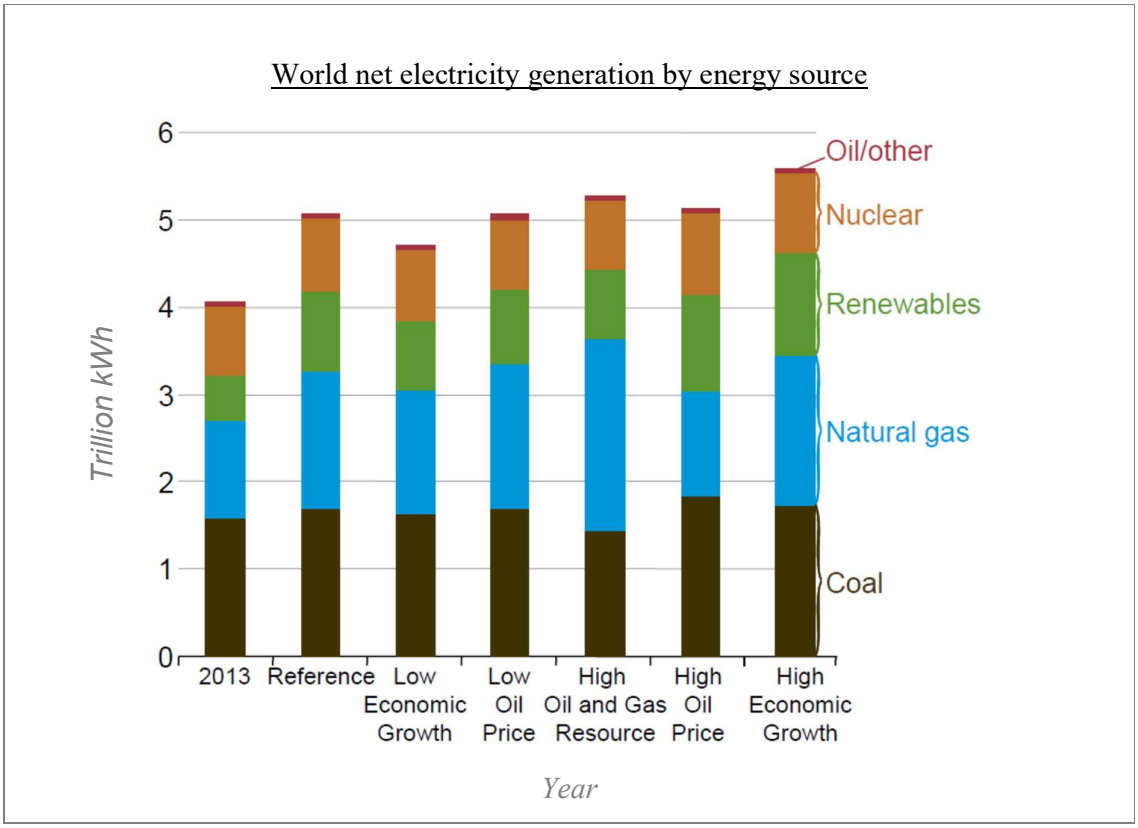

Figure 2.2: Projected world electricity generation by energy source from 2010 to 2040 (Energy Information Administration, 2015)

Due to concerns about the environmental consequences of greenhouse gas emissions, projected growth in renewable and nuclear energy supply is significant. However, due to the Fukushima incident in 2011, projected growth of nuclear power might indeed be less than anticipated. It can be seen that fossil fuels are projected to remain the predominant fuel used in electricity generation (Energy Information Administration, 2015).

2.2.2 *Thermal efficiency*

Thermal efficiency indicates the ratio of energy output to energy input. Energy is lost throughout the system from the initial input to the final output. Figure 2.3 indicates the flow of energy for a typical 500 MW subcritical boiler.

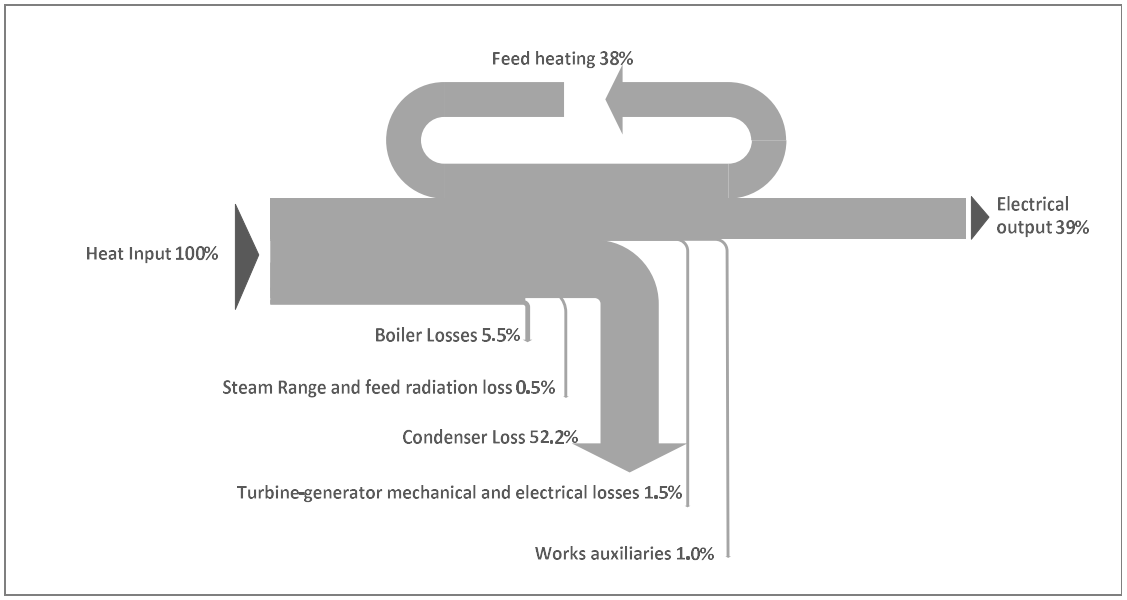

Figure 2.3: Sankey diagram for a typical 500 MW subcritical pulverised coal-fired boiler (Coal Industry Advisory Board, 2010)

Based on the illustrated concept, the thermal efficiency can be shown in the simplified Equation 2.1 (Sonntag et al., 2003).

$$\eta_{thermal} = \frac{Energy_{In}}{Energy_{Out}} \quad (2.1)$$

The majority of steam power plants are based on the concept of the Rankine cycle.

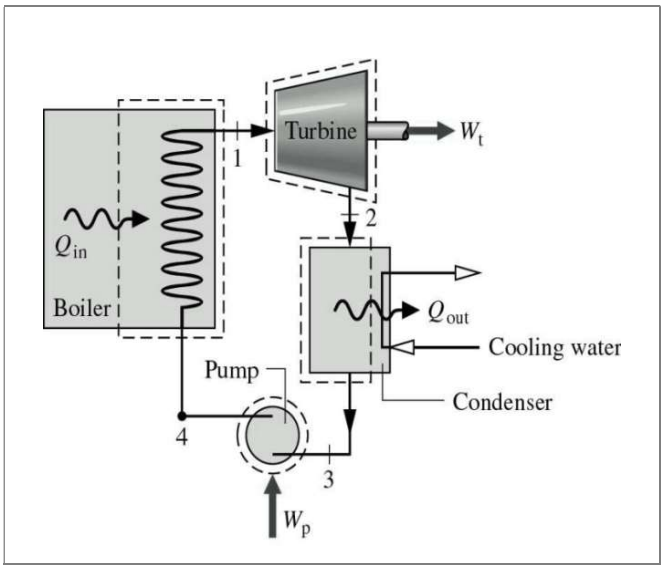

Figure 2.4: Rankine cycle (Moran & Shapiro, 2004)

Variations of the Rankine cycle are discussed further on in this study. However, the simple Rankine cycle, which indicates the primary components of a coal-fired power plant, is shown in Figure 2.4. Boiler, turbine, and turbine and pump losses are relatively insignificant. Therefore, from Equation 2.1 and Figure 2.4, it can be concluded that the majority of the losses in a Rankine cycle occur in the condenser. The average efficiencies of fossil fuel power plants and primary movers from 2007 to 2012 are indicated in Table 2.1 (Energy Information Administration, 2012).

	Coal efficiency	Petroleum efficiency	Natural gas efficiency
2007			
Steam generator	33.59%	32.81%	32.68%
Gas turbine		25.82%	29.33%
Internal combustion		32.66%	33.53%
Combined cycle		31.10%	45.03%
2008			
Steam generator	33.66%	32.95%	32.88%
Gas turbine		25.63%	29.47%
Internal combustion		32.72%	34.21%
Combined cycle		31.06%	44.65%
2009			
Steam generator	33.62%	32.97%	32.72%
Gas turbine		25.60%	29.52%
Internal combustion		32.72%	34.26%
Combined cycle		31.84%	44.87%
2010			
Steam generator	33.64%	33.29%	32.76%
Gas turbine		25.49%	29.44%
Internal combustion		32.72%	34.41%
Combined cycle		32.58%	44.78%
2011			
Steam generator	33.69%	32.76%	32.76%
Gas turbine		25.02%	29.49%
Internal combustion		32.72%	34.38%
Combined cycle		32.04%	44.88%
2012			
Steam generator	33.76%	32.94%	32.86%
Gas turbine		25.05%	29.67%
Internal combustion		32.76%	34.15%
Combined cycle		33.47%	44.81%

Table 2.1: Average efficiencies by energy source, 2007 to 2012 (Energy Information Administration, 2012)

As mentioned, it is clear that the low efficiency of coal-fired power plants is due to significant losses in the process, specifically the condenser.

2.2.3 Steam power plants in South Africa's power generation sector

Fossil fuels, especially coal, are projected to remain the main source for electricity generation. In light of the Fukushima incident, electricity supply has moved even more towards coal power generation. Coal consumption is projected to rise by 1.3% annually from 2013 to 2040 (Energy Information Administration, 2015).

Worldwide, 40% of electricity generation is coal fired. Coal-fired electricity generation is also projected to grow by 1.8% per year from 2010 to 2040 (Energy Information Administration, 2015).

Existing coal-fired power plants are, however, perceived as being relatively inefficient. The global average of coal-fired power plants' overall thermal efficiency is 28 to 33% (World Coal Association, 2006), (Sloss, 2011) and (Energy Information Administration, 2014a), indicating that less than half of the heat supplied by coal is converted into useful energy. Even though it can be seen that the world's electricity generation remains dependent on coal-fired power plants, there are concerns around "waste", leading to the inefficiency of coal-fired power generation.

South Africa has the highest amount of coal reserves (33 421 million tons) in Africa, and about 95% of Africa's coal is located in South Africa (Energy Information Administration, 2011). Consequently, most of South Africa's power generation is by means of coal-fired power plants. South Africa's state utility, Eskom, generates 95% of South Africa's power, and about 90% of Eskom's power is generated by means of coal-fired power plants (Department of Energy, 2014).

South Africa's installed coal-fired power generation system mostly consists of subcritical units with a thermal efficiency below 40% as indicated in Table 2.2.

Power station	Cooling		Design efficiency at rated turbine maximum continuous rating (MCR)	Installed capacity
	Dry or wet	Notes on wet or dry cooling	Percentage	MW
Tutuka	Wet		38.0%	3 654
Lethabo	Wet		37.8%	3 708
Majuba	Wet	Three units wet cooling	37.7%	4 100
Duvha	Wet		37.6%	3 600
Matla	Wet		37.6%	3 600
Kriel	Wet		36.9%	3 000
Arnot	Wet		35.6%	2 100
Matimba	Dry	Direct dry cooling (fans)	35.6%	3 990
Kendal	Dry	Indirect dry cooling (natural convection cooling towers)	35.3%	4 116
Majuba	Dry	Three units direct forced cooling	35.3%	
Hendrina	Wet		34.2%	2 000
Camden	Wet		33.4%	1 600
Grootvlei	Wet	One unit direct forced cooling	32.9%	1 200
Komati	Wet		30.0%	1 000

Table 2.2: List of South Africa's coal-fired power plants indicating the thermal efficiency of each power station (Eskom, 2014)

As previously mentioned, the largest losses in a coal-fired power plant are the ones that occur at the condenser. The inefficiency of South Africa's coal-fired power plants directly contribute to a direct release of heat and a high amount of CO_2 into the atmosphere.

2.2.4 The environmental effect of fossil fuel power stations

Coal-fired power plants have regulations that dictate the allowable amount of harmful emissions released by the power plant, such as particulate matter, NOx and SOx. The majority of these emissions can be controlled by implementing existing measures or technologies, like flue gas desulphurisation (FGD). There are, however, no measures in place to regulate CO_2 emissions or direct heat emitted from a coal-fired power plant.

	2015 'existing plant' limit (mg/Nm^3 at 10% O_2)	2020 'new plant' limit (mg/Nm^3 at 10% O_2)
Particulate matter	100	50
Sulphur dioxide	3 500	500
Oxides of nitrogen (NO_x as NO_2)	1 100	750

Table 2.3: Emission standards for coal-fired power plants in South Africa (Eskom, 2012)

CO_2 will become a regulated greenhouse gas emission in the future. The 21st session of the Conference of the Parties (COP 21 to the United Nations Framework Convention on Climate Change (UNFCCC), which was held in France in 2015, aimed to establish a legally binding agreement with countries to reduce greenhouse gas emissions in order to limit global warming to below 2 °C (United Nations Environmental Program, 2015). South Africa also aims introduce carbon tax in 2016 (The Carbon Report, 2014).

An existing coal-fired power plant's CO_2 emissions can be reduced by increasing its thermal efficiency. An increase in efficiency of 1% will reduce CO_2 emissions by 2% to 3% (World Coal Association, 2014). Utilisation of waste heat has become a popular manner to increase the efficiency of a system.

2.3 Waste heat and its utilisation

As mentioned, a significant amount of heat used in coal-fired power generation is lost throughout the cycle. Lost heat or waste heat throughout the cycle decreases the efficiency of the power plant. Therefore, utilising all forms of waste heat will significantly increase the thermal efficiency of the power plant.

Waste heat can be classified into three categories: low-grade, medium-grade and high-grade waste heat (Kacludis et al., 2012). The grade of waste heat depends on the temperature of the

source. Table 2.4 indicates the temperature range of each source class and an example of the source in industry, along with possible applications.

Heat source class	Example of industrial heat sources	Temperature range °C	Applications
High > 650 °C	Nickel refining furnace Steel electric arc furnace Basic oxygen furnace Aluminum reverberatory furnace Steel reheat furnace Fume incinerators and thermal oxidisers Glass melting furnace Coke oven Copper refining furnace	1 370 to 1 650 1 370 to 1 650 1 200 1 100 to 1 200 930 to 1 040 650 to 1 430 1 300 to 1 540 650 to 1 000 760 to 820	• High-quality thermal energy • Industrial plant for large-scale materials manufacturing • Waste heat to power (WH2P) • Combined heat and power (CHP) • Combined heat, cooling and power (trigeneration)
Medium 230 to 650 °C	Steam boiler exhaust Gas turbine exhaust Reciprocating engine exhaust Heat treating furnace Drying and baking furnace Ceramic kilns Cement kilns	230 to 480 370 to 540 320 to 590 430 to 650 230 to 590 450 to 620 450 to 620	• Medium-quality thermal energy • Traditional fossil fuel power and steam generation • Industrial plants for large-scale materials manufacturing • On-site and distributed power generation • Typical heat sources for bottoming cycle applications • Combined cycle power generation • WH2P • CHP • Trigeneration
Low < 230 °C	Process steam condensate Hot process liquids and solids Drying, baking and curing ovens Heat recovery steam generator (HRSG) exhaust Ethylene furnace exhaust Gas-fired boiler exhaust Cooling water return, furnace doors Cooling water return, annealing furnaces Cooling water return, internal combustion engines Cooling water return, refrigeration condensers	50 to 90 30 to 230 90 to 230 70 to 230 70 to 230 70 to 230 30 to 50 70 to 230 70 to 120 30 to 40	• Low-quality thermal energy • Industrial plants for light materials, pulp/paper, plastics, food, pharmaceuticals and biological materials processing • CHP • Trigeneration • Process water and air heating and cooling

Table 2.4: Classification of waste heat sources (Kacludis, et al., 2012)

Current methods used to utilise waste heat in coal-fired power plants include reheating, economisers, deaerating heaters, FWHs and air heaters (Petchers, 2003). These methods are, however, used for medium-grade waste heat.

Currently, few methods are implemented to utilise low-grade waste heat in coal-fired power plants. However, the potential for low-grade waste heat utilisation is significant.

2.4 Low-grade waste heat

It is clear that a significant loss of heat occurs in the condenser in coal-fired power plants. The waste heat at the condenser can also serve as a source of low-grade waste heat, with minor modifications to the power plant. Therefore, there is significant potential to utilise this source of low-grade waste heat in a system to increase the power plant's efficiency.

Low-grade heat recovery methods to increase the thermal efficiency of a cycle usually involve an organic Rankine cycle (ORC) or a variation thereof. An ORC is similar to a normal Rankine cycle, but the cycle temperatures and pressures are lower than those of the normal Rankine cycle, and usually involve a working fluid other than water (Chen et al., 2010).

2.4.1 Low-grade waste heat utilisation technologies

Cycles used in industry and studied for waste heat applications are the ORC, regenerative ORC, supercritical ORC, carbon dioxide transcritical power cycle, Kalina cycle, Goswami cycle and a trilateral flash cycle. Each of these cycles is briefly discussed below.

2.4.1.1 Organic Rankine cycle

An ORC, like a normal Rankine cycle, has the usual components of a Rankine cycle, such as the boiler or evaporator, expander, condenser and pump. The difference is that with the organic Rankine cycle, the working fluid is chosen to suit the low temperature and pressure of the cycle.

A basic ORC is indicated in Figure 2.5 and the ORC's Temperature-entropy (T-s) diagram is indicated in Figure 2.6. The working fluid in the ORC is heated by means of the low-grade waste heat source or evaporator to either a saturated or superheated vapour, depending on the conditions of the system. Figure 2.6 indicates a superheated vapour at T_3 exiting the low-grade waste heat heat exchanger. The superheated vapour then enters an expander or turbine and generates work. The fluid is then cooled in a condenser to a saturated liquid at T_1. The working fluid then enters a pump to increase its pressure, before entering the low-grade waste heat heat exchanger again (Cuda, 2012).

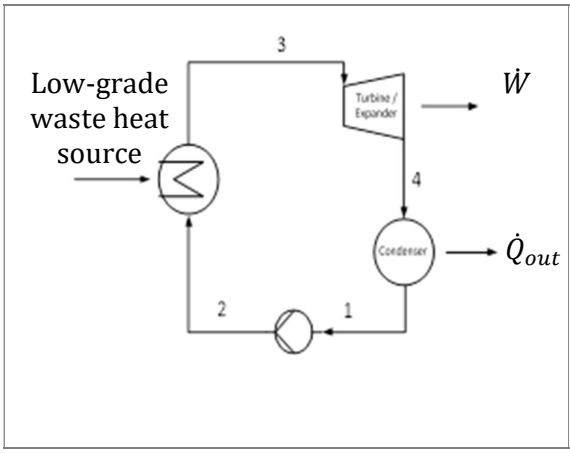

Figure 2.5: A simple ORC plant (Saleh, et al., 2007)

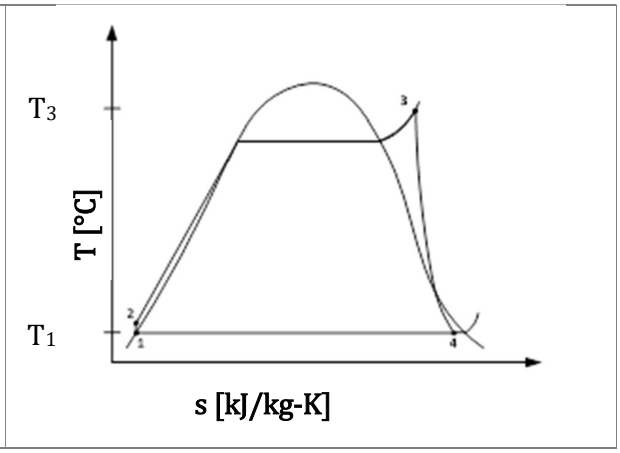

Figure 2.6: T-s diagram of an ORC (Saleh, et al., 2007)

The ORC described above is the basic ORC. Variations to this cycle, along with other technologies, are discussed below, indicating the benefits of each variation or concept.

2.4.1.2 Regenerative organic Rankine cycle

The regenerative ORC is similar to the normal ORC. However, the fluid exiting the expander or turbine might still be in the superheated phase. This occurs when the saturated vapour line on the T-s diagram has a negative slope. This is a characteristic of a dry fluid, (Chen, et al., 2006). The characteristics of working fluids are discussed further on in this chapter.

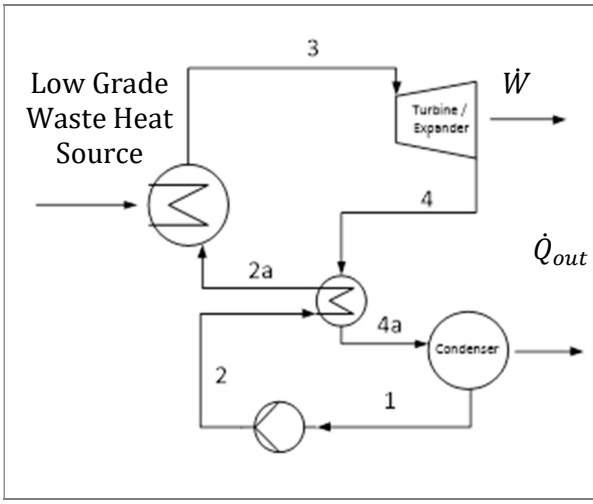

Figure 2.7: An ORC with a dry working fluid and regeneration (Cuda, 2012)

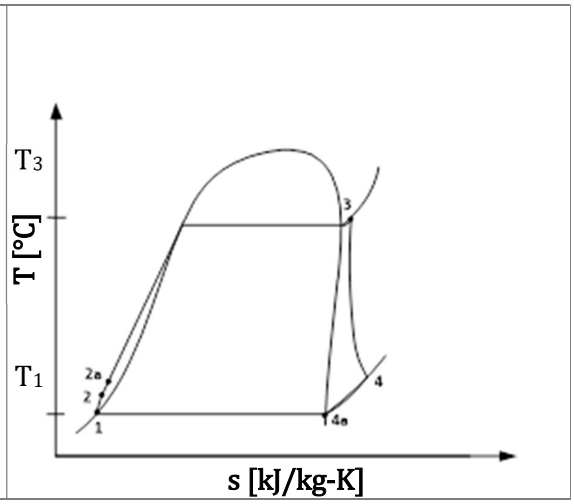

Figure 2.8: T-s diagram of a regenerative ORC (Saleh, et al., 2007)

The superheated fluid, exiting the turbine or expander therefore still has the potential to release some heat. Consequently, in the regenerative ORC, the superheated fluid exits the turbine and enters a heat exchanger or FWH, as indicated in Figure 2.7. The fluid then enters the condenser as a saturated vapour and condenses to a saturated liquid at T_1.

The working fluid, after passing through a pump, enters the regenerator or FWH before entering the low-grade waste heat heat exchanger or evaporator. The regenerative ORC is also indicated in Figure 2.8 on a T-s diagram. The regenerative ORC will have a higher thermal efficiency than the simple ORC (Saleh, et al., 2007).

2.4.1.3 Supercritical organic Rankine cycle

In a supercritical ORC, the pressure of the working fluid passing through the evaporator is above the critical pressure. In Figure 2.9 it can be seen that the working fluid avoids the mixture phase when passing through the boiler, therefore reducing the losses incurred during this phase change. The efficiency of this cycle is therefore also higher than a normal ORC (Chen, et al., 2006).

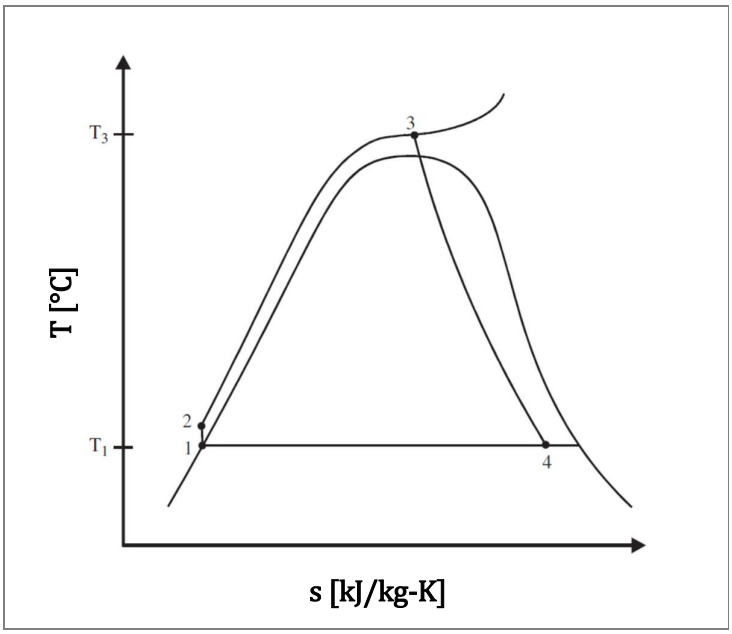

Figure 2.9: Supercritical ORC (Saleh, et al., 2007)

2.4.1.4 Carbon dioxide transcritical power cycle

Chen et al. (2006) studied the trans-critical carbon dioxide power cycle. The cycle operates in a manner similar to the regenerative ORC and the supercritical ORC, but the working fluid is CO_2. This system was compared to a classic regenerative ORC, and was found to provide a higher power output and to be more compact (Chen, et al., 2006).

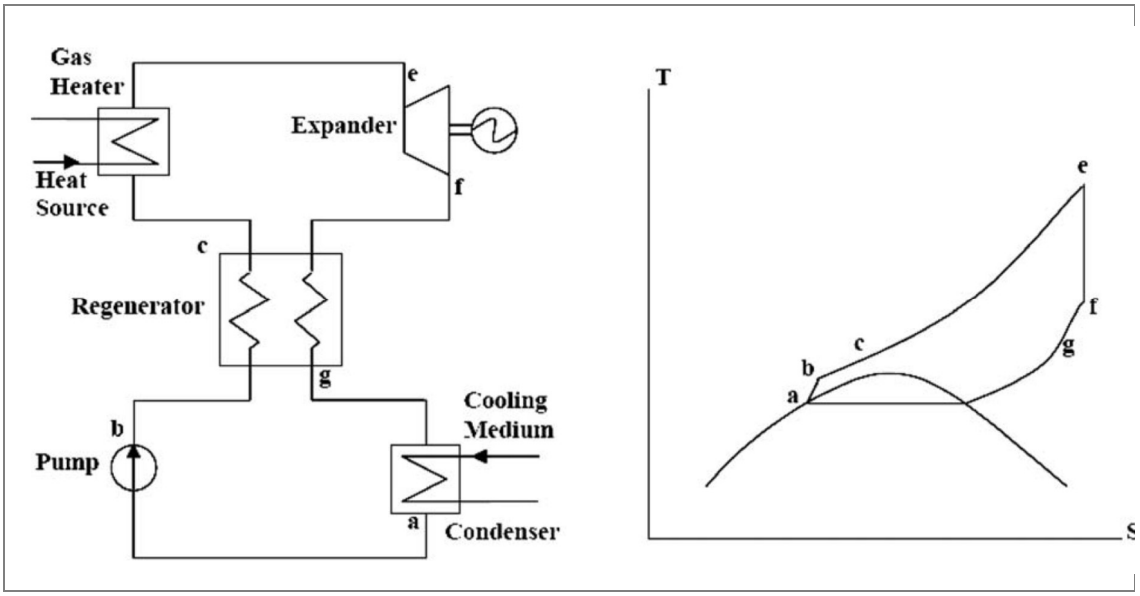

Figure 2.10: Transcritical CO_2 power cycle (Chen, et al., 2006)

The benefits of the transcritical CO_2 cycle is that the working fluid temperature matches that of the low-grade waste heat source, as indicated in the T-s diagram in, avoiding the pinching problems incurred with a classical ORC due to phase change (Larjola, 1995).

The critical temperature of CO_2 is 31.1 ºC, which is low when one considers the condensation process. In South Africa, condensation normally occurs close to this temperature or at a temperature a little higher than this temperature (Clark, 2013). Its application is therefore limited.

2.4.1.5 Kalina cycle

The Kalina cycle, unlike a classic ORC, uses a non-azeotropic mixture, which consists of NH_3 and H_2O as working fluids. Similar to the transcritical CO_2 cycle, the Kalina cycle's working fluid temperature also matches that of the heat source better due to the volatility of the ammonia in the NH_3-H_2O mixture as indicated in Figure 2.11. During the phase-changing process, the more volatile ammonia changes state first, which causes a better match to the temperature profile. The Kalina cycle, at a specific mixture, performs better than the ORC at moderate pressures (Hettiarachchi, et al., 2007).

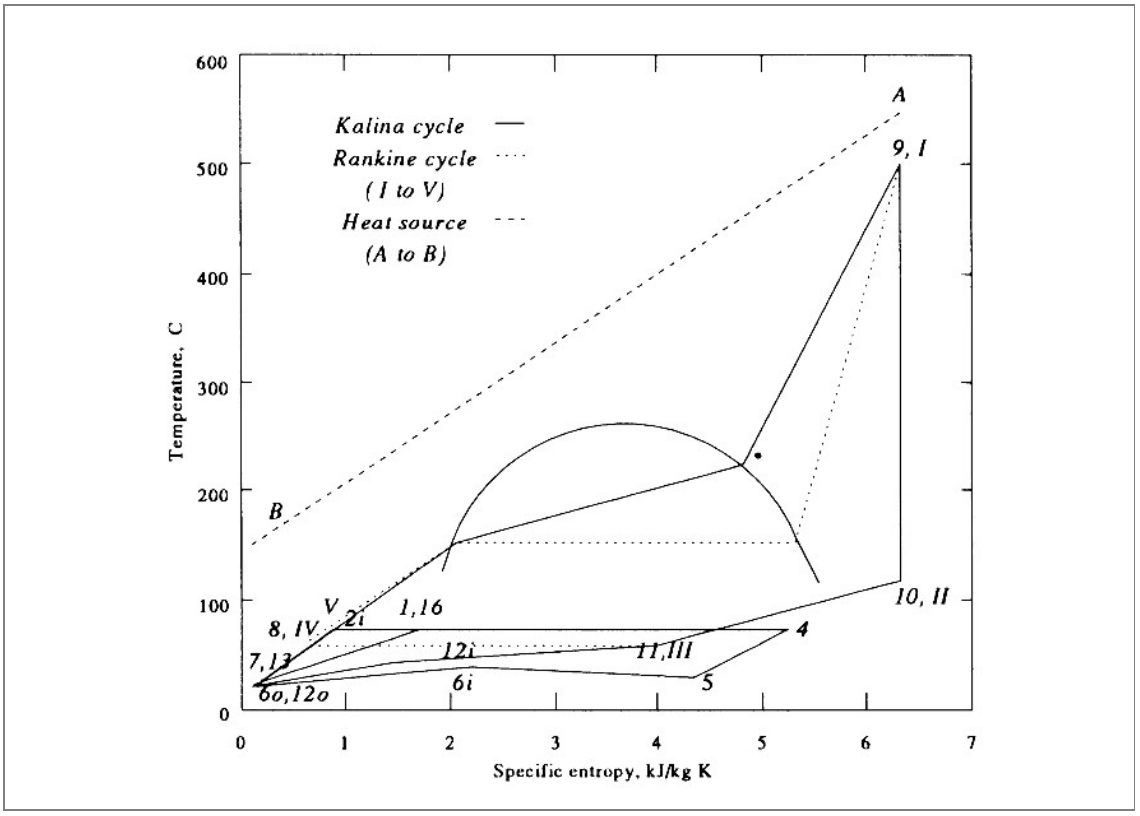

Figure 2.11: T-s diagram of a Kalina cycle compared to a Rankine cycle (Nag & Gupta, 1998)

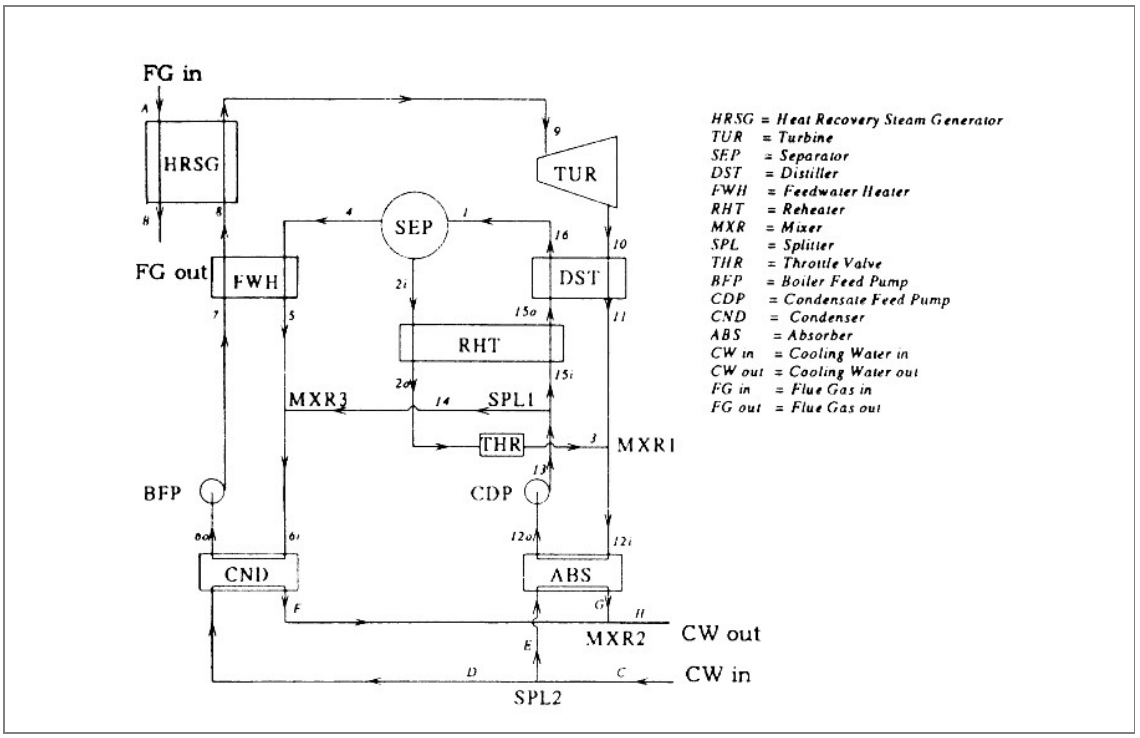

Figure 2.12: Component diagram of the Kalina cycle (Nag & Gupta, 1998)

2.4.1.6 Goswami cycle

Like the Kalina cycle, the Goswami cycle uses a mixture of ammonia and water as a working fluid. However, the cycle is configured to utilise waste heat and produce both power and cooling from waste heat (Padilla, et al., 2012). Due to the fact that the cycle produces both power and cooling, comparing the efficiencies with an ORC or Kalina cycle presents complications.

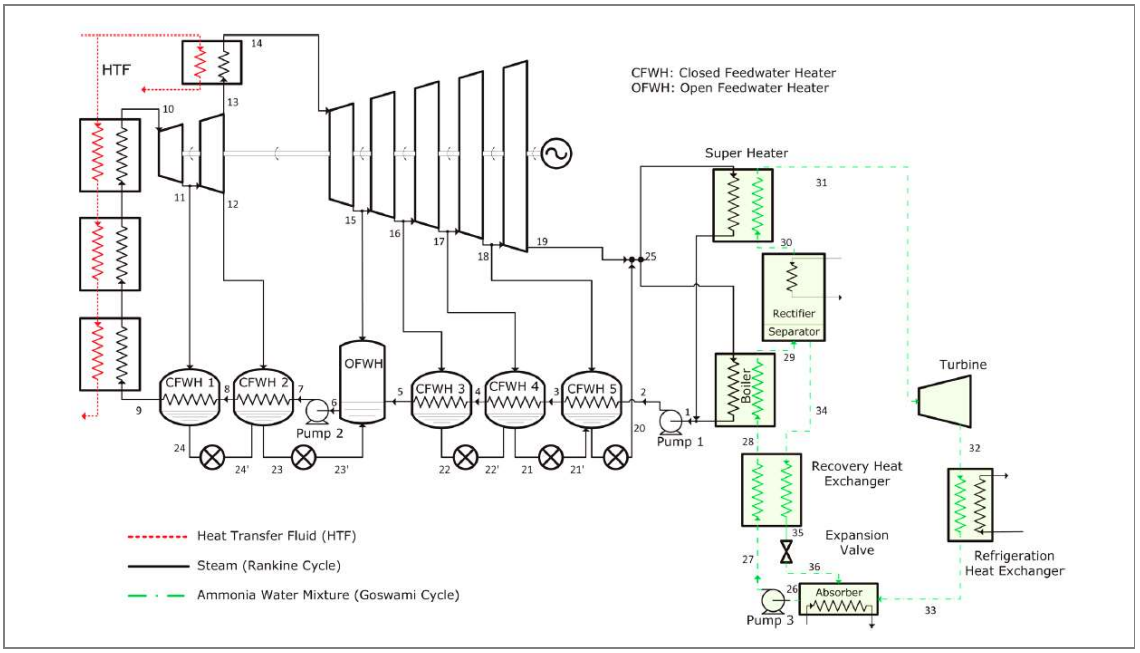

Figure 2.13: The Goswami cycle using waste heat from a Rankine cycle (Padilla, et al., 2012)

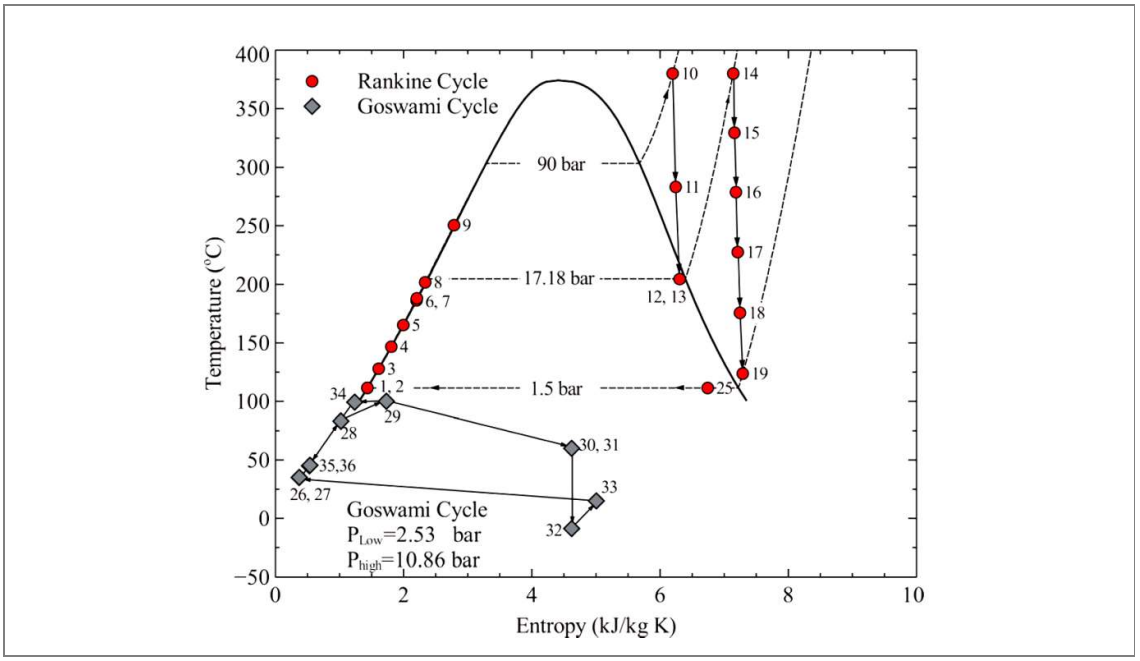

Figure 2.14: T-s diagram of the Goswami and Rankine cycles (Padilla, et al., 2012)

The benefit of the cycle is that, should the application call for cooling, the Goswami cycle can produce up to half the output in cooling, depending on the heat source (Vijayaraghavan & Goswami, 2005). Figure 2.13 indicates a component diagram of a Rankine cycle along with a Goswami cycle. From the T-s diagram of the cycle, presented in Figure 2.14, it can be seen that cooling is achieved at temperatures from -5 to -8 ºC, depending on the heat source, cycle conditions and cycle setup.

2.4.1.7 Trilateral flash cycle

The trilateral flash cycle, which is indicated in Figure 2.15, is in principle similar to a classic ORC when considering the component diagram. However, the trilateral flash cycle differs fundamentally in the sense that expansion starts from a saturated liquid phase. Point 2 in Figure 2.15 is therefore a saturated liquid. Heat transfer is therefore via liquid to liquid, which causes a closer temperature profile. Consequently, the pinching problem that occurs due to phase change is eliminated. The fact that the working fluid is an ammonia-water mixture also emphasises the close temperature profile between the heat source and the working fluid. The energy losses are therefore significantly reduced (Paanu, et al., 2012).

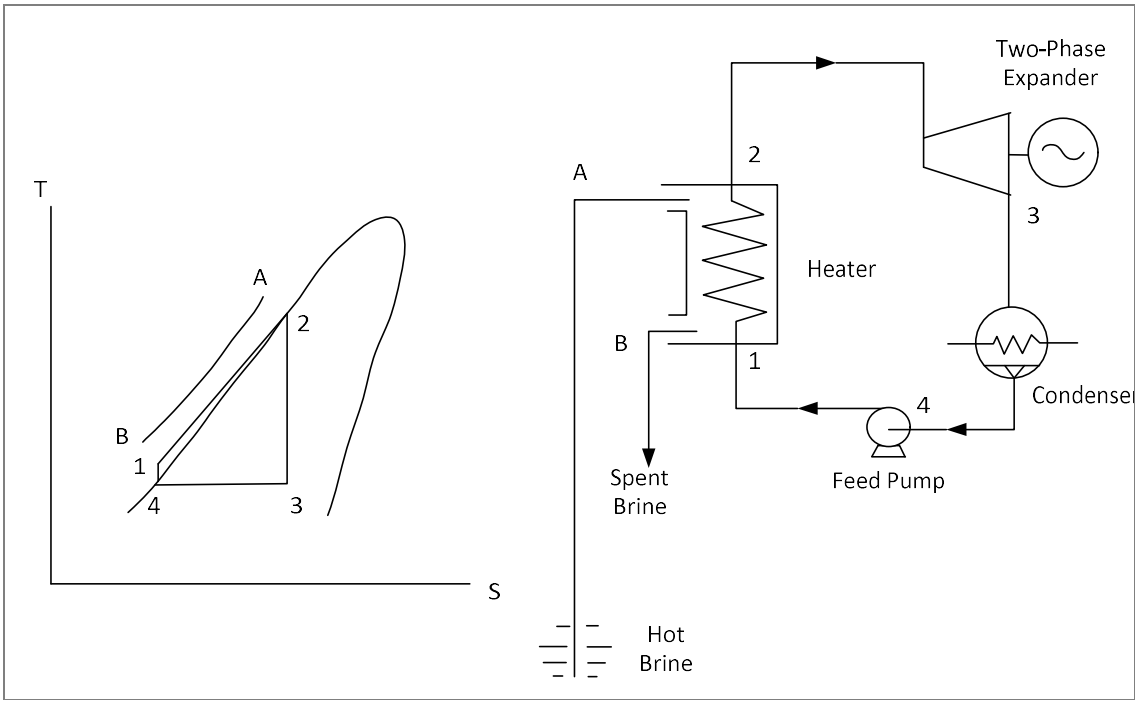

Figure 2.15: The trilateral flash cycle (Smith, et al., 1995)

2.5 Working fluids

When analysing the cycles discussed, it is clear that the working fluid plays a significant role in the performance of the cycle. The working fluid should clearly suit the operating conditions. The working fluid with the optimal performance under certain operating conditions should be selected for the application.

2.5.1 Classification of working fluids

When analysing a working fluid for an application, one can classify the working fluid as either a dry, wet or isentropic working fluid. The type of working fluid is classified by looking at the slope of the saturated vapour curve on the T-s diagram of a specific working fluid (Chen, et al., 2010). Figure 2.16 indicates this principle clearly.

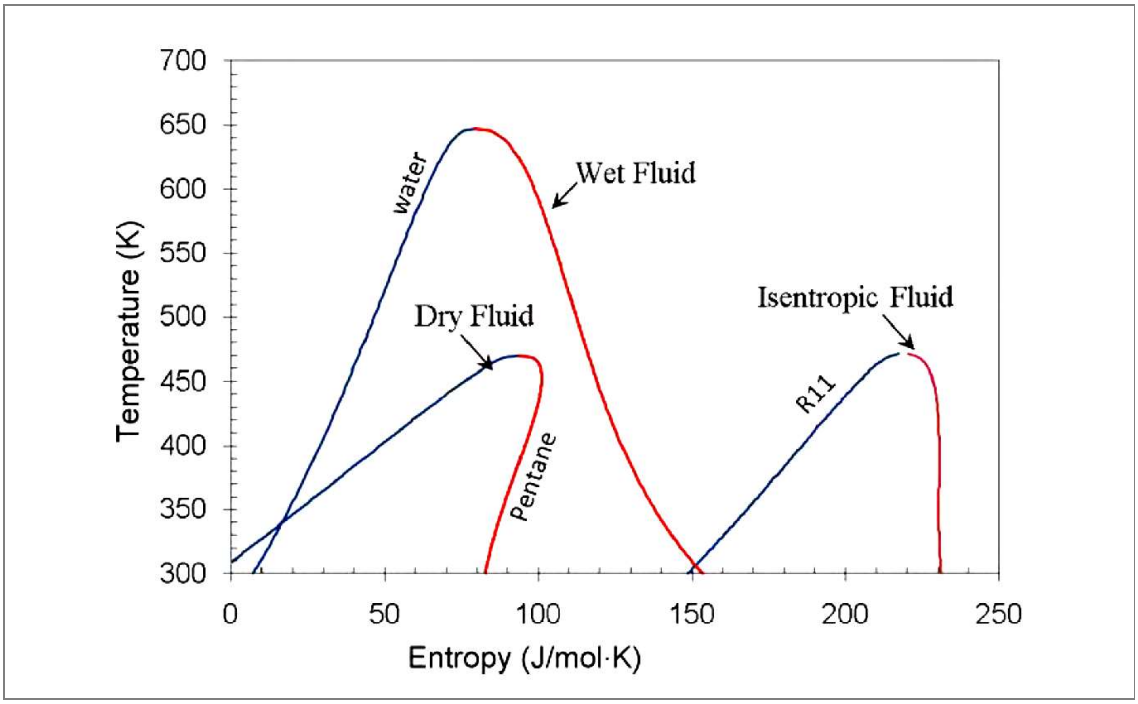

Figure 2.16: Diagram indicating the types of working fluids (Chen, et al., 2010)

The slope of the saturated vapour curve is defined as $\xi = ds/dT$. If $\xi > 0$, then the fluid is a dry fluid. If $\xi \approx 0$, then the fluid is an isentropic fluid. If $\xi < 0$, then the fluid is a wet fluid. Equation 2.2 indicates an expression by which the slope can be calculated (Lui, et al., 2004).

$$\xi = \frac{C_p}{T_H} - \frac{\left(\frac{\eta T_{rH}}{1-T_{rH}}\right)+1}{T_H^2}\,\Delta H_H \qquad (2.2)$$

Taking the above into account, along with conditions such as the heat source and condensing temperatures for example, the heat recovery cycle can be modified to obtain optimal operating conditions.

For example, a normal ORC that utilises a dry fluid as a working fluid is usually still in the superheated phases, after expansion. This presents an opportunity to utilise the available heat for feedwater heating before entering the condenser as a saturated vapour (Chen, et al., 2010).

The cycle can therefore be modified to obtain optimum results. Another factor that should be taken into account is the characteristics of the working fluid. A working fluid's characteristics, like the critical temperature or critical pressure, can limit the operating conditions of the ORC. Refer to Table 3.4 for a list of working fluids.

2.5.2 Constraints on working fluids

The working fluid's constraints should also be taken into account when assessing a low-grade W2P cycle. One of the key factors to consider is the environmental aspects with regard to certain working fluids. Ozone depletion and the global warming potential of working fluids should also be carefully considered. Due to these issues, some working fluids are being phased out by 2020 or 2030. These fluids include R113, R114, R115, R-11, R-12, R-21, R-22, R-123, R-124, R141b and R142b (Chen, et al., 2010).

Other aspects to consider with regard to a working fluid are listed below in Table 2.5.

Aspect to consider	Explanation
Critical point	The critical point of a working fluid might be below the condensation temperature of the system, which makes it unsuitable for the application.
Stability and compatibility	Some working fluids deteriorate at higher temperatures. The working fluid should also be non-corrosive and compatible with the material it is in contact with.
Availability and cost	Low-grade waste heat recovery working fluids are traditionally expensive and care should be taken when deciding on a working fluid.
Safety	Fluid should preferably be non-corrosive, non-flammable and non-toxic.
Influence of latent heat, density and specific heat	High latent heat and density, along with a low specific heat, absorb more energy and the components required can be reduced in size.
Effectiveness of superheating	The rate of the divergence of the constant pressure line determines the effectiveness of superheating and is a function of the properties of the working fluid.

Table 2.5: Working fluid properties and considerations (Chen, et al., 2010)

2.6 The boiling condenser used for waste heat recovery

A new manner proposed to utilise low-grade waste heat to generate power is to implement a BC cycle. Sharifpur (2007) proposed the implementation of a BC in a fossil fuel power plant to increase its thermal efficiency. The proposed cycle functions on the principle that the BC cycle is implemented on a steam Rankine cycle. The steam Rankine cycle is slightly modified and the BC is implemented in the steam Rankine cycle to replace the function of a condenser. On the steam side of the BC, the steam enters as a vapour at a certain temperature and pressure, and condenses to a saturated liquid. The BC is designed to function in a similar way to the core

of the BWR. The steam therefore condenses in tubes in the BC. A working fluid, which recovers the waste heat in the cycle, flows in the channels on the outside of the tubes and absorbs the waste heat from the condensation process on the steam side. The working fluid then enters a cycle similar to a normal ORC (Sharifpur, 2007). The implementation of a BC cycle can be seen below in Figure 2.17. The T-s diagram of the BC cycle is similar to the T-s diagram of a normal ORC cycle, as indicated in Figure 2.6.

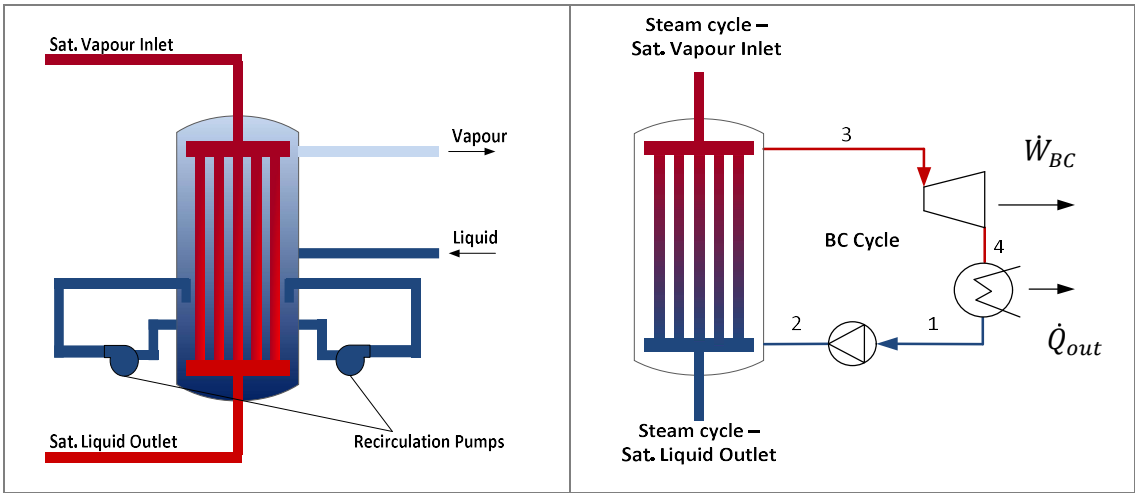

Figure 2.17: Diagram of a BC and a BC cycle implemented on a steam Rankine cycle (Sharifpur, 2007)

Implementation of the BC cycle showed increases in the overall thermal efficiency of the power generation cycle. Consequently, there is a reduction in the direct heat released by the power plant, as well as a reduction in the release of CO_2.

2.7 Conclusion

The energy demand is rising and most of the energy is projected to still be generated from fossil fuel power plants. Coal-fired power plants in South Africa are and will remain the main source of electricity. However, the most common coal-fired power plants in South Africa, namely subcritical coal-fired power plants, generally have a thermal efficiency lower than 36%. This implies that a substantial amount of heat is lost or wasted throughout the cycle, with the majority of the losses occurring in the condenser.

The waste heat from a cycle can be categorised according to high-, medium-, and low-grade waste heat. Several methods have been studied and implemented to recover high- and medium-grade waste heat. However, with most of the losses occurring in the condenser, it would be worthwhile to see if methods can be implemented to recover heat from this low-grade waste heat source.

Different cycles have been studied where heat can be recovered from low-grade waste heat sources, such as the ORC, regenerative ORC, supercritical ORC, transcritical CO_2 cycle, Kalina cycle, Goswami cycle and the trilateral flash cycle. Features and benefits of each of these cycles were discussed. The key issue in these cycles is the working fluids. When selecting a working fluid for an application, it is imperative to keep the constraints and characteristics of the working fluid in mind.

A new method to recover waste heat, specifically in steam Rankine cycles, namely the BC cycle, was also discussed. A study of this cycle's implementation preliminarily indicates an increase in thermal efficiency.

3. BOILING CONDENSER CYCLE AND METHOD OF ANALYSIS

3.1 Introduction

This chapter will discuss the method used and assumptions made in the analysis of an existing South African fossil fuel power plant where the BC is implemented. The South African power plant is discussed first, after which the configuration and assumptions around the simple BC cycle are discussed. The method of analysis used and assumptions made for the analysis of a BC cycle with FWHs and heat exchangers will also be discussed.

3.2 Komati Power Station

Komati Power Station is the oldest operational fossil fuel power station in South Africa. This power station has the lowest overall thermal efficiency of all the local power stations, (Eskom, 2013). It was therefore decided to conduct this study on the Komati Power Station.

3.2.1 Komati Power Station cycle information

The Komati Power Station has an installed capacity of 1 000 MW and was mothballed in 1990. However, due to an increasing power demand in South Africa, refurbishment and modernisation was conducted on the Komati Power Station, and six of the nine units are operational again and supplying electricity to South Africa's grid (Siemens, 2012).

Not all the units at Komati Power Station have the same configuration. Units 6 and 7 have the same configuration with an installed capacity of 125 MW (Eskom, 2010). It was decided that the configuration for units 6 and 7 are used for the analysis and implementation of the BC, as the heat balance diagrams for unit 6 and 7 have been updated recently.

Komati Power Station's units 6 and 7 heat balance diagram (Clark, 2013) is indicated in Figure 3.1. With the information supplied by each node, the thermal efficiency, along with the Carnot efficiency, was calculated to serve as a basis of reference.

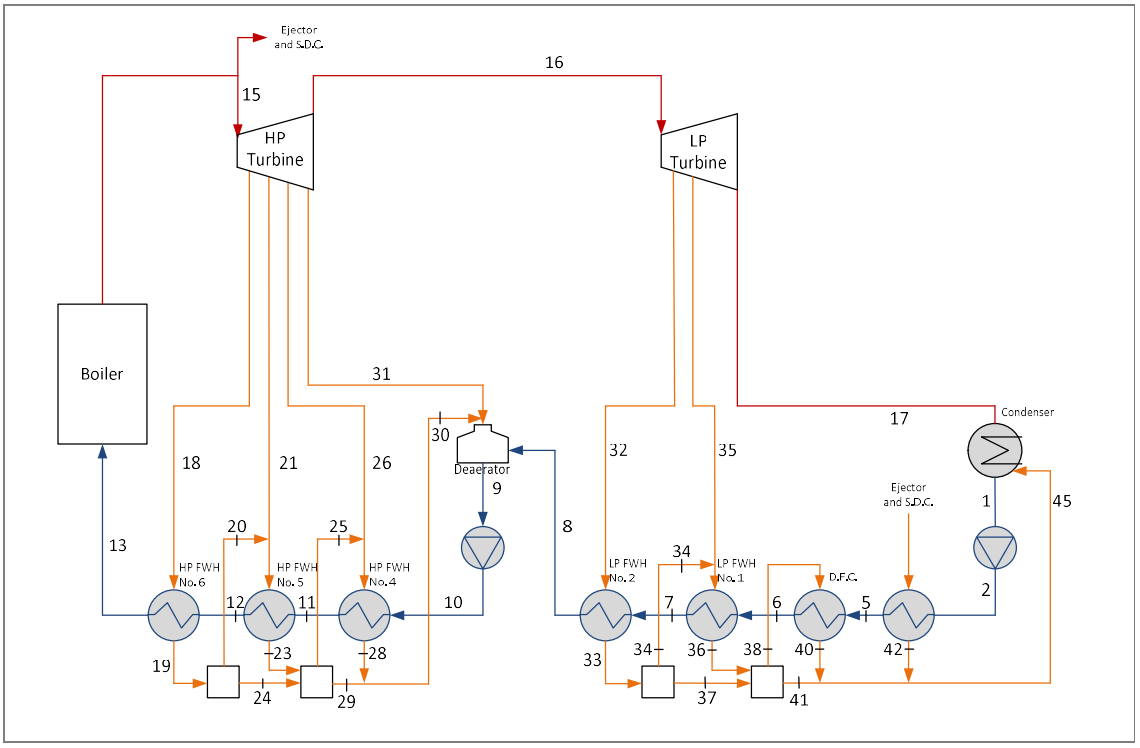

Figure 3.1: Komati Power Station Unit 6 heat balance diagram (Clark, 2013)

The T-s diagram of the heat balance diagram in indicated in Figure 3.2.

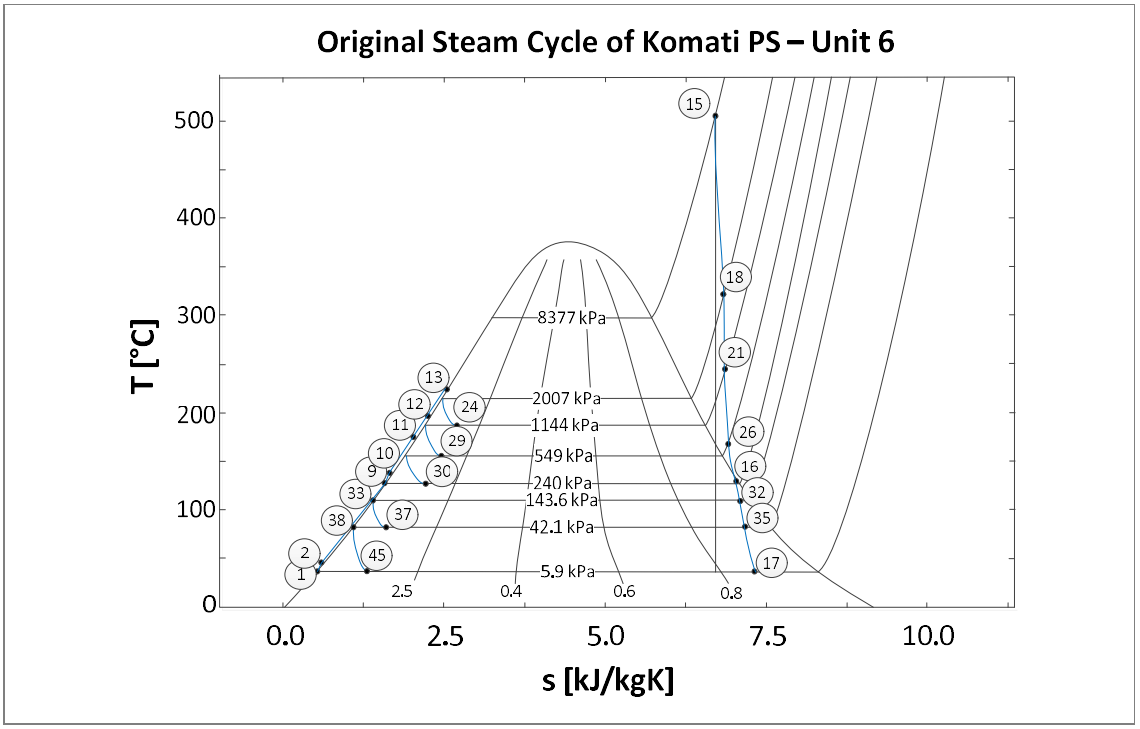

Figure 3.2: T-s diagram of the original steam cycle for the Komati Power Station – units 6 and 7

The state of each node indicated in figures 3.1 and 3.2 is given below in Table 3.1, along with the assumptions made for the analysis of the cycle.

Node	Temperature (°C)	Mass flow (kg/s)	Enthalpy (kJ/kg)	Assumption	Validation of assumption
1	36	103.48	150.6	Steady state	Analysis is conducted where conditions are monitored long after start up. All the devices are considered steady-flow devices. Therefore there is little change in properties over time (Cengel & Boles, 2006).
2	36	103.48	151.4		
5	47.4	103.48	198.3		
6	42.4	103.48	178.0		
7	71.6	103.48	300.2	First law simplification: $\Delta pe \cong 0$ $\Delta ke \cong 0$	Potential energy changes are negligible and kinetic energy changes are very small compared to the change in enthalpy in the system (Cengel & Boles, 2006).
8	104.5	103.48	438.5		
9	126.1	126.35	529.8		
10	127.6	126.35	542.3		
11	152.6	126.35	648.9	Perfectly insulated components ($\dot{Q} = 0$)	Heat losses throughout the system are negligible (Cengel & Boles, 2006).
12	183	126.35	780.9		
13	210	126.35	900.5		
15	510	126.35	3 418.8		
16	126.9	103.06	2 664.7		
17	36	90.69	2 253.7	Efficiency of pumps $\eta_p = 0.9$	Assuming the pumps are relatively modern, it is safe to implement the indicated efficiency as pump efficiency, normally ranging from 0.7 – 0.9 (Engineering Edge, 2006).
18	347.3	6.87	3 132.5		
19	212.6	6.87	909.4		
20		0.42	2 781		
21	245.8	7.42	2 948.6	Adiabatic turbine and pump ($\dot{Q} = 0$)	Turbines are relatively well insulated and heat losses through pumps are small. Therefore, it is safe to assume these components as adiabatic (Cengel & Boles, 2006).
23	185.8	7.83	788.9		
24	185.8	6.45	788.9		
25		0.91	2 751.6		
26	178.1	5.44	2 804	Heat transfer work = 0	For heat transfer components (boiler, condenser, FWHs, de-aerators, etc.), there will be no work done on the fluid
28	155.4	6.35	655.5		
29	155.4	13.38	655.5		
30	155.4	19.73	655.5		
31	165.2	3.14	2 796.5	Efficiency of turbine $\eta_t = 0.9 - 0.95$	Where the efficiency of the turbine was not incorporated, this efficiency was assumed. The reason are that the efficiency of the installed turbines was approximately 0.87 and an efficiency of 0.9 to 0.95 is generally accepted for large turbines (Engineering Edge, 2006).
32	110.1	6.78	2 593.2		
33	101.1	6.78	461.6		
34		0.6	1 887.3		
35	77.1	5.59	2 438.5	Negligible pressure losses	Pressure drops are usually small (Cengel & Boles, 2006) and are not taken into account, unless specified clearly by Eskom, in the heat balance diagrams.
36	77.1	6.19	322.9		
37	77.1	6.19	322.9		
38		0.69	2 433		
40	47.4	0.69	198.3		
41	47.4	11.68	198.3		
42	36	0.41	376.768		
45	36	12.78	204.1		

Table 3.1: Thermodynamic state of each node for the steam cycle of the Komati Power Station (Clark, 2013) and assumptions made for this analysis

The information mentioned above was used to determine work and heat input or output, the thermal efficiency of the cycle and the Carnot, or maximum, efficiency of the cycle. In order to determine this, certain standard assumptions had to be made. The assumptions made for the analysis are also indicated in Table 3.1: Thermodynamic state of each node for the steam cycle of the Komati Power Station (Clark, 2013) and assumptions made for this analysis . Further assumptions related to specific components and configurations are discussed where applicable.

The energy balance simplification, along with assumptions from Table 3.1, results in the following formulae used for the analysis.

The energy balance (Cengel & Boles, 2006) for a steady state flow process is given as:

$$\dot{Q}_{in} + \dot{W}_{in} + \Sigma_{in}\dot{m}\left(h + \frac{V^2}{2} + gz\right) = \dot{Q}_{out} + \dot{W}_{out} + \Sigma_{out}\dot{m}\left(h + \frac{V^2}{2} + gz\right) \quad \textbf{(3.1)}$$

The assumptions, for the property of the node, used or referred to in the analysis are indicated in the equation by means of superscripts and brackets.

Simplifying Equation 3.1 for the boiler, condenser, pumps and turbines results in the following:

$$\dot{Q}_{boiler} = \dot{m}_{13}\left[h_{13}^{sh,g}(P_{13};T_{13}) - h_{15}^{c,f}(P_{15};T_{15})\right] \quad \text{[kW]} \quad \textbf{(3.2)}$$

$$\dot{Q}_{condenser} = \left[\dot{m}_{17}h_{17}^{sat.fg}(T_{17};x_{17}) + \dot{m}_{45}h_{45}^{sat.fg}(T_{45};x_{45}) - \dot{m}_{1}h_{1}^{sat.f}(T_{1})\right] \text{[kW]} \quad \textbf{(3.3)}$$

$$\dot{W}_{p,cond} = \dot{m}_{1}\left[h_{1}^{sat.f}(T_{1}) - h_{2}^{c,f}(P_{2};T_{2})\right] \quad \text{[kW]} \quad \textbf{(3.4)}$$

$$\dot{W}_{p,boil} = \dot{m}_{9}\left[h_{9}^{sat,f}(P_{9}) - h_{10}^{c,f}(P_{10};T_{10})\right] \quad \text{[kW]} \quad \textbf{(3.5)}$$

$$\dot{W}_{HP,t} = \dot{m}_{15}h_{15}^{sh,g}(P_{15};T_{15}) - \dot{m}_{18}h_{18}^{sh,g}(P_{18};T_{18}) - \dot{m}_{21}h_{21}^{sh,g}(P_{21};T_{21}) - \dot{m}_{26}h_{26}^{sh,g}(P_{26};T_{26}) - \dot{m}_{31}h_{31}^{sh,g}(P_{31};T_{31}) - \dot{m}_{16}h_{16}^{sat,fg}(P_{16};x_{16}) \quad \text{[kW]} \quad \textbf{(3.6)}$$

$$\dot{W}_{LP,t} = \dot{m}_{16}h_{16}^{sat,fg}(P_{16};x_{16}) - \dot{m}_{32}h_{32}^{sat,fg}(P_{32};x_{32}) - \dot{m}_{35}h_{35}^{sat,fg}(P_{35};x_{35}) - \dot{m}_{17}h_{17}^{sat,fg}(P_{35};x_{35}) - \dot{m}_{16}h_{16}^{sat,fg}(P_{16};x_{16}) \quad \text{[kW]} \quad \textbf{(3.7)}$$

All the actual properties were given by Eskom (Clark, 2013). The program, incorporating the above assumptions and methodology, corresponds to the heat balance diagrams given by Eskom (Clark, 2013).

The thermal efficiency of the cycle was determined by means of Equation 3.8. The thermal efficiency, by considering the heat input from the fuel as the calorific value of the coal, given by Eskom, (Clark, 2013), is indicated in Equation 3.9.

$$\eta_{th} = \frac{\dot{W}_{net}}{\dot{Q}_{in}} = \frac{\dot{W}_{HP,t} + \dot{W}_{LP,t} + \dot{W}_{p,cond} + \dot{W}_{p,boil}}{\dot{Q}_{boiler}} \quad \textbf{(3.8)}$$

$$\eta_{th,fuel} = \frac{\dot{W}_{net}}{\dot{Q}_{in}} = \frac{\dot{W}_{HP,t} + \dot{W}_{LP,t} + \dot{W}_{p,cond} + \dot{W}_{p,boil}}{\dot{Q}_{Fuel\ heat}} \quad \textbf{(3.9)}$$

The maximum/ideal efficiency of the cycle can be indicated by the Carnot efficiency:

$$\eta_{th,Carnot} = 1 - \frac{T_L}{T_H} = 1 - \frac{T_{17}}{T_{15}} \quad \textbf{(3.10)}$$

The results indicated in Table 3.2 were obtained from the simplification of the first law for each component, utilising the assumptions and equations above.

$\dot{Q}_{condenser}$	**191 412 kW**
$\dot{Q}_{boiler}$	318 187 kW
$\dot{Q}_{Fuel}$	382 940 kW
$\dot{W}_{total\ turbine}$	128 931 kW
η_{Carnot}	60.52%
$\eta_{Thermal}$	40.0%
$\eta_{Thermal\ with\ fuel\ heat}$	33.24%

Table 3.2: Analysis of the original steam cycle

With a low overall efficiency, Komati Power Station appears to create an opportunity for analysis by implementing the BC.

3.3 The boiling condenser cycle

The simple BC cycle, along with all the different configurations tested in order to achieve a higher efficiency, will now be discussed. The assumptions and method of each configuration will also be discussed.

3.3.1 Modified cycle

For implementation of the BC cycle, the original cycle is modified theoretically in such a way to provide sufficient heat to the BC. Nodes 8 and 16, as well as the condensation temperature for the implementation of the BC, are kept at the state as in the original cycle (Sharifpur, 2007). The modified system is indicated in Figure 3.3.

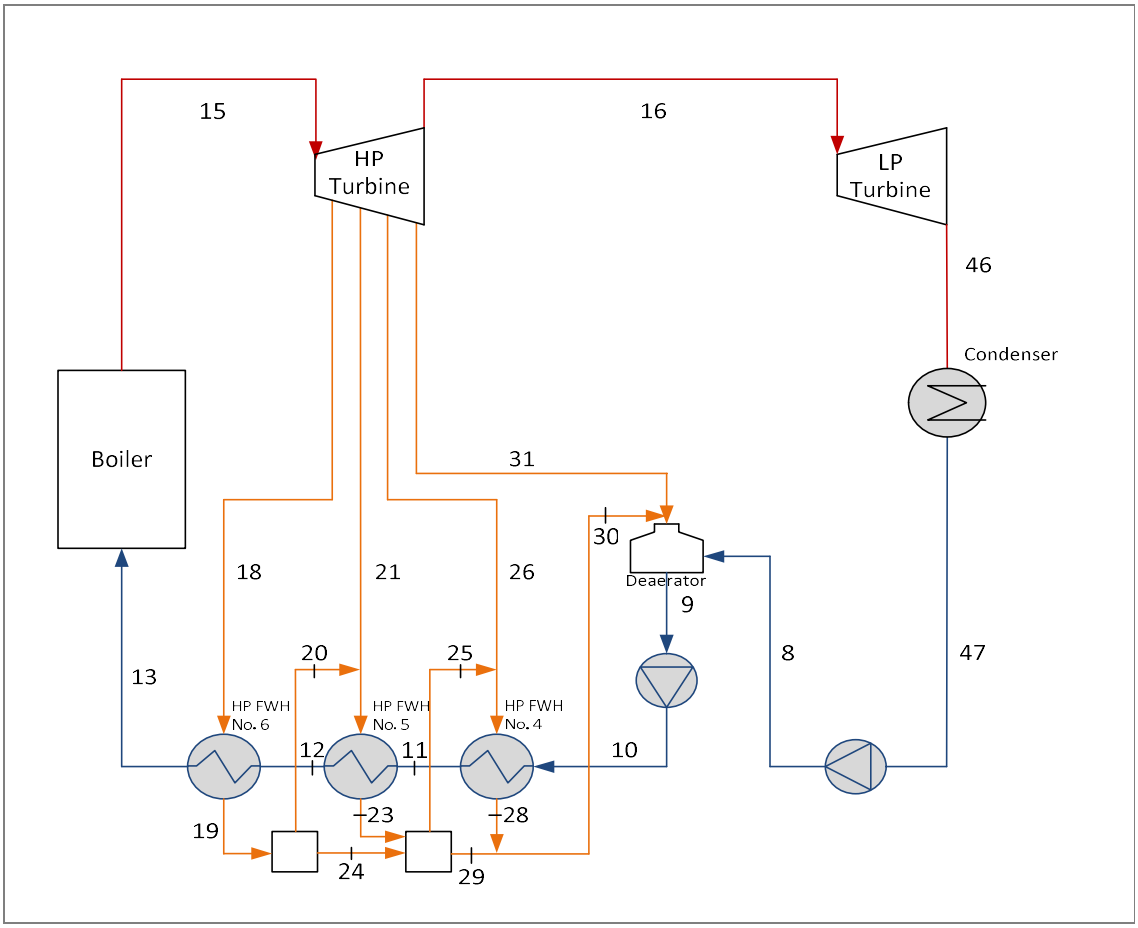

Figure 3.3: Component diagram of the modified thermal cycle

This configuration will serve as the basis for the BC. Seeing that nodes 46 and 47 are unknown, the system had to be analysed to determine the state of these nodes. Iteratively, the temperature at node 47 could be determined. The following equations, (Cengel & Boles, 2006) and method indicated in Figure 3.4 were implemented for the iteration.

$$\eta_{p,cond} = \frac{\dot{w}_{p,actual}}{\dot{w}_{p,ideal}} \quad \text{[kJ/kg]} \quad \textbf{(3.11)}^{1}$$

$$w_{p,actual} = h_{8,a}^{c,f}(P_8; T_8) - h_{47}^{sat,f}(T_{47}) \quad \text{[kJ/kg]} \quad \textbf{(3.12)}$$

$$w_{p,ideal} = h_{8,i}^{c,f}(P_8; s_{8,i}) - h_{47}^{sat,f}(T_{47}) \quad \text{[kJ/kg]} \quad \textbf{(3.13)}$$

[1] The pump efficiency indicated in Table 3.1 was used.

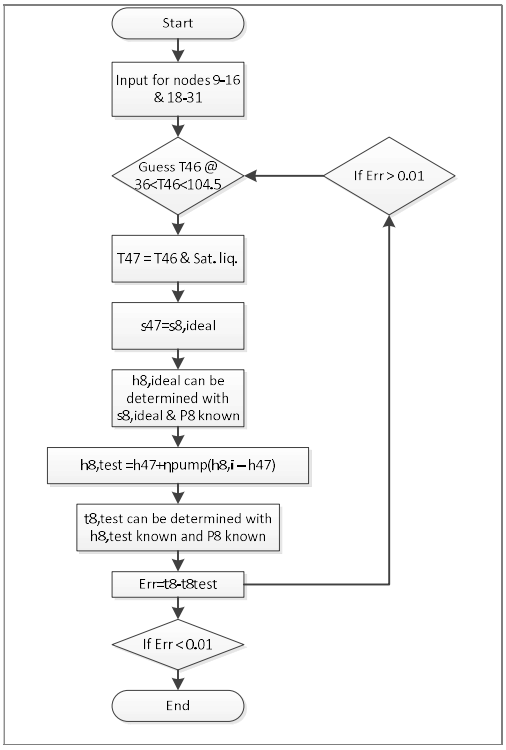

Figure 3.4: Iteration method for T_{46}

T_{46} should be somewhere between the lowest temperature in the original cycle, which is 36 °C, and T_8, which is 104.5 °C. A temperature was assumed for T_{46} within this designated range. T_{47} is equal to T_{46}, as condensation occurs at a constant temperature (Cengel & Boles, 2006). The state of 47 is a saturated liquid. The entropy, s_{46}, at this point could then be determined. In an ideal pump, the entropy at the inlet and at the outlet of the pump are equal. Therefore, the ideal entropy at node 8, $s_{8,ideal}$, was known. Consequently, the ideal enthalpy at node 8, $h_{8,ideal}$, could be determined from $s_{8,ideal}$ and P_8. Equations 3.11 to 3.13 were used to calculate the actual enthalpy at node 8. With the actual enthalpy and pressure at node 8 known, the test temperature at node 8 could be determined with EES. The difference between the actual temperature at node 8 (104.5 °C) and the test temperature was then determined. Based on the nature of the difference, an increment of 0.1 was either added to or subtracted from the previous guess value of T_{46}. The process described above was repeated. The iteration continued until the accuracy criteria were met and T_{46} was determined.

Following the determination of T_{46}, the state of T_{46} can also be determined. By assuming an isentropic turbine, the ideal state of node 46 can also be determined.

$$s_{16}^{sh,g}(P_{16};T_{16}) = s_{46}^{sa\ .gf}(T_{46}) \qquad (3.14)$$

With the temperature and the ideal entropy at node 46 known, its ideal/isentropic properties can be determined. Incorporating a turbine efficiency for the component in the calculations of work output will compensate for the assumption that the component is ideal.

The state of each node is indicated in Table 3.3 and the T-s diagram of the modified cycle is indicated in Figure 3.5. The analysis of the cycle is similar to that of the original cycle. It can be seen that there is less expansion and therefore less work from the low-pressure turbine in the modified cycle. The T-s diagram and formulae used will also be discussed.

Node	Temperature (°C)	Mass flow (kg/s)	Enthalpy (kJ/kg)
8	104.5	103.48	438.5
9	126.1	126.35	529.8
10	127.6	126.35	542.3
11	152.6	126.35	648.9
12	183	126.35	780.9
13	210	126.35	900.5
15	510	126.35	3 418.8
16	126.9	103.06	2664.7
18	347.3	6.87	3 132.5
19	212.6	6.87	909.4
20		0.42	2 781
21	245.8	7.42	2 948.6
23	185.8	7.83	788.9
24	185.8	6.45	788.9
25		0.91	2 751.6
26	178.1	5.44	2 804
28	155.4	6.35	655.5
29	155.4	13.38	655.5
30	155.4	19.73	655.5
31	165.2	3.14	2 796.5
46	104	103.5	2 457
47	104	103.5	436

Table 3.3: The state of each node for the modified system

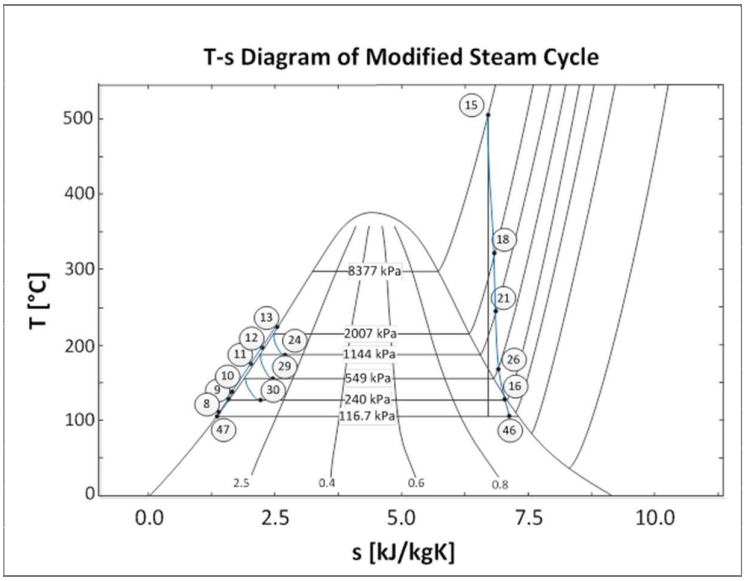

Figure 3.5: T-s diagram of the modified thermal cycle of the Komati Power Station

The formulae adapted and used for the modified cycle are indicated below. Equations, 3.2, 3.4, 3.6, 3.8 and 3.9 are used as is for the modified cycle.

$$\dot{Q}_{condenser} = \left[\dot{m}_{46} h_{46}^{sat.fg}(T_{46}; x_{46}) + \dot{m}_{47} h_{47}^{sat.fg}(T_{47}; x_{47})\right] \quad \text{[kW]} \quad \textbf{(3.15)}$$

$$\dot{W}_{p,cond} = \dot{m}_{47}\left[h_{47}^{sat.f}(T_{47}) - h_{8}^{c.f}(P_8; T_8)\right] \quad \text{[kW]} \quad \textbf{(3.16)}$$

$$\dot{W}_{LP,t} = \dot{m}_{16} h_{16}^{sat,fg}(P_{16}; x_{16}) - \dot{m}_{46} h_{46}^{sat,fg}(P_{46}; x_{46}) \quad \text{[kW]} \quad \textbf{(3.17)}$$

$$\eta_{th,Carnot} = 1 - \frac{T_L}{T_H} = 1 - \frac{T_{46}}{T_{15}} \quad \textbf{(3.18)}$$

The results obtained for this configuration are discussed in Chapter 4. This configuration, and consequently the states of each node as described above, forms the basis of the steam cycle for the implementation of the BC.

3.3.2 Configuration of simple BC cycle

As mentioned, the original cycle was theoretically modified slightly for the BC to be implemented. The method of analysing the BC theoretically implemented at the Komati Power Station will now be discussed.

Figure 3.6 indicates the theoretical BC cycle. The BC replaces the traditional condenser. The heat recovered in the BC from the steam cycle, where saturated water vapour of a certain quality enters the BC at node 46 and exits the BC as saturated liquid at node 47, is absorbed by a working fluid, usually an organic fluid or refrigerant that passes through the tube bundles of the BC. On the BC cycle side, the working fluid exits the BC at node 48, either as a saturated or superheated vapour, and passes through the BC turbine to node 49 to generate useful work. After expansion, the working fluid will enter a condenser and exit as a saturated liquid at node 50. The working fluid will then be pumped to a certain pressure and enter the BC at node 51.

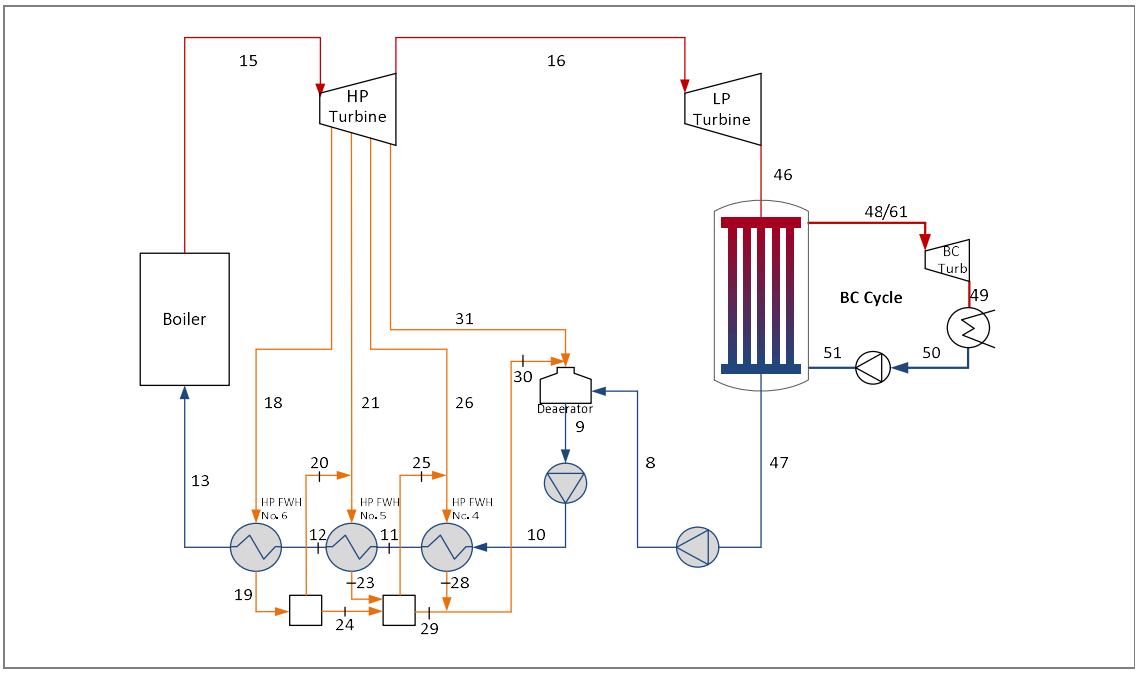

Figure 3.6: Component diagram of the Komati Power Station with the BC

Several different working fluids were tested in the BC cycle. The working fluids, listed in Table 3.4 and numbered 1 to 73, were suitable for the application. The working fluids numbered 74 to 105 were not suitable for the BC cycle and did not present useful results. Working fluids were suitable for the application based on two main criteria, namely the temperature of the

critical point of the working fluid and the physical properties of the working fluid at the outlet of the BC. If critical point temperature of the working fluid is lower than condensing temperature at node 49 then the working fluid is not suitable for the application. If the properties of the working fluid are such that the quality of the outlet of the BC turbine is too low, it was not considered for the application. The environmental implications and cost of the working fluid were not taken into account in choosing a working fluid. These factors are discussed in Chapter 5.

Working fluid tested									
1	R11	22	R22	43	Cyclohexane	64	Nitrous oxide	85	D4
2	R113	23	R236ea	44	Cyclopentane	65	n-Octane	86	D5
3	R114	24	R236fa	45	Deuterium oxide	66	n-Pentane	87	Ethyl benzene
4	R12	25	R245fa	46	Diethyl ether	67	n-Undecane	88	Hydrogen chloride
5	R123	26	R32	47	Dimethyl carbonate	68	Propane	89	Hydrogen sulphide
6	R1233zd(E)	27	R365mfc	48	Dimethyl ether	69	SES36	90	ISCEON89
7	R1234yf	28	R40	49	Ethanol	70	Sulphur dioxide	91	Isohexane
8	R1234ze(E)	29	R41	50	FC72	71	Trans-2-butene	92	Isopentane
9	R1234ze(Z)	30	R500	51	FC87	72	R116	93	Md4m
10	R124	31	R502	52	HFE7000	73	R13	94	Mdm
11	R1243zf	32	R600	53	HFE7100	74	R13B1	95	Methanol
12	R125	33	R600a	54	HFE7500	75	R14	96	M-Xylene
13	R134a	34	R718	55	Isobutane	76	R23	97	n-Decane
14	R141b	35	RC318	56	Isobutene	77	R404A	98	n-Nonane
15	R142b	36	Acetone	57	Isopropanol	78	R407c	99	o-Xylene
16	R143a	37	Ammonia	58	MM	79	R410A	100	Propylene
17	R143m	38	Benzene	59	n-Butane	80	R423A	101	p-Xylene
18	R152a	39	Butene C6	60	n-Dodecane	81	R507A	102	Sulphur hexafluoride
19	R161	40	Fluoroketone	61	Neopentane	82	R508B	103	Toluene
20	R218	41	Carbonyl sulphide	62	n-Heptane	83	R744		
21	R227ea	42	Cis-2-butene	63	n-Hexane	84	Carbon dioxide		

Table 3.4: Working fluids tested on the BC cycle (Engineering Equation Solver, 2015)

The characteristics of the working fluid also had a significant impact on the results. Slight changes in the system can increase the results, purely because of the characteristics of the working fluid (Chen, et al., 2010). The BC cycle, as illustrated in Figure 3.6, was therefore tested in two different scenarios:

- In the first scenario, the outlet conditions of the BC turbine were “fixed” at 36 °C with a quality of 0.9.
- In the second scenario, the inlet conditions of the BC turbine were “fixed” at 100 °C as a saturated vapour.

Figure 3.7 indicates the T-s diagrams of the two tested scenarios. Scenario 2 was specifically tested for the benefits of using a dry fluid (Chen, et al., 2010). A dry fluid presents the benefit that the state of the working fluid at the outlet of the BC turbine is still in a superheated state and presents the opportunity to utilise the additional heat in regeneration.

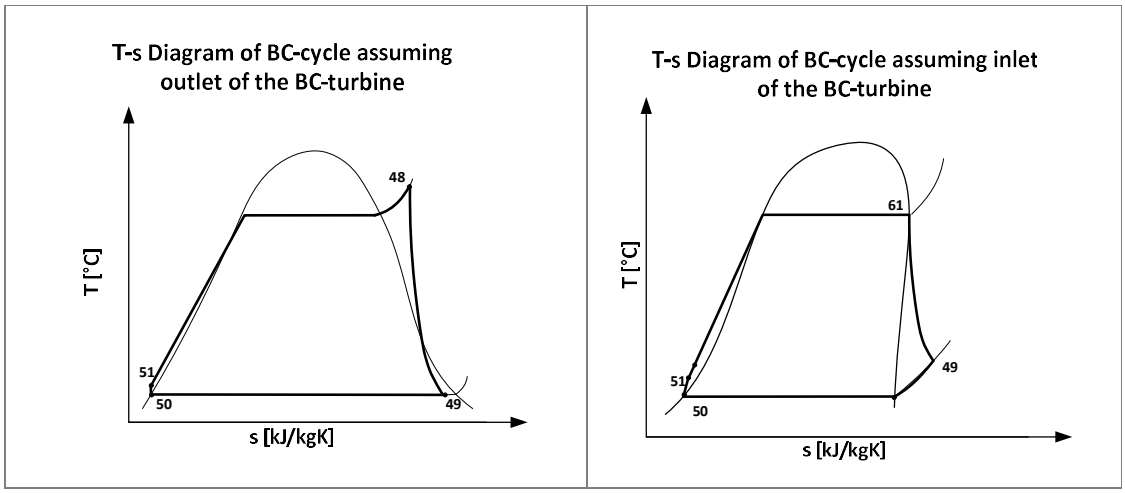

Figure 3.7: T-s diagrams of a simple BC cycle (Figure 3.6) for the two different scenarios tested

For Scenario 1 and Scenario 2, the steam side of the cycle, shown in Figure 3.6, is assumed to have the properties and states indicated in Table 3.3. Table 3.5 below indicates the state of each node in the BC cycle for both scenarios and the assumptions made of each of the nodes to determine the state at that node. The enthalpy and mass flow rates are functions of the working fluid. Therefore, such information is only discussed in Chapter 4 when the results for each configuration are discussed.

Scenario 1			Scenario 2		
Node	**Temperature (°C)**	**Assumption**	**Node**	**Temperature (°C)**	**Assumption**
48	100	$s_{48} = s_{49,i}$ $P_{48}@(T_{48},s_{48})$ [kPa] $h_{48,i}@(T_{48},s_{48,i})$ [kJ/kg][2]	**61**	100	$x_{61}=1$ P_{61} = Sat. P@T_{61} [kPa] $h_{61}@(P_{61},x_{61})$ [kJ/kg]
49	36	$x_{49}=0.9$ P_{49} = Sat.P @T_{49} [kPa] $h_{49}@(T_{49},x_{49})$ [kJ/kg]	**49**	36	$s_{49,i}=s_{61}$ $P_{49} = P_{50}$ $h_{49,i}@(P_{49},s_{49,i})$[1] $x_{49}@(P_{49},s_{49})$
50	36	$x_{50}=0$ $P_{50} = P_{49}$ $h_{50}@(T_{50},x_{50})$ [kJ/kg] $v_{50}@(T_{50},x_{50})$ [m^3/kg]	**50**	36	$x_{50}=0$ P_{50} = Sat.P @T_{50} [kPa] $h_{50}@(T_{50},x_{50})$ [kJ/kg]
51	f(assump.)	$P_{51} = P_{48}$ $v_{51}=v_{50}$ (incompressible liquid and small temperature difference) $h_{51} = \left(\frac{1}{\eta_p} v_{51}[P_{51} - P_{50}]\right) + h_{50}$	**51**	f(assump.)	$s_{51,i}=s_{50}$ $P_{51}=P_{61}$ $h_{51,i}@(P_{51},s_{51,i})$[1]

Table 3.5: The state of each node for the BC cycle for Scenario 1 and Scenario 2 and the assumptions made

[2] A turbine and pump efficiency is applied in the calculations to compensate for the ideal conditions assumed at nodes 48, 49 and 51. The value of the turbine and pump efficiencies are indicated in Table 3.1.

Note that two different methods were used to determine the enthalpy of node 51 for scenarios 1 and 2. This is purely illustrative, as the two methods produce the same results. Either of the methods can therefore be used to determine h_{51}.

Equations, 3.2, 3.5, 3.6 and 3.15 to 3.18 are used to analyse the steam cycle, along with the following formulae, which are adapted and used for the BC cycle, for both scenarios. The results obtained for this configuration are discussed in Chapter 4.

$$\eta_{th,with\ BC} = \frac{\dot{W}_{total}}{\dot{Q}_{boiler}} \tag{3.19}$$

$$\dot{W}_{total} = \dot{W}_{HP,t} + \dot{W}_{LP,t} + \dot{W}_{P,cond} + \dot{W}_{P,boil} + \dot{W}_{BC,t} + \dot{W}_{BC,p} \quad \text{[kW]} \tag{3.20}$$

$$\dot{W}_{BC,t} = \dot{m}_{BC}\eta_t(h_{48/61} - h_{49}) \quad \text{[kW]} \tag{3.21}$$

$$\dot{W}_{BC,p} = \dot{m}_{BC}\left(\frac{1}{\eta_p}\right)(h_{50} - h_{51}) \,/\, \frac{1}{\eta_p}\dot{m}_{BC}v_{50}(P_{50} - P_{51}) \quad \text{[kW]} \tag{3.22}$$

$$\dot{m}_{BC} = \dot{m}_{47}\left(\frac{h_{46}-h_{47}}{h_{48/61}-h_{51}}\right) \quad \text{[kg/s]} \tag{3.23}$$

The temperature assumptions for node 50 at 36 °C and node 48/61 at 100 °C were made based on the following reasoning:

- Node 50, the node indicating the condensation temperature, was assumed to be the same as the condensation temperature achieved in the original cycle, namely 36 °C. This is a valid assumption due to the fact that the properties of the working fluids used in the BC cycle release less heat during condensation than water does. Therefore, the available cooling towers will easily achieve this temperature. The assumptions made around the inlet and outlet of the BC turbine that govern the inlet of the condenser are such that less heat is rejected to the cooling towers than in the original cycle. This is seen in Chapter 4.
- Node 48/61, the node indicating the outlet of the BC, was assumed to have a temperature of 100 °C. This assumption was based on literature suggesting that the heat source has a temperature below 150 °C (Tchanche, et al., 2014), with a minimum heat source of 100 °C (Chen, et al., 2010). Figure 3.8 indicates a similar process to the BC, where it can be seen that the assumption of Node 48/61 at 100 °C is also valid.

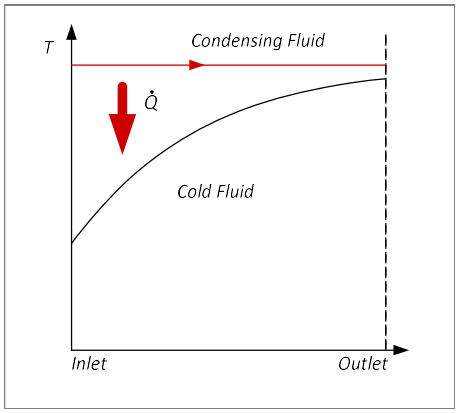

Figure 3.8: Variation in fluid temperature when one fluid is condensing (Cengel, 2006)

Under these conditions, the BC cycle indicates that an increase in thermal efficiency can be achieved. The system where the BC cycle is implemented can therefore be tested under different configurations to obtain an even higher thermal efficiency. Theoretical configurations were tested where traditional methods mentioned in Chapter 2.3, such as regeneration and feed water heating, can be implemented to achieve this. The cycle was therefore tested with different configurations and with all the working fluids indicated in Table 2.1.The configurations tested are discussed in the following sections.

3.3.3 Simple BC cycle without low-pressure turbine

The waste heat source temperature used in the BC cycle and indicated in Section 3.3.2 could be seen as being relatively low. The system can theoretically be changed to obtain a higher temperature source in the BC cycle before the working fluid enters the BC turbine. Several methods can be implemented to achieve this. The method proposed in this section is indicated in Figure 3.9.

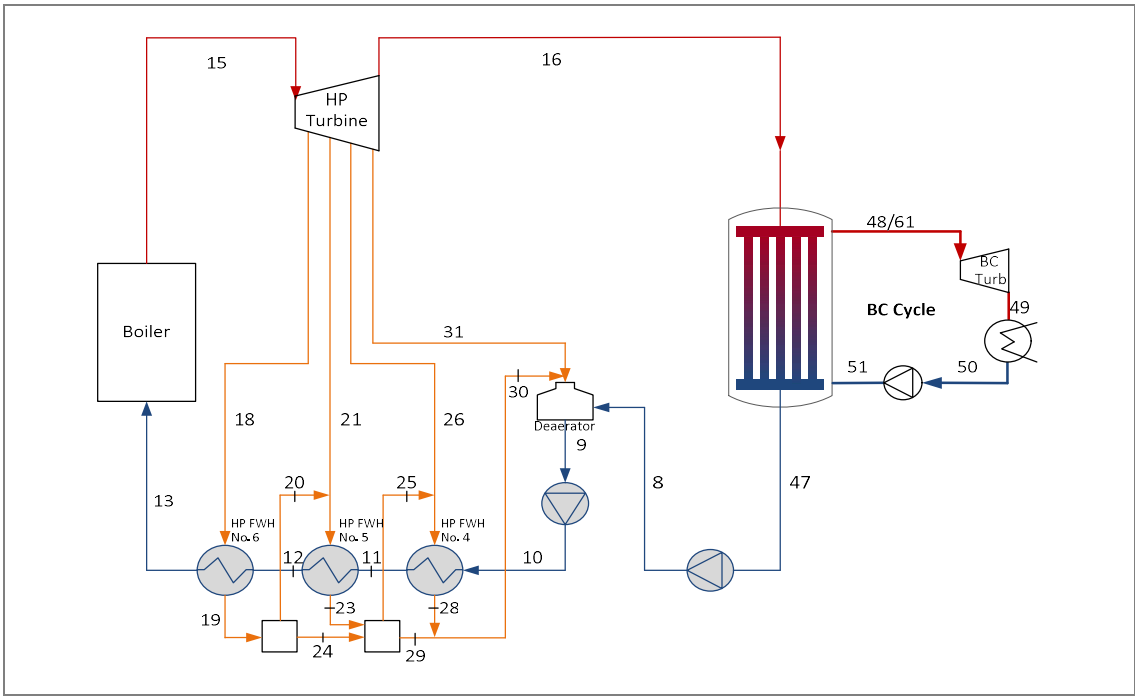

Figure 3.9: Component diagram of the Komati Power Station without a low-pressure turbine with the BC

The low-pressure turbine is theoretically removed from the steam cycle. The steam entering the BC is therefore at a higher temperature; however, the loss of the work from the low-pressure turbine on the steam side could eliminate the benefit of the higher temperature in the BC. The methods and assumption used for this configuration is indicated below. The results are discussed in Chapter 4. The nodal information and T-s diagram for the cycle is indicated in Table 3.6 and Figure 3.10 respectively.

Node	Temperature (°C)	Mass flow (kg/s)	Enthalpy (kJ/kg)
8	104.5	103.48	438.5
9	126.1	126.35	529.8
10	127.6	126.35	542.3
11	152.6	126.35	648.9
12	183	126.35	780.9
13	210	126.35	900.5
15	510	126.35	3 418.8
16	126.9	103.06	2 664.7
18	347.3	6.87	3 132.5
19	212.6	6.87	909.4
20		0.42	2 781
21	245.8	7.42	2 948.6
23	185.8	7.83	788.9
24	185.8	6.45	788.9
25		0.91	2 751.6
26	178.1	5.44	2 804
28	155.4	6.35	655.5
29	155.4	13.38	655.5
30	155.4	19.73	655.5
31	165.2	3.14	2 796.5
47	104	103.5	436

Table 3.6: The state of each node for a BC without a low-pressure steam turbine

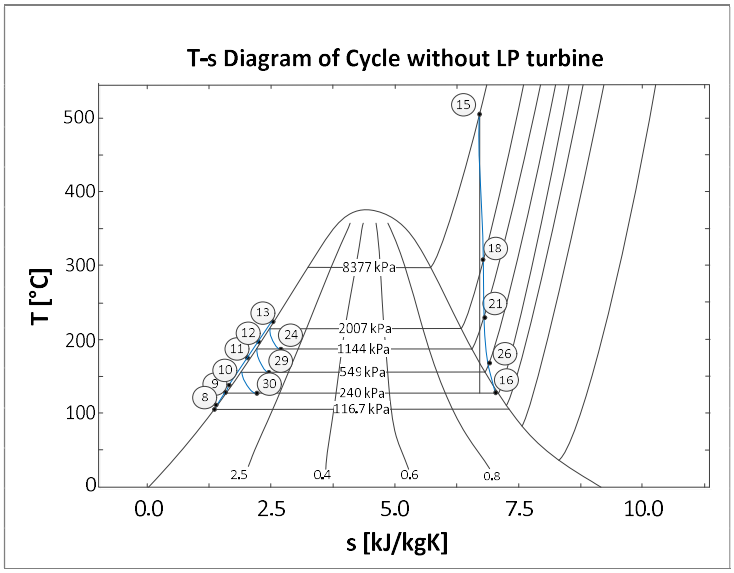

Figure 3.10: T-s diagram for the BC cycle without a low-pressure turbine

The cycle was tested for both scenarios discussed in Section 3.3.2, namely where the inlet and outlet conditions of the BC turbine was fixed. The T-s diagram of the BC cycle, without low-pressure turbine, is similar to the T-s diagram indicated in Figure 3.7. However, the temperature of node 48 is higher for both scenarios. Table 3.7 indicates the assumptions made for these two scenarios.

Scenario 1			Scenario 2		
Node	**Temp-erature (°C)**	**Assumption**	**Node**	**Temp-erature (°C)**	**Assumption**
48	120	$s_{48} = s_{49,i}$ $P_{48}@(T_{48},s_{48})$ [kPa] $h_{48,i}@(T_{48},s_{48,i})$ [kJ/kg][3]	**61**	120	$x_{61}=1$ P_{61} = Sat. P@T_{61} [kPa] $h_{61}@(P_{61},x_{61})$ [kJ/kg]
49	36	$x_{49}=0.9$ P_{49} = Sat.P @T_{49} [kPa] $h_{49}@(T_{49},x_{49})$ [kJ/kg]	**49**	36	$s_{49,i}=s_{61}$ $P_{49} = P_{50}$ $h_{49,i}@(P_{49},s_{49,i})^2$ $x_{49}@(P_{49},s_{49})$
50	36	$x_{50}=0$ $P_{50} = P_{49}$ $h_{50}@(T_{50},x_{50})$ [kJ/kg] $v_{50}@(T_{50},x_{50})$ [m^3/kg]	**50**	36	$x_{50}=0$ P_{50} = Sat.P @T_{50} [kPa] $h_{50}@(T_{50},x_{50})$ [kJ/kg]
51	f(assump.)	$P_{51} = P_{48}$ $v_{51}=v_{50}$ (incompressible liquid and small temperature difference) $h_{51} = \left(\frac{1}{\eta_p} v_{51}[P_{51} - P_{50}]\right) + h_{50}$	**51**	f(assump.)	$s_{51,i}=s_{50}$ $P_{51}=P_{61}$ $h_{51,i}@(P_{51},s_{51,i})^2$

Table 3.7: The state of each node for the BC cycle without a low-pressure turbine for scenarios 1 and 2, and the assumptions made

The equations used for the analysis of this cycle differ only slightly from those used for the normal BC cycle. Equations, 3.2, 3.5, 3.6 and 3.15 to 3.18 are used to analyse the steam cycle. Equations 3.19, 3.21 and 3.22 are used for the BC side, along with the following equations that were modified to accommodate the removal of the steam side's low-pressure turbine.

$$\dot{W}_{total} = \dot{W}_{HP,t} + \dot{W}_{P,cond} + \dot{W}_{P,boil} + \dot{W}_{BC,t} + \dot{W}_{BC,p} \quad \text{[kW]} \quad \textbf{(3.24)}$$

$$\dot{m}_{BC} = \dot{m}_{16}\left(\frac{h_{16}-h_{47}}{h_{48/61}-h_{51}}\right) \quad \text{[kg/s]} \quad \textbf{(3.25)}$$

The temperature assumed at node 48/61 at 120 °C follows the same arguments discussed in Section 3.3.2. The higher temperature entering the BC consequently allows for a higher temperature to enter the BC cycle's turbine. The working fluids tested for this configuration are the same as those indicated in Table 3.4.

This method indicates some benefits. However, some of the working fluids used in the BC cycle had "dry" fluid characteristics. Therefore, the state of the working fluid exiting the turbine of the BC was still in the superheated phase, which can be seen as a waste if not utilised.

3.3.4 Regeneration

As mentioned, dry fluids implemented in a low-grade waste heat cycle present the opportunity to utilise these characteristics for regeneration. Scenario 2, which is described in sections 3.3.2 and 3.3.3, served as a basis to discern which working fluids tested in the BC cycle can be used

[3] A turbine and pump efficiency is applied in the calculations to compensate for the ideal conditions assumed at nodes 48, 49 and 51. The value of the turbine and pump efficiencies are indicated in Table 3.1.

for regeneration. The analysis indicates which working fluid tested in the configuration was in the superheated phase at the outlet of the BC turbine. Implementing regeneration will be beneficial, as it may present an increase in the thermal efficiency of the cycle (Drescher & Bruggemann, 2006), (Yekoladio, 2013) and (Saleh, et al., 2007).

3.3.4.1 Simple BC cycle with regeneration from the BC outlet

The configuration utilised for Scenario 2, described in Section 3.3.2, was modified in such a way that a heat exchanger is installed in the BC cycle where the outlet of the BC turbine, still in the superheated phase, enters the heat exchanger and heats the working fluid that enters the BC. The theoretical configuration is indicated in Figure 3.11.

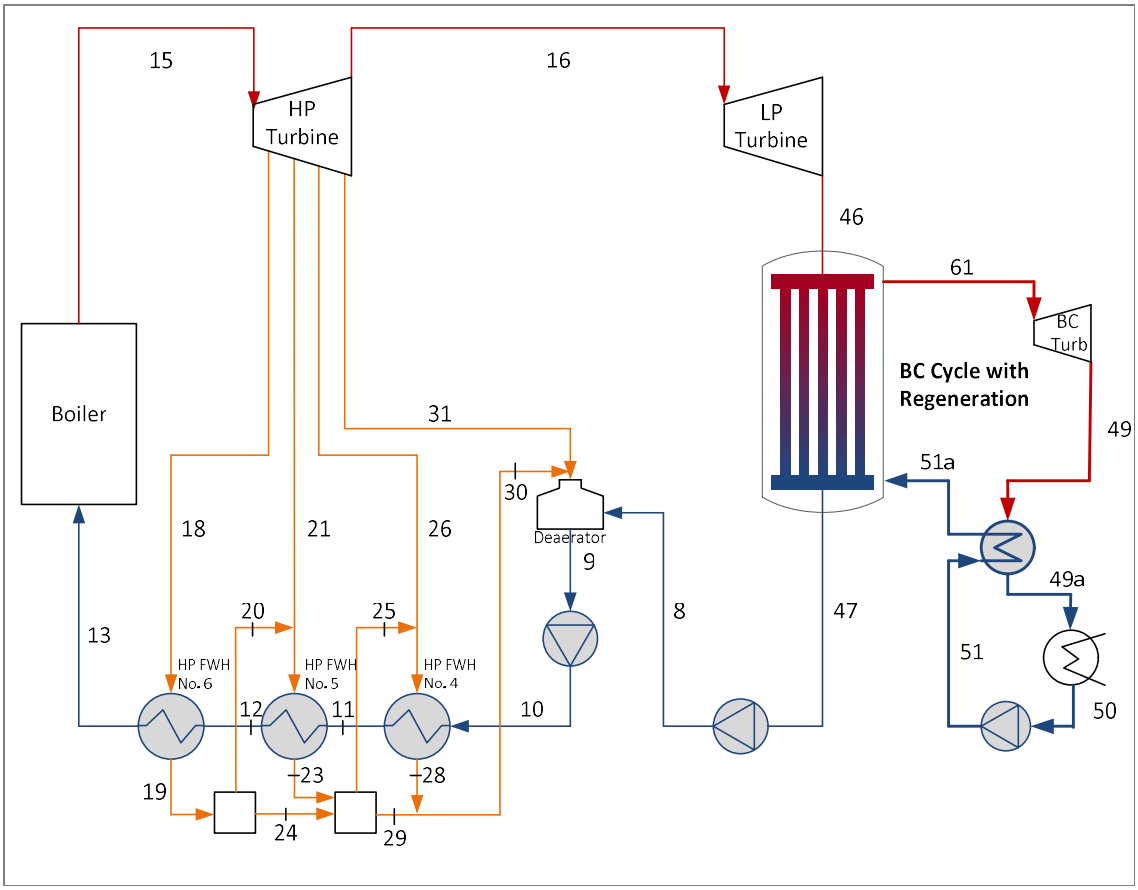

Figure 3.11: Component diagram of the Komati Power Station with a BC and regeneration from the BC outlet

The T-s diagram for this cycle, along with the method used to analyse the regeneration in the BC cycle, is indicated in Figure 3.12. It can be seen that the working fluid, at the outlet of the BC turbine, is in a superheated state. After expansion in the BC turbine to the condensation pressure, the working fluid will enter a heat exchanger at node 49 as a superheated vapour and exit the heat exchanger at node 49a. The working fluid will then pass through the condenser,

to be pumped to the cycle pressure (P_{61}), It will then enter the heat exchanger again, absorbing the heat rejected by the superheated vapour, to enter the BC at node 51a.

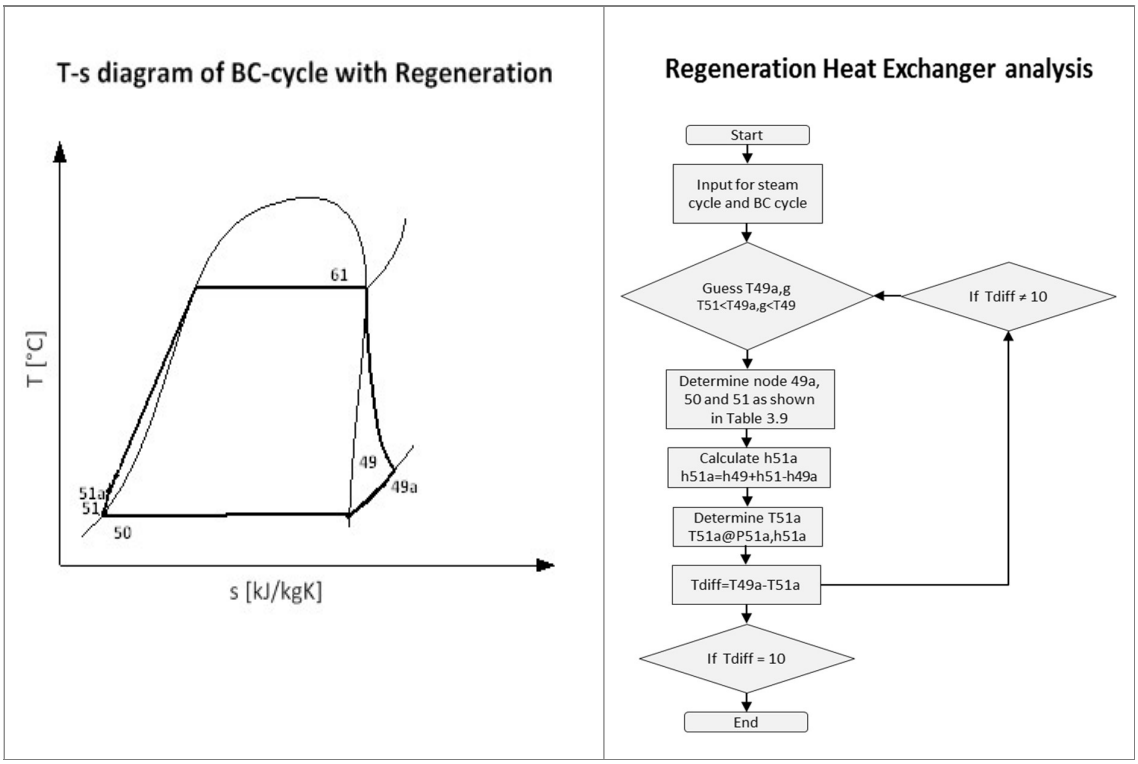

Figure 3.12: T-s diagram of a BC cycle with regeneration

The assumptions around the heat exchanger are based on an iteration method, where the main criteria centres around the assumption that the outlet temperatures of the heat exchangers differ by 10 degrees. The heat exchanger will be designed such that this is accomplished.

As mentioned, the tests conducted in Section 3.3.2 indicate which working fluids are suitable for this application, i.e. which working fluids were in the superheated state at node 49. Table 3.8: Working fluids tested on a simple BC cycle that includes indicates the working fluids tested.

Working fluids tested - simple BC cycle with regeneration							
1	R113	10	R365mfc	19	Dimethyl carbonate	28	n-Butane
2	R114	11	R600	20	FC72	29	n-Dodecane
3	R12	12	R600a	21	FC87	30	Neopentane
4	R123	13	RC318	22	HFE7000	31	n-Heptane
5	R1233zd(E)	14	Butene	23	HFE7100	32	n-Hexane
6	R141b	15	C6 Fluoroketone	24	HFE7500	33	n-Octane
7	R236ea	16	Cyclohexane	25	Isobutane	34	n-Pentane
8	R236fa	17	Cyclopentane	26	Isobutene	35	n-Undecane
9	R245fa	18	Diethyl ether	27	MM	36	SES36

Table 3.8: Working fluids tested on a simple BC cycle that includes regeneration from the outlet of a BC turbine

The steam cycle's node information remains similar to that indicated in Table 3.3. The node information and assumptions made for the BC are indicated below in Table 3.9. It should be noted that the temperature of nodes 49, 51 and 51a depends on the fluid properties.

BC cycle with regeneration		
Node	**Temperature (°C)**	**Assumption**
61	100	$x_{61}=1$ P_{61} = Sat. P@T_{61} [kPa] $h_{61}@(P_{61},x_{61})$ [kJ/kg]
49	f(working fluid @indicated assumptions)	$s_{49,i}=s_{61}$ $P_{49} = P_{50}$ $T_{49}@(P_{49},s_{49})$ $h_{49,i}@(P_{49},s_{49,i})$[4]
49a	f(working fluid @ indicated assumptions)[5]	$P_{49a}=P_{49}$ $h_{49a}@(P_{49a},T_{49a})$
50	36	$x_{50}=0$ P_{50} = Sat.P @T_{50} [kPa] $h_{50}@(T_{50},x_{50})$ [kJ/kg]
51	f(working fluid @indicated assumptions)	$s_{51,i}=s_{50}$ $P_{51}=P_{61}$ $h_{51,i}@(P_{51},s_{51,i})$[2]
51 a	f(working fluid @indicated assumptions)[6]	$P_{51a}=P_{61}$ h_{51a} = f(energy balance over the heat exchanger) $T_{51a}@(P_{51a},h_{51a})$

Table 3.9: Node information and assumptions for a BC cycle with regeneration from the outlet of the BC turbine

Equations, 3.2, 3.5, 3.6 and 3.15 to 3.22 are used to analyse the steam cycle, along with the following formulae that are adapted and used for the BC cycle with regeneration.

$$\dot{m}_{BC} = \dot{m}_{47}\left(\frac{h_{46}-h_{47}}{h_{61}-h_{51a}}\right) \quad \text{[kg/s]} \quad \textbf{(3.26)}$$

$$h_{51a} = h_{49} - h_{49a} + h_{51} \quad \text{[kJ/kg]} \quad \textbf{(3.27)}$$

This configuration did not result in an increase in thermal efficiency above that of the reference thermal efficiency of 40%. The results are indicated in Appendix B. It should be noted that due

[4] A turbine and pump efficiency is applied in the calculations to compensate for the ideal conditions assumed at nodes 49 and 51.
[5] The conditions around the heat exchanger were assumed as indicated at node 51.a. T_{49} was iterated till these conditions were met.
[6] The EES program's philosophy was written such that the heat exchanger's cold outlet temperature, i.e. node 51a, should be 10°C lower than the heat exchanger's hot outlet conditions.

to the configuration not indicating a gain in thermal efficiency, it was not deemed economical to further the study of this configuration by adding heat exchangers from the steam cycle.

3.3.4.2 BC cycle without a low-pressure turbine and with regeneration or feedwater heating

The configuration, where the BC cycle was implemented under Scenario 2 and the low-pressure turbine on the steam side was removed, as described in Section 3.3.3, was modified in such a way to include a heat exchanger in the BC cycle. The outlet of the BC turbine, still in the superheated phase, enters the heat exchanger and heats the working fluid entering the BC. The theoretical configuration is indicated in Figure 3.13.

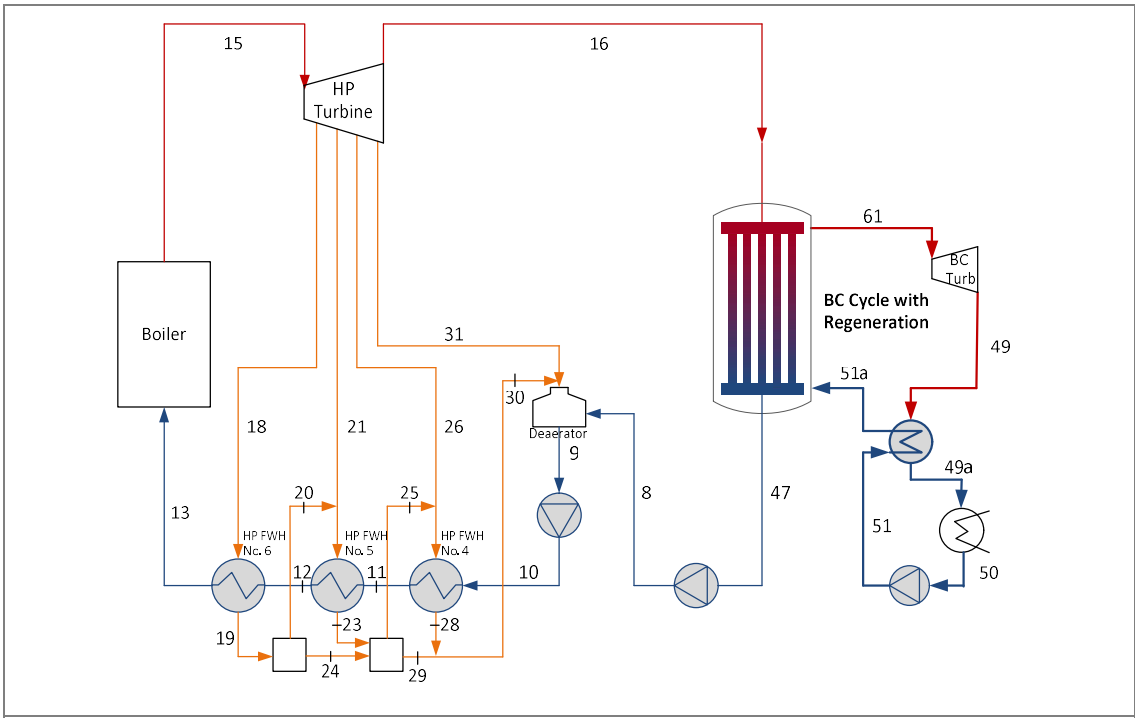

Figure 3.13: Component diagram of the Komati Power Station without a low-pressure turbine, including a BC and regeneration

Scenario 2, which is explained in Section 3.3.3, also served to indicate which working fluids were suitable for a theoretical configuration that includes regeneration, i.e. fluids that were superheated at the outlet of the BC turbine and Table 3.10 indicates the working fluids that were suitable and tested for this configuration.

Working fluid tested - BC cycle, without a low-pressure steam turbine, with regeneration in a BC cycle							
1	R113	10	R600a	18	FC87	26	n-Dodecane
2	R114	11	Butene	19	HFE7000	27	Neopentane
3	R123	12	C6 Fluoroketone	20	HFE7100	28	n-Heptane
4	R1233zd(E)	13	Cyclohexane	21	HFE7500	29	n-Hexane
5	R141b	14	Cyclopentane	22	Isobutane	30	n-Octane
6	R236ea	15	Diethyl ether	23	Isobutene	31	n-Pentane

7	R245fa	16	Dimethyl carbonate	24	MM	32	n-Undecane
8	R365mfc	17	FC72	25	n-Butane	33	SES36
9	R600						

Table 3.10: Working fluids tested on a simple BC cycle, which includes regeneration, without a low-pressure steam turbine

The steam cycle will have the properties indicated in Table 3.6 and Figure 3.10. The T-s diagram of the BC cycle, which is indicated in Figure 3.13, is similar to the T-s diagram indicated in Figure 3.12. However, the temperature of node 61 is higher at 120 °C. The method of analysis around the regeneration heat exchanger will also remain the same as indicated in Figure 3.12.

The working fluid in the BC side will therefore exit the BC turbine at node 49 as a superheated vapour and enter a heat exchanger where heat is rejected. The working fluid will exit the heat exchanger at node 49a and then enter a condenser and exit as a saturated liquid at 36 °C. The working fluid will then be pumped to the cycle pressure of P_{61} and enter the heat exchanger at node 51. The working fluid will then absorb the heat, rejected from nodes 49 to 49a, and enter the BC at node 51a. The working fluid will then pass through the BC and exit at node 61 as a saturated vapour at 120 °C, to pass through the BC turbine again.

A BC cycle with regeneration, without a low-pressure steam turbine		
Node	**Temperature (°C]**	**Assumption**
61	120	$x_{61}=1$ P_{61} = Sat. P@T_{61} [kPa] $h_{61}@(P_{61},x_{61})$ [kJ/kg]
49	f(working fluid @indicated assumptions)	$s_{49,i}=s_{61}$ $P_{49} = P_{50}$ $T_{49}@(P_{49},s_{49})$ $h_{49,i}@(P_{49},s_{49,i})$[7]
49a	f(working fluid @ indicated assumptions) [8]	$P_{49a}=P_{49}$ $h_{49a}@(P_{49a},T_{49a})$
50	36	$x_{50}=0$ P_{50} = Sat.P @T_{50} [kPa] $h_{50}@(T_{50},x_{50})$ [kJ/kg]
51	f(working fluid @indicated assumptions)	$s_{51,i}=s_{50}$ $P_{51}=P_{61}$ $h_{51,i}@(P_{51},s_{51,i})$[2]
51a	f(working fluid @indicated assumptions)[9]	$P_{51a}=P_{61}$ h_{51a} = f(energy balance over the heat exchanger) $T_{51a}@(P_{51a},h_{51a})$

Table 3.11: Node information and assumptions for a BC cycle with regeneration, without a low-pressure steam turbine

[7] A turbine and pump efficiency is applied in the calculations to compensate for the ideal conditions assumed at nodes 49 and 51.
[8] The conditions around the heat exchanger were assumed as indicated at node 51.a. T_{49} was iterated till these conditions were met.
[9] The EES program's philosophy was written such that the heat exchanger's cold outlet temperature, i.e. node 51a, should be 10°C lower than the heat exchanger's hot outlet conditions.

The equations used for the analysis of this cycle differ only slightly from those used for the normal BC cycle. Equations, 3.2, 3.5, 3.6 and 3.15 to 3.18 are used to analyse the steam cycle. Equations 3.19, 3.21 and 3.22 are used for the BC side, along with the equations below, which were modified to accommodate the removal of the steam side's low-pressure turbine and the BC cycle with regeneration.

$$\dot{W}_{total} = \dot{W}_{HP,t} + \dot{W}_{P,cond} + \dot{W}_{P,boil} + \dot{W}_{BC,t} + \dot{W}_{BC,p} \quad \text{[kW]} \quad \textbf{(3.28)}$$

$$\dot{m}_{BC} = \dot{m}_{16}\left(\frac{h_{16}-h_{47}}{h_{61}-h_{51a}}\right) \quad \text{[kg/s]} \quad \textbf{(3.29)}$$

$$h_{51a} = h_{49} - h_{49a} + h_{51} \quad \text{[kJ/kg]} \quad \textbf{(3.30)}$$

Due to the higher temperature obtained at the inlet of the BC turbine by removing the low-pressure steam turbine, the dry working fluids will exit the BC turbine at a higher temperature. Consequently, more heat is released to the working fluid before entering the BC. This however did not cause the thermal efficiency of the cycle to rise above the reference thermal efficiency of 40%. The results will be shown in Appendix B, but similar to the case discussed in Section 3.3.4.1, it will be assumed as uneconomical to further the study in this configuration.

3.3.5 BC cycle with regeneration from the BC turbine and heat exchangers

The cycles described in sections 3.3.2 to 3.3.4 indicate an increase in thermal efficiency. However, it would be beneficial to implement other concepts in the BC cycle to investigate whether a further increase in thermal efficiency is possible. Concepts that were theoretically implemented in this section included additional heat exchangers and regeneration from the BC turbine.

However, the manner in which regeneration is implemented here differs from that indicated in Section 3.3.4. The heat source for the regeneration is supplied from the BC turbine. Figure 3.14 indicates the BC cycle with regeneration or feed water heating with a tap-off from the BC turbine, along with the T-s diagram of the BC cycle indicating this concept.

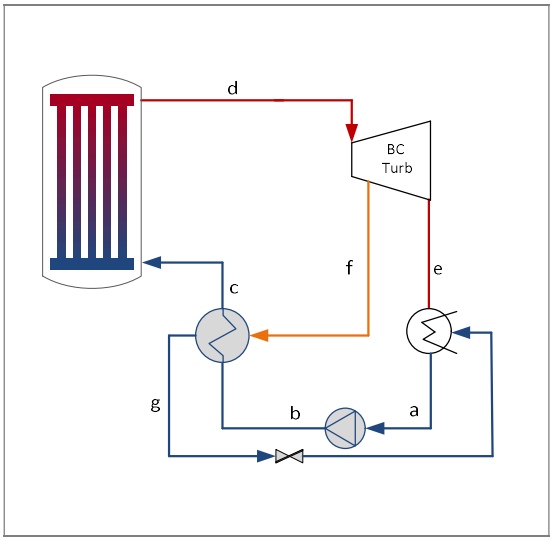

Figure 3.14: A BC cycle with a FWH

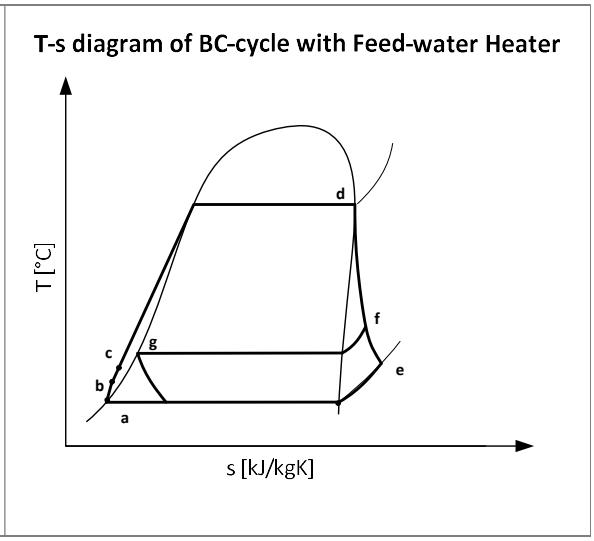

Figure 3.15: T-s diagram of a BC cycle with a FWH

The working fluid enters the turbine at node d after being heated in the BC and expands to node e. Between nodes d and e, working fluid, which is at a certain pressure, is tapped off to the FWH where heat is released, and consequently exits the FWH at node g as a saturated liquid at the tap-off pressure. The tap-off stream then enters the condenser again to join the main BC cycle.

The rest of the working fluid, after exiting the BC turbine at e, enters a condenser and is pumped from a saturated liquid at the condensation pressure at node a to the cycle pressure at node b. The working fluid then enters the FWH and absorbs heat from the tap-off stream to exit the FWH at a higher temperature at node c. The working fluid then enters the BC and absorbs the steam cycle heat to a temperature of node d to enter the BC turbine again. Feedwater heating in this application will increase the thermal efficiency and decrease the irreversible losses in the system (Habib & Zubair, 1992).

It should be noted that the tap-off pressure feeding into the FWH has to be determined by finding the optimum efficiency for a certain tap-off pressure that relates to a specific tap-off mass flow rate. This tap-off pressure has to be determined via the optimisation of a range of pressure, usually varying between the inlet and the outlet pressure of the BC turbine. A mass balance over the FWH gives an indication of what the mass flow rate for a specific tap-off pressure should be. It is evident that an optimum efficiency is obtained at a certain mass flow rate and tap-off pressure as indicated in Figure 3.16.

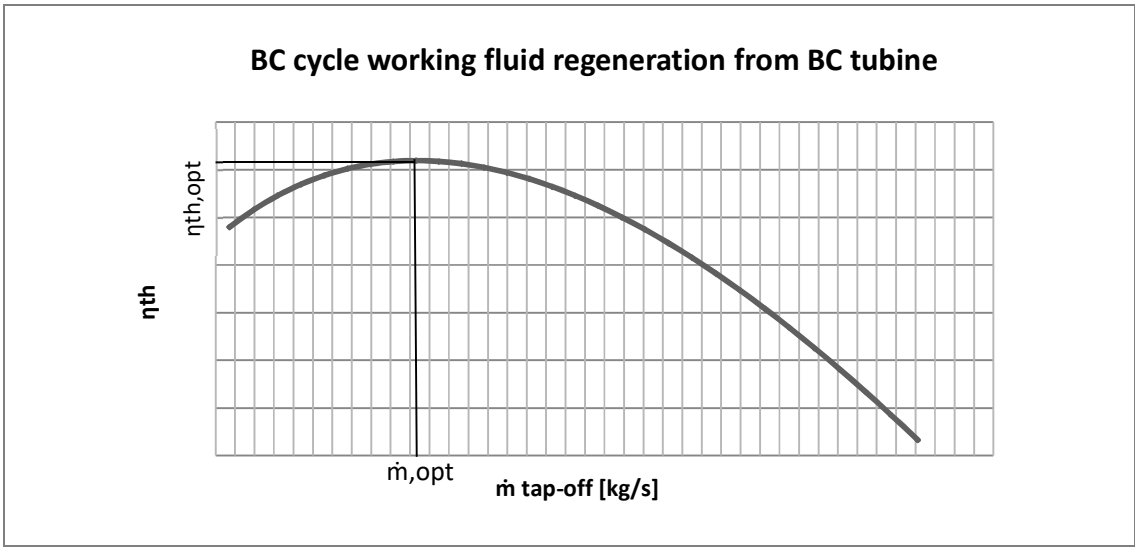

Figure 3.16: Example of optimum efficiency achieved at the specific tap-off mass flow rate of a FWH

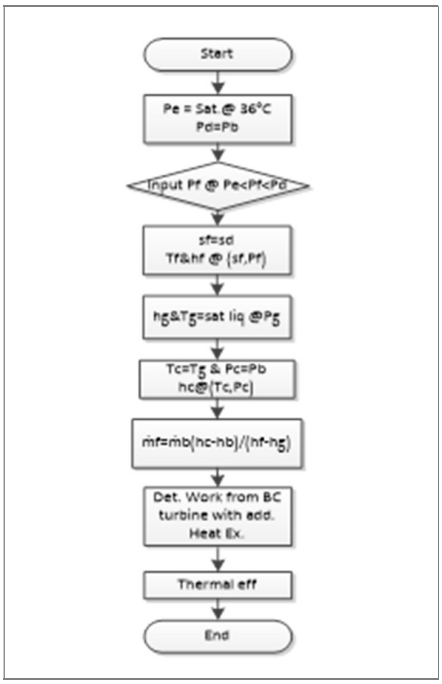

Figure 3.17: Flow diagram of method to calculate the tap-off mass flow rate for a FWH

The method to determine the tap-off mass flow rate, feeding into the FWH, is indicated in Figure 3.17. It can be seen that a tap-off pressure directly relates to a tap-off mass flow rate, where the optimum mass flow rate can be determined within the tap-off pressure range. More than one FWH can also be implemented, with each additional FWH increasing the thermal efficiency of the cycle. The limit to the number of FWHs being implemented is based on the balance between practicality and the increase in efficiency, (Sonntag, et al., 2003). Second and third FWHs are analysed in a manner similar to the method indicated above and are discussed in more detail further on in this chapter. Implementing an additional heat exchanger in the BC cycle can also result in an increase in the thermal efficiency of the cycle where heat is obtained from the steam cycle.

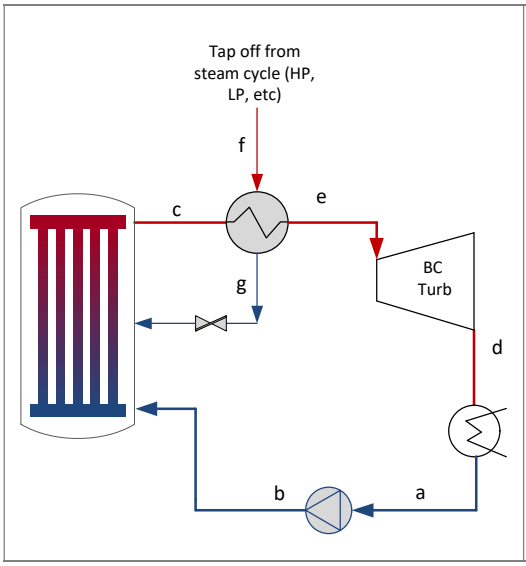

Figure 3.18: A BC cycle with an additional heat exchanger from the steam cycle

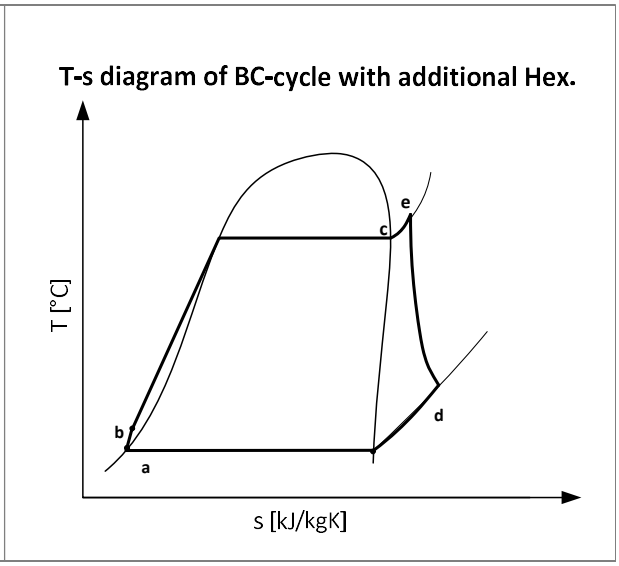

Figure 3.19: T-s diagram with an additional heat exchanger from the steam cycle

Figure 3.18 and Figure 3.19 indicate the component diagram and the T-s diagram of the theoretical cycle where an additional heat exchanger, is implemented with steam from the steam cycle. Figure 3.20 indicates the T-s diagram of the steam cycle with a tap-off to the heat exchanger in the BC cycle. This tap-off can come from either the high-pressure turbine or the low-pressure turbine in the steam side.

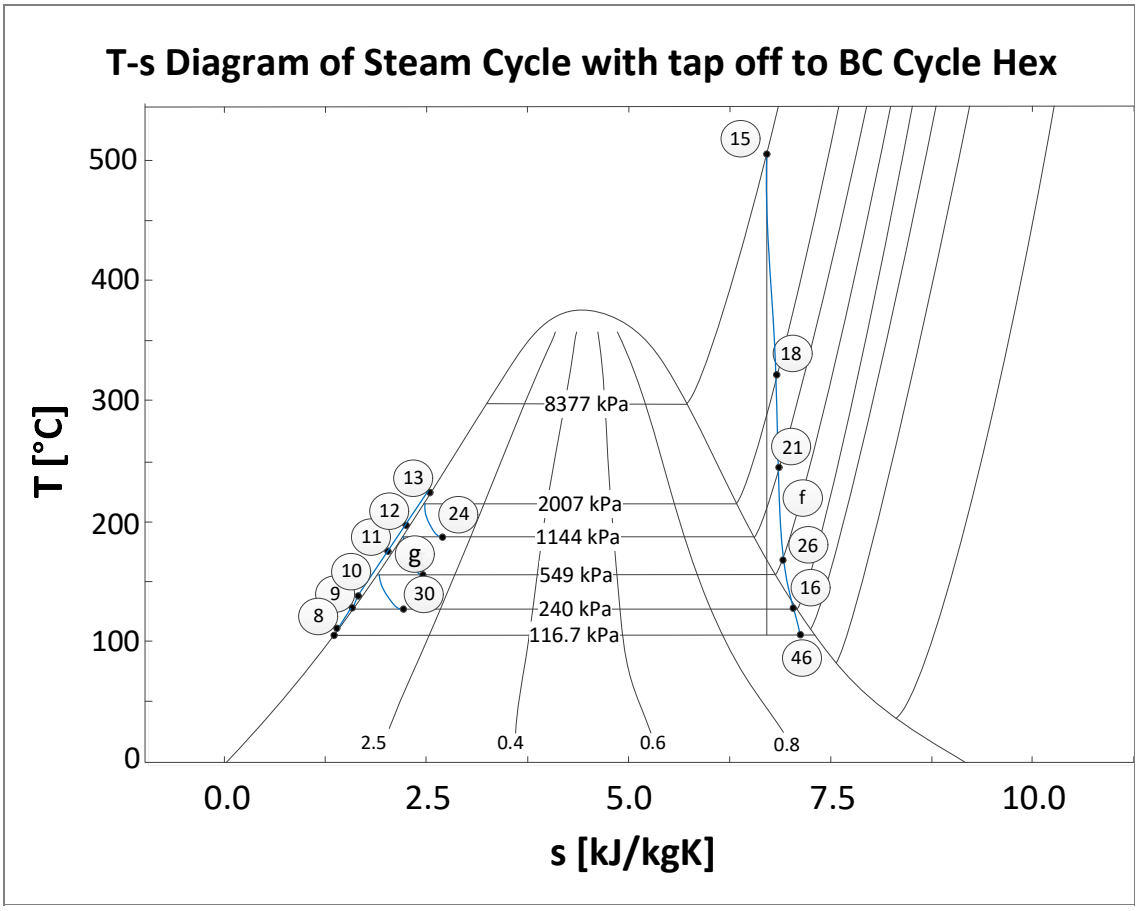

Figure 3.20: T-s diagram of the steam cycle with tap-off to the BC cycle heat exchanger

The tap-off pressure from the steam cycle can be at any pressure within the range from the inlet to outlet pressures of either the high-pressure or the low-pressure turbine. An optimum tap-off pressure and related mass flow rate can also be determined, in a similar manner as the method indicated in Figure 3.17 and Figure 3.22. The tap-off pressure from the steam cycle relates directly to the tap-off mass flow rate. Consequently, an optimum tap-off mass flow rate can be determined. The outlet temperature T_e was assumed to be slightly lower than the outlet temperature of the heat exchanger's steam side T_g. Therefore, the heat exchanger is chosen and designed in such a way that this can be accomplished. The design of the heat exchangers will not fall within the scope of this study.

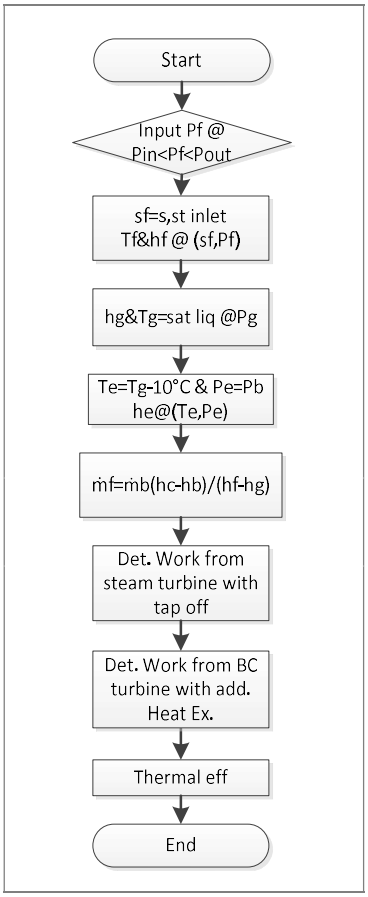

Figure 3.22: Flow diagram indicating the process of heat exchange

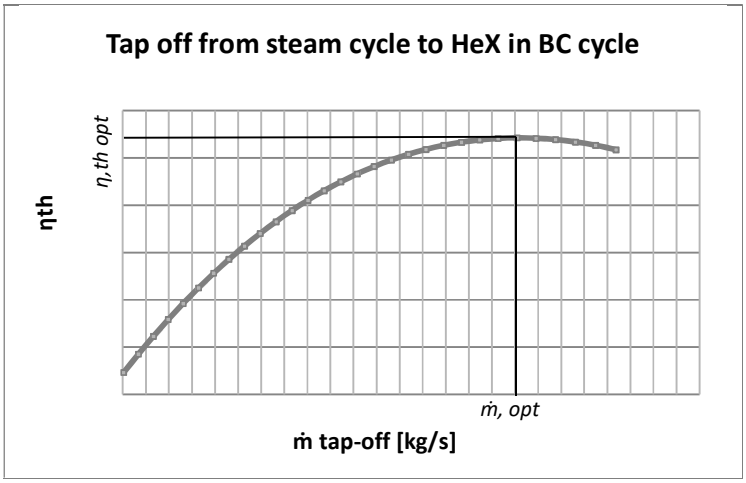

Figure 3.21: Example of optimum efficiency achieved at a specific tap-off mass flow rate for a heat exchanger with tap-off from the steam cycle

This theoretical configuration indicates an increase in efficiency when implemented on the BC cycle with certain working fluids.

It should be noted that one can combine the concept of a heat exchanger with tap-off from the steam cycle and the concept of the BC cycle FWHs. This combined theoretical concept was also tested and is discussed in detail further on in this chapter. However, the basis of this concept is discussed here.

Figure 3.23 indicates the theoretical cycle, where the BC cycle includes both a heat exchanger with tap-off from the steam side and a BC cycle FWH. It should be assumed that, for this configuration, the concept of the heat exchanger implemented in the BC cycle, with tap-off from the steam cycle, would have been tested and optimum results would have been obtained for each working fluid, as indicated in Figure 3.21. These optimum conditions for the steam cycle heat exchanger are used in the BC cycle where FWHs are implemented. The method described in Figure 3.17 and Figure 3.18 will then be implemented to obtain the optimal conditions for the BC cycle FWH.

This theoretical configuration indicates a further increase in the thermal efficiency of the cycle. Implementing two or more FWHs in the BC cycle will indicate a larger increase in the thermal efficiency of the cycle. The method and results of this configuration are discussed further in chapters 3 and 4 respectively.

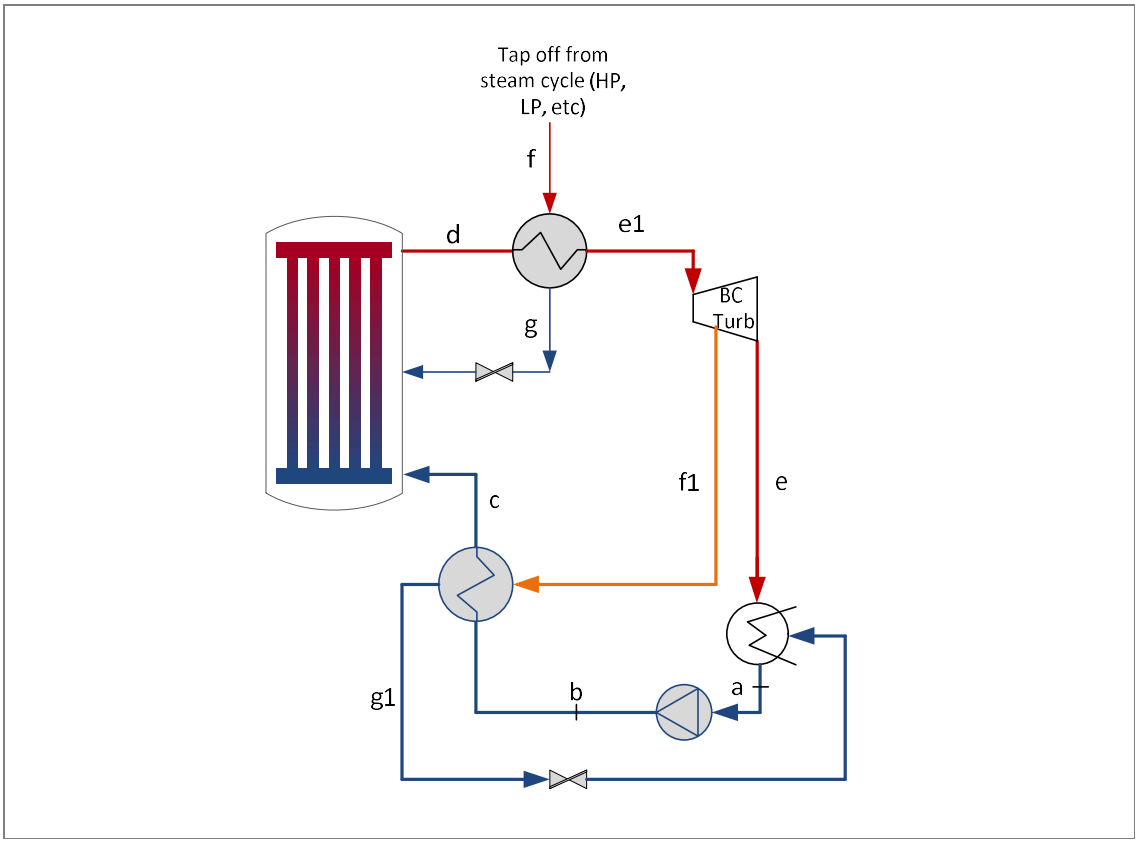

Figure 3.23: A BC cycle with an additional heat exchanger from the steam cycle and BC cycle feedwater heating

3.3.5.1 Quadratic approximation method and maximum efficiency of the tap-off pressure

As indicated in Figure 3.16 and Figure 3.21, an optimum tap-off pressure and related tap-off mass flow rate will result in an optimum cycle thermal efficiency.

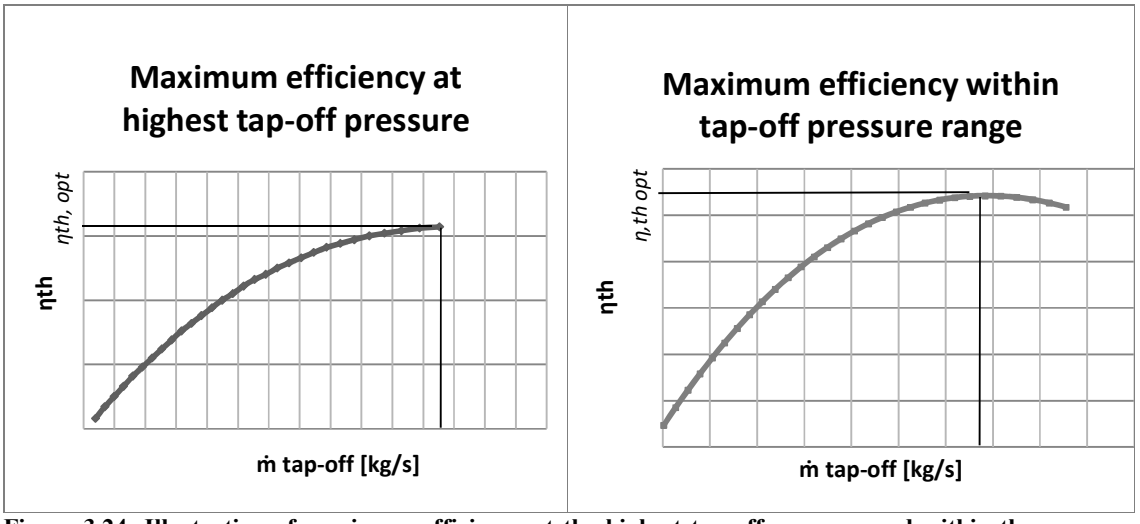

Figure 3.24: Illustration of maximum efficiency at the highest tap-off pressure and within the pressure range

Certain working fluids, which are tested in the BC cycle in the two different configurations, indicate a clear maximum efficiency at the highest tap-off pressure of the tap-off pressure range. However, other working fluids indicate a maximum thermal efficiency somewhere within the pressure range. The two different scenarios are indicated in Figure 3.24.

The optimum cycle thermal efficiency within this pressure range should therefore be determined. Quadratic approximation was used to estimate the curve best suited for the data obtained within the tap-off pressure range for both the scenario where steam was tapped off and used in a heat exchanger in the BC cycle and where the BC cycle had feed water heating, within a certain tolerance. The relative convergence tolerance used to find the maximum efficiency implementing quadratic approximation was 0.0001 (Engineering Equation Solver, 2015).

The curve would typically have the domain as the tap-off mass flow rate, which is a function of the tap-off pressure, and the range as the calculated thermal efficiency of the tested configuration. Once the quadratic function has been obtained for the specific working fluid and the specific configuration, the derivative of the function, which is equated to zero, will indicate the mass flow rate and consequently the tap-off pressure where the optimum efficiency is obtained (Stewart, 2003).

The above was done for all configurations where a heat exchanger, a FWH or a combination of the two was implemented. The tested configurations will now be discussed, indicating the theoretical configuration, nodal information of the steam and the BC cycle, along with the T-s diagrams of the steam and the BC cycle, followed by the equations used for the configuration and the working fluids tested for the configuration. As mentioned, the results are discussed in Chapter 4.

3.3.5.2 BC cycle with FWHs

The BC cycle with feed water heating from the BC turbine was theoretically tested as described above in Section 3.3.5. Figure 3.25 indicates the theoretical component diagram of the BC cycle that is implemented at the Komati Power Station, where one FWH is implemented and tested as described above.

The assumptions made for the BC cycle are similar to those explained in Section 3.3.2 and Figure 3.7, i.e. that the configuration was tested where the inlet of the BC turbine was assumed

to be fixed at a certain condition and where the outlet of the BC turbine was assumed to be fixed at a certain condition.

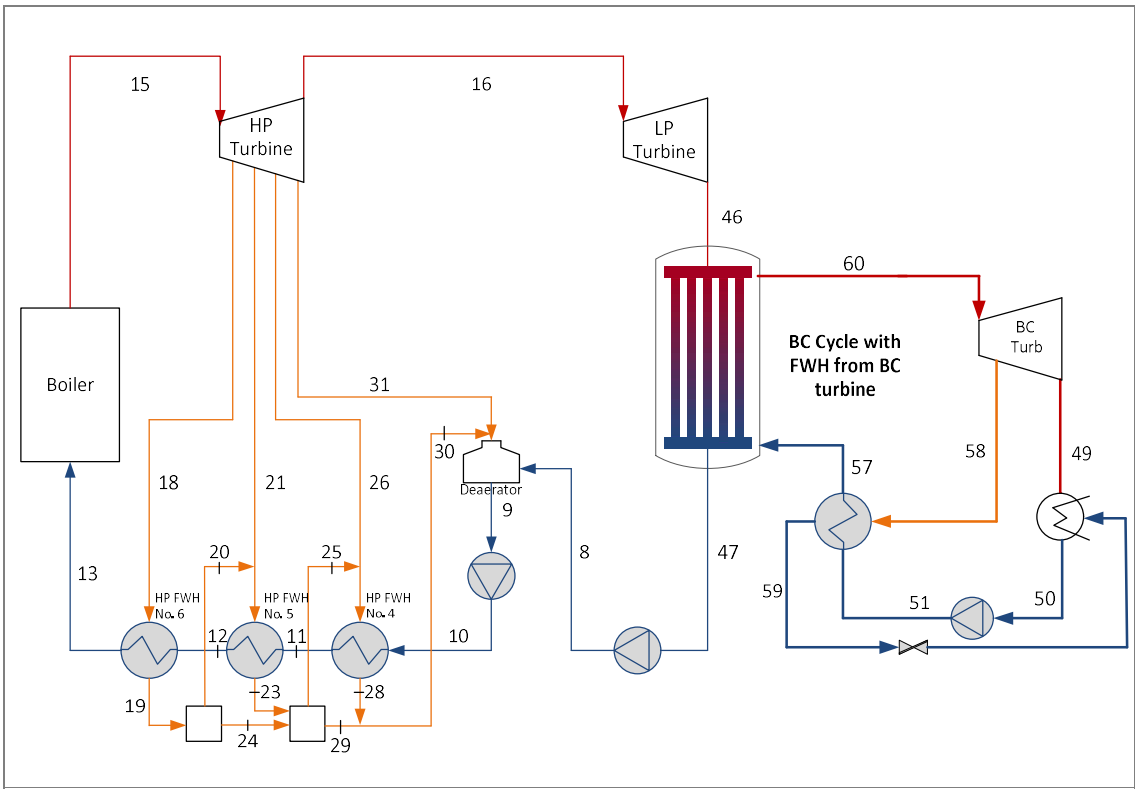

Figure 3.25: A BC cycle with one FWH – BC turbine as the source

For the cycle indicated in Figure 3.25 and for the cycle with more than one FWH in the BC cycle, the nodal information for the steam side will remain as stated in Table 3.3 and Figure 3.5. It is indicated again in this subsection for ease of reference.

Node	Temperature (°C)	Mass flow (kg/s)	Enthalpy (kJ/kg)
8	104.5	103.48	438.5
9	126.1	126.35	529.8
10	127.6	126.35	542.3
11	152.6	126.35	648.9
12	183	126.35	780.9
13	210	126.35	900.5
15	510	126.35	3 418.8
16	126.9	103.06	2 664.7
18	347.3	6.87	3 132.5
19	212.6	6.87	909.4
20		0.42	2 781
21	245.8	7.42	2 948.6
23	185.8	7.83	788.9
24	185.8	6.45	788.9
25		0.91	2 751.6
26	178.1	5.44	2 804
28	155.4	6.35	655.5
29	155.4	13.38	655.5
30	155.4	19.73	655.5
31	165.2	3.14	2796.5
46	104	103.5	2 457
47	104	103.5	436

Table 3.12: The state of each node for the modified system

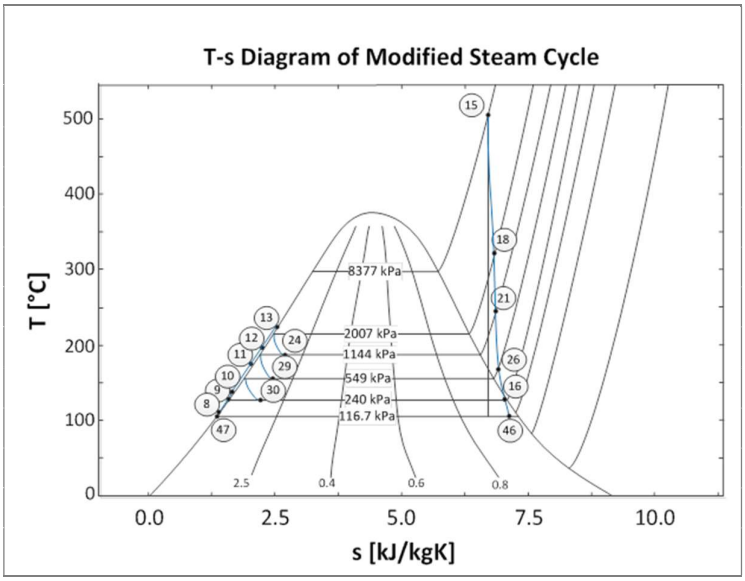

Figure 3.26: T-s diagram of a modified thermal cycle at the Komati Power Station

The nodal information and assumptions for the BC cycle, which includes FWHs, are indicated in Table 3.13 for scenarios 1 and 2.

Scenario 1			Scenario 2		
Node	**Temperature (°C)**	**Assumption**	**Node**	**Temperature (°C)**	**Assumption**
60	100	$s_{48} = s_{49,i}$ $P_{48}@(T_{48},s_{48})$ [kPa] $h_{48,i}@(T_{48},s_{48,i})$ [kJ/kg][10]	**60**	100	$x_{60}=1$ P_{60} = Sat. P@T_{60} [kPa] $h_{60}@(P_{60},x_{60})$ [kJ/kg]
49	36	$x_{49}=0.9$ P_{49} = Sat.P @T_{49} [kPa] $h_{49}@(T_{49},x_{49})$ [kJ/kg]	**49**	36	$s_{49,i}=s_{61}$ $P_{49} = P_{50}$ $h_{49,i}@(P_{49},s_{49,i})$[5] $x_{49}@(P_{49},s_{49})$
50	36	$x_{50}=0$ $P_{50} = P_{49}$ $h_{50}@(T_{50},x_{50})$ [kJ/kg] $v_{50}@(T_{50},x_{50})$ [m^3/kg]	**50**	36	$x_{50}=0$ P_{50} = Sat.P @T_{50} [kPa] $h_{50}@(T_{50},x_{50})$ [kJ/kg]
51	f(assump.)	$P_{51} = P_{48}$ $v_{51}=v_{50}$ (incompressible liquid and small temperature difference) $h_{51} = \left(\frac{1}{\eta_p} v_{51}[P_{51} - P_{50}]\right) + h_{50}$	**51**	f(assump.)	$s_{51,i}=s_{50}$ $P_{51}=P_{61}$ $h_{51,i}@(P_{51},s_{51,i})$[5]
57	$T_{57}=T_{59}$ [11]	$P_{57}=P_{51}$ $h_{57}@(T_{57},P_{57})$ [kJ/kg]	**57**	$T_{57}=T_{59}$ [6]	$P_{57}=P_{51}$ $h_{57}@(T_{57},P_{57})$ [kJ/kg]
58	f(assump.)	$P_{58}=P_{guess}$ ($P_{60}<P_{58}<P_{49}$) $s_{58,i}=s_{60}$[5] $h_{58}@(s_{58},P_{58})$ [kJ/kg]	**58**	f(assump.)	$P_{58}=P_{guess}$ $P_{58}=P_{guess}$ ($P_{60}<P_{58}<P_{49}$) $s_{58,i}=s_{60}$[5] $h_{58}@(s_{58},P_{58})$ [kJ/kg]
59	$T_{59}=T_{sat}@P_{59}$	$x_{59}=0$ $P_{59}=P_{58}$ $h_{59}@(x_{59},P_{59})$ [kJ/kg]	**59**	$T_{59}=T_{sat}@P_{59}$	$x_{59}=0$ $P_{59}=P_{58}$ $h_{59}@(x_{59},P_{59})$ [kJ/kg]

Table 3.13: The state of each node for the BC cycle, with one FWH, for scenarios 1 and 2, and the assumptions made

Due to the fact that the properties of the working fluids, tested in the mentioned configuration, were not such dominant factors in the design of the cycle, there will be no mention of the working fluids tested for this configuration and the configurations mentioned henceforth. All the working fluids tested are listed in Appendix B, Table B1.

Equations, 3.2, 3.5, 3.6 and 3.15 to 3.18 are used to analyse the steam cycle, along with the following formulae, adapted and used for the BC cycle with one FWH for scenarios 1 and 2.

[10] A turbine and pump efficiency is applied in the calculations to compensate for the ideal conditions assumed at nodes 60, 49, 51 and 58.
[11] (Sonntag, et al., 2003)

$$\eta_{th,with\ BC} = \frac{\dot{W}_{total}}{\dot{Q}_{boiler}} \quad \textbf{(3.31)}$$

$$\dot{W}_{total} = \dot{W}_{HP,t} + \dot{W}_{LP,t} + \dot{W}_{P,cond} + \dot{W}_{P,boil} + \dot{W}_{BC,t} + \dot{W}_{BC,p} \quad \text{[kW]} \quad \textbf{(3.32)}$$

$$\dot{W}_{BC,t} = \eta_t[\dot{m}_{BC}h_{60} - \dot{m}_{58}h_{58} - (\dot{m}_{BC} - \dot{m}_{58})h_{49}] \quad \text{[kW]} \quad \textbf{(3.33)}$$

$$\dot{m}_{BC} = \dot{m}_{47}\left(\frac{h_{46}-h_{47}}{h_{60}-h_{57}}\right) \quad \text{[kg/s]} \quad \textbf{(3.34)}$$

$$\dot{m}_{58} = \dot{m}_{BC}\left(\frac{h_{57}-h_{51}}{h_{58}-h_{59}}\right) \quad \text{[kg/s]} \quad \textbf{(3.35)}$$

It can be seen in Equation 3.35 and Table 3.13 that the tap-off mass flow rate is a function of the tap-off pressure. As discussed in Section 3.3.5, an optimum mass flow rate and related tap-off pressure would have been determined for a specific working fluid tested in this configuration with either Scenario 1 or Scenario 2.

The configuration was also tested with more than one FWH implemented in the BC cycle. Figure 3.27 indicates the theoretical cycle where more than one FWH is implemented in the BC cycle. The steam cycle for this configuration will remain as indicated in Figure 3.26 and Table 3.12.

The second FWH is implemented either between the BC pump and the first FWH, i.e. between node 51 and the first FWH or between the first FWH and the BC, i.e. between node 57 and the BC. In this section, the second FWH was implemented between the BC pump and the first FWH. The optimum tap-off pressure for the first FWH was already determined for each working fluid. One can therefore assume that the first FWH's operating conditions will remain at the optimum tap-off pressure. The optimum operating conditions should therefore be found for the second FWH. The process indicated above is again implemented to obtain the optimum efficiency of the cycle with the second FWH, with the tap-off pressure for the second FWH to be between the tap-off pressure of the first FWH and the condensation pressure, i.e. P_{58} and P_{49}.

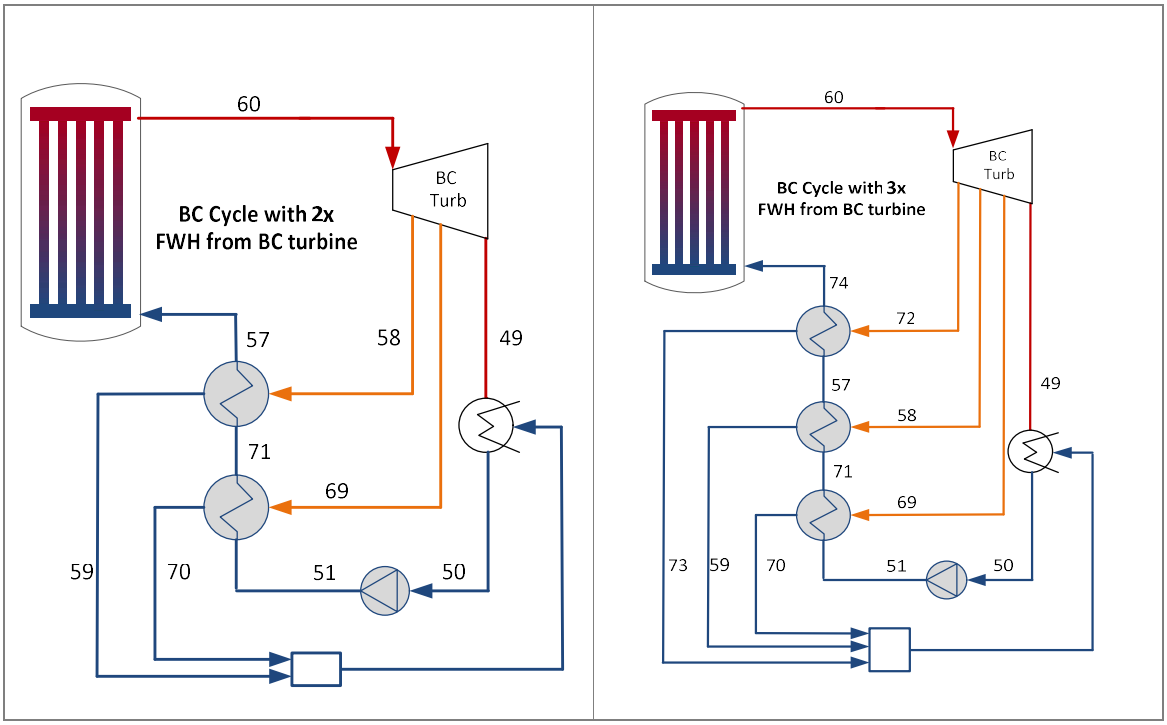

Figure 3.27: BC cycle with two and three FWHs

Each additional FWH will increase the thermal efficiency of the cycle. However, a play-off will have to be made between efficiency increase and the cost of additional FWHs (Sonntag, et al., 2003). This study limited the number of FWHs to three. The T-s diagrams of the BC cycle with two and three FWHs are indicated in Figure 3.28. The tap-off pressure range and tap-off pressures to the FWHs are unique to each working fluid used in the BC cycle. Table 3.14 indicates the nodal information and assumptions for the configuration where two FWHs are used.

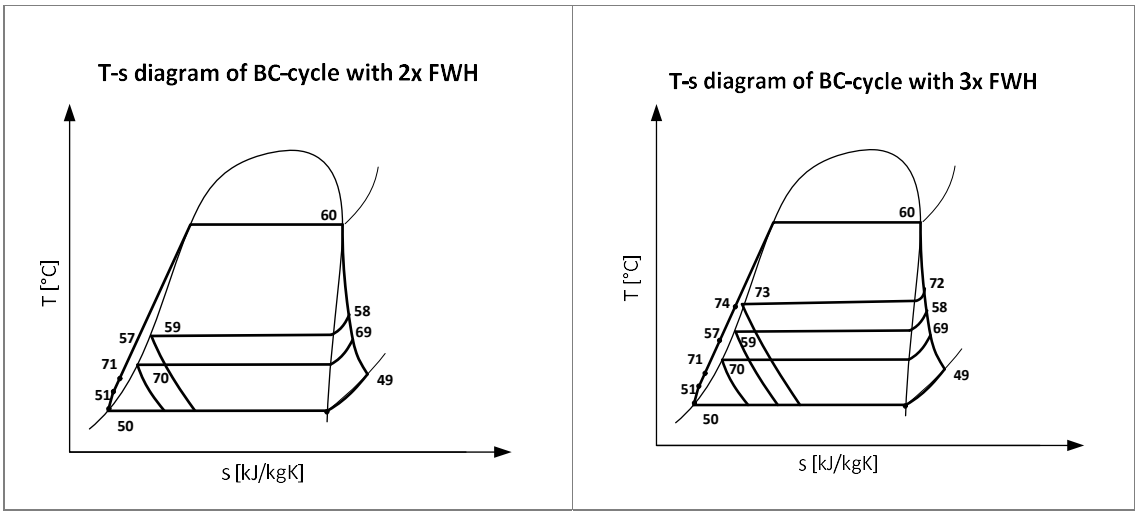

Figure 3.28: T-s diagrams of BC cycles with two and three FWHs

Scenario 1			Scenario 2		
Node	**Temperature (°C)**	**Assumption**	**Node**	**Temperature (°C)**	**Assumption**
60	100	$s_{48} = s_{49,i}$ P_{48}@(T_{48},s_{48}) [kPa] $h_{48,i}$@(T_{48},$s_{48,i}$) [kJ/kg][12]	**60**	100	x_{60}=1 P_{60} = Sat. P@T_{60} [kPa] h_{60}@(P_{60},x_{60}) [kJ/kg]
49	36	x_{49}=0.9 P_{49} = Sat.P @T_{49} [kPa] h_{49}@(T_{49},x_{49}) [kJ/kg]	**49**	36	$s_{49,i}$=s_{61} P_{49} = P_{50} $h_{49,i}$@(P_{49},$s_{49,i}$)[7] x_{49}@(P_{49},s_{49})
50	36	x_{50}=0 P_{50} = P_{49} h_{50}@(T_{50},x_{50}) [kJ/kg] v_{50}@(T_{50},x_{50}) [m^3/kg]	**50**	36	x_{50}=0 P_{50} = Sat.P @T_{50} [kPa] h_{50}@(T_{50},x_{50}) [kJ/kg]
51	f(assump.)	P_{51} = P_{48} v_{51}=v_{50} (incompressible liquid and small temperature difference) $h_{51} = \left(\frac{1}{\eta_p} v_{51}[P_{51} - P_{50}]\right) + h_{50}$	**51**	f(assump.)	$s_{51,i}$=s_{50} P_{51}=P_{61} $h_{51,i}$@(P_{51},$s_{51,i}$)[7]
57	T_{57}=T_{59} [13]	P_{57}=P_{51} h_{57}@(T_{57},P_{57}) [kJ/kg]	**57**	T_{57}=T_{59} [8]	P_{57}=P_{51} h_{57}@(T_{57},P_{57}) [kJ/kg]
58	f(assump.)	P_{58}@opt eff of 1x FWH $s_{58,i}$=s_{60}[7] h_{58}@(s_{58},P_{58}) [kJ/kg]	**58**	f(assump.)	P_{58}@opt eff of 1x FWH $s_{58,i}$=s_{60}[7] h_{58}@(s_{58},P_{58}) [kJ/kg]
59	T_{59}=T_{sat}@P_{59}	x_{59}=0 P_{59}=P_{58} h_{59}@(x_{59},P_{59}) [kJ/kg]	**59**	T_{59}=T_{sat}@P_{59}	x_{59}=0 P_{59}=P_{58} h_{59}@(x_{59},P_{59}) [kJ/kg]
69	f(assump.)	P_{69}=P_{guess} (P_{49}<P_{69}<P_{58}) $s_{69,i}$=s_{60}[7] h_{69}@(s_{69},P_{69}) [kJ/kg]	**69**	f(assump.)	P_{69}=P_{guess} (P_{49}<P_{69}<P_{58}) $s_{69,i}$=s_{60}[7] h_{69}@(s_{69},P_{69}) [kJ/kg]
70	T_{59}=T_{sat}@P_{59}	x_{70}=0 P_{70}=P_{69} h_{70}@(x_{70},P_{70}) [kJ/kg]	**70**	T_{59}=T_{sat}@P_{59}	x_{70}=0 P_{70}=P_{69} h_{70}@(x_{70},P_{70}) [kJ/kg]
71	T_{71}=T_{70}	P_{71}=P_{51} h_{71}@(T_{71},P_{71}) [kJ/kg]	**71**	T_{71}=T_{70}	P_{71}=P_{51} h_{71}@(T_{71},P_{71}) [kJ/kg]

Table 3.14: The state of each node for the BC cycle, with two FWHs for scenarios 1 and 2, and the assumptions made

Equations 3.2, 3.5, 3.6, 3.15 to 3.18 and 3.31 to 3.35 are used to analyse the steam and BC cycle, along with the following formulae, adapted and used for the BC cycle with two FWHs for scenarios 1 and 2.

[12] A turbine and pump efficiency is applied in the calculations to compensate for the ideal conditions assumed at nodes 60, 49, 51, 58 and 69.
[13] (Sonntag, et al., 2003)

$$\dot{W}_{BC,t} = \eta_t[\dot{m}_{BC}h_{60-} - \dot{m}_{69}h_{69} - \dot{m}_{58}h_{58} - (\dot{m}_{BC} - \dot{m}_{58} - \dot{m}_{69})h_{49}] \quad \text{[kW]} \quad \textbf{(3.36)}$$

$$\dot{m}_{69} = \dot{m}_{BC}\left(\frac{h_{71}-h_{51}}{h_{69}-h_{70}}\right) \quad \text{[kg/s]} \quad \textbf{(3.37)}$$

When adding a third FWH, the analysis is conducted according to a method similar to that indicated above. The nodal information and assumptions for a configuration with three FWHs are indicated in Table 3.15.

Scenario 1			Scenario 2		
Node	**Temperature (°C)**	**Assumption**	**Node**	**Temperature (°C)**	**Assumption**
60	100	$s_{48} = s_{49,i}$ P_{48}@(T_{48},s_{48}) [kPa] $h_{48,i}$@(T_{48},$s_{48,i}$) [kJ/kg][14]	**60**	100	x_{60}=1 P_{60} = Sat. P@T_{60} [kPa] h_{60}@(P_{60},x_{60}) [kJ/kg]
49	36	x_{49}=0.9 P_{49} = Sat.P @T_{49} [kPa] h_{49}@(T_{49},x_{49}) [kJ/kg]	**49**	36	$s_{49,i}$=s_{61} P_{49} = P_{50} $h_{49,i}$@(P_{49},$s_{49,i}$)[9] x_{49}@(P_{49},s_{49})
50	36	x_{50}=0 P_{50} = P_{49} h_{50}@(T_{50},x_{50}) [kJ/kg] v_{50}@(T_{50},x_{50}) [m^3/kg]	**50**	36	x_{50}=0 P_{50} = Sat.P @T_{50} [kPa] h_{50}@(T_{50},x_{50}) [kJ/kg]
51	f(assump.)	P_{51} = P_{48} v_{51}=v_{50} (incompressible liquid and small temperature difference) $h_{51} = \left(\frac{1}{\eta_p} v_{51}[P_{51} - P_{50}]\right) + h_{50}$	**51**	f(assump.)	$s_{51,i}$=s_{50} P_{51}=P_{61} $h_{51,i}$@(P_{51},$s_{51,i}$)[9]
57	T_{57}=T_{59} [15]	P_{57}=P_{51} h_{57}@(T_{57},P_{57}) [kJ/kg]	**57**	T_{57}=T_{59} [10]	P_{57}=P_{51} h_{57}@(T_{57},P_{57}) [kJ/kg]
58	f(assump.)	P_{58}@opt eff of 1x FWH $s_{58,i}$=s_{60}[9] h_{58}@(s_{58},P_{58}) [kJ/kg]	**58**	f(assump.)	P_{58}@opt eff of 1x FWH $s_{58,i}$=s_{60}[9] h_{58}@(s_{58},P_{58}) [kJ/kg]
59	T_{59}=T_{sat}@P_{59}	x_{59}=0 P_{59}=P_{58} h_{59}@(x_{59},P_{59}) [kJ/kg]	**59**	T_{59}=T_{sat}@P_{59}	x_{59}=0 P_{59}=P_{58} h_{59}@(x_{59},P_{59}) [kJ/kg]
69	f(assump.)	P_{69}@opt eff of 2x FWH $s_{69,i}$=s_{60}[9] h_{69}@(s_{69},P_{69}) [kJ/kg]	**69**	f(assump.)	P_{69}@opt eff of 2x FWH $s_{69,i}$=s_{60}[9] h_{69}@(s_{69},P_{69}) [kJ/kg]
70	T_{59}=T_{sat}@P_{59}	x_{70}=0 P_{70}=P_{69} h_{70}@(x_{70},P_{70}) [kJ/kg]	**70**	T_{59}=T_{sat}@P_{59}	x_{70}=0 P_{70}=P_{69} h_{70}@(x_{70},P_{70}) [kJ/kg]
71	T_{71}=T_{70}	P_{71}=P_{51} h_{71}@(T_{71},P_{71}) [kJ/kg]	**71**	T_{71}=T_{70}	P_{71}=P_{51} h_{71}@(T_{71},P_{71}) [kJ/kg]
72	f(assump.)	P_{72}=P_{guess} (P_{58}<P_{72}<P_{60}) $s_{72,i}$=s_{60}[9] h_{72}@(s_{72},P_{72}) [kJ/kg]	**72**	f(assump.)	P_{72}=P_{guess} (P_{58}<P_{72}<P_{60}) $s_{72,i}$=s_{60}[9] h_{72}@(s_{72},P_{72}) [kJ/kg]
73	T_{73}=T_{sat}@P_{73}	x_{73}=0 P_{73}=P_{72} h_{73}@(x_{73},P_{73}) [kJ/kg]	**73**	T_{73}=T_{sat}@P_{73}	x_{73}=0 P_{73}=P_{72} h_{73}@(x_{73},P_{73}) [kJ/kg]
74	T_{74}=T_{73}	P_{74}=P_{51} h_{74}@(T_{74},P_{74}) [kJ/kg]	**74**	T_{74}=T_{73}	P_{74}=P_{51} h_{74}@(T_{74},P_{74}) [kJ/kg]

Table 3.15: The state of each node for the BC cycle with three FWHs for scenarios 1 and 2, and the assumptions made

[14] A turbine and pump efficiency is applied in the calculations to compensate for the ideal conditions assumed at nodes 60, 49, 51, 58, 69 and 72.
[15] (Sonntag, et al., 2003)

Equations, 3.2, 3.5, 3.6, 3.15 to 3.18 and 3.31 to 3.36 are used to analyse the steam and BC cycle, along with the following formula, adapted and used for the BC cycle with three FWHs for scenarios 1 and 2.

$$\dot{W}_{BC,t} = \eta_t[\dot{m}_{BC}h_{60} - \dot{m}_{72}h_{72} - \dot{m}_{58}h_{58} - \dot{m}_{69}h_{69} - (\dot{m}_{BC} - \dot{m}_{58} - \dot{m}_{72} - \dot{m}_{69})h_{49}] \quad \text{[kW]} \quad \textbf{(3.38)}$$

$$\dot{m}_{BC} = \dot{m}_{47}\left(\frac{h_{46}-h_{47}}{h_{60}-h_{57}}\right) \quad \text{[kg/s]} \quad \textbf{(3.39)}$$

$$\dot{m}_{72} = \dot{m}_{BC}\left(\frac{h_{74}-h_{57}}{h_{72}-h_{73}}\right) \quad \text{[kg/s]} \quad \textbf{(3.40)}$$

Theoretically, adding FWHs to scenarios where one has added a heat exchanger with tap-off from the steam cycle was also tested and is discussed in further detail below.

3.3.5.3 BC cycle without low-pressure turbine and FWHs

Combinations of concepts were tested to see whether an even higher increase in thermal efficiency can be obtained. The concept shown in Figure 3.29 indicates a combination of the concept discussed in Section 3.3.3 (a Simple BC cycle without low-pressure turbine) and Section 3.3.5.2 (a BC cycle with FWHs). The concept was tested with one, two and three FWHs, implementing the method described in the mentioned chapters.

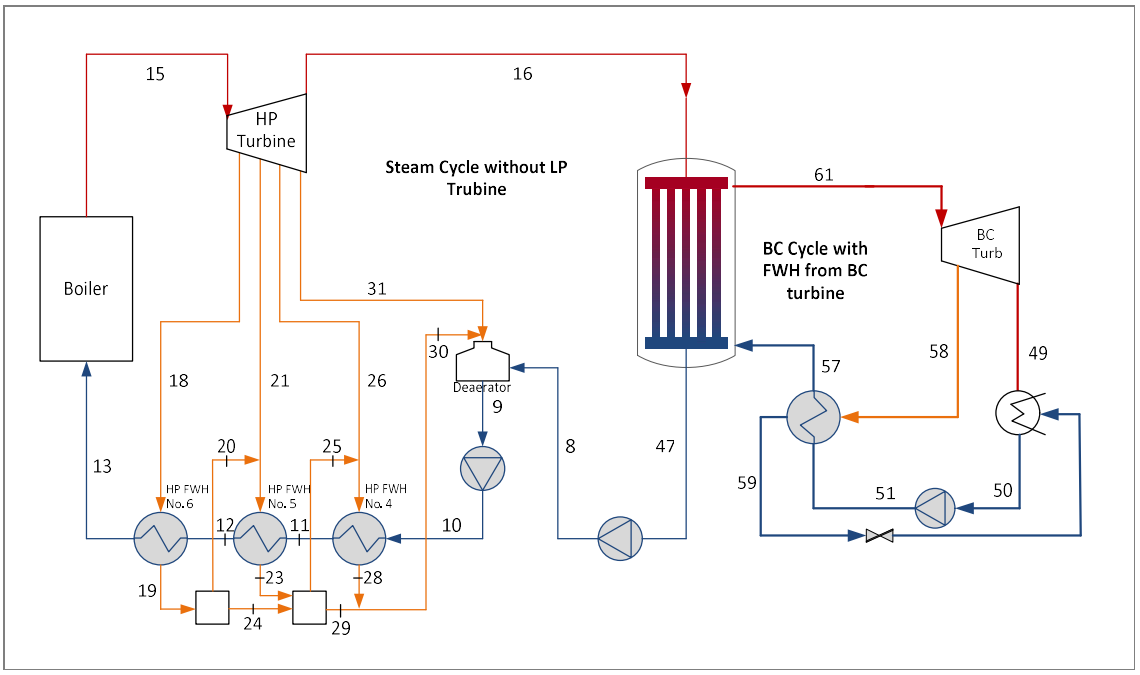

Figure 3.29: Component diagram of the Komati Power Station without a low-pressure turbine, including a BC and one FWH

The cycle's T-s diagram for the steam and BC cycle are similar to that already indicated in Figure 3.10, Figure 3.15 and Figure 3.28, respectively. The nodal information on the steam side will remain as indicated in Table 3.6.

The node information for the BC cycle with one, two and three FWHs, remains exactly as indicated in Table 3.14 and Table 3.15. The node that differs is node 60, which changes to node 61, with information as indicated below in Table 3.16.

Scenario 1			Scenario 2		
Node	**Temperature (°C)**	**Assumption**	**Node**	**Temperature (°C)**	**Assumption**
61	120	$s_{48} = s_{49,i}$ $P_{48}@(T_{48},s_{48})$ [kPa] $h_{48,i}@(T_{48},s_{48,i})$ [kJ/kg][16]	61	120	$x_{60}=1$ P_{60} = Sat. P@T_{60} [kPa] $h_{60}@(P_{60},x_{60})$ [kJ/kg]

Table 3.16: The state of node 61 for the BC cycle without a steam-cycle low-pressure turbine with one, two and three FWHs for scenarios 1 and 2, and the assumptions made

The equations implemented for the analysis have been mentioned in Section 3.3.3 and chapter 3.3.5.2, but are repeated for clarity. These equations will apply for scenarios 1 and 2.

$$\dot{Q}_{boiler} = \dot{m}_{13}\left[h_{13}^{sh,g}(P_{13};T_{13}) - h_{15}^{c,f}(P_{15};T_{15})\right] \quad \text{[kW]} \quad \textbf{(3.41)}$$

$$\dot{W}_{p,boil} = \dot{m}_{9}\left[h_{9}^{sat,f}(P_{9}) - h_{10}^{c,f}(P_{10};T_{10})\right] \quad \text{[kW]} \quad \textbf{(3.42)}$$

$$\dot{W}_{HP,t} = \dot{m}_{15}h_{15}^{sh,g}(P_{15};T_{15}) - \dot{m}_{18}h_{18}^{sh,g}(P_{18};T_{18}) - \dot{m}_{21}h_{21}^{sh,g}(P_{21};T_{21}) - \dot{m}_{26}h_{26}^{sh,g}(P_{26};T_{26}) - \dot{m}_{31}h_{31}^{sh,g}(P_{31};T_{31}) - \dot{m}_{16}h_{16}^{sat,fg}(P_{16};x_{16}) \quad \text{[kW]} \quad \textbf{(3.43)}$$

$$\dot{W}_{p,cond} = \dot{m}_{47}\left[h_{47}^{sat.f}(T_{47}) - h_{8}^{c,f}(P_{8};T_{8})\right] \quad \text{[kW]} \quad \textbf{(3.44)}$$

$$\eta_{th,Carnot} = 1 - \frac{T_L}{T_H} = 1 - \frac{T_{47}}{T_{15}} \quad \textbf{(3.45)}$$

$$\eta_{th,with\ BC} = \frac{\dot{W}_{total}}{\dot{Q}_{boiler}} \quad \textbf{(3.46)}$$

$$\dot{W}_{total} = \dot{W}_{HP,t} + \dot{W}_{P,cond} + \dot{W}_{P,boil} + \dot{W}_{BC,t} + \dot{W}_{BC,p} \quad \text{[kW]} \quad \textbf{(3.47)}$$

For the BC cycle, the following equations are used, depending on whether one, two or three FWHs are implemented.

$$\dot{W}_{BC,p} = \dot{m}_{BC}\left(\frac{1}{\eta_p}\right)(h_{50} - h_{51}) \,/\, \frac{1}{\eta_p}\dot{m}_{BC}v_{50}(P_{50} - P_{51}) \quad \text{[kW]} \quad \textbf{(3.48)}$$

[16] A turbine and pump efficiency is applied in the calculations to compensate for the ideal conditions assumed at node 61.

For one FWH:

$$\dot{W}_{BC,t} = \eta_t[\dot{m}_{BC}h_{61} - \dot{m}_{58}h_{58} - (\dot{m}_{BC} - \dot{m}_{58})h_{49}] \quad \text{[kW]} \quad \textbf{(3.49)}$$

$$\dot{m}_{BC} = \dot{m}_{47}\left(\frac{h_{46}-h_{47}}{h_{61}-h_{57}}\right) \quad \text{[kg/s]} \quad \textbf{(3.50)}$$

$$\dot{m}_{58} = \dot{m}_{BC}\left(\frac{h_{57}-h_{51}}{h_{58}-h_{59}}\right) \quad \text{[kg/s]} \quad \textbf{(3.51)}$$

For two FWHs:

$$\dot{W}_{BC,t} = \eta_t[\dot{m}_{BC}h_{61-} - \dot{m}_{69}h_{69} - \dot{m}_{58}h_{58} - (\dot{m}_{BC} - \dot{m}_{58} - \dot{m}_{69})h_{49}] \quad \text{[kW]} \quad \textbf{(3.52)}$$

$$\dot{m}_{69} = \dot{m}_{BC}\left(\frac{h_{71}-h_{51}}{h_{69}-h_{70}}\right) \quad \text{[kg/s]} \quad \textbf{(3.53)}$$

$$\dot{m}_{BC} = \dot{m}_{47}\left(\frac{h_{46}-h_{47}}{h_{61}-h_{57}}\right) \quad \text{[kg/s]} \quad \textbf{(3.54)}$$

For three FWHs:

$$\dot{W}_{BC,t} = \eta_t[\dot{m}_{BC}h_{61} - \dot{m}_{72}h_{72} - \dot{m}_{58}h_{58} - \dot{m}_{69}h_{69} - (\dot{m}_{BC} - \dot{m}_{58} - \dot{m}_{72} - \dot{m}_{69})h_{49}] \quad \text{[kW]} \quad \textbf{(3.55)}$$

$$\dot{m}_{BC} = \dot{m}_{47}\left(\frac{h_{46}-h_{47}}{h_{61}-h_{57}}\right) \quad \text{[kg/s]} \quad \textbf{(3.56)}$$

$$\dot{m}_{72} = \dot{m}_{BC}\left(\frac{h_{74}-h_{57}}{h_{72}-h_{73}}\right) \quad \text{[kg/s]} \quad \textbf{(3.57)}$$

3.3.5.4 BC cycle with tap-off from a low-pressure turbine and FWHs

This section will cover the method followed to evaluate the performance of the theoretical cycle, where the BC cycle is implemented with a heat exchanger with tap-off from the low-pressure turbine. The cycle was also analysed where FWHs were added to the BC cycle.

3.3.5.4.1 BC cycle with tap-off from a low-pressure turbine

The concept where a heat exchanger is theoretically included in the BC cycle, where steam is fed into the heat exchanger from the low-pressure turbine, is indicated in Figure 3.30. The concept indicates steam being tapped off from the low-pressure turbine at a certain pressure, which is obtained via the simulation that is discussed below, and feeds into a heat exchanger that is positioned in the BC cycle. The steam enters at node 53 and releases heat to the working fluid in the BC cycle. The steam then leaves the heat exchanger as saturated liquid water at the tap-off pressure at node 56. The saturated liquid water then enters the BC to leave at node 47. Similarly, the working fluid enters the heat exchanger at node 48, under the conditions described previously in the chapter, absorbs the heat and enters the BC turbine at an elevated temperature, where T_{52} is assumed to be a couple of degrees lower than T_{56}.

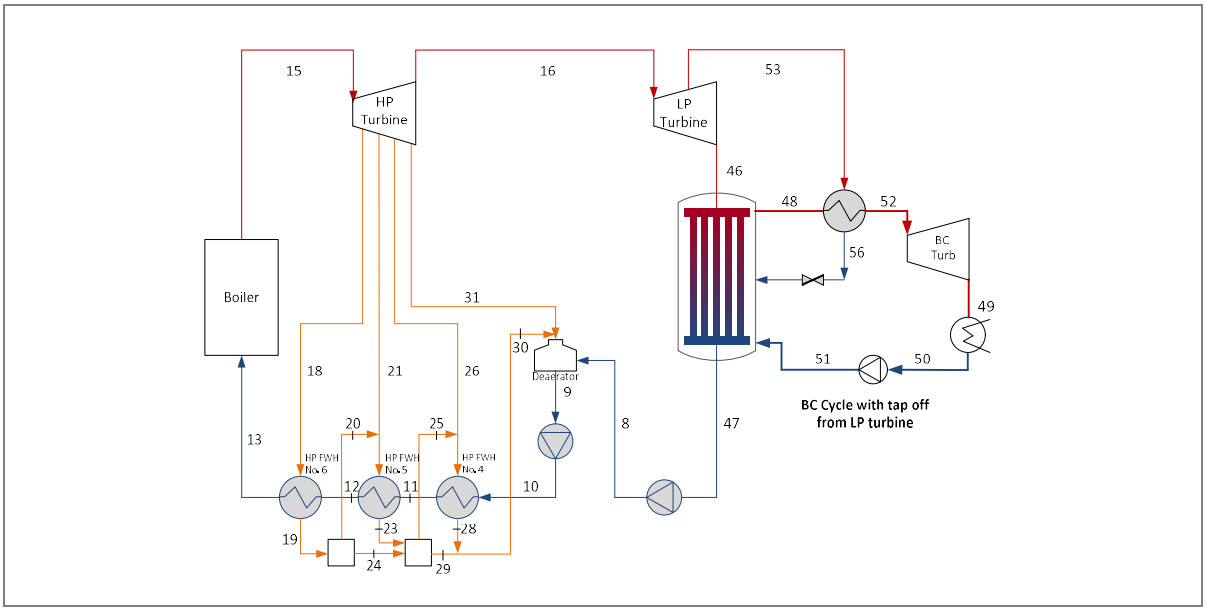

Figure 3.30: Component diagram of the Komati Power Station with tap-off from a low-pressure turbine into the BC cycle

The steam cycle's nodal information and the T-s diagram are similar to that explained in Section 3.3.5. However, the tap-off from the low-pressure turbine affects the steam side's mass flow rates as the mass flow rates are a function of the tap-off pressure and the BC cycle's working fluid properties. Table 3.17 and Figure 3.31 indicate the steam cycle nodal properties related to Figure 3.30. Note that the tap-off pressure, P_{53}, was chosen from a pressure range between P_{16} and P_{46}. For each tap-off pressure, a corresponding tap-off mass flow rate was calculated.

Node	Temperature (°C)	Mass flow (kg/s)	Enthalpy (kJ/kg)
8	104.5	103.48	438.5
9	126.1	126.35	529.8
10	127.6	126.35	542.3
11	152.6	126.35	648.9
12	183	126.35	780.9
13	210	126.35	900.5
15	510	126.35	3 418.8
16	126.9	103.06	2 664.7
18	347.3	6.87	3 132.5
19	212.6	6.87	909.4
20		0.42	2 781
21	245.8	7.42	2 948.6
23	185.8	7.83	788.9
24	185.8	6.45	788.9
25		0.91	2 751.6
26	178.1	5.44	2 804
28	155.4	6.35	655.5
29	155.4	13.38	655.5
30	155.4	19.73	655.5
31	165.2	3.14	2 796.5
46	104	[17]	2 457
47	104	[12]	436
53	$T_{53}@(s_{53},P_{53})$[18]	[12]	$h_{53}@(s_{53},P_{53})$[13]
56	$T_{56}=T_{sat}@(P_{56}=P_{53})$	[12]	$h_{56}@h_f@P_{56}$

Table 3.17: The state of each node for the steam cycle with tap-off from a low-pressure turbine

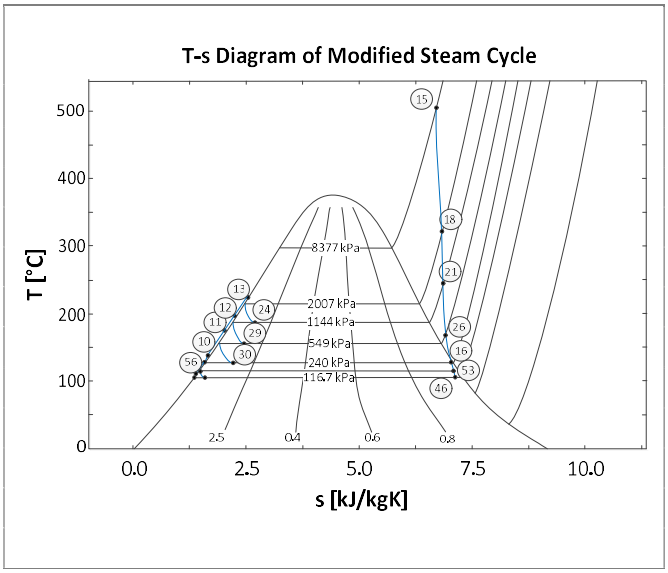

Figure 3.31: T-s diagram of a steam cycle at the Komati Power Station – with tap-off from a low-pressure turbine

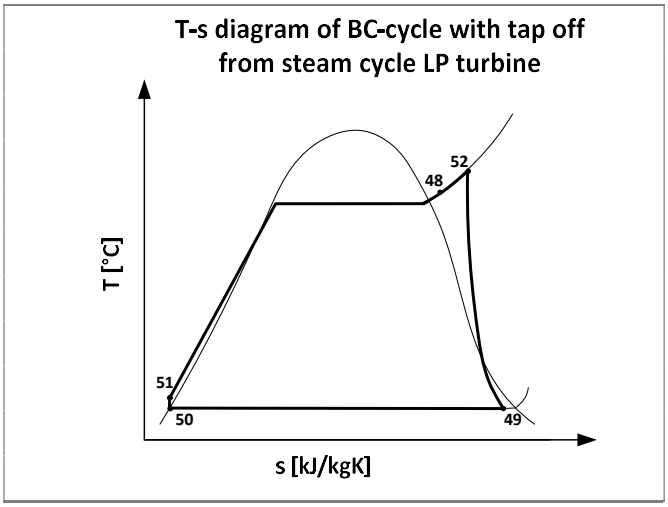

Figure 3.32: T-s diagrams of the BC cycle with tap-off from a low-pressure steam turbine

Including a heat exchanger in the BC cycle, with tap-off from the steam side, should increase the temperature of the working fluid in the BC cycle from T_{48} to T_{52}, further into the superheated region, before entering the turbine. Consequently, the work of the BC cycle turbine will increase. Depending on the properties of the working fluid, this configuration could increase the thermal efficiency of the cycle.

[17] The mass flow rates of these nodes are a function of the tap-off pressure and working fluid properties. Consequently, it differs for each scenario. See equations related to this configuration for further information.
[18] P_{53} was chosen such that $P_{43} < P_{53} < P_{16}$. Under ideal conditions, the entropy at node 53 was assumed as follows: $s_{53} = s_{16}$.

Figure 3.32 indicates the T-s diagram of the BC cycle for this configuration. The properties for the BC cycle are indicated in Table 3.18.

Scenario 1			Scenario 2		
Node	**Temperature (°C)**	**Assumption**	**Node**	**Temperature (°C)**	**Assumption**
48	100	$s_{48} = s_{49,i}$ $P_{48}@(T_{48},s_{48})$ [kPa] $h_{48,i}@(T_{48},s_{48,i})$ [kJ/kg][19]	**61**	100	$x_{60}=1$ P_{60} = Sat. P@T_{60} [kPa] $h_{60}@(P_{60},x_{60})$ [kJ/kg]
49	36	$x_{49}=0.9$ P_{49} = Sat.P @T_{49} [kPa] $h_{49}@(T_{49},x_{49})$ [kJ/kg]	**49**	36	$s_{49,i}=s_{61}$ $P_{49} = P_{50}$ $h_{49,i}@(P_{49},s_{49,i})$[14] $x_{49}@(P_{49},s_{49})$
50	36	$x_{50}=0$ $P_{50} = P_{49}$ $h_{50}@(T_{50},x_{50})$ [kJ/kg] $v_{50}@(T_{50},x_{50})$ [m^3/kg]	**50**	36	$x_{50}=0$ P_{50} = Sat.P @T_{50} [kPa] $h_{50}@(T_{50},x_{50})$ [kJ/kg]
51	f(assump.)	$P_{51} = P_{48}$ $v_{51}=v_{50}$ (incompressible liquid and small temperature difference) $h_{51} = \left(\frac{1}{\eta_p} v_{51}[P_{51} - P_{50}]\right) + h_{50}$	**51**	f(assump.)	$s_{51,i}=s_{50}$ $P_{51}=P_{61}$ $h_{51,i}@(P_{51},s_{51,i})$[14]
52	$T_{52}=T_{56}$ -10 [20]	$P_{52}=P_{51}$ $h_{52}@(T_{52},P_{52})$ [kJ/kg]	**52**	$T_{52}=T_{56}$ -10 [15]	$P_{52}=P_{51}$ $h_{52}@(T_{52},P_{52})$ [kJ/kg]

Table 3.18: The state of each node of the BC cycle, with tap-off from the steam-side low-pressure turbine for scenario 1 and 2, and the assumptions made

The equations used to analyse this cycle are repeated below for the sake of convenience, along with additional equations required for the analysis of the modification.

The equations for the complete cycle required to determine the thermal efficiency of the cycle are as follows:

$$\eta_{th,with\ BC} = \frac{\dot{W}_{total}}{\dot{Q}_{boiler}} \quad \textbf{(3.58)}$$

$$\eta_{th,fuel} = \frac{\dot{W}_{total}}{\dot{Q}_{in}} \quad \textbf{(3.59)}$$

$$\eta_{th,Carnot} = 1 - \frac{T_L}{T_H} = 1 - \frac{T_{50}}{T_{15}} \quad \textbf{(3.60)}$$

$$\dot{W}_{total} = \dot{W}_{HP,t} + \dot{W}_{LP,t} + \dot{W}_{P,cond} + \dot{W}_{P,boil} + \dot{W}_{BC,t} + \dot{W}_{BC,p} \quad [\text{kW}] \quad \textbf{(3.61)}$$

[19] A turbine and pump efficiency is applied in the calculations to compensate for the ideal conditions assumed at nodes 48, 49 and 51.
[20] The outlet temperature of the heat exchanger on the BC side is assumed to be slightly lower than the outlet temperature of the heat exchanger on the steam side (Cengel, 2006).

The equations related to the steam cycle are as follows:

$$\dot{Q}_{boiler} = \dot{m}_{13}\left[h_{13}^{sh,g}(P_{13};T_{13}) - h_{15}^{c,f}(P_{15};T_{15})\right] \quad \text{[kW]} \quad \textbf{(3.62)}$$

$$\dot{W}_{p,boil} = \dot{m}_{9}\left[h_{9}^{sat,f}(P_{9}) - h_{10}^{c,f}(P_{10};T_{10})\right] \quad \text{[kW]} \quad \textbf{(3.63)}$$

$$\dot{W}_{HP,t} = \dot{m}_{15}h_{15}^{sh,g}(P_{15};T_{15}) - \dot{m}_{18}h_{18}^{sh,g}(P_{18};T_{18}) - \dot{m}_{21}h_{21}^{sh,g}(P_{21};T_{21}) - \dot{m}_{26}h_{26}^{sh,g}(P_{26};T_{26}) - \dot{m}_{31}h_{31}^{sh,g}(P_{31};T_{31}) - \dot{m}_{16}h_{16}^{sat,fg}(P_{16};x_{16}) \quad \text{[kW]} \quad \textbf{(3.64)}$$

$$\dot{W}_{p,cond} = \dot{m}_{47}\left[h_{47}^{sat.f}(T_{47}) - h_{8}^{c,f}(P_{8};T_{8})\right] \quad \text{[kW]} \quad \textbf{(3.65)}$$

$$\dot{W}_{LP,t} = \dot{m}_{16}h_{16}^{sat,fg}(P_{16};x_{16}) - \dot{m}_{53}h_{53}^{sh,g}(P_{53};s_{53}) - \dot{m}_{46}h_{46}^{sat,fg}(P_{46};x_{46}) \quad \text{[kW]} \quad \textbf{(3.66)}$$

Equations related to the BC cycle are as follows:

$$\dot{W}_{BC,t} = \dot{m}_{BC}\eta_{t}(h_{52} - h_{49}) \quad \text{[kW]} \quad \textbf{(3.67)}$$

$$\dot{W}_{BC,p} = \dot{m}_{BC}\left(\frac{1}{\eta_p}\right)(h_{50} - h_{51}) \,/\, \frac{1}{\eta_p}\dot{m}_{BC}v_{50}(P_{50} - P_{51}) \quad \text{[kW]} \quad \textbf{(3.68)}$$

$$\dot{m}_{BC} = \frac{\dot{m}_{16}(h_{46} - h_{47}) + \dot{m}_{53}(h_{57} - h_{46})}{h_{48} - h_{51}} \quad \text{[kg/s]} \quad \textbf{(3.69)}$$

$$\dot{m}_{53} = \frac{\dot{m}_{BC}(h_{52} - h_{48/61})}{h_{53} - h_{56}} \quad \text{[kg/s]} \quad \textbf{(3.70)}$$

In Chapter 4, it is evident that an optimum tap-off mass flow rate is obtained for each working fluid, where the thermal efficiency for this configuration reaches a maximum, as explained briefly in Section 3.3.5 and Figure 3.24.

3.3.5.4.2 Tap-off from low-pressure turbine and FWHs

An increase in thermal efficiency is expected for the cycle with tap-off from the low-pressure steam turbine, as discussed in Section 3.3.5.4.1, where it can be seen that a certain tap-off mass flow rate from the low-pressure turbine corresponds to the maximum thermal efficiency of the cycle, which relates to the specific tap-off pressure of node 53. The addition of FWHs should increase the thermal efficiency of the cycle as well. In the section that follows, FWHs are added to the theoretical configuration indicated in Figure 3.30.

Figure 3.33 indicates this theoretical configuration. The steam cycle's properties will remain as indicated in Section 3.3.5.4.1 and Table 3.17. The tap-off pressure from the steam cycle, P_{53}, is fixed in this section at the tap-off pressure where maximum thermal efficiency was achieved for the specific working fluid.

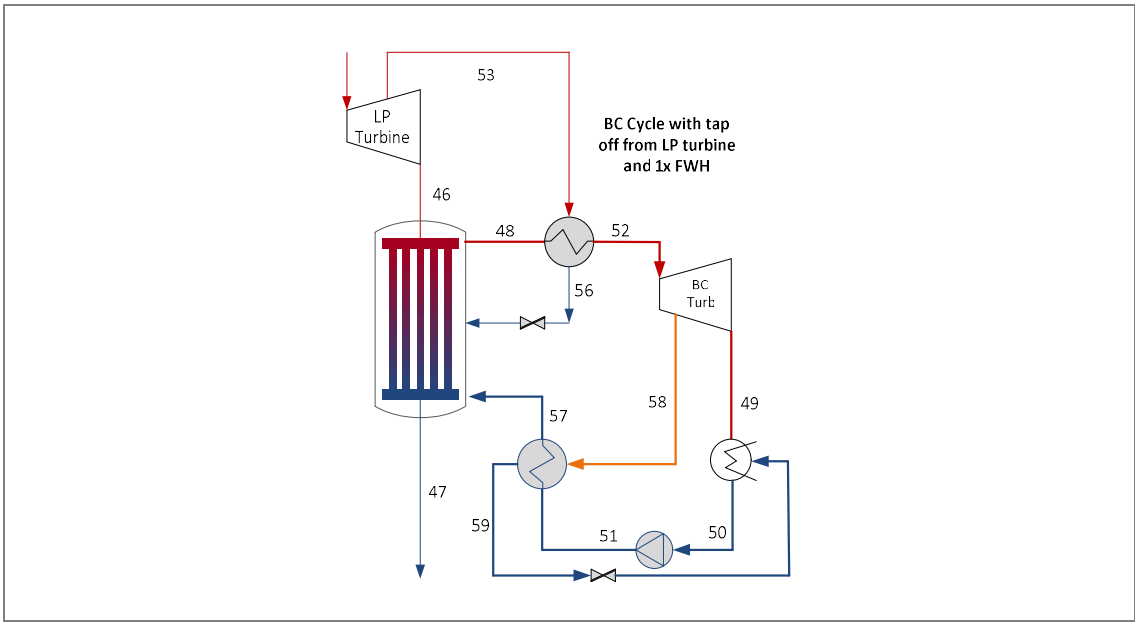

Figure 3.33: Component diagram of the Komati Power Station with tap-off from a low-pressure turbine into the BC cycle and BC cycle FWH

The BC cycle side, for this configuration, is analysed as indicated in Section 3.3.5.2. The main difference is that the inlet temperature of the BC turbine is higher for this configuration. Consequently, the FWH tap-off pressure range ($P_{49} < P_{58} < P_{52}$) is larger and is again a function of the properties of the working fluid. The properties at each node of the BC cycle are indicated in Table 3.19. The assumptions made for each node are also indicated in this table.

This configuration was tested with only one FWH because the results of the cycle without a FWH, as indicated in Section 3.3.5.4.1, did not heed a very large increase in thermal efficiency. Consequently, the theoretical cycle, a BC cycle with tap-off from a low-pressure turbine, including two or more FWHs, is not expected to have a significant increase in thermal efficiency. However, for illustrative purposes, the cycle was tested with one FWH.

Scenario 1			Scenario 2		
Node	**Temperature (°C)**	**Assumption**	**Node**	**Temperature (°C)**	**Assumption**
48	100	$s_{48} = s_{49,i}$ $P_{48}@(T_{48},s_{48})$ [kPa] $h_{48,i}@(T_{48},s_{48,i})$ [kJ/kg][21]	**61**	100	$x_{60}=1$ P_{60} = Sat. P@T_{60} [kPa] $h_{60}@(P_{60},x_{60})$ [kJ/kg]
49	36	$x_{49}=0.9$ P_{49} = Sat.P @T_{49} [kPa] $h_{49}@(T_{49},x_{49})$ [kJ/kg]	**49**	36	$s_{49,i}=s_{61}$ $P_{49} = P_{50}$ $h_{49,i}@(P_{49},s_{49,i})$[16] $x_{49}@(P_{49},s_{49})$
50	36	$x_{50}=0$ $P_{50} = P_{49}$ $h_{50}@(T_{50},x_{50})$ [kJ/kg] $v_{50}@(T_{50},x_{50})$ [m^3/kg]	**50**	36	$x_{50}=0$ P_{50} = Sat.P @T_{50} [kPa] $h_{50}@(T_{50},x_{50})$ [kJ/kg]
51	f(assump.)	$P_{51} = P_{48}$ $v_{51}=v_{50}$ (incompressible liquid and small temperature difference) $h_{51} = \left(\frac{1}{\eta_p} v_{51}[P_{51} - P_{50}]\right) + h_{50}$	**51**	f(assump.)	$s_{51,i}=s_{50}$ $P_{51}=P_{61}$ $h_{51,i}@(P_{51},s_{51,i})$[16]
52	$T_{52}=T_{56}$ -6 [22]	$P_{52}=P_{51}$ $h_{52}@(T_{52},P_{52})$ [kJ/kg]	**52**	$T_{52}=T_{56}$ -6 [17]	$P_{52}=P_{51}$ $h_{52}@(T_{52},P_{52})$ [kJ/kg]
57	$T_{57}=T_{59}$ [23]	$P_{57}=P_{51}$ $h_{57}@(T_{57},P_{57})$ [kJ/kg]	**57**	$T_{57}=T_{59}$ [18]	$P_{57}=P_{51}$ $h_{57}@(T_{57},P_{57})$ [kJ/kg]
58	f(assump.)	$P_{58}=P_{guess}$ ($P_{52}<P_{58}<P_{49}$) $s_{58,i}=s_{52}$[16] $h_{58}@(s_{58},P_{58})$ [kJ/kg]	**58**	f(assump.)	$P_{58}=P_{guess}$ ($P_{52}<P_{58}<P_{49}$) $s_{58,i}=s_{52}$[16] $h_{58}@(s_{58},P_{58})$ [kJ/kg]
59	$T_{59}=T_{sat}@P_{59}$	$x_{59}=0$ $P_{59}=P_{58}$ $h_{59}@(x_{59},P_{59})$ [kJ/kg]	**59**	$T_{59}=T_{sat}@P_{59}$	$x_{59}=0$ $P_{59}=P_{58}$ $h_{59}@(x_{59},P_{59})$ [kJ/kg]

Table 3.19: The state of each node for the BC cycle, with tap-off from the steam-side low-pressure turbine for scenarios 1 and 2 and FWHs in the BC cycle, including the assumptions made

Equations 3.58 to 3.66, 3.68 and 3.70 indicated in Section 3.3.5.4.1 are also used in the analysis of this cycle. The additional equations below will apply to this configuration with the addition of a FWH.

$$\dot{W}_{BC,t} = \eta_t[\dot{m}_{BC}h_{52} - \dot{m}_{58}h_{58} - (\dot{m}_{BC} - \dot{m}_{58})h_{49}] \quad \text{[kW]} \quad \textbf{(3.71)}$$

$$\dot{m}_{BC} = \frac{\dot{m}_{16}(h_{46}-h_{47})+\dot{m}_{53}(h_{56}-h_{46})}{h_{48}-h_{57}} \quad \text{[kg/s]} \quad \textbf{(3.72)}$$

[21] A turbine and pump efficiency is applied in the calculations to compensate for the ideal conditions assumed at nodes 48, 49, 51 and 58.
[22] The outlet temperature of the heat exchanger on the BC side is assumed to be slightly lower than the outlet temperature of the heat exchanger on the steam side (Cengel, 2006).
[23] (Sonntag, et al., 2003)

$$\dot{m}_{58} = \dot{m}_{BC}\left(\frac{h_{57}-h_{51}}{h_{58}-h_{59}}\right) \quad \text{[kg/s]} \quad \textbf{(3.73)}$$

3.3.5.5 BC cycle with tap-off before low-pressure turbines and FWHs

The configuration was also tested for the theoretical scenario, where, instead of tapping off from the low-pressure turbine on the steam side, tap-off occurred from the steam side's low-pressure inlet. This scenario was tested along with feed water heating in the BC cycle.

3.3.5.5.1 BC cycle with tap-off before low-pressure turbines

The concept where a heat exchanger is theoretically included in the BC cycle, with steam fed into the heat exchanger from the inlet to the low-pressure turbine, is indicated in Figure 3.34. The concept indicates steam being tapped off from the inlet pipe of the low-pressure turbine at the steam low-pressure turbine inlet pressure and temperature. The mass flow rate of the tap-off from the low-pressure inlet is a function of the properties of the working fluid. The steam enters at node 54 and releases heat to the working fluid in the BC cycle. The steam then leaves the heat exchanger as saturated liquid water at the tap-off pressure at node 55. The saturated liquid water then enters the BC to leave at node 47. Similarly, the working fluid enters the heat exchanger at node 48, under the conditions described previously in the chapter, absorbs the heat and enters the BC turbine at an elevated temperature, where T_{52} is assumed to be a couple of degrees lower than T_{55}.

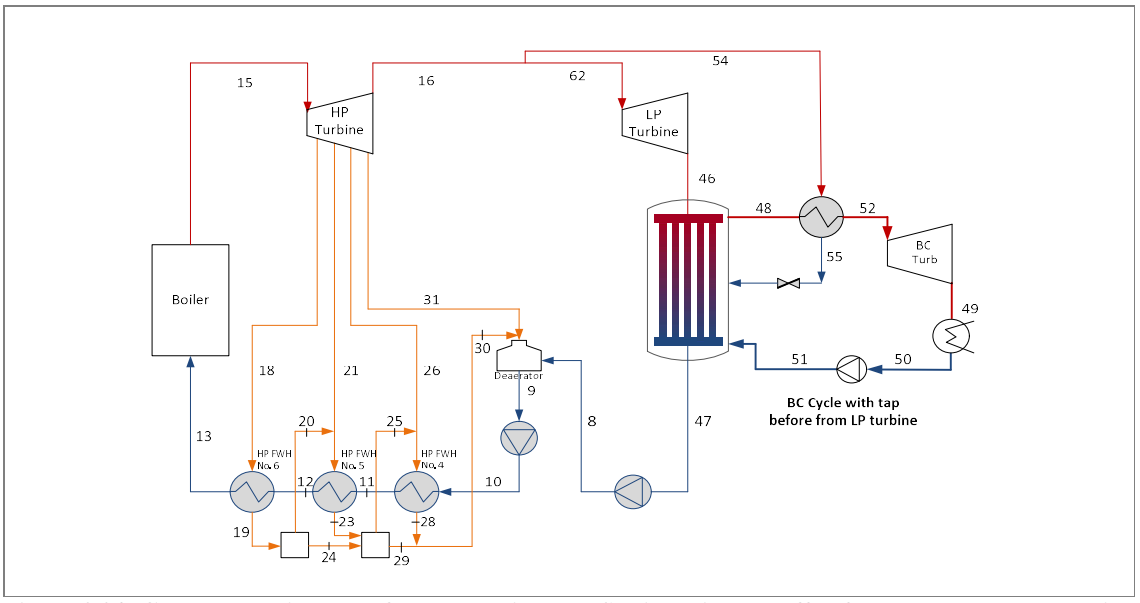

Figure 3.34: Component diagram of the Komati Power Station with tap-off before a low-pressure turbine into the BC cycle

The steam cycle's nodal information and the T-s diagram are similar to that explained in Section 3.3.5. Table 3.17 and Figure 3.31 indicate the steam cycle nodal properties related to

Figure 3.34. Each working fluid tested in the BC cycle will have a corresponding tap-off mass flow rate.

Node	Temperature (°C)	Mass flow (kg/s)	Enthalpy (kJ/kg)
8	104.5	103.48	438.5
9	126.1	126.35	529.8
10	127.6	126.35	542.3
11	152.6	126.35	648.9
12	183	126.35	780.9
13	210	126.35	900.5
15	510	126.35	3 418.8
16	126.9	103.06	2 664.7
18	347.3	6.87	3 132.5
19	212.6	6.87	909.4
20		0.42	2 781
21	245.8	7.42	2 948.6
23	185.8	7.83	788.9
24	185.8	6.45	788.9
25		0.91	2 751.6
26	178.1	5.44	2 804
28	155.4	6.35	655.5
29	155.4	13.38	655.5
30	155.4	19.73	655.5
31	165.2	3.14	2 796.5
46	104	[24]	2 457
47	104	[19]	436
54	$T_{54}=T_{16}$	[19]	$h_{54}=h_{16}$
55	$T_{55}=T_{sat}@(P_{55}=P_{16})$	[19]	$h_{55}=h_f@P_{55}$

Table 3.20: The state of each node for the steam cycle with tap-off before a low-pressure turbine

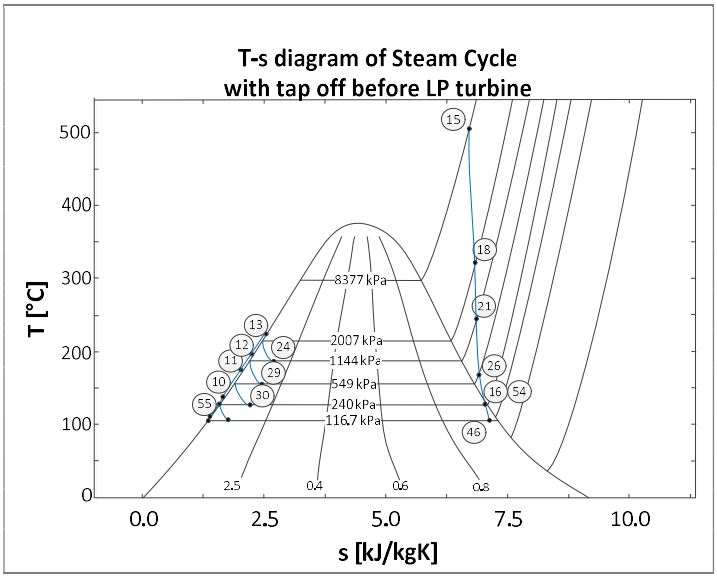

Figure 3.35: T-s diagram of the steam cycle at the Komati Power Station – with tap-off before a low-pressure turbine

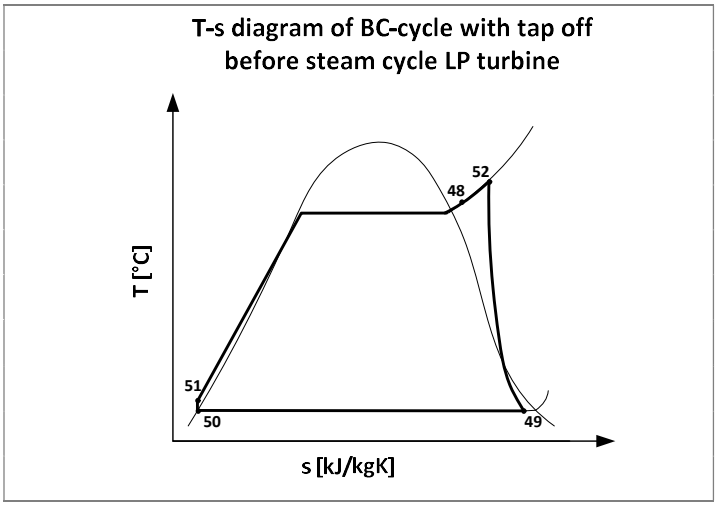

Figure 3.36: T-s diagrams of a BC cycle with tap-off before a low-pressure steam turbine

Including a heat exchanger in the BC cycle with tap-off from the steam side should increase the temperature of the working fluid in the BC cycle from T_{48} to T_{52} further into the superheated region before entering the BC turbine. Consequently, the work of the BC cycle turbine will increase. Depending on the properties of the working fluid, this configuration could increase the thermal efficiency of the cycle.

[24] The mass flow rates of these nodes are a function of the working fluid properties. Consequently, they differ for each working fluid tested in the BC cycle. See the equations related to this configuration for further information.

Figure 3.36 indicates the T-s diagram of the BC cycle for this configuration. The properties for the BC cycle are indicated in Table 3.21.

Scenario 1			Scenario 2		
Node	**Temperature (°C)**	**Assumption**	**Node**	**Temperature (°C)**	**Assumption**
48	100	$s_{48} = s_{49,i}$ $P_{48}@(T_{48},s_{48})$ [kPa] $h_{48,i}@(T_{48},s_{48,i})$ [kJ/kg][25]	**61**	100	$x_{60}=1$ P_{60} = Sat. P@T_{60} [kPa] $h_{60}@(P_{60},x_{60})$ [kJ/kg]
49	36	$x_{49}=0.9$ P_{49} = Sat.P @T_{49} [kPa] $h_{49}@(T_{49},x_{49})$ [kJ/kg]	**49**	36	$s_{49,i}=s_{61}$ $P_{49} = P_{50}$ $h_{49,i}@(P_{49},s_{49,i})$[20] $x_{49}@(P_{49},s_{49})$
50	36	$x_{50}=0$ $P_{50} = P_{49}$ $h_{50}@(T_{50},x_{50})$ [kJ/kg] $v_{50}@(T_{50},x_{50})$ [m^3/kg]	**50**	36	$x_{50}=0$ P_{50} = Sat.P @T_{50} [kPa] $h_{50}@(T_{50},x_{50})$ [kJ/kg]
51	f(assump.)	$P_{51} = P_{48}$ $v_{51}=v_{50}$ (incompressible liquid and small temperature difference) $h_{51} = \left(\frac{1}{\eta_p} v_{51}[P_{51} - P_{50}]\right) + h_{50}$	**51**	f(assump.)	$s_{51,i}=s_{50}$ $P_{51}=P_{61}$ $h_{51,i}@(P_{51},s_{51,i})$[20]
52	$T_{52}=T_{55}$ -6 [26]	$P_{52}=P_{51}$ $h_{52}@(T_{52},P_{52})$ [kJ/kg]	**52**	$T_5=T_{55}$ -6 [21]	$P_{52}=P_{51}$ $h_{52}@(T_{52},P_{52})$ [kJ/kg]

Table 3.21: The state of each node for the BC cycle with tap-off from the steam-side low-pressure turbine for scenarios 1 and 2, including the assumptions made

The equations used for the analysis of this cycle are repeated below for the sake of convenience, along with additional equations required for the analysis of the modification.

The equations for the complete cycle, which are required to determine the thermal efficiency of the cycle, are as follows:

$$\eta_{th,with\ BC} = \frac{\dot{W}_{total}}{\dot{Q}_{boiler}} \quad (3.74)$$

$$\eta_{th,fuel} = \frac{\dot{W}_{total}}{\dot{Q}_{in}} \quad (3.75)$$

$$\eta_{th,Carnot} = 1 - \frac{T_L}{T_H} = 1 - \frac{T_{50}}{T_{15}} \quad (3.76)$$

[25] A turbine and pump efficiency is applied in the calculations to compensate for the ideal conditions assumed at nodes 48, 49 and 51.
[26] The outlet temperature of the heat exchanger on the BC side is assumed to be slightly lower than the outlet temperature of the heat exchanger on the steam side (Cengel, 2006).

$$\dot{W}_{total} = \dot{W}_{HP,t} + \dot{W}_{LP,t} + \dot{W}_{P,cond} + \dot{W}_{P,boil} + \dot{W}_{BC,t} + \dot{W}_{BC,p} \quad [\text{kW}] \quad \textbf{(3.77)}$$

The equations related to the steam cycle are as follows:

$$\dot{Q}_{boiler} = \dot{m}_{13}\left[h_{13}^{sh,g}(P_{13};T_{13}) - h_{15}^{c,f}(P_{15};T_{15})\right] \quad [\text{kW}] \quad \textbf{(3.78)}$$

$$\dot{W}_{p,boil} = \dot{m}_{9}\left[h_{9}^{sat,f}(P_{9}) - h_{10}^{c,f}(P_{10};T_{10})\right] \quad [\text{kW}] \quad \textbf{(3.79)}$$

$$\dot{W}_{HP,t} = \dot{m}_{15}h_{15}^{sh,g}(P_{15};T_{15}) - \dot{m}_{18}h_{18}^{sh,g}(P_{18};T_{18}) - \dot{m}_{21}h_{21}^{sh,g}(P_{21};T_{21}) - \dot{m}_{26}h_{26}^{sh,g}(P_{26};T_{26}) - \dot{m}_{31}h_{31}^{sh,g}(P_{31};T_{31}) - \dot{m}_{16}h_{16}^{sat,fg}(P_{16};x_{16}) \quad [\text{kW}] \quad \textbf{(3.80)}$$

$$\dot{W}_{p,cond} = \dot{m}_{47}\left[h_{47}^{sat.f}(T_{47}) - h_{8}^{c,f}(P_{8};T_{8})\right] \quad [\text{kW}] \quad \textbf{(3.81)}$$

$$\dot{W}_{LP,t} = \dot{m}_{62}h_{62}^{sat,fg}(P_{62};x_{62}) - \dot{m}_{46}h_{46}^{sat,fg}(P_{46};x_{46}) \quad [\text{kW}] \quad \textbf{(3.82)}$$

$$\dot{m}_{62} = \dot{m}_{16} - \dot{m}_{54} \quad [\text{kg/s}] \quad \textbf{(3.83)}$$

Equations related to the BC cycle are as follows:

$$\dot{W}_{BC,t} = \dot{m}_{BC}\eta_t(h_{52} - h_{49}) \quad [\text{kW}] \quad \textbf{(3.84)}$$

$$\dot{W}_{BC,p} = \dot{m}_{BC}\left(\frac{1}{\eta_p}\right)(h_{50} - h_{51}) \,/\, \frac{1}{\eta_p}\dot{m}_{BC}v_{50}(P_{50} - P_{51}) \quad [\text{kW}] \quad \textbf{(3.85)}$$

$$\dot{m}_{BC} = \frac{\dot{m}_{16}(h_{46} - h_{47}) + \dot{m}_{54}(h_{55} - h_{46})}{h_{48} - h_{51}} \quad [\text{kg/s}] \quad \textbf{(3.86)}$$

$$\dot{m}_{54} = \frac{\dot{m}_{BC}(h_{52} - h_{48/61})}{h_{54} - h_{55}} \quad [\text{kg/s}] \quad \textbf{(3.87)}$$

It is seen in Chapter 4 that an optimum tap-off mass flow rate is obtained for each working fluid, where the thermal efficiency for this configuration reaches a maximum, as explained briefly in Section 3.3.5 and Figure 3.24.

3.3.5.5.2 Tap-off before low-pressure turbine and FWHs

Certain working fluids tested in the cycle and discussed in Section 3.3.5.5.1 indicate an increase in thermal efficiency, where the increase is related to the working fluid tested in the BC cycle. The cycles where an increase in thermal efficiency above 40% was achieved were also tested with the implementation of FWHs. The addition of FWHs should increase the thermal efficiency of the cycle further. In the following section, FWHs are added to the theoretical configuration indicated in Figure 3.34.

Figure 3.37 indicates this theoretical configuration. The steam cycle's properties will remain as indicated in Section 3.3.5.5.1 and Table 2.1. The tap-off mass flow rate from the steam cycle, $\dot{m}_{54}$, is fixed in this section for the specific working fluid tested in the BC cycle.

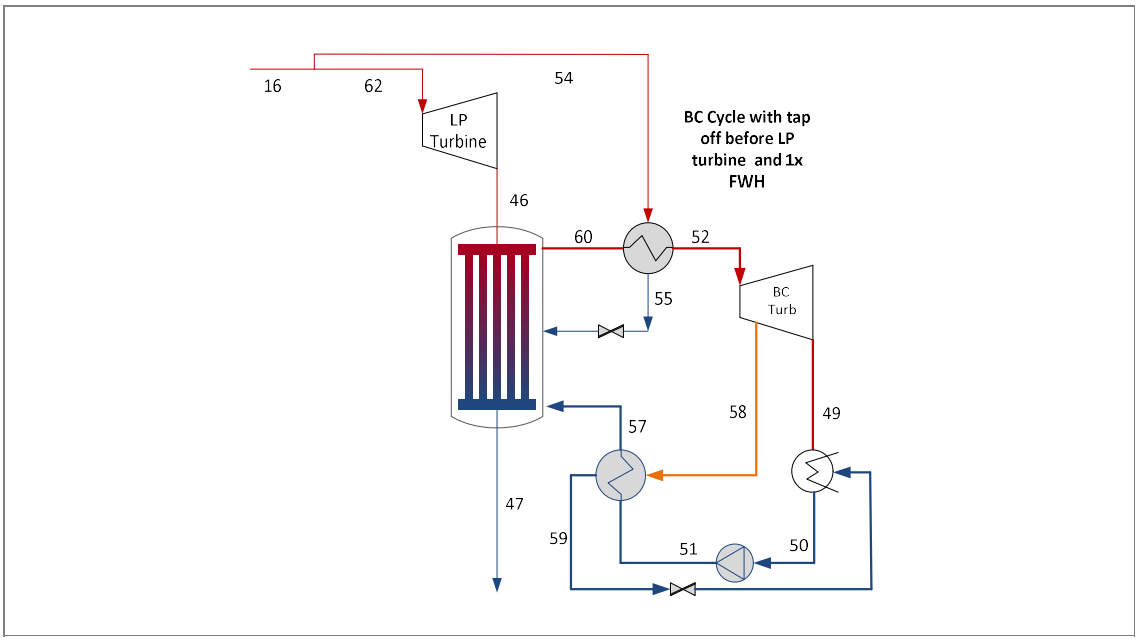

Figure 3.37: Component diagram of the Komati Power Station with tap-off before a low-pressure turbine into the BC cycle and BC cycle FWH

The BC cycle side, for this configuration, is analysed as indicated in Section 3.3.5.2. The main difference is that the inlet temperature of the BC turbine is higher for this configuration. Consequently, the FWH tap-off pressure range ($P_{49} < P_{58} < P_{52}$) is larger and is again a function of the properties of the working fluid. The properties at each node of the BC cycle are indicated in Table 3.22. The assumptions made for each node are also indicated in this table.

Similar to Section 3.3.5.4.2, this configuration was also tested with only one FWH as the results of the cycle without a FWH, as indicated in Section 3.3.5.4.1, did not heed a very large increase in thermal efficiency. Consequently, the theoretical cycle, the BC cycle with tap-off from a low-pressure turbine, including two or more FWHs, will not be economically viable. However, the cycle was tested with one FWH for illustrative purposes.

Scenario 1			Scenario 2		
Node	**Temperature (°C)**	**Assumption**	**Node**	**Temperature (°C)**	**Assumption**
60	100	$s_{60} = s_{60,i}$; $P_{60}@(T_{60},s_{60})$ [kPa] $h_{60,i}@(T_{60},s_{60,i})$ [kJ/kg][27]	**61**	100	$x_{61}=1$; P_{61} = Sat. P@T_{61} [kPa] $h_{61}@(P_{61},x_{61})$ [kJ/kg]
49	36	$x_{49}=0.9$ P_{49} = Sat.P @T_{49} [kPa] $h_{49}@(T_{49},x_{49})$ [kJ/kg]	**49**	36	$s_{49,i}=s_{61}$ $P_{49} = P_{50}$ $h_{49,i}@(P_{49},s_{49,i})$[22] $x_{49}@(P_{49},s_{49})$
50	36	$x_{50}=0$; $P_{50} = P_{49}$ $h_{50}@(T_{50},x_{50})$ [kJ/kg] $v_{50}@(T_{50},x_{50})$ [m^3/kg]	**50**	36	$x_{50}=0$ P_{50} = Sat.P @T_{50} [kPa] $h_{50}@(T_{50},x_{50})$ [kJ/kg]
51	f(assump.)	$P_{51} = P_{48}$ $v_{51}=v_{50}$ (incompressible liquid and small temperature difference) $h_{51} = \left(\frac{1}{\eta_p} v_{51}[P_{51} - P_{50}]\right) + h_{50}$	**51**	f(assump.)	$s_{51,i}=s_{50}$ $P_{51}=P_{61}$ $h_{51,i}@(P_{51},s_{51,i})$[22]
52	$T_{52}=T_{56}$ -6 [28]	$P_{52}=P_{51}$ $h_{52}@(T_{52},P_{52})$ [kJ/kg]	**52**	$T_{52}=T_{56}$ -6 [23]	$P_{52}=P_{51}$ $h_{52}@(T_{52},P_{52})$ [kJ/kg]
57	$T_{57}=T_{59}$ [29]	$P_{57}=P_{51}$ $h_{57}@(T_{57},P_{57})$ [kJ/kg]	**57**	$T_{57}=T_{59}$ [24]	$P_{57}=P_{51}$ $h_{57}@(T_{57},P_{57})$ [kJ/kg]
58	f(assump.)	$P_{58}=P_{guess}$ ($P_{52}<P_{58}<P_{49}$) $s_{58,i}=s_{52}$[16] $h_{58}@(s_{58},P_{58})$ [kJ/kg]	**58**	f(assump.)	$P_{58}=P_{guess}$ ($P_{52}<P_{58}<P_{49}$) $s_{58,i}=s_{52}$[16] $h_{58}@(s_{58},P_{58})$ [kJ/kg]
59	$T_{59}=T_{sat}@P_{59}$	$x_{59}=0$ $P_{59}=P_{58}$ $h_{59}@(x_{59},P_{59})$ [kJ/kg]	**59**	$T_{59}=T_{sat}@P_{59}$	$x_{59}=0$ $P_{59}=P_{58}$ $h_{59}@(x_{59},P_{59})$ [kJ/kg]

Table 3.22: The state of each node for the BC cycle with tap-off before the steam-side low-pressure turbine for scenarios 1 and 2 and FWHs in the BC cycle, including the assumptions made

Equations 3.74 to 3.83 and 3.85, which are indicated in Section 3.3.5.5.1, were used in the analysis of this cycle. The additional equations indicated below will apply to this configuration with the addition of a FWH.

$$\dot{W}_{BC,t} = \eta_t[\dot{m}_{BC}h_{52} - \dot{m}_{58}h_{58} - (\dot{m}_{BC} - \dot{m}_{58})h_{49}] \quad \text{[kW]} \quad \textbf{(3.88)}$$

$$\dot{m}_{BC} = \frac{\dot{m}_{16}(h_{46}-h_{47})+\dot{m}_{53}(h_{56}-h_{46})}{h_{48}-h_{57}} \quad \text{[kg/s]} \quad \textbf{(3.89)}$$

$$\dot{m}_{58} = \dot{m}_{BC}\left(\frac{h_{57}-h_{51}}{h_{58}-h_{59}}\right) \quad \text{[kg/s]} \quad \textbf{(3.90)}$$

[27] A turbine and pump efficiency is applied in the calculations to compensate for the ideal conditions assumed at nodes 48, 49, 51 and 58.
[28] The outlet temperature of the heat exchanger on the BC side is assumed to be slightly lower than the outlet temperature of the heat exchanger on the steam side (Cengel, 2006).
[29] (Sonntag, et al., 2003)

3.3.5.6 BC cycle with tap-off in a high-pressure turbine and FWHs

The configuration was also tested for the theoretical scenario where steam was tapped off from the high-pressure turbine into a heat exchanger in the BC turbine. This scenario was also tested with feed water heating in the BC cycle.

3.3.5.6.1 BC cycle with tap-off in high-pressure turbine

The concept where a heat exchanger is theoretically included in the BC cycle with steam fed into the heat exchanger from the high-pressure turbine in the steam side is indicated in Figure 3.38. The concept indicates steam being tapped off from the high-pressure turbine at a certain pressure, which is obtained via the simulation that is discussed below and feeds into a heat exchanger that is positioned in the BC cycle. The steam enters at node 66 and releases heat to the working fluid in the BC cycle. The steam then leaves the heat exchanger as saturated liquid water at the tap-off pressure at node 68. The saturated liquid water then enters the BC to leave at node 47. Similarly, the working fluid enters the heat exchanger at node 48 under the conditions described previously in the chapter, absorbs the heat and enters the BC turbine at an elevated temperature, where T_{67} is assumed to be a couple of degrees lower than T_{68}.

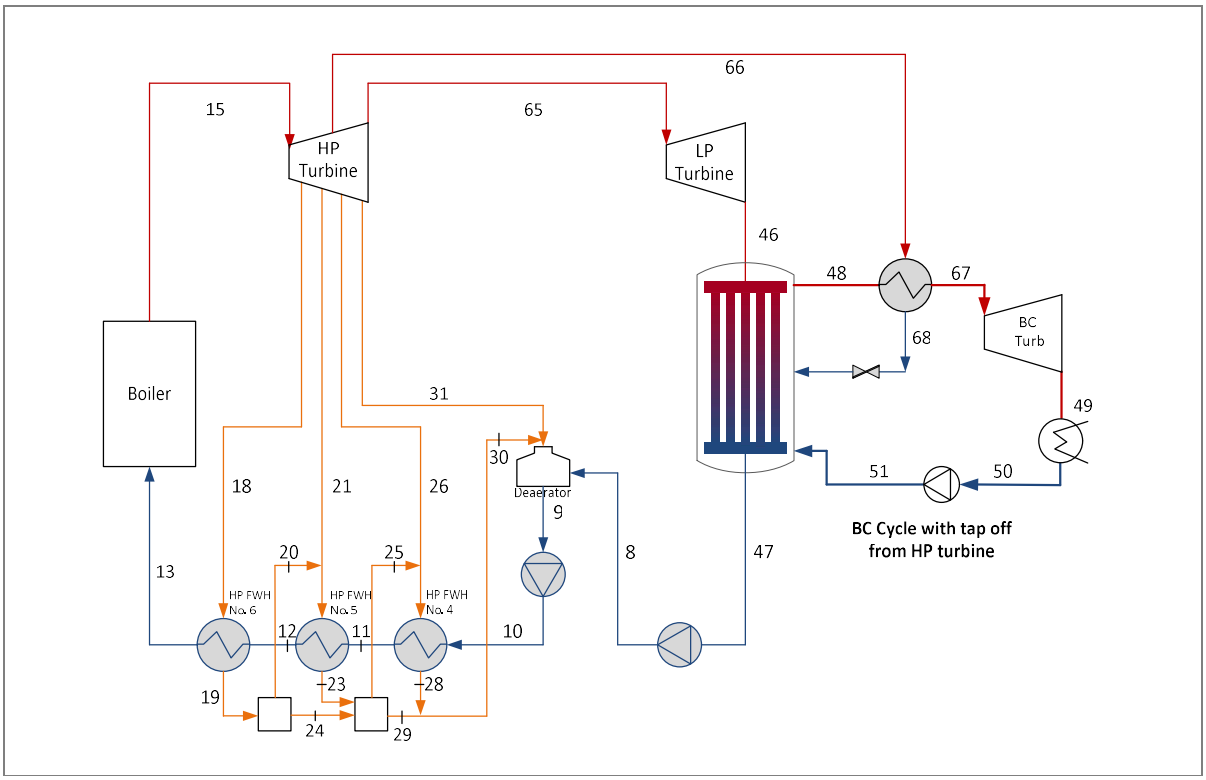

Figure 3.38: Component diagram of the Komati Power Station with tap-off from a high-pressure turbine into the BC cycle

The steam cycle's nodal information and the T-s diagram is indicated in Table 3.23. The tap-off from the high-pressure turbine affects the steam side's mass flow rates. The tap-off mass flow rates are a function of the tap-off pressure and the BC cycle's working fluid properties. Table 3.23 and Figure 3.39 indicate the steam cycle nodal properties related to Figure 3.38. The tap-off pressure from the high-pressure turbine, P_{66}, was chosen from the pressure range between high-pressure turbine inlet and outlet pressures, i.e. P_{15} to P_{16}. For each tap-off pressure, a corresponding tap-off mass flow rate was calculated.

Node	Temperature (°C)	Mass flow (kg/s)	Enthalpy (kJ/kg)
8	104.5	103.48	438.5
9	126.1	126.35	529.8
10	127.6	126.35	542.3
11	152.6	126.35	648.9
12	183	126.35	780.9
13	210	126.35	900.5
15	510	126.35	3 418.8
65	126.9	[25]	2 664.7
18	347.3	6.87	3 132.5
19	212.6	6.87	909.4
20		0.42	2 781
21	245.8	7.42	2 948.6
23	185.8	7.83	788.9
24	185.8	6.45	788.9
25		0.91	2 751.6
26	178.1	5.44	2 804
28	155.4	6.35	655.5
29	155.4	13.38	655.5
30	155.4	19.73	655.5
31	165.2	3.14	2 796.5
46	104	[30]	2 457
47	104	103.48	436
66	$T_{66}@(s_{66},P_{66})$[31]	[25]	$h_{66}@(s_{66},P_{66})$[26]
68	$T_{68}=T_{sat}@(P_{68}=P_{66})$	[25]	$h_{68}@h_f@P_{68}$

Table 3.23: The state of each node for the steam cycle with tap-off from a high-pressure turbine

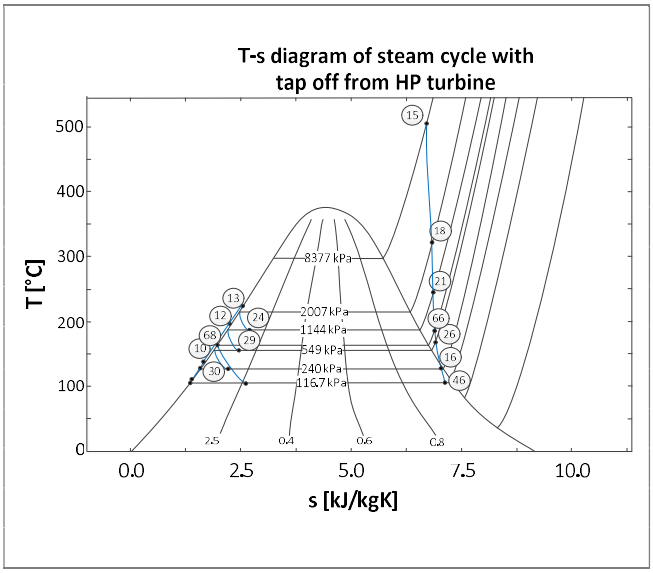

Figure 3.39: T-s diagram of the steam cycle of the Komati Power Station – with tap-off from a high-pressure turbine

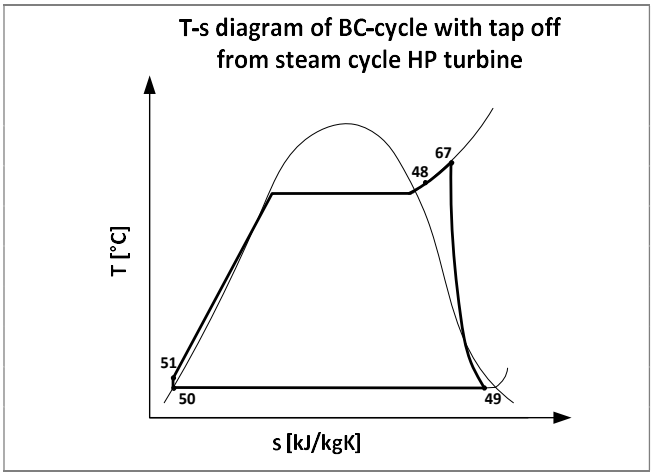

Figure 3.40: T-s diagrams of the BC cycle with tap-off from a high-pressure steam turbine

[30] $\dot{m}_{46,47,66,68} = f$ (P_{66}, working fluid properties); $\dot{m}_{46,47,66,68}$ differs for each scenario; See equations related to this configuration for further information.

[31] P_{66} was chosen such that $P_{16} < P_{66} < P_{15}$. Under ideal conditions, the entropy at node 66 was assumed as follows: $s_{66}=s_{15}$

Figure 3.40 indicates the T-s diagram of the BC cycle for this configuration. The properties of the BC cycle are indicated in Table 3.24.

Scenario 1			Scenario 2		
Node	**Temperature (°C)**	**Assumption**	**Node**	**Temperature (°C)**	**Assumption**
48	100	$s_{48} = s_{49,i}$ $P_{48}@(T_{48},s_{48})$ [kPa] $h_{48,i}@(T_{48},s_{48,i})$ [kJ/kg][32]	**61**	100	$x_{60}=1$ P_{60} = Sat. P@T_{60} [kPa] $h_{60}@(P_{60},x_{60})$ [kJ/kg]
49	36	$x_{49}=0.9$ P_{49} = Sat.P @T_{49} [kPa] $h_{49}@(T_{49},x_{49})$ [kJ/kg]	**49**	36	$s_{49,i}=s_{61}$ $P_{49} = P_{50}$ $h_{49,i}@(P_{49},s_{49,i})$[27] $x_{49}@(P_{49},s_{49})$
50	36	$x_{50}=0$ $P_{50} = P_{49}$ $h_{50}@(T_{50},x_{50})$ [kJ/kg] $v_{50}@(T_{50},x_{50})$ [m^3/kg]	**50**	36	$x_{50}=0$ P_{50} = Sat.P @T_{50} [kPa] $h_{50}@(T_{50},x_{50})$ [kJ/kg]
51	f(assump.)	$P_{51} = P_{48}$ $v_{51}=v_{50}$ (incompressible liquid and small temperature difference) $h_{51} = \left(\frac{1}{\eta_p} v_{51}[P_{51} - P_{50}]\right) + h_{50}$	**51**	f(assump.)	$s_{51,i}=s_{50}$ $P_{51}=P_{61}$ $h_{51,i}@(P_{51},s_{51,i})$[27]
67	$T_{67}=T_{68}$ - 6 [33]	$P_{67}=P_{51}$ $h_{67}@(T_{67},P_{67})$ [kJ/kg]	**67**	$T_{67}=T_{68}$ - 6 [28]	$P_{67}=P_{51}$ $h_{67}@(T_{67},P_{67})$ [kJ/kg]

Table 3.24: The state of each node for the BC cycle with tap-off from a steam-side high-pressure turbine for scenarios 1 and 2, including the assumptions made

The equations used for the analysis of this cycle are repeated below, along with additional equations required for the analysis of the modification. The equations for the complete cycle, which are required to determine the thermal efficiency of the cycle, are as follows:

$$\eta_{th,with\ BC} = \frac{\dot{W}_{total}}{\dot{Q}_{boiler}} \quad \textbf{(3.91)}$$

$$\eta_{th,fuel} = \frac{\dot{W}_{total}}{\dot{Q}_{in}} \quad \textbf{(3.92)}$$

$$\eta_{th,Carnot} = 1 - \frac{T_L}{T_H} = 1 - \frac{T_{50}}{T_{15}} \quad \textbf{(3.93)}$$

$$\dot{W}_{total} = \dot{W}_{HP,t} + \dot{W}_{LP,t} + \dot{W}_{P,cond} + \dot{W}_{P,boil} + \dot{W}_{BC,t} + \dot{W}_{BC,p} \quad \text{[kW]} \quad \textbf{(3.94)}$$

[32] A turbine and pump efficiency is applied in the calculations to compensate for the ideal conditions assumed at nodes 48, 49 and 51.
[33] The outlet temperature of the heat exchanger on the BC side is assumed to be slightly lower than the outlet temperature of the heat exchanger on the steam side (Cengel, 2006).

The equations related to the steam cycle are as follows:

$$\dot{Q}_{boiler} = \dot{m}_{13}\left[h_{13}^{sh,g}(P_{13};T_{13}) - h_{15}^{c,f}(P_{15};T_{15})\right] \quad \text{[kW]} \quad \textbf{(3.95)}$$

$$\dot{W}_{p,boil} = \dot{m}_{9}\left[h_{9}^{sat,f}(P_{9}) - h_{10}^{c,f}(P_{10};T_{10})\right] \quad \text{[kW]} \quad \textbf{(3.96)}$$

$$\dot{W}_{HP,t} = \dot{m}_{15}h_{15}^{sh,g}(P_{15};T_{15}) - \dot{m}_{18}h_{18}^{sh,g}(P_{18};T_{18}) - \dot{m}_{21}h_{21}^{sh,g}(P_{21};T_{21}) - \dot{m}_{26}h_{26}^{sh,g}(P_{26};T_{26}) - \dot{m}_{31}h_{31}^{sh,g}(P_{31};T_{31}) - \dot{m}_{66}h_{66}^{sh,g}(P_{66};s_{66}) - \dot{m}_{16}h_{16}^{sat,fg}(P_{16};x_{16}) \quad \text{[kW]} \quad \textbf{(3.97)}$$

$$\dot{W}_{p,cond} = \dot{m}_{47}\left[h_{47}^{sat.f}(T_{47}) - h_{8}^{c,f}(P_{8};T_{8})\right] \quad \text{[kW]} \quad \textbf{(3.98)}$$

$$\dot{W}_{LP,t} = \dot{m}_{65}h_{65}^{sat,fg}(P_{65};x_{65}) - h_{46}^{sat,fg}(P_{46};x_{46}) \quad \text{[kW]} \quad \textbf{(3.99)}$$

$$\dot{m}_{65} = \dot{m}_{15} - \dot{m}_{18} - \dot{m}_{21} - \dot{m}_{26} - \dot{m}_{31} - \dot{m}_{66} \quad \text{[kg/s]} \quad \textbf{(3.100)}$$

Equations related to the BC cycle are as follows:

$$\dot{W}_{BC,t} = \dot{m}_{BC}\eta_t(h_{67} - h_{49}) \quad \text{[kW]} \quad \textbf{(3.101)}$$

$$\dot{W}_{BC,p} = \dot{m}_{BC}\left(\frac{1}{\eta_p}\right)(h_{50} - h_{51}) \;/\; \frac{1}{\eta_p}\dot{m}_{BC}v_{50}(P_{50} - P_{51}) \quad \text{[kW]} \quad \textbf{(3.102)}$$

$$\dot{m}_{BC} = \frac{\dot{m}_{65}(h_{46} - h_{47}) + \dot{m}_{66}(h_{68} - h_{46})}{h_{48} - h_{51}} \quad \text{[kg/s]} \quad \textbf{(3.103)}$$

$$\dot{m}_{66} = \frac{\dot{m}_{BC}(h_{67} - h_{48/61})}{h_{66} - h_{68}} \quad \text{[kg/s]} \quad \textbf{(3.104)}$$

An optimum tap-off mass flow rate is obtained where the thermal efficiency for this configuration reaches a maximum, as explained briefly in Section 3.3.5 and Figure 3.24.

3.3.5.6.2 Tap-off from the high-pressure turbine and FWHs

The addition of FWHs to the theoretical cycle discussed in Section 3.3.5.6.1 should increase the thermal efficiency of the cycle even further. In the section that follows, FWHs are added to the theoretical configuration indicated in Figure 3.38.

Figure 3.41 indicates this theoretical configuration. The steam cycle's properties will remain as indicated in Section 3.3.5.4.1 and Table 3.17. The tap-off pressure from the steam cycle, P_{66}, is fixed in this section at the tap-off pressure where maximum thermal efficiency was achieved for the specific working fluid.

For this configuration, the BC cycle side is analysed as indicated in Section 3.3.5.2. However, the inlet temperature of the BC turbine is higher for this configuration. Consequently, the FWH

tap-off pressure range ($P_{4\,9} < P_{58} < P_{67}$) is larger and is again a function of the properties of the working fluid.

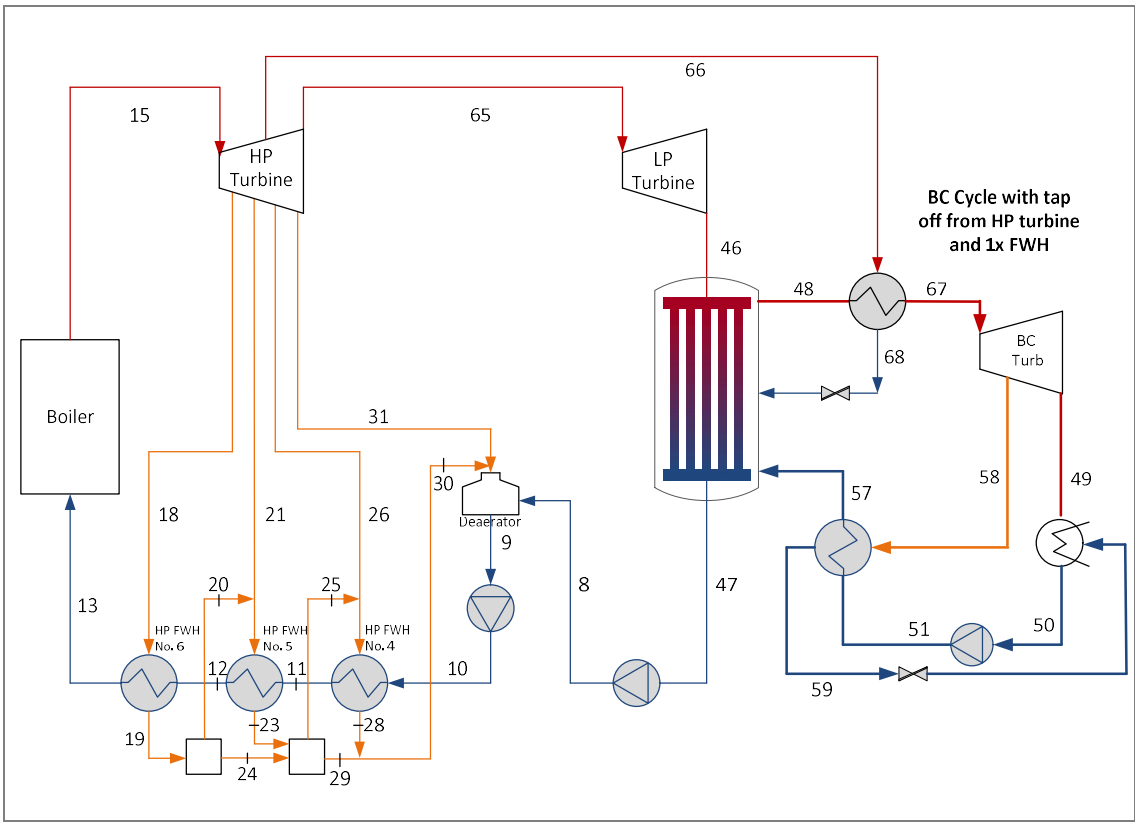

Figure 3.41: Component diagram of the Komati Power Station with tap-off from a high-pressure turbine into the BC cycle, and a BC cycle with one FWH

This configuration was tested with only one, two and three FWHs because the results of the cycle without a FWH, as indicated in Section 3.3.5.6.1, heeded an indication of an increase in thermal efficiency. Consequently, the theoretical cycle, BC cycle with tap-off in high-pressure turbine, including one, two and three FWHs, is expected to indicate an even further increase in thermal efficiency.

The implementation of FWHs were explained in detail in Section 3.3.5.2. For illustrative purposes, the cycle with one FWH is discussed in more detail. However, the cycle with two and three FWHs will follow the same method as indicated in Section 3.3.5.2. It will not be necessary to go into further detail with regard to this configuration in this chapter. The theoretical configuration is, however, indicated and briefly discussed.

The properties at each node of the BC cycle are indicated in Table 3.25. The assumptions made for each node are also indicated in this table.

Scenario 1			Scenario 2		
Node	**Temperature (°C)**	**Assumption**	**Node**	**Temperature (°C)**	**Assumption**
48	100	$s_{48} = s_{49,i}$ $P_{48}@(T_{48},s_{48})$ [kPa] $h_{48,i}@(T_{48},s_{48,i})$ [kJ/kg][34]	**61**	100	$x_{60}=1$ P_{60} = Sat. P@T_{60} [kPa] $h_{60}@(P_{60},x_{60})$ [kJ/kg]
49	36	$x_{49}=0.9$ P_{49} = Sat.P @T_{49} [kPa] $h_{49}@(T_{49},x_{49})$ [kJ/kg]	**49**	36	$s_{49,i}=s_{61}$ $P_{49} = P_{50}$ $h_{49,i}@(P_{49},s_{49,i})$[29] $x_{49}@(P_{49},s_{49})$
50	36	$x_{50}=0$ $P_{50} = P_{49}$ $h_{50}@(T_{50},x_{50})$ [kJ/kg] $v_{50}@(T_{50},x_{50})$ [m^3/kg]	**50**	36	$x_{50}=0$ P_{50} = Sat.P @T_{50} [kPa] $h_{50}@(T_{50},x_{50})$ [kJ/kg]
51	f(assump.)	$P_{51} = P_{48}$ $v_{51}=v_{50}$ (incompressible liquid and small temperature difference) $h_{51} = \left(\frac{1}{\eta_p} v_{51}[P_{51} - P_{50}]\right) + h_{50}$	**51**	f(assump.)	$s_{51,i}=s_{50}$ $P_{51}=P_{61}$ $h_{51,i}@(P_{51},s_{51,i})$[29]
67	$T_{67}=T_{68}$ - 6 [35]	$P_{67}=P_{51}$ $h_{67}@(T_{67},P_{67})$ [kJ/kg]	**67**	$T_{67}=T_{68}$ - 6 [30]	$P_{67}=P_{51}$ $h_{67}@(T_{67},P_{67})$ [kJ/kg]
57	$T_{57}=T_{59}$ [36]	$P_{57}=P_{51}$ $h_{57}@(T_{57},P_{57})$ [kJ/kg]	**57**	$T_{57}=T_{59}$ [31]	$P_{57}=P_{51}$ $h_{57}@(T_{57},P_{57})$ [kJ/kg]
58	f(assump.)	$P_{58}=P_{guess}$ ($P_{52}<P_{58}<P_{49}$) $s_{58,i}=s_{52}$[29] $h_{58}@(s_{58},P_{58})$ [kJ/kg]	**58**	f(assump.)	$P_{58}=P_{guess}$ ($P_{52}<P_{58}<P_{49}$) $s_{58,i}=s_{52}$[29] $h_{58}@(s_{58},P_{58})$ [kJ/kg]
59	$T_{59}=T_{sat}@P_{59}$	$x_{59}=0$ $P_{59}=P_{58}$ $h_{59}@(x_{59},P_{59})$ [kJ/kg]	**59**	$T_{59}=T_{sat}@P_{59}$	$x_{59}=0$ $P_{59}=P_{58}$ $h_{59}@(x_{59},P_{59})$ [kJ/kg]

Table 3.25: The state of each node for the BC cycle with tap-off from a steam-side high-pressure turbine for scenarios 1 and 2, and FWHs in the BC cycle, including the assumptions made

Equations 3.91 to 3.100, 3.102 and 3.104, which are indicated in Section 3.3.5.6.1, are used in the analysis of this cycle. The additional equations indicated below will apply to this configuration with the addition of a FWH.

$$\dot{W}_{BC,t} = \eta_t[\dot{m}_{BC}h_{67} - \dot{m}_{58}h_{58} - (\dot{m}_{BC} - \dot{m}_{58})h_{49}] \quad \text{[kW]} \quad \textbf{(3.105)}$$

$$\dot{m}_{BC} = \frac{\dot{m}_{65}(h_{46}-h_{47})+\dot{m}_{66}(h_{68}-h_{46})}{h_{48}-h_{57}} \quad \text{[kg/s]} \quad \textbf{(3.106)}$$

$$\dot{m}_{58} = \dot{m}_{BC}\left(\frac{h_{57}-h_{51}}{h_{58}-h_{59}}\right) \quad \text{[kg/s]} \quad \textbf{(3.107)}$$

[34] A turbine and pump efficiency is applied in the calculations to compensate for the ideal conditions assumed at nodes 48, 49, 51 and 58.
[35] The outlet temperature of the heat exchanger on the BC side is assumed to be slightly lower than the outlet temperature of the heat exchanger on the steam side (Cengel, 2006).
[36] (Sonntag, et al., 2003)

3.3.5.7 BC cycle without a low-pressure turbine and tap-off from a high-pressure turbine and FWHs

The concept where the low-pressure turbine has been removed was discussed in Section 3.3.3. The concept where a heat exchanger is theoretically included in the BC cycle with steam fed into the heat exchanger from the steam side has been discussed for several different configurations. In this section, a theoretical configuration was tested where these two configurations were combined, i.e. where steam was tapped off from the high-pressure turbine into a heat exchanger in the BC turbine and the low-pressure steam turbine was removed. This scenario was also tested with feedwater heating in the BC cycle.

3.3.5.7.1 BC cycle with tap-off in a high-pressure turbine and without the low-pressure turbine

In this section, a heat exchanger is theoretically included in the BC cycle, with steam fed into the heat exchanger from the steam side's high-pressure turbine, as indicated in Figure 3.42.

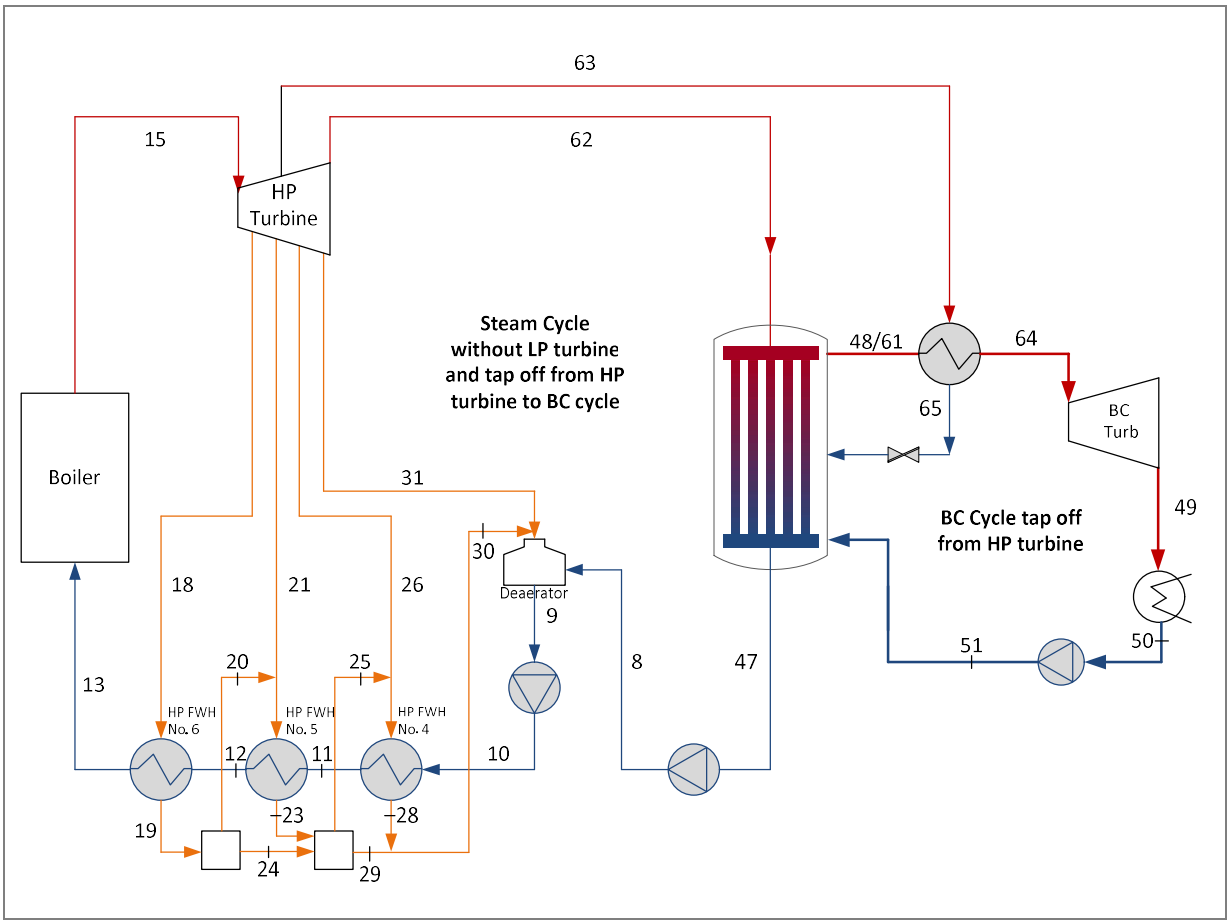

Figure 3.42: Component diagram of the Komati Power Station without a low-pressure turbine and with tap-off from a high-pressure turbine into the BC cycle

The concept indicates steam being tapped off from the high-pressure turbine at a certain pressure, which is obtained via the simulation that is discussed below and feeds into a heat exchanger positioned in the BC cycle. The steam enters at node 63 and releases heat to the working fluid in the BC cycle. The steam then leaves the heat exchanger as saturated liquid water at the tap-off pressure at node 65. The saturated liquid water then enters the BC to leave at node 47.

Similarly, the working fluid on the BC cycle side enters the heat exchanger at node 48/61 under the conditions described previously in this chapter, absorbs the heat and enters the BC turbine at an elevated temperature. Again, the increase in temperature before the BC turbine will increase the work done by the BC turbine.

The inlet temperature of the BC turbine, $T_{64,}$ is assumed to be a couple of degrees lower than T_{65} (Cengel, 2006), the outlet temperature of the steam side of the heat exchanger.

The tap-off from the high-pressure turbine affects the steam side's mass flow rates. The tap-off mass flow rates are a function of the tap-off pressure and the BC cycle's working fluid properties. Table 3.26 and Figure 3.43 indicate the steam cycle nodal properties related to Figure 3.42. The tap-off pressure from the high-pressure turbine, P_{63}, was chosen from the pressure range between the high-pressure turbine inlet and outlet pressures, i.e. P_{15} to P_{62}. For each tap-off pressure, a corresponding tap-off mass flow rate was calculated.

Node	Temperature (°C)	Mass flow (kg/s)	Enthalpy (kJ/kg)
8	104.5	103.48	438.5
9	126.1	126.35	529.8
10	127.6	126.35	542.3
11	152.6	126.35	648.9
12	183	126.35	780.9
13	210	126.35	900.5
15	510	126.35	3 418.8
18	347.3	6.87	3 132.5
19	212.6	6.87	909.4
20		0.42	2 781
21	245.8	7.42	2 948.6
23	185.8	7.83	788.9
24	185.8	6.45	788.9
25		0.91	2 751.6
26	178.1	5.44	2 804
28	155.4	6.35	655.5
29	155.4	13.38	655.5
30	155.4	19.73	655.5
31	165.2	3.14	2 796.5
47	104	103.48	436
62	126.9	[37]	2 664.7
63	$T_{63}@(s_{63},P_{63})$[38]	[32]	$h_{63}@(s_{63},P_{63})$[33]
65	$T_{65}=T_{sat}@(P_{65}=P_{65})$	[32]	$h_{65}@h_f@P_{65}$

Table 3.26: The state of each node for the steam cycle without a low-pressure turbine and tap-off from the high-pressure turbine

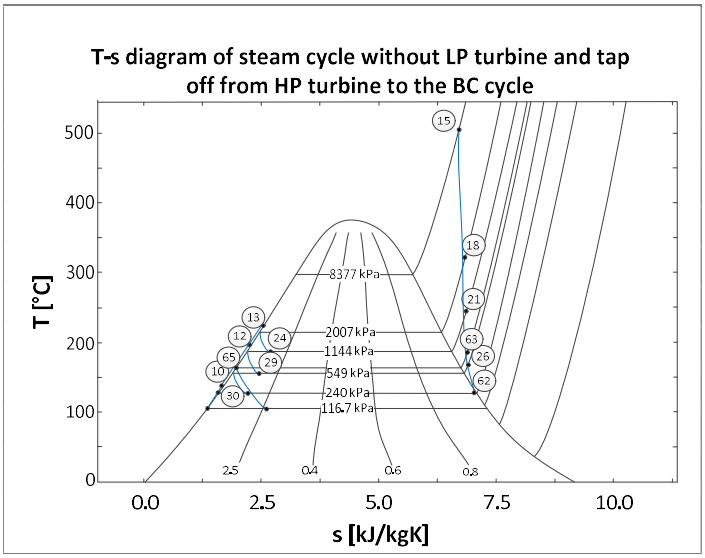

Figure 3.43: T-s diagram of the steam cycle of the Komati Power Station without a low-pressure turbine – with tap-off from a high-pressure turbine

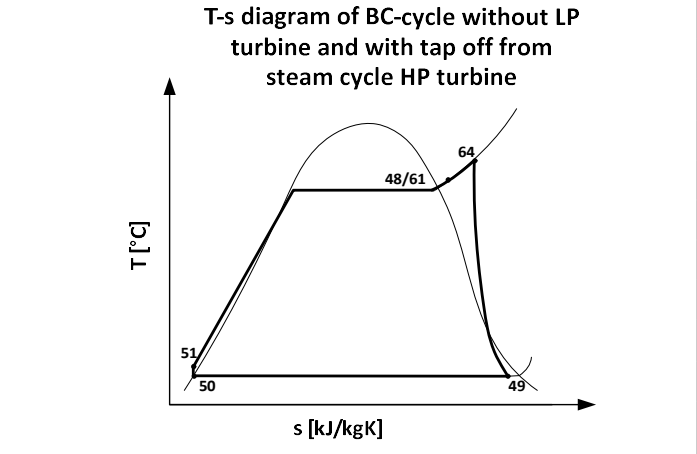

Figure 3.44: T-s diagrams of a BC cycle without a low-pressure turbine and tap-off from a high-pressure steam turbine

Figure 3.44 indicates the T-s diagram of the BC cycle for this configuration. The properties for the BC cycle are indicated in Table 3.27.

[37] $\dot{m}_{62,63,65} = f(P_{63}$,working fluid properties); $\dot{m}_{62,63,65}$ differs for each scenario.
[38] P_{63} was chosen: $P_{62} < P_{63} < P_{15}$; under ideal conditions assumed, i.e.: $s_{63} = s_{15}$.

Scenario 1			Scenario 2		
Node	**Temperature (°C)**	**Assumption**	**Node**	**Temperature (°C)**	**Assumption**
48	120	$s_{48} = s_{49,i}$ $P_{48}@(T_{48},s_{48})$ [kPa] $h_{48,i}@(T_{48},s_{48,i})$ [kJ/kg][39]	**61**	120	$x_{60}=1$ P_{60} = Sat. P@T_{60} [kPa] $h_{60}@(P_{60},x_{60})$ [kJ/kg]
49	36	$x_{49}=0.9$ P_{49} = Sat.P @T_{49} [kPa] $h_{49}@(T_{49},x_{49})$ [kJ/kg]	**49**	36	$s_{49,i}=s_{61}$ $P_{49} = P_{50}$ $h_{49,i}@(P_{49},s_{49,i})$[34] $x_{49}@(P_{49},s_{49})$
50	36	$x_{50}=0$ $P_{50} = P_{49}$ $h_{50}@(T_{50},x_{50})$ [kJ/kg] $v_{50}@(T_{50},x_{50})$ [m^3/kg]	**50**	36	$x_{50}=0$ P_{50} = Sat.P @T_{50} [kPa] $h_{50}@(T_{50},x_{50})$ [kJ/kg]
51	f(assump.)	$P_{51} = P_{48}$ $v_{51}=v_{50}$ (Incompressible liq. & small temp. diff.) $h_{51} = \left(\frac{1}{\eta_p} v_{51}[P_{51} - P_{50}]\right) + h_{50}$	**51**	f(assump.)	$s_{51,i}=s_{50}$ $P_{51}=P_{61}$ $h_{51,i}@(P_{51},s_{51,i})$[34]
64	$T_{64}=T_{65}$ - 6 [40]	$P_{64}=P_{51}$ $h_{64}@(T_{64},P_{64})$ [kJ/kg]	**64**	$T_{64}=T_{65}$ - 6 [35]	$P_{64}=P_{51}$ $h_{64}@(T_{64},P_{64})$ [kJ/kg]

Table 3.27: The state of each node for the BC cycle without a low-pressure turbine and tap-off from the steam-side high-pressure turbine for scenarios 1 and 2, including the assumptions made

The equations used for the analysis of this cycle are repeated below, along with additional equations required for the analysis of the modification. The equations for the complete cycle required to determine the thermal efficiency of the cycle are as follows:

$$\eta_{th,with\ BC} = \frac{\dot{W}_{total}}{\dot{Q}_{boiler}} \quad \textbf{(3.108)}$$

$$\eta_{th,fuel} = \frac{\dot{W}_{total}}{\dot{Q}_{in}} \quad \textbf{(3.109)}$$

$$\eta_{th,Carnot} = 1 - \frac{T_L}{T_H} = 1 - \frac{T_{50}}{T_{15}} \quad \textbf{(3.110)}$$

$$\dot{W}_{total} = \dot{W}_{HP,t} + \dot{W}_{LP,t} + \dot{W}_{P,cond} + \dot{W}_{P,boil} + \dot{W}_{BC,t} + \dot{W}_{BC,p} \quad \text{[kW]} \quad \textbf{(3.111)}$$

The equations related to the steam cycle are as follows:

$$\dot{Q}_{boiler} = \dot{m}_{13}\left[h_{13}^{sh,g}(P_{13};T_{13}) - h_{15}^{c,f}(P_{15};T_{15})\right] \quad \text{[kW]} \quad \textbf{(3.112)}$$

$$\dot{W}_{p,boil} = \dot{m}_{9}\left[h_{9}^{sat,f}(P_{9}) - h_{10}^{c,f}(P_{10};T_{10})\right] \quad \text{[kW]} \quad \textbf{(3.113)}$$

[39] η_p & η_t are applied in order for the ideal conditions assumed at nodes 48/61, 49 and 51.
[40] T_{out} of the heat exchanger on the BC side is assumed to be less than T_{out} of the heat exchanger on the steam side (Cengel, 2006).

$$\dot{W}_{HP,t} = \dot{m}_{15}h_{15}^{sh,g}(P_{15};T_{15}) - \dot{m}_{18}h_{18}^{sh,g}(P_{18};T_{18}) - \dot{m}_{21}h_{21}^{sh,g}(P_{21};T_{21}) - \dot{m}_{26}h_{26}^{sh,g}(P_{26};T_{26}) - \dot{m}_{31}h_{31}^{sh,g}(P_{31};T_{31}) - \dot{m}_{63}h_{63}^{sh,g}(P_{63};s_{63}) - \dot{m}_{62}h_{62}^{sat,fg}(P_{62};x_{62})$$ [kW] **(3.114)**

$$\dot{W}_{p,cond} = \dot{m}_{47}\left[h_{47}^{sat.f}(T_{47}) - h_{8}^{c,f}(P_8;T_8)\right]$$ [kW] **(3.115)**

$$\dot{m}_{62} = \dot{m}_{15} - \dot{m}_{18} - \dot{m}_{21} - \dot{m}_{26} - \dot{m}_{31} - \dot{m}_{63}$$ [kg/s] **(3.116)**

Equations related to the BC cycle are as follows:

$$\dot{W}_{BC,t} = \dot{m}_{BC}\eta_t(h_{64} - h_{49})$$ [kW] **(3.117)**

$$\dot{W}_{BC,p} = \dot{m}_{BC}\left(\frac{1}{\eta_p}\right)(h_{50} - h_{51}) \,/\, \frac{1}{\eta_p}\dot{m}_{BC}v_{50}(P_{50} - P_{51})$$ [kW] **(3.118)**

$$\dot{m}_{BC} = \frac{\dot{m}_{63}h_{65} - \dot{m}_{62}h_{47} + \dot{m}_{62}h_{62}}{h_{48/61} - h_{51}}$$ [kg/s] **(3.119)**

$$\dot{m}_{63} = \frac{\dot{m}_{BC}(h_{64} - h_{48/61})}{h_{63} - h_{65}}$$ [kg/s] **(3.120)**

An optimum tap-off mass flow rate is obtained where the thermal efficiency for this configuration reaches a maximum for the tap-off pressure and related tap-off mass flow rate.

3.3.5.7.2 Tap-off from the high-pressure turbine and FWHs

The addition of FWHs to the theoretical cycle discussed in Section 3.3.5.7.1 should increase the thermal efficiency of the cycle even further. In the section that follows, FWHs are added to the theoretical configuration indicated in Figure 3.42.

Figure 3.45 indicates this theoretical configuration. The steam cycle's properties will remain as indicated in Section 3.3.5.7.1 and Table 3.26. The tap-off pressure from the steam cycle, P_{63}, is fixed in this section at the tap-off pressure where maximum thermal efficiency was achieved for the specific working fluid.

For this configuration, the BC cycle side is analysed as indicated in Section 3.3.5.2. However, the inlet temperature of the BC turbine is higher for this configuration. Consequently, the FWH tap-off pressure range ($P_{4\,9} < P_{58} < P_{64}$) is larger and is again a function of the properties of the working fluid.

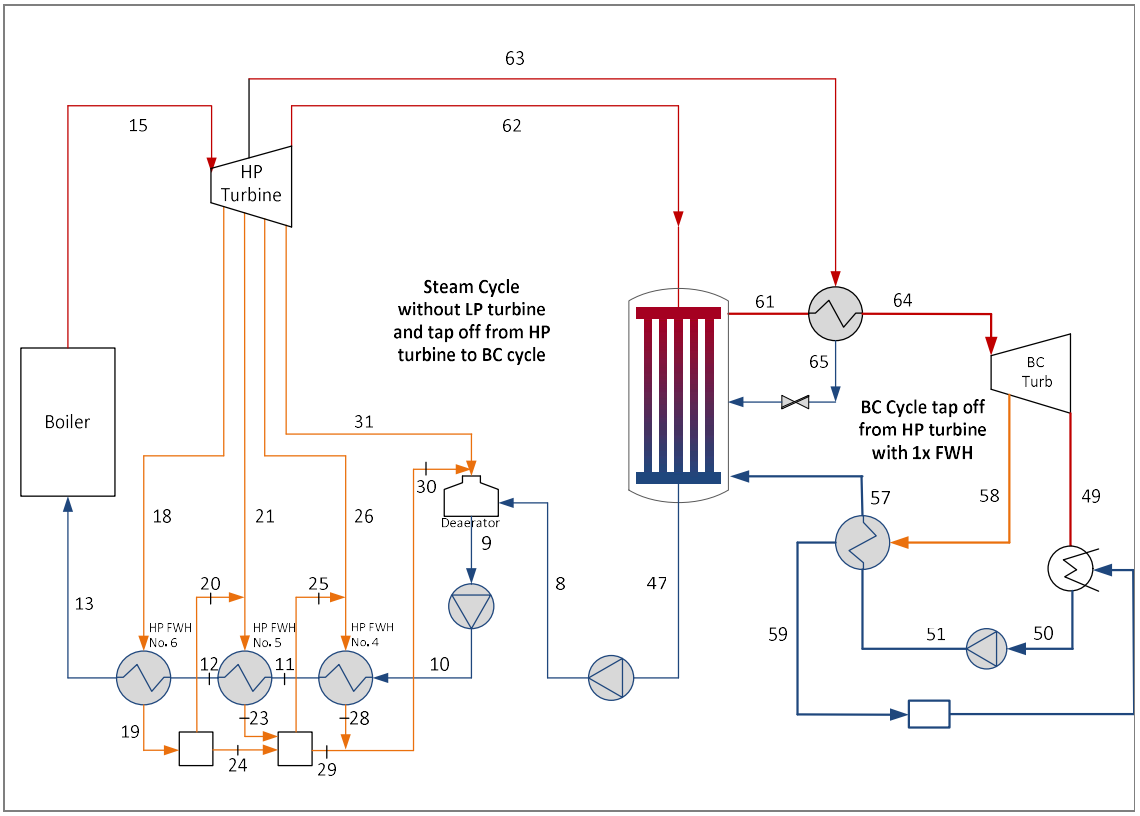

Figure 3.45: Component diagram of the Komati Power Station without a low-pressure turbine and tap-off from a high-pressure turbine into the BC cycle, and a BC cycle and one FWH

This configuration was tested with only one, two and three FWHs because the results of the cycle without a FWH, as indicated in Section 3.3.5.6.1, heeded an indication of an increase in thermal efficiency. Consequently, the theoretical cycle, the BC cycle with tap-off in a high-pressure turbine and without the low-pressure turbine, but with two and three FWHs, is expected to indicate an even further increase in thermal efficiency.

The implementation of FWHs was explained in detail in Section 3.3.5.2. For illustrative purposes, the cycle with one FWH is discussed in more detail. However, the cycle with two and three FWHs will follow the same method as indicated in Section 3.3.5.2. It will therefore not be necessary to go into further detail on this configuration in this chapter. However, the theoretical configuration will be indicated and briefly discussed.

The properties at each node of the BC cycle are indicated in Table 3.28. The assumptions made for each node are also indicated in this table.

Scenario 1			Scenario 2		
Node	**Temperature (°C)**	**Assumption**	**Node**	**Temperature (°C)**	**Assumption**
48	120	$s_{48} = s_{49,i}$ $P_{48}@(T_{48},s_{48})$ [kPa] $h_{48,i}@(T_{48},s_{48,i})$ [kJ/kg][41]	**61**	120	$x_{60}=1$ P_{60} = Sat. P@T_{60} [kPa] $h_{60}@(P_{60},x_{60})$ [kJ/kg]
49	36	$x_{49}=0.9$ P_{49} = Sat.P @T_{49} [kPa] $h_{49}@(T_{49},x_{49})$ [kJ/kg]	**49**	36	$s_{49,i}=s_{61}$ $P_{49} = P_{50}$ $h_{49,i}@(P_{49},s_{49,i})$[36] $x_{49}@(P_{49},s_{49})$
50	36	$x_{50}=0$ $P_{50} = P_{49}$ $h_{50}@(T_{50},x_{50})$ [kJ/kg] $v_{50}@(T_{50},x_{50})$ [m^3/kg]	**50**	36	$x_{50}=0$ P_{50} = Sat.P @T_{50} [kPa] $h_{50}@(T_{50},x_{50})$ [kJ/kg]
51	f(assump.)	$P_{51} = P_{48}$ $v_{51}=v_{50}$ (incompressible liquid and small temperature difference) $h_{51} = \left(\frac{1}{\eta_p} v_{51}[P_{51} - P_{50}]\right) + h_{50}$	**51**	f(assump.)	$s_{51,i}=s_{50}$ $P_{51}=P_{61}$ $h_{51,i}@(P_{51},s_{51,i})$[36]
64	$T_{64}=T_{65}$ - 6 [42]	$P_{64}=P_{51}$ $h_{64}@(T_{64},P_{64})$ [kJ/kg]	**64**	$T_{64}=T_{65}$ - 6 [37]	$P_{64}=P_{51}$ $h_{64}@(T_{64},P_{64})$ [kJ/kg]
57	$T_{57}=T_{59}$ [43]	$P_{57}=P_{51}$ $h_{57}@(T_{57},P_{57})$ [kJ/kg]	**57**	$T_{57}=T_{59}$ [38]	$P_{57}=P_{51}$ $h_{57}@(T_{57},P_{57})$ [kJ/kg]
58	f(assump.)	$P_{58}=P_{guess}$ ($P_{52}<P_{58}<P_{49}$) $s_{58,i}=s_{52}$[29] $h_{58}@(s_{58},P_{58})$ [kJ/kg]	**58**	f(assump.)	$P_{58}=P_{guess}$ ($P_{52}<P_{58}<P_{49}$) $s_{58,i}=s_{52}$[29] $h_{58}@(s_{58},P_{58})$ [kJ/kg]
59	$T_{59}=T_{sat}@P_{59}$	$x_{59}=0$ $P_{59}=P_{58}$ $h_{59}@(x_{59},P_{59})$ [kJ/kg]	**59**	$T_{59}=T_{sat}@P_{59}$	$x_{59}=0$ $P_{59}=P_{58}$ $h_{59}@(x_{59},P_{59})$ [kJ/kg]

Table 3.28: The state of each node for the BC cycle without a low-pressure turbine, and tap-off from the steam-side high-pressure turbine for scenarios 1 and 2, and FWHs in the BC cycle, including the assumptions made

Equations 3.114 to 3.122, 3.124 and 3.126, which are indicated in Section 3.3.5.7.1, are used in the analysis of this cycle. The additional equations indicated below will apply to this configuration with the addition of a FWH.

$$\dot{W}_{BC,t} = \eta_t[\dot{m}_{BC}h_{64} - \dot{m}_{58}h_{58} - (\dot{m}_{BC} - \dot{m}_{58})h_{49}] \quad \text{[kW]} \quad \textbf{(3.121)}$$

$$\dot{m}_{BC} = \frac{\dot{m}_{62}h_{62} - \dot{m}_{47}h_{47} + \dot{m}_{65}h_{65}}{h_{48/61} - h_{51}} \quad \text{[kg/s]} \quad \textbf{(3.122)}$$

[41] A turbine and pump efficiency is applied in the calculations to compensate for the ideal conditions assumed at nodes 48, 49, 51 and 58.
[42] T_{out} of the heat exchanger on the BC side is assumed to be less than T_{out} of the heat exchanger on the steam side (Cengel, 2006).
[43] (Sonntag, et al., 2003)

$$\dot{m}_{58} = \dot{m}_{BC}\left(\frac{h_{57}-h_{51}}{h_{58}-h_{59}}\right) \quad \text{[kg/s]} \quad \textbf{(3.123)}$$

3.4 Conclusion

Chapter 3 discussed the methods used to theoretically analyse the proposed application of the BC at the Komati Power Station. The method and assumptions are also indicated in this section.

Nineteen configurations were tested in which the BC was implemented. For each configuration, several different working fluids were tested. A total of 103 working fluids were tested in the simple BC cycle and 71 of these fluids indicated usable results. The 71 working fluids were tested in all other configurations.

The tested configurations included concepts such as regeneration, including heat exchangers in the BC cycle where steam is tapped off from the steam cycle, and FWHs in the BC cycle, with tap-off from the BC turbine. The tested configurations included the following:

- A Configuration of simple BC cycle
- A Simple BC cycle without low-pressure turbine
- A BC cycle with Regeneration
- A BC cycle without a low-pressure turbine and with regeneration or feedwater heating
- A BC cycle with FWHs
- A BC cycle without low-pressure turbine and FWHs
- A BC cycle with tap-off from a low-pressure turbine
- A BC cycle with Tap-off from low-pressure turbine and FWHs
- A BC cycle with tap-off before low-pressure turbine
- A BC cycle with Tap-off before low-pressure turbine and FWHs
- A BC cycle with tap-off in high-pressure turbine
- BC cycle with tap-off in a high-pressure turbine and FWHs
- BC cycle with tap-off in a high-pressure turbine and without the low-pressure turbine
- BC cycle without a low-pressure turbine and tap-off from a high-pressure turbine and FWHs

More than one FWH was also added to certain configurations, which were chosen due to the increase in thermal efficiency without a FWH.

Figure 3.46 indicates the configurations discussed in Chapter 3. These configurations are mapped out to indicate the process in Chapter 4. The tested configurations indicated an increase in thermal efficiency. The results are discussed in Chapter 4.

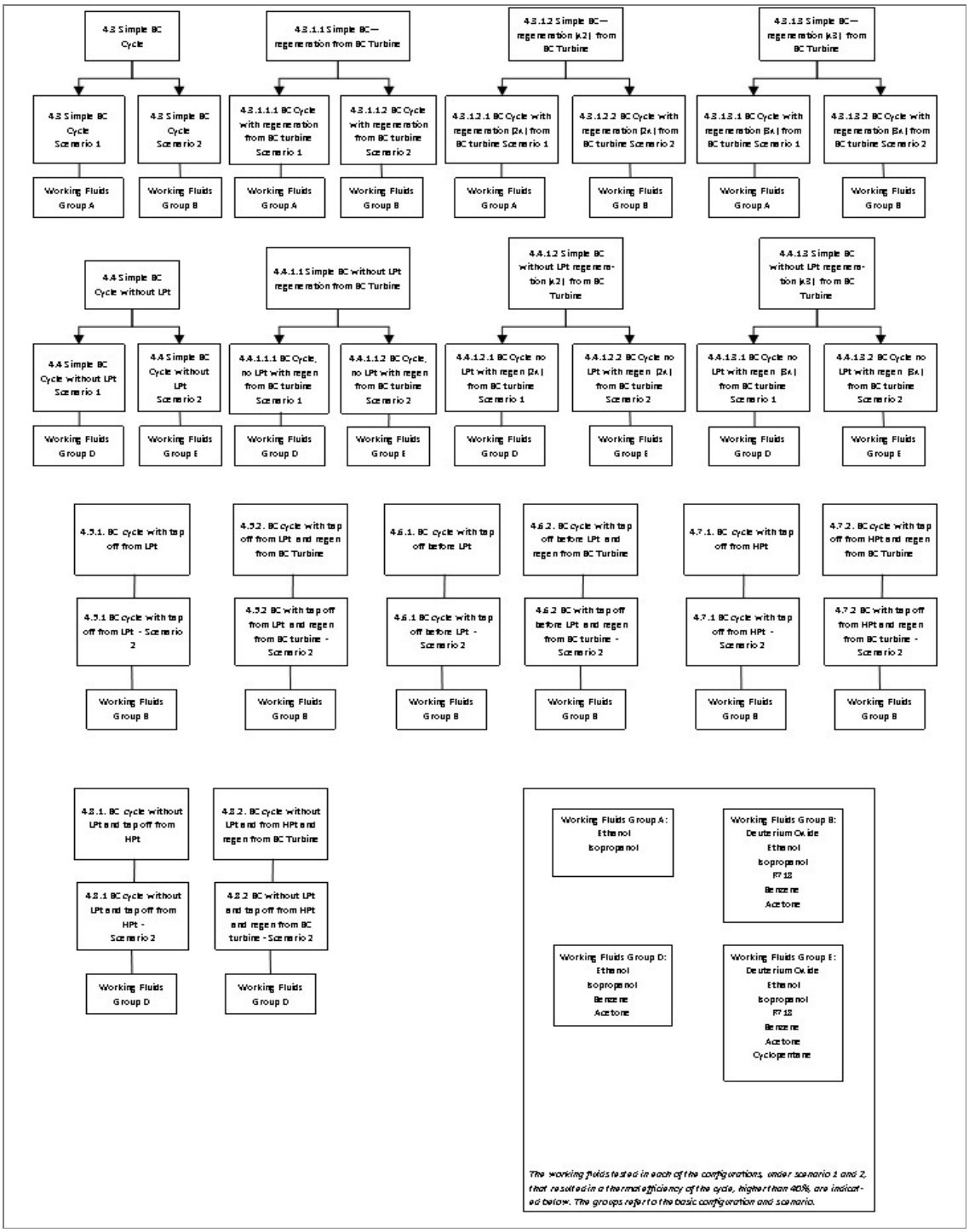

Figure 3.46: Map of the tested configurations

4. RESULTS OF ANALYSIS

4.1 Introduction

The purpose of this chapter is to discuss the results obtained by implementing the BC method to utilise low-grade waste heat from Komati Power Station's thermal power plant. The configurations and working fluids that indicated a thermal efficiency higher than 40%, the thermal efficiency of Komati Power Station's Unit 6, are discussed in this chapter. A diagram of the tested configuration is indicated in Annexure A. The configurations and working fluids that did not indicate a thermal efficiency higher than 40% are indicated in Appendix B, along with the results obtained for the configurations that had a tap-off pressure range, with the corresponding thermal efficiency of each tap-off pressure.

4.2 Modified cycle

The modified system discussed in Section 3.3.1 is indicated again in Figure 4.1 below.

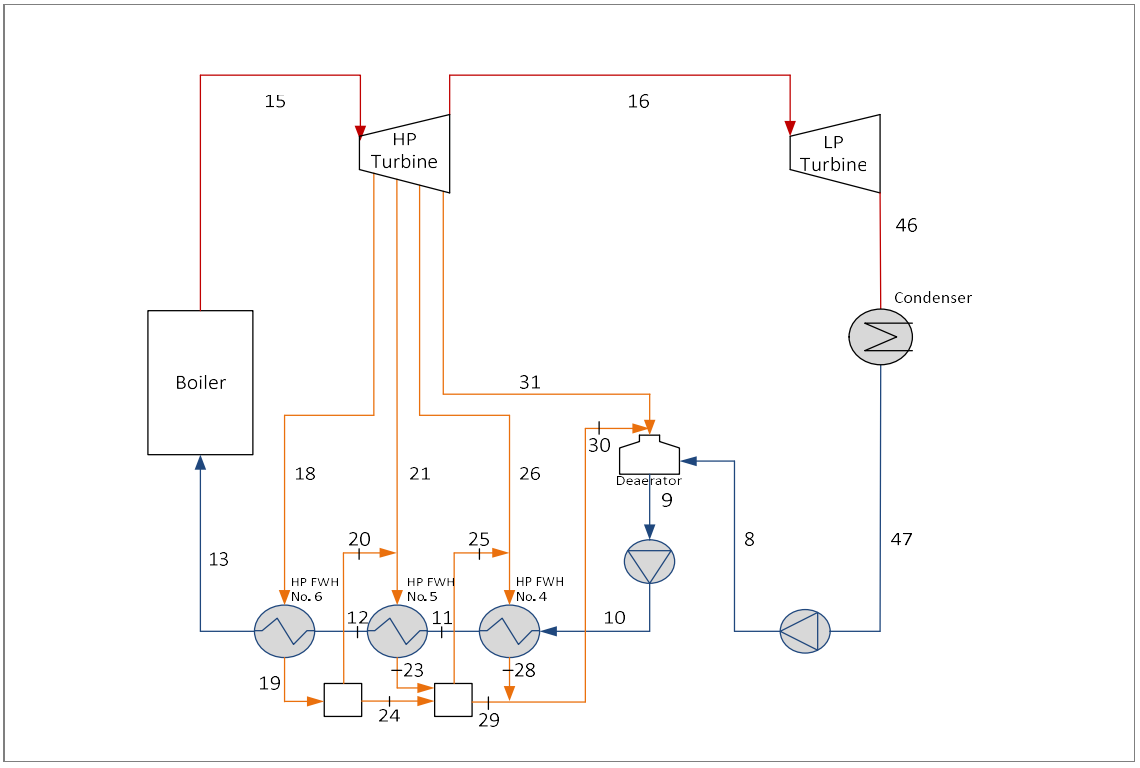

Figure 4.1: Component diagram of the modified thermal cycle

As mentioned, Komati Power Station's thermal cycle was theoretically modified slightly to accommodate the BC. The modified cycle was analysed to serve as a basis for the implementation of the BC cycle. The results of the analysis are indicated in Table 4.1, along with the results of the original cycle to serve as a reference for comparison against the modified cycle and the rest of the theoretical cycles indicated in this section.

Original steam cycle	
$\dot{Q}_{condenser}$	191 412 kW
$\dot{Q}_{boiler}$	318 187 kW
$\dot{Q}_{Fuel}$	382 940 kW
$\dot{W}_{total\ turbine}$	128 931 kW
η_{Carnot}	60.52%
$\eta_{Thermal}$	40.0%
$\eta_{Thermal\ with\ fuel\ heat}$	33.24%

Modified steam cycle	
$\dot{Q}_{condenser}$	217 975 kW
$\dot{Q}_{boiler}$	318 187 kW
$\dot{Q}_{Fuel}$	382 940 kW
$\dot{W}_{total\ turbine}$	100 312 kW
η_{Carnot}	51.85%
$\eta_{Thermal}$	31.53%
$\eta_{Thermal\ with\ fuel\ heat}$	26.2%

Table 4.1: Analysis of the original steam cycle and modified steam cycle

4.3 Configuration of simple BC cycle

The theoretical configuration, where the BC was implemented at the Komati Power Station, is indicated again in Figure 4.2.

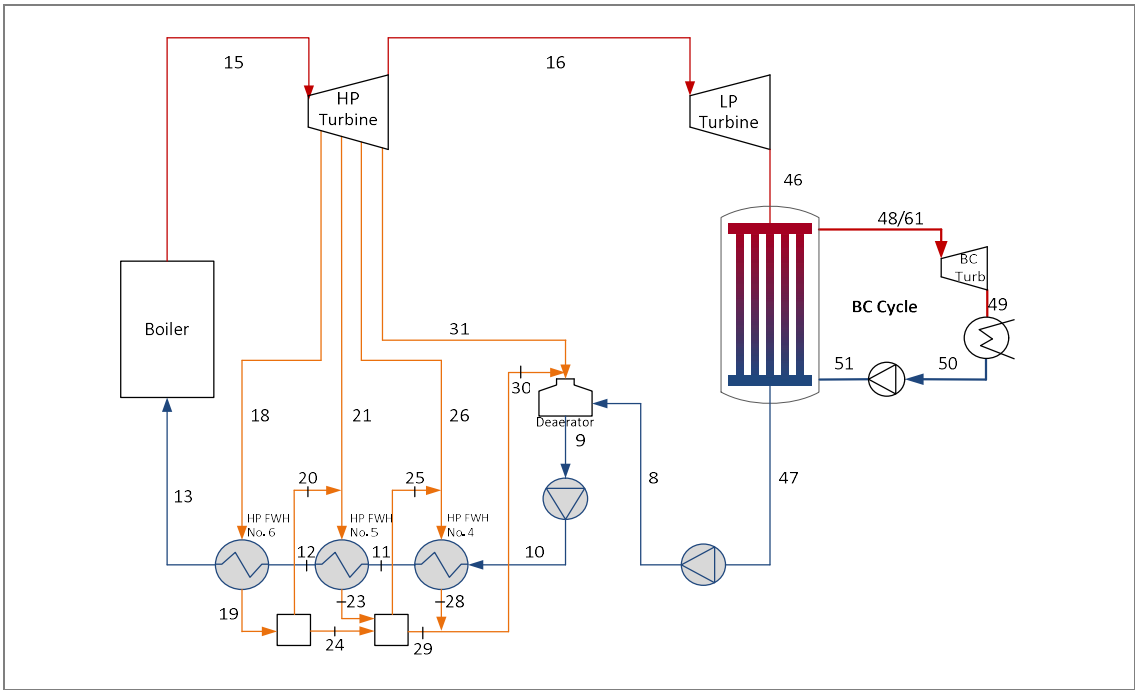

Figure 4.2: Component diagram of the Komati Power Station with a BC

It was mentioned that the BC cycle was tested in two scenarios: where the outlet conditions of the BC turbine were fixed at 36 °C with a quality 0.9, and where the inlet of the BC turbine was fixed as a saturated vapour at 100 °C. A relatively small increase in thermal efficiency was obtained for this configuration with these two scenarios when tested with the working fluids that were listed in Section 3.3.2 and Table 3.4: Working fluids tested on the BC cycle .

Scenario 1, where the outlet of the BC turbine was fixed, indicated a maximum increase of 0.4%. Therefore, the maximum thermal efficiency of the BC cycle for Scenario 1 was 40.4%. The working fluid tested in the BC cycle that produced the higher efficiency was ethanol. Only two working fluids tested in the mentioned configuration indicated an efficiency higher than 40%. The results for Scenario 1 are indicated in Table 4.2.

The theoretical implementation of the BC cycle on Komati Power Station's Unit 6 under the assumptions described for Scenario 2 also indicated an increase in thermal efficiency. The working fluids listed in Table 3.4 were tested. Six of the tested working fluids indicated an increase in thermal efficiency above 40%. The results are indicated in Table 4.2. A maximum increase of 0.83% was achieved for this configuration with assumptions made for Scenario 2, indicating a maximum thermal efficiency of 40.83% for the working fluid R718.

	Working fluid	$\eta_{th,BC}$[44]	Efficiency increase	Gain in useful work (kW)	$\dot{m}_{BC}$ (kg/s)
Scenario 1: Outlet of BC turbine fixed	Ethanol	40.4	0.4	1 296	228.6
	Isopropanol	40.1	0.1	260	286
Scenario 2: Inlet of BC turbine fixed	R718	40.83	0.83	2 621	87.86
	Deuterium oxide	40.76	0.76	2 428	94.71
	Ethanol	40.43	0.43	1 362	223.6
	Isopropanol	40.16	0.16	517.9	267.7
	Benzene	40.14	0.14	428.1	445.5
	Acetone	40.08	0.08	242.1	373.4

Table 4.2: Results of the analysis conducted on the Komati Power Station when implementing a simple BC cycle

In addition to the increase in efficiency and the increase in useful work is also indicated in Table 4.2. It is clear that, as the gain in useful work increases, the thermal efficiency of the cycle also increases.

The mass flow rates required for the BC cycle for this configuration is relatively low, which indicates that the equipment necessary for this cycle could be small and consequently, more economically viable.

The results from this chapter indicate that the implementation of the BC cycle increased the thermal efficiency of Komati Power Station. It is therefore worthwhile to continue with the

[44] Refer to the figure related to the discussed configuration to associate the thermal efficiency indicated to the specific tested configuration.

mentioned configurations to theoretically test whether a further increase in thermal efficiency can be achieved.

4.3.1 Simple BC cycle with regeneration from the BC turbine

4.3.1.1 Simple BC cycle with regeneration (one FWH) from the BC turbine

The working fluids tested in the simple BC cycle, which indicated an increase in thermal efficiency of above 40% (see Table 4.2), are tested in the theoretical configuration where regeneration from the BC turbine is implemented on the cycle under the Scenario 1 and Scenario 2 assumptions discussed in Chapter 3. These working fluids are ethanol and isopropanol.

The benefits of an increase in thermal efficiency are discussed in further detail in Chapter 5, along with the appropriateness of the working fluids that indicated an increase for the suggested theoretical configuration.

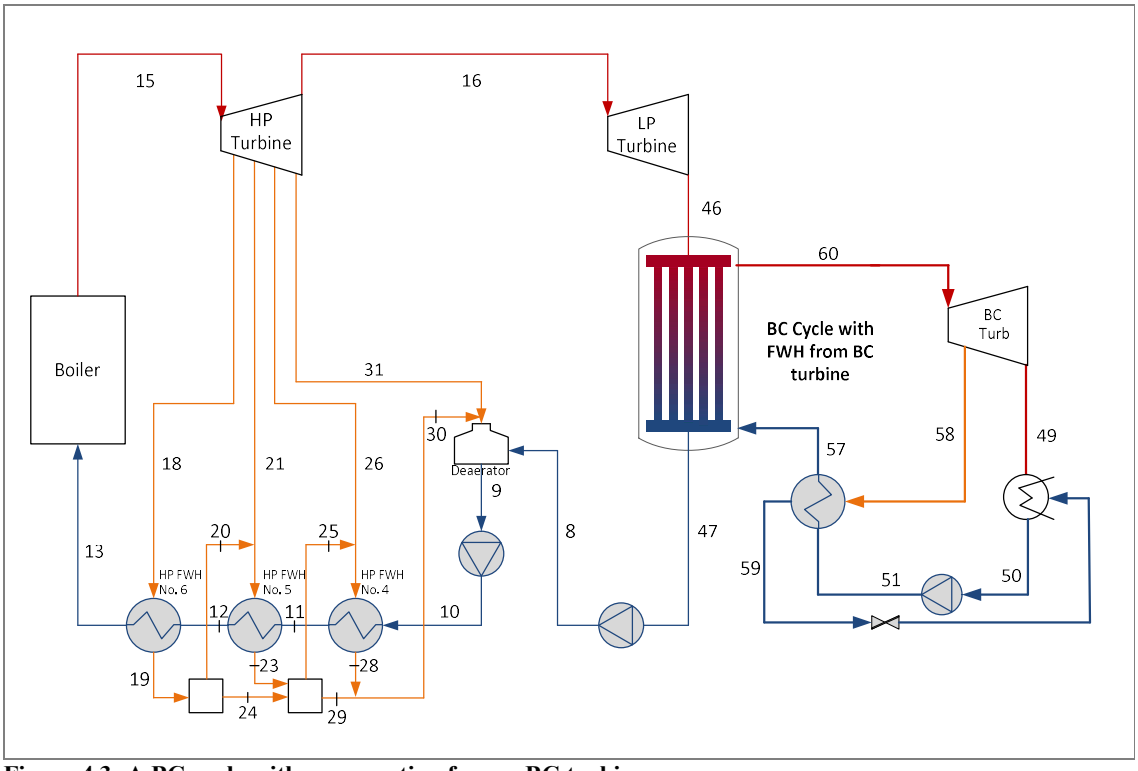

Figure 4.3: A BC cycle with regeneration from a BC turbine

It should be noted that the results of implementing one, two or three FWHs are indicated and discussed fully for this configuration to show the range of tap-off mass flow rates and differences obtained for each working fluid for each configuration. The maximum thermal efficiencies and corresponding results obtained for any consequent configurations that included

FWHs will only be tabulated as the final data obtained for consequent configurations with FWHs presented similar to that indicated in Figure 4.4 and Figure 4.5. Figures, similar to and Figure 4.5 of the results obtained for the consequent configurations are indicated in Annexure B.

As mentioned, the configurations with regeneration from the BC turbine or feed water heating were tested under the assumptions of scenarios 1 and 2. Scenario 1 assumptions fixed the outlet of the BC turbine under certain conditions and Scenario 2 conditions fixed the inlet of the BC turbine under certain conditions. The results for each scenario are indicated and discussed below.

4.3.1.1.1 Simple BC cycle with regeneration from BC turbine – Scenario 1

The results from the working fluids tested under Scenario 1 assumptions in the configuration shown in Figure 4.3 are indicated in Figure 4.4, where the tap-off mass flow rate calculated for each tap-off pressure is indicated against the cycle's thermal efficiency at each specific tap-off mass flow rate. As discussed in Chapter 3, a maximum thermal efficiency is obtained within this range of tap-off pressures. The range of tap-off pressure is specific to each working fluid and scenario. The tap-off pressure from the BC turbine to the FWH ranged from the BC turbine inlet pressure to the BC turbine outlet pressure.

The tap-off pressure for the two working fluids tested under Scenario 1 assumptions was 14.65 to 224.7 kPa for ethanol and 11.56 to 194 kPa for isopropanol. The tap-off pressures were determined based on the assumptions discussed in Chapter 3. These are shown again in Table 4.3 for ease of reference. The maximum efficiency for the tap-off pressure range for each working fluid was determined by means of the method discussed in Chapter 3.

Scenario 1		
Node	**Temperature (°C)**	**Assumption**
60	100	$s_{48} = s_{49,i}$ & $P_{48}@(T_{48},s_{48})$ [kPa] $h_{48,i}@(T_{48},s_{48,i})$ [kJ/kg]
49	36	x_{49}=0.9 & P_{49} = Sat.P @T_{49} [kPa] $h_{49}@(T_{49},x_{49})$ [kJ/kg]

Table 4.3: Nodal information for a BC cycle under Scenario 1 assumptions

Theoretically, implementing one FWH had a significant influence on the overall thermal efficiency of the cycle. The configuration with ethanol as a working fluid indicated a 2.06% increase in thermal efficiency compared to the original thermal efficiency of the cycle and a 1.66% increase in thermal efficiency compared to the simple BC cycle. The optimum thermal

efficiency for this configuration was obtained at a tap-off pressure of 58.39 kPa, with a corresponding tap-off mass flow rate of 22.95 kg/s.

Working fluid	$\eta_{th,\,BC}$[45]	Efficiency increase	Gain in useful work (kW)	$\dot{m}_{BC}$ (kg/s)	$\dot{m}_{58}$ (kg/s)	P_{58} (kPa)
Ethanol	42.062271	2.062271	6 556	242.6652	22.95	58.39
Isopropanol	41.854954	1.854954	5 896	309.4241	36.51	42.29

Table 4.4: Results of the analysis conducted on the Komati Power Station with tap-off from a BC turbine when implementing regeneration on a simple BC cycle under Scenario 1 assumptions

Figure 4.4 indicates the efficiency for the range of tap-off pressures from the BC turbine. It can be seen that the tap-off pressure range is unique to each working fluid and that the maximum efficiency is achieved at a tap-off pressure unique to each working fluid within the tap-off pressure range.

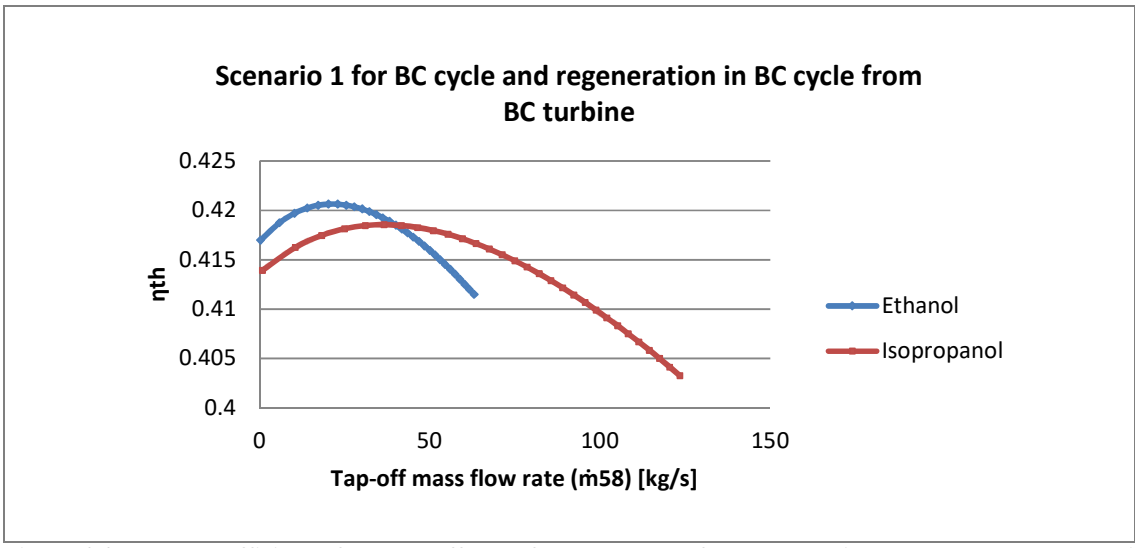

Figure 4.4: Thermal efficiency for a tap-off mass flow rate range for the analysis conducted on the Komati Power Station, with regeneration in a BC cycle from a BC turbine under Scenario 1 assumptions

4.3.1.1.2 Simple BC cycle with regeneration from the BC turbine – Scenario 2

Similarly, the working fluids that were tested in the simple BC cycle, under Scenario 2 assumptions, which indicated an increase in thermal efficiency above 40%, were tested in the theoretical configuration indicated in Figure 4.3.

[45] Refer to the figure related to the discussed configuration to associate the thermal efficiency indicated to the specific tested configuration.

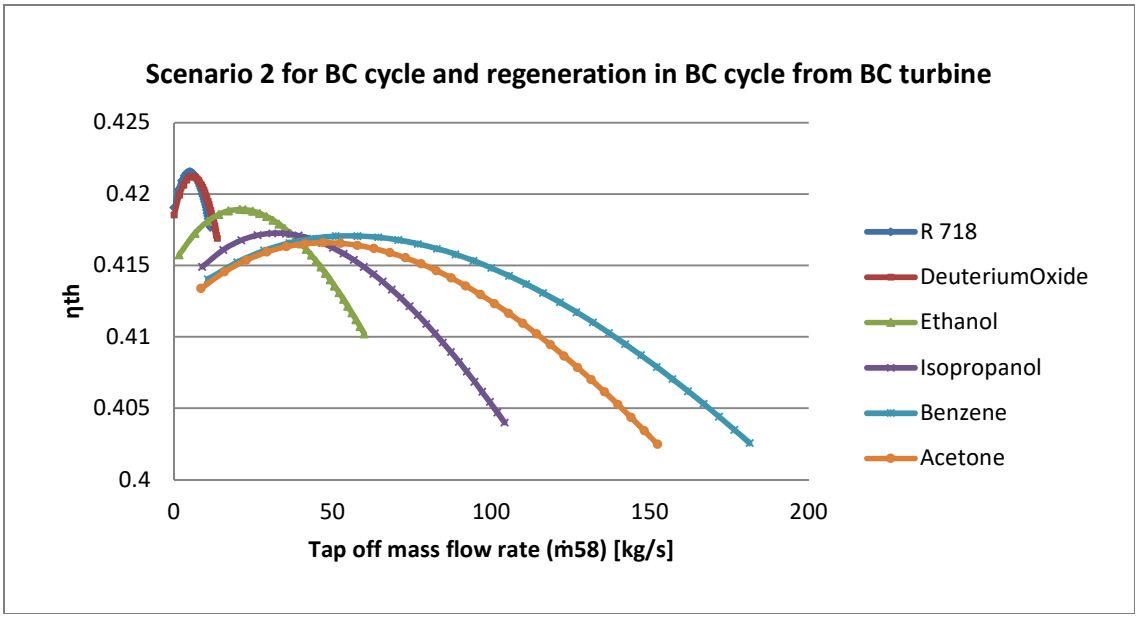

Figure 4.5: Thermal efficiency for the tap-off mass flow rate range for the analysis conducted on the Komati Power Station, with regeneration in a BC cycle from a BC turbine under Scenario 2 assumptions

The analysis was conducted as described in Chapter 3 and the tap-off pressure from the BC turbine feeding into the FWH was based on the assumptions shown again in Table 4.6. The tap-off pressure range was to be between the BC cycle turbine inlet and outlet pressures, i.e. P_{60} and P_{49}.

Scenario 2		
Node	**Temperature (°C)**	**Assumption**
60	100	$x_{60}=1$ & P_{60} = Sat. P@T_{60} [kPa] $h_{60}@(P_{60},x_{60})$ [kJ/kg]
49	36	$s_{49,i}=s_{61}$; $P_{49} = P_{50}$ $h_{49,i}@(P_{49},s_{49,i})$ & $x_{49}@(P_{49},s_{49})$

Table 4.5: Results of the analysis conducted on the Komati Power Station with tap-off from a BC turbine when implementing regeneration on a simple BC cycle under Scenario 1 assumptions

An optimum thermal efficiency is obtained within this tap-off pressure and corresponding mass flow rate range. Again, it can be seen that each working fluid tested in this configuration indicated a maximum thermal efficiency at a specific tap-off pressure and corresponding mass flow rate. The maximum thermal efficiency achieved for each tested working fluid is indicated in Table 4.6.

Working fluid	$\eta_{th,BC}$[46]	Efficiency increase	Gain in useful work (kW)	$\dot{m}_{BC}$ (kg/s)	$\dot{m}_{58}$ (kg/s)	P_{58} (kPa)
R718	42.1562	2.1562	6 854	91.41034	4.93592	24.45
Deuterium oxide	42.1247	2.1247	6 754	98.89942	5.77453	22.13
Ethanol	41.8922	1.8922	6 015	239.31767	20.78587	55.01
Isopropanol	41.726	1.726	5 486	292.44217	32.49091	43.34
Benzene	41.7073	1.7073	5 426	487.70581	55.47995	56.18
Acetone	41.6588	1.6588	5 272	409.54504	47.57585	122.53

Table 4.6: Results of the analysis conducted on the Komati Power Station with tap-off from a BC turbine when implementing regeneration on a simple BC cycle under Scenario 2 assumptions

It can be seen that the working fluid R718 indicated the highest increase in efficiency for this specific configuration with an increase of 2.16% compared to the thermal efficiency of the original cycle. This efficiency was achieved at a tap-off pressure of 24.45 kPa and a corresponding tap-off mass flow rate of 4.93 kg/s.

Implementing the FWH on the BC cycle under Scenario 2 assumptions increased the thermal efficiency of the cycle by 1.33% compared to the thermal efficiency of the simple BC cycle under Scenario 2 assumptions.

An increase of 6.85 MW in useful work was achieved with this working fluid in this configuration.

4.3.1.2 Simple BC cycle with regeneration (two FWHs) from the BC turbine

The theoretical configuration was tested with an additional FWH, as described in Chapter 3. An additional FWH was added in the BC cycle between the outlet of the pump and the first FWH, as indicated in Figure 4.6.

[46] Refer to the figure related to the discussed configuration to associate the thermal efficiency indicated to the specific tested configuration.

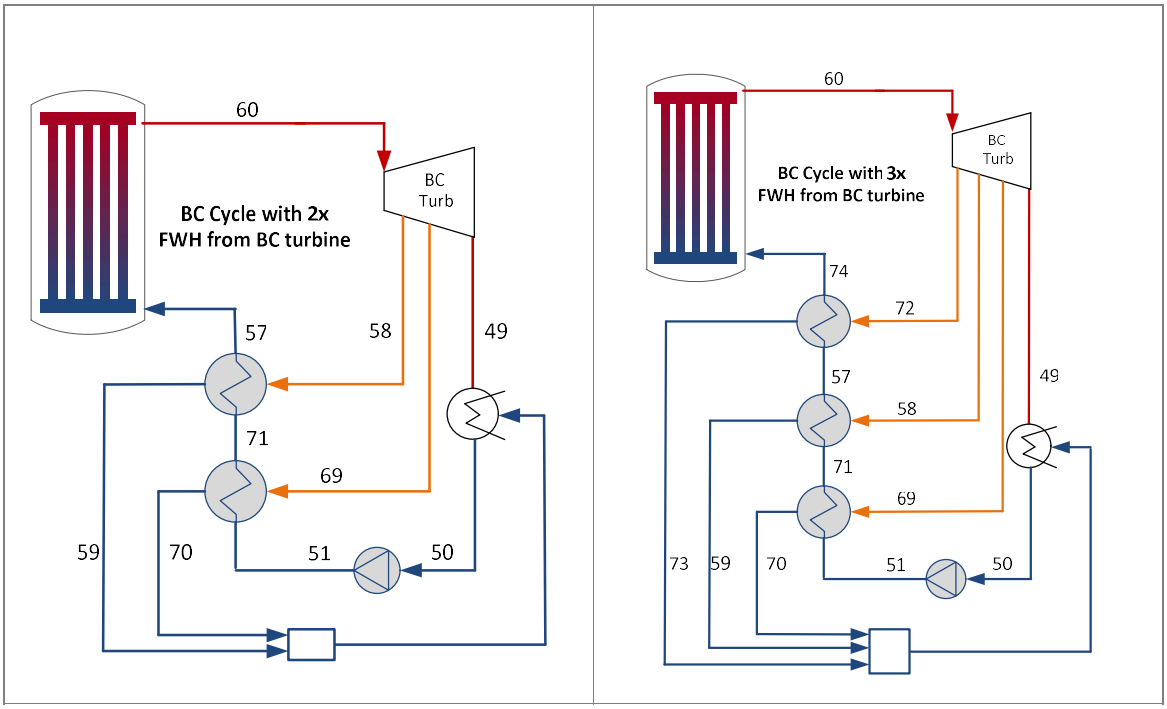

Figure 4.6: A BC cycle with two and three FWHs

This theoretical configuration, where a second FWH was added to the cycle, was also tested under Scenario 1 and Scenario 2 assumptions. The results are discussed below.

4.3.1.2.1 BC cycle with regeneration (two FWHs) from the BC turbine – Scenario 1

The working fluids tested for the configuration indicated in Figure 4.3 were also tested under Scenario 1 assumptions for the configuration indicated in Figure 4.6. Ethanol and isopropanol were therefore tested with the assumptions and method discussed in Chapter 3.

The tap-off pressure from the BC turbine to the second FWH was therefore in the pressure range between P_{58} and P_{49}, where P_{58} and P_{49} were specific to each working fluid. P_{58} specifically was determined, as discussed in Section 4.3.1.1.1 and fixed at the tap-off pressure that resulted in the maximum thermal efficiency of the cycle for each working fluid. Similar to the configuration of one FWH, the maximum thermal efficiency of the cycle with the additional FWH was also achieved within the tap-off pressure range and corresponding mass flow rate range. Figure 4.7 indicates the thermal efficiency of the cycle for the tap-off mass flow rate range applicable to each working fluid tested in the configuration.

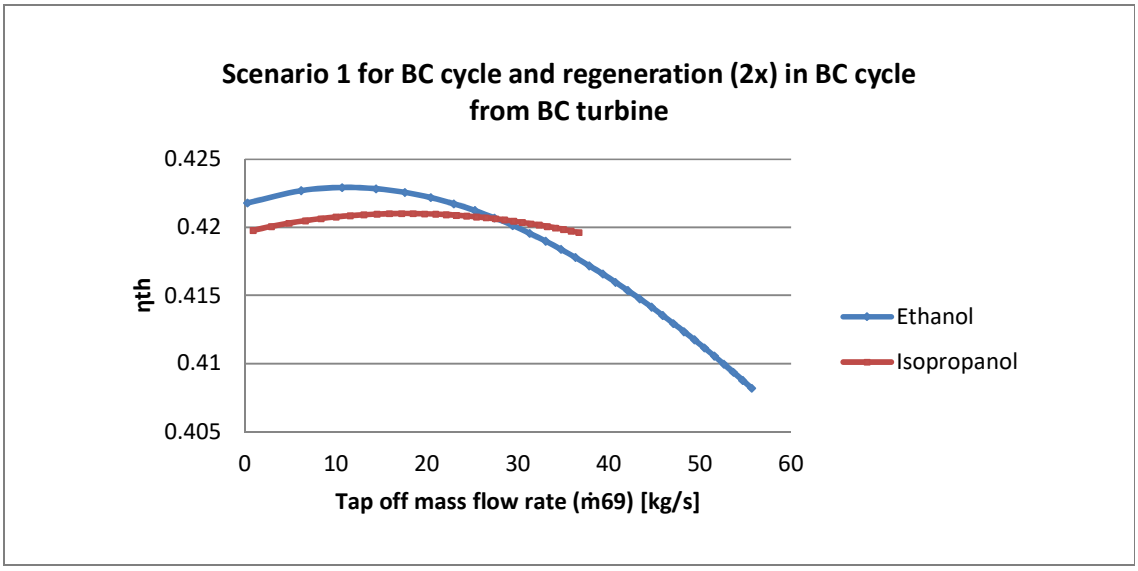

Figure 4.7: Thermal efficiency for a tap-off mass flow rate range for analysis conducted at the Komati Power Station, with regeneration (two FWHs) in a BC cycle from a BC turbine under Scenario 1 assumptions

The maximum thermal efficiency obtained for this configuration, along with the conditions related to the maximum thermal efficiency, is indicated in Table 4.7.

The maximum thermal efficiency achieved with a second FWH under Scenario 1 assumptions was 42.29%, which is an increase of 2.29% compared to the original thermal efficiency of the cycle and an increase of 0.23% in thermal efficiency compared to the BC cycle with one FWH under Scenario 1 assumptions. These results were achieved by theoretically implementing ethanol as a working fluid.

Again, it can be seen that the increase in useful work of 7,2 MW was theoretically achieved this configuration and assumptions.

Working fluid	$\eta_{th,\,BC}$[47]	Efficiency increase	Gain in useful work (kW)	$\dot{m}_{BC}$ (kg/s)	$\dot{m}_{69}$ (kg/s)	P_{69} (kPa)
Ethanol	42.293159	2.293159	7 290	245.1175	10.68	29.46
Isopropanol	42.102155	2.102155	6 683	312.5126	17.2	22.51

Table 4.7: Results of the analysis conducted on the Komati Power Station with tap-off from a BC turbine when implementing regeneration (two FWHs) on a simple BC cycle under Scenario 1 assumptions

4.3.1.2.2 BC cycle with regeneration (two FWHs) from the BC turbine – Scenario 2

The analysis of the configuration where a second FWH was added to the BC cycle was similarly conducted under Scenario 2 assumptions. The six working fluids that indicated an increase in thermal efficiency were also tested in this configuration. As mentioned, the tap-off pressure,

[47] Refer to the figure related to the discussed configuration to associate the thermal efficiency indicated to the specific tested configuration.

which ranged from P_{58} to P_{49}, was unique to each working fluid and a maximum thermal efficiency was obtained for each working fluid within this tap-off range. The thermal efficiency achieved for each tap-off pressure's corresponding mass flow rate for each working fluid tested in this configuration is indicated in Figure 4.8.

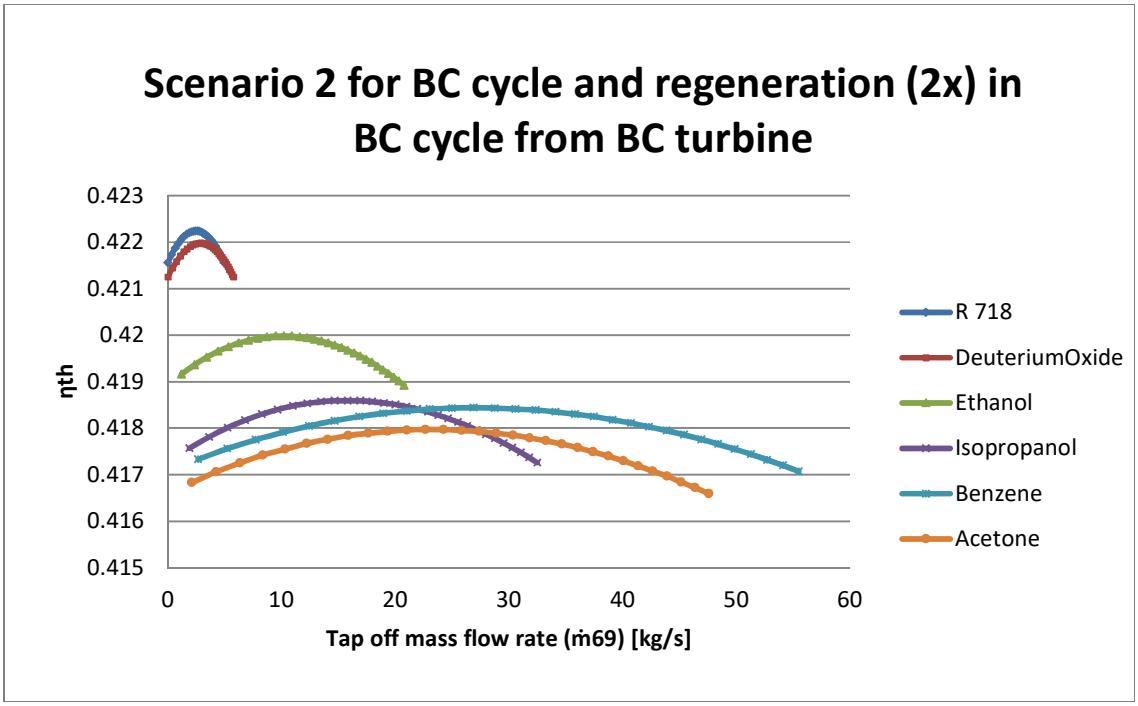

Figure 4.8: Thermal efficiency for the tap-off mass flow rate range for the analysis conducted at the Komati Power Station, with regeneration (two FWHs) in a BC cycle from a BC turbine

The maximum thermal efficiency obtained for this configuration for each working fluid tested is indicated in Table 4.8. R718 again indicated the highest thermal efficiency at 42.22% with an increase of 2.22% compared to the original steam cycle and an increase of 0.067% compared to the configuration where the BC cycle included only one FWH.

Working fluid	$\eta_{th,\ BC}$	Efficiency increase	Gain in useful work (kW)	$\dot{m}_{BC}$ (kg/s)	$\dot{m}_{69}$ (kg/s)	P_{69} (kPa)
R718	42.224	2.224	7 070	91.41044	2.47054	12.3663
Deuterium oxide	42.198	2.198	6 987	98.89942	2.8888	11.0319
Ethanol	41.998	1.998	6 352	239.3177	10.16281	29.3947
Isopropanol	41.859	1.859	5 910	292.4422	15.77852	23.208
Benzene	41.844	1.844	5 860	487.7058	26.99051	34.95478
Acetone	41.797	1.797	5 711	409.545	23.81094	79.90023

Table 4.8: Results of the analysis conducted on the Komati Power Station with tap-off from a BC turbine when implementing regeneration (two FWHs) in a simple BC cycle

4.3.1.3 Simple BC cycle with regeneration (three FWHs) from a BC turbine

The theoretical configuration tested with a third FWH in the BC cycle, as indicated in Figure 4.6, was also tested under the assumptions of scenarios 1 and 2. The third FWH would theoretically be installed between the first FWH and the inlet of the BC.

For the theoretical implementation of the third FWH, the tap-off pressures to the first and second FWHs from the BC turbine, i.e. P_{58} and P_{69}, were fixed for this theoretical configuration at the tap-off pressures that resulted in the maximum thermal efficiency of the cycle, which was unique to each working fluid. The results obtained for this configuration are discussed for scenarios 1 and 2.

4.3.1.3.1 A BC cycle with regeneration (three FWHs) from the BC turbine – Scenario 1

The working fluids ethanol and isopropanol were tested for this theoretical configuration under the assumptions of Scenario 1. The tap-off pressure range for each working fluid, as discussed above, was unique to each working fluid and similarly to the configurations discussed above, and indicated a maximum thermal efficiency within the tap-off range.

The thermal efficiency obtained for each tap-off pressure and working fluid is indicated in Figure 4.9. The maximum thermal efficiency, along with the conditions around the maximum thermal efficiency, is indicated in Table 4.9.

Working fluid	$\eta_{th,\,BC}$	Efficiency increase	Gain in useful work (kW)	$\dot{m}_{BC}$ (kg/s)	$\dot{m}_{72}$ (kg/s)	P_{72} (kPa)
Ethanol	42.395307	2.395307	7 615	255.4037	11.38	98.36
Isopropanol	42.255664	2.255664	7 171	330.5519	20.4	72.85

Table 4.9: Results of the analysis conducted on the Komati Power Station, with tap-off from a BC turbine when implementing regeneration (three FWHs) on a simple BC cycle under Scenario 1 assumptions

A total increase in thermal efficiency of 2.39% was achieved compared to the thermal efficiency of the original cycle, and an increase of 0.1% was achieved compared to the configuration with two FWHs. An increase in useful work and consequent reduction in heat rejection was also achieved.

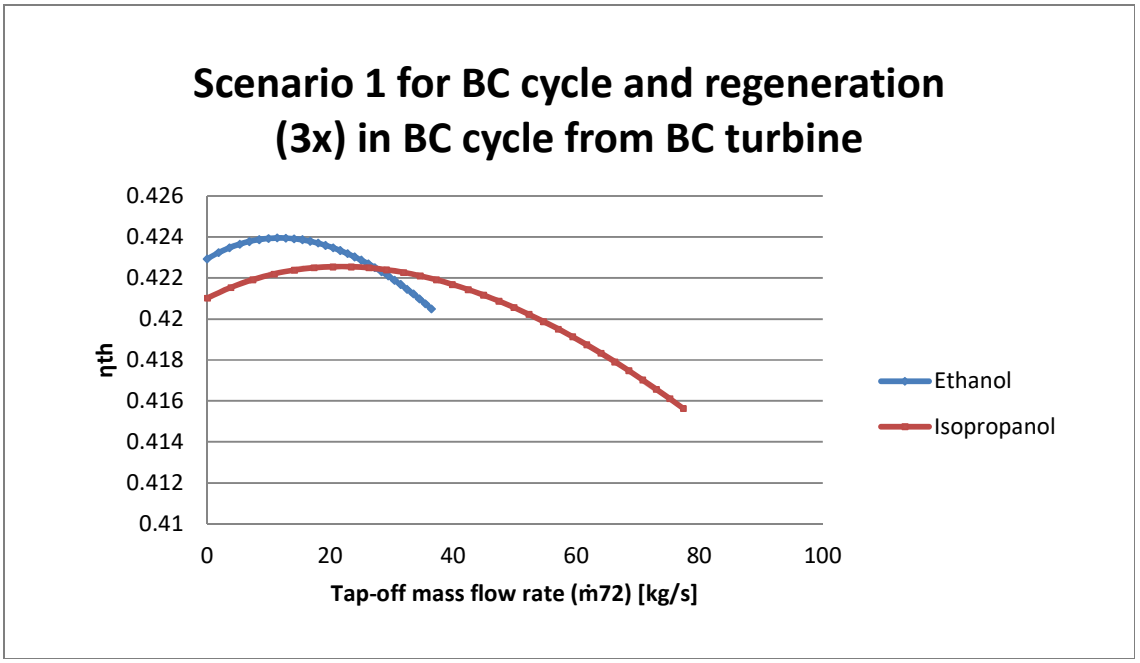

Figure 4.9: Thermal efficiency for the tap-off mass flow rate range for analysis conducted on the Komati Power Station, with regeneration (three FWHs) in a BC cycle from a BC turbine under Scenario 1 assumptions

The addition of FWHs and the increase in thermal efficiency for each FWH is discussed later in this chapter.

4.3.1.3.2 A BC cycle with regeneration (three FWHs) from a BC turbine – Scenario 2

The addition of a third FWH to the BC cycle was also tested under Scenario 2 conditions. The assumptions and method discussed in Chapter 3 were used for this analysis. The tested working fluids, indicated in Table 4.10, again had a unique tap-off pressure range and corresponding tap-off mass flow rate range.

Again, it can be seen in Figure 4.10 that the maximum thermal efficiency for each working fluid was achieved within the tap-off pressure related to the working fluid. R718 indicated the highest increase in thermal efficiency at 42.29%, which indicates an increase of 2.29% in thermal efficiency compared to the original steam cycle's thermal efficiency.

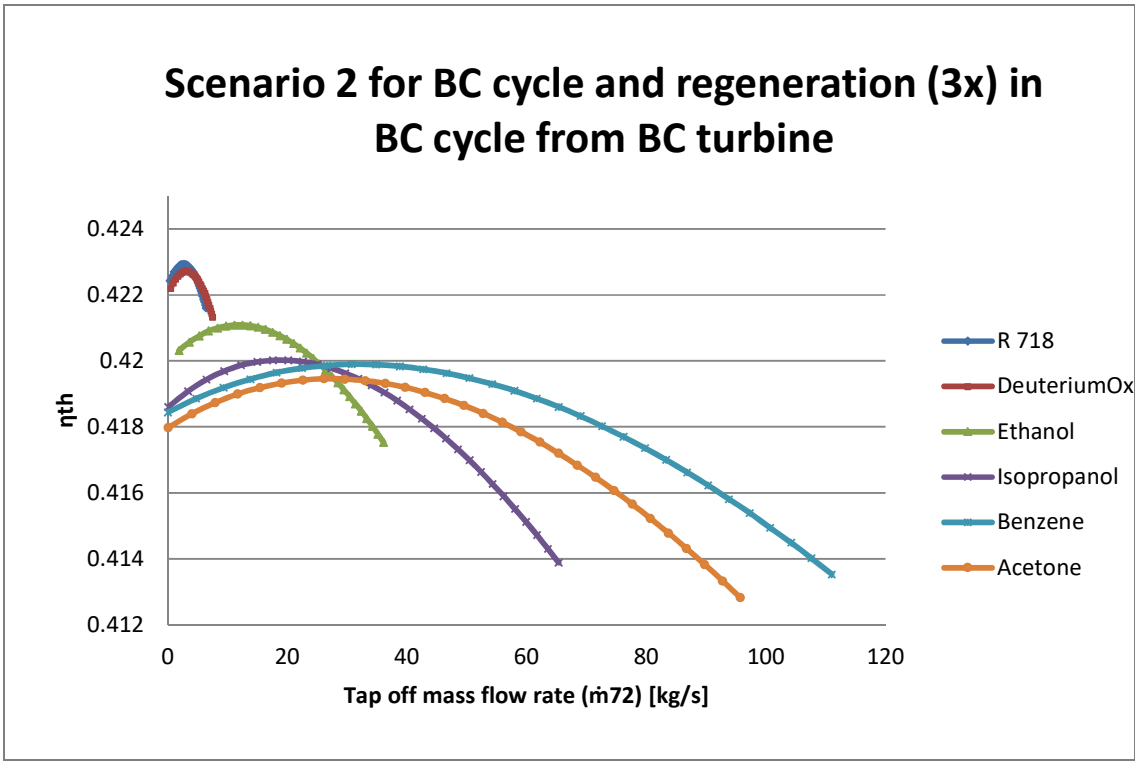

Figure 4.10: Thermal efficiency for the tap-off mass flow rate range for analysis conducted on the Komati Power Station with regeneration (three FWHs) in a BC cycle from a BC turbine

There was again a significant increase in useful work and a reduction in heat rejected at the BC cycle's condenser.

Working fluid	$\eta_{th,\,BC}$[48]	Efficiency increase	Gain in useful work (kW)	$\dot{m}_{BC}$ (kg/s)	$\dot{m}_{69}$ (kg/s)	P_{69} (kPa)
R718	42.293	2.293	7 290	93.848	2.646	46.24
Deuterium oxide	42.273	2.273	7 225	101.74817	3.102	42.49
Ethanol	42.11	2.11	6 707	250.01308	11.87	97.69
Isopropanol	42.003	2.003	6 367	309.15101	18.83	76.93
Benzene	41.99	1.99	6 325	515.97346	31.91	87.28
Acetone	41.946	1.946	6 186	433.71333	27.33	185.1

Table 4.10: Results of the analysis conducted on the Komati Power Station, with tap-off from a BC turbine, when implementing regeneration (three FWHs) in a simple BC cycle

4.3.1.4 Gain in efficiency for each added FWH

It would be worthwhile to briefly look into the increase in thermal efficiency for each FWH added to the BC cycle. Each FWH added to the system indicated an increase in thermal efficiency. The addition of a second FWH, for example, indicated a smaller increase in thermal efficiency compared to the addition of one FWH. Similarly, the addition of a third FWH

[48] Refer to the figure related to the discussed configuration to associate the thermal efficiency indicated to the specific tested configuration.

indicated a smaller increase in thermal efficiency compared to the addition of a second FWH. This concept is indicated theoretically in Figure 4.11 and Figure 4.12.

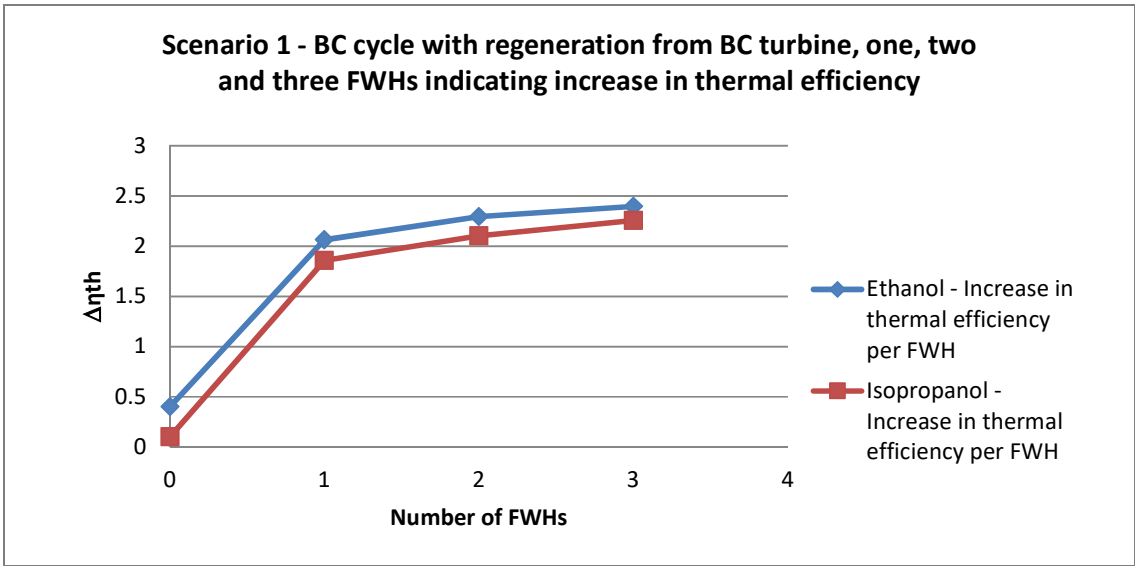

Figure 4.11: The increase in thermal efficiency of the cycle vs the number of regeneration units implemented on a simple BC cycle with assumptions under Scenario 1

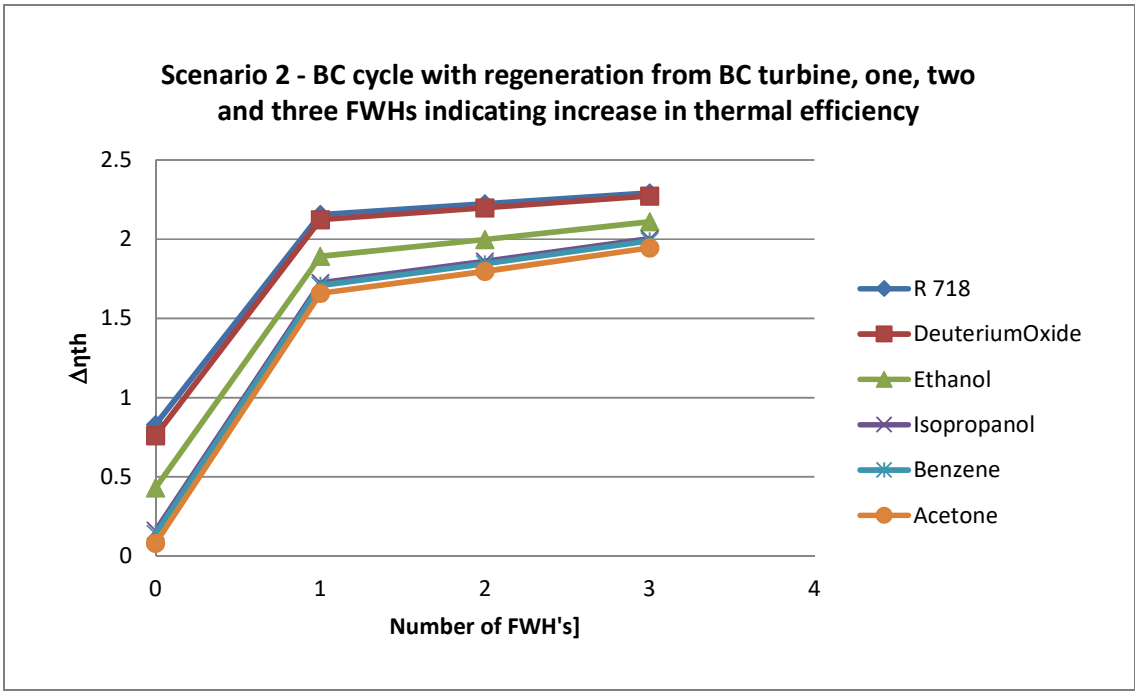

Figure 4.12: Thermal efficiency of the cycle vs the number of regeneration units implemented on a simple BC cycle with assumptions under Scenario 2

It is clear that the addition of each FWH causes an increase in thermal efficiency in the cycle. However, the increase in thermal efficiency is smaller for each additional FWH. The benefit of an additional FWH should therefore be weighed against other factors, of which cost is probably the most important.

4.3.2 Concluding remarks and data presented in the following configurations

Section 4.3 indicated the results obtained when implementing the BC cycle, adding regeneration from the outlet of the BC turbine and adding regeneration from the BC turbine (to FWHs). The results of each configuration were discussed and, where applicable, represented graphically.

The principles discussed in this section are repeated in the following configurations. The tap-off mass flow rate for any of the following configurations, for example, is unique in the assumptions and working fluid properties. The data that is presented is very similar to that indicated and discussed in Section 4.3. Therefore, to avoid unnecessary repetition, the following sections will indicate only optimum results obtained and should be read keeping the principles of Section 4.3 in mind. The graphic representation of the data of the following sections is indicated in Annexure B.

4.4 Simple BC cycle without a low-pressure turbine

The simple BC cycle without a low-pressure turbine was also tested to see whether it would be beneficial to increase the temperature at the outlet of the BC before the inlet of the BC turbine. The theoretical configuration is indicated again in Figure 4.13.

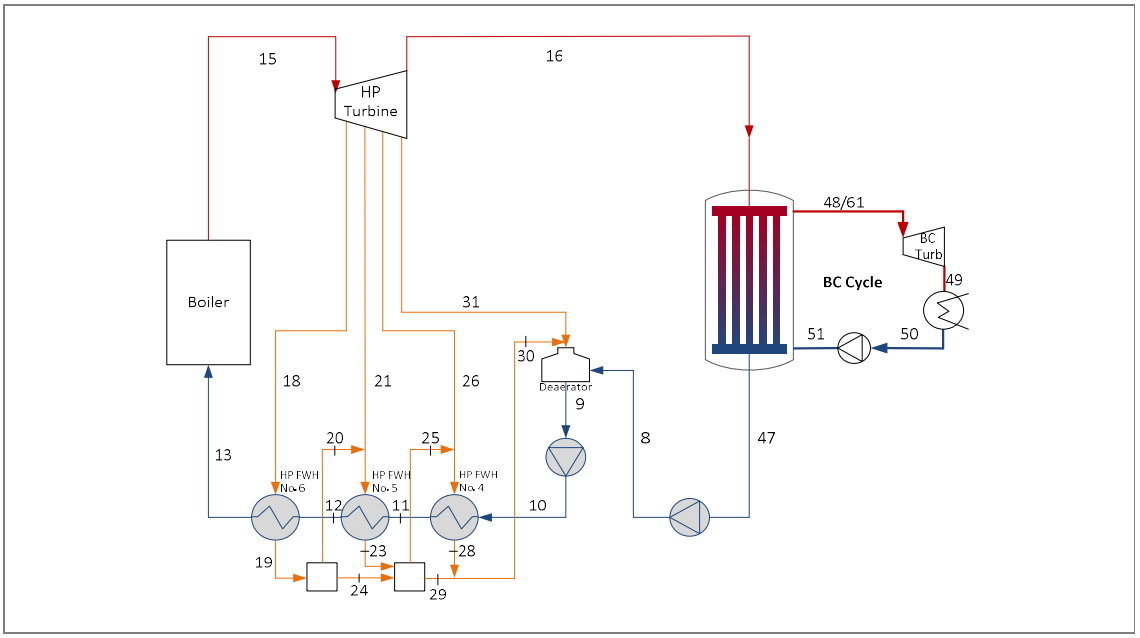

Figure 4.13: Component diagram of the Komati Power Station without a low-pressure turbine with a BC

The results obtained when testing the working fluids listed in Table 3.4 for the above configuration is indicated in Table 4.11.

	Working fluid	$\eta_{th,\ BC}$	Efficiency increase	Gain in useful work (kW)	$\dot{m}_{BC}$ (kg/s)
Scenario 1: Outlet of BC turbine fixed	Ethanol	40.75	0.75	2 376	227.2
	Isopropanol	40.2	0.2	645.1	285.4
	Acetone	40.11	0.11	329	399.6
	Benzene	40.09	0.09	287	491.1
Scenario 2: Inlet of BC turbine fixed	R718	41.41	1.41	4 464	89.89
	Deuterium oxide	41.32	1.32	4 193	96.88
	Ethanol	40.75	0.75	2 393	226.3
	Isopropanol	40.33	0.33	1 044	267.8
	Benzene	40.32	0.32	1 025	440
	Acetone	40.25	0.25	781.5	373.7
	Cyclopentane	40.04	0.04	133.5	456.9

Table 4.11: Results of the analysis conducted on the Komati Power Station without a steam-side low-pressure turbine when implementing a simple BC cycle

Theoretically, removing the low-pressure turbine and implementing the BC indicated an increase in thermal efficiency, more so than with the steam side's low-pressure turbine. It can be seen from Table 4.11 that Scenario 1 indicated an increase in thermal efficiency of 0.75% and Scenario 2 indicated an increase in thermal efficiency of 1.41% when compared to the original steam cycle.

Scenario 1 had an increase in useful work of 2.3 MW. Similarly, Scenario 2 indicates an increase of 4.5 MW in useful work. The indicated values were compared to the original steam cycle.

The mass flow rates required in the BC cycle were also relatively low. Scenario 1 had a $\dot{m}_{BC}$ of 227.2 kg/s, while Scenario 2 had a $\dot{m}_{BC}$ of 89.89 kg/s.

4.4.1 A BC cycle without a low-pressure turbine and regeneration with tap-off from BC turbine

4.4.1.1 A BC cycle without a low-pressure turbine and regeneration (one FWH) from the BC turbine

The BC cycle without a low-pressure turbine was also tested with regeneration from the BC turbine. The configuration with one FWH is indicated again in Figure 4.14.

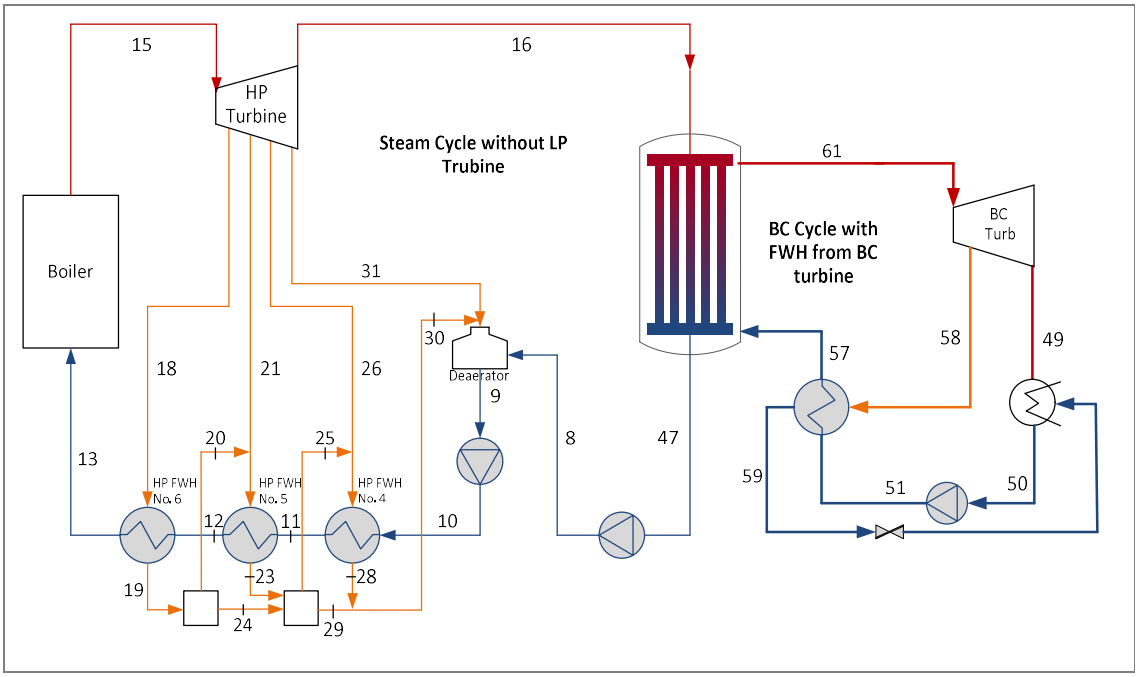

Figure 4.14: Component diagram of the Komati Power Station without a low-pressure turbine, including a BC and one FWH

4.4.1.1.1 A BC cycle without a low-pressure turbine and regeneration (one FWH) from the BC turbine – Scenario 1

The method described in Section 3.3.5.3 was implemented and the results for Scenario 1 are shown below. Each working fluid had a unique tap-off pressure and corresponding mass flow rate range with a maximum thermal efficiency of the cycle achieved within this tap-off pressure range. The working fluids that were tested in the configuration without any form of regeneration and that indicate an increase in thermal efficiency above 40% (see Table 4.11) were used in the analysis where one FWH was added (see Figure 4.14) under Scenario 1 assumptions. The results are shown in Table 4.12.

Working fluid	$\eta_{th,\,BC}$	Efficiency increase	Gain in useful work (kW)	$\dot{m}_{BC}$ (kg/s)	$\dot{m}_{58}$ (kg/s)	P_{58} (kPa)
Ethanol	41.49	1.49	4 748	252.3	28.17	72.83
Isopropanol	41.1	1.1	3 500	325.8	47.69	55.09
Benzene	41.02	1.02	3 240	563.7	86.38	66.67
Acetone	41.03	1.03	3 279	458.4	70.04	144.9

Table 4.12: Results of the analysis conducted on the Komati Power Station without a low-pressure turbine when implementing a simple BC cycle with regeneration (one FWH) from the BC turbine under Scenario 1 assumptions

The configuration with ethanol as a working fluid indicates the highest increase in thermal efficiency for this specific configuration at 1.49%. The addition of one FWH increased the

thermal efficiency of the cycle by 0.74% compared to the BC cycle without a FWH. An increase of 4.7 MW in useful work could theoretically be achieved.

4.4.1.1.2 A BC cycle without a low-pressure turbine and regeneration (one FWH) from the BC turbine – Scenario 2

Similarly, the results obtained for the theoretical configuration tested with the working fluids that indicate an increase in thermal efficiency above 40% under the assumptions of Scenario 2 without a FWH are indicated in Table 4.13. Again, it can be noted that each working fluid had a unique tap-off range from the BC turbine and that a maximum thermal efficiency for the cycle was obtained within this tap-off range. The maximum thermal efficiency was consequently obtained for the specific tap-off pressure and corresponding mass flow rate for each working fluid. This is indicated in Table 4.13.

The maximum increase of 1.96% in efficiency was obtained for R718 compared to the original steam cycle with an increase of 6.2 MW in useful. The maximum tap-off pressure occurred at 33.78 kPa with a corresponding mass flow rate of 6.75 kg/s.

Working fluid	$\eta_{th,\,BC}$	Efficiency increase	Gain in useful work (kW)	$\dot{m}_{BC}$ (kg/s)	$\dot{m}_{58}$ (kg/s)	P_{58} (kPa)
R718	41.96	1.96	6 246	96.46	6.747	33.78
Deuterium oxide	41.92	1.92	6 088	104.4	7.88	30.68
Ethanol	41.5	1.5	4 762	251.3	27.96	72.9
Isopropanol	41.2	1.2	3 822	303.9	42.18	56.32
Benzene	41.2	1.2	3 810	499.8	69.88	68.66
Acetone	41.14	1.14	3 636	426	61.54	147.5
Cyclopentane	40.95	0.95	3 030	524.3	79.88	176.8

Table 4.13: Results of the analysis conducted at the Komati Power Station without a low-pressure turbine when implementing a simple BC cycle with regeneration from a BC turbine under Scenario 2 assumptions

4.4.1.2 A BC cycle without a low-pressure turbine and regeneration (two FWHs) from a BC turbine

Similar to the simple BC cycle, the BC cycle without a low-pressure steam turbine was also tested with a second FWH under Scenario 1 and Scenario 2 conditions.

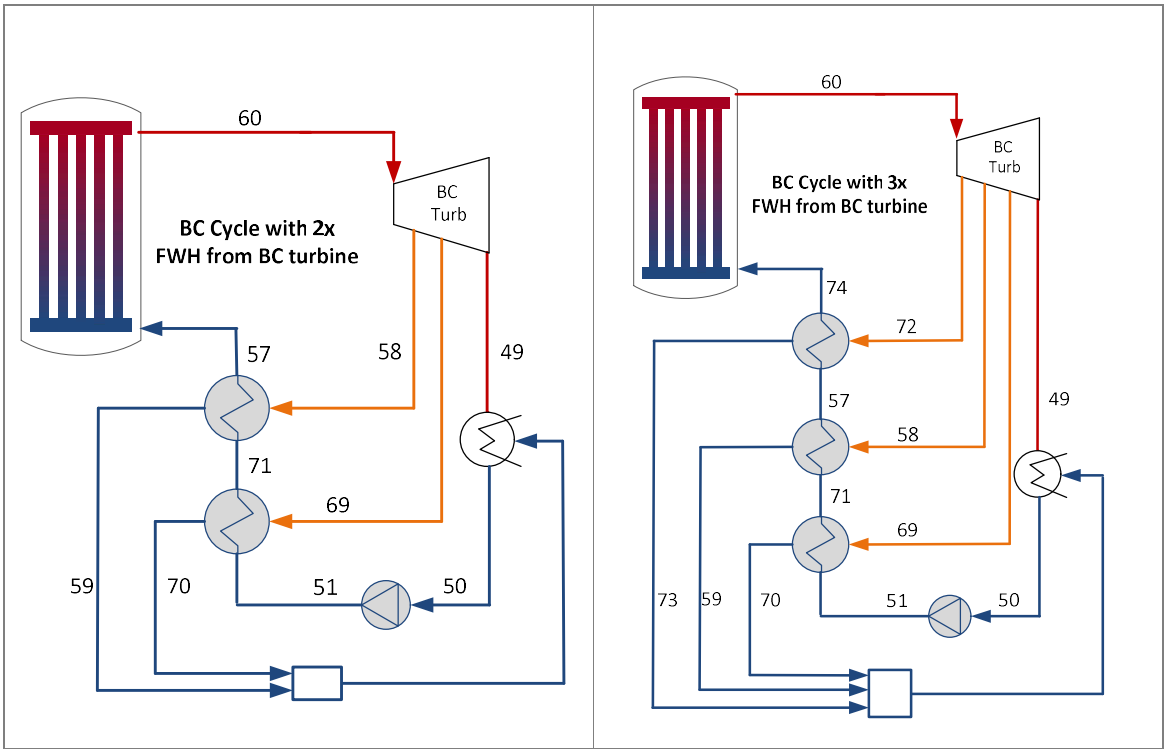

Figure 4.15: A BC cycle with two and three FWHs

4.4.1.2.1 A BC cycle without a low-pressure turbine and regeneration (two FWHs) from the BC turbine – Scenario 1

With the addition of a second FWH to the configuration where the low-pressure turbine had been removed, the configuration was tested under Scenario 1 conditions. The maximum thermal efficiency of the cycle was obtained with the working fluid of ethanol. The increase in efficiency with the additional FWH was 1.66% at the tap-off pressure of 34.45 kPa, compared to the original cycle, as indicated in Table 4.14.

Working fluid	$\eta_{th,\,BC}$	Efficiency increase	Gain in useful work (kW)	$\dot{m}_{BC}$ (kg/s)	$\dot{m}_{69}$ (kg/s)	P_{69} (kPa)
Ethanol	41.6647	1.6647	5 291	252.3	13.68	34.45
Isopropanol	41.3196	1.3196	4 193	325.8	22.92	26.62
Benzene	41.2461	1.2461	3 959	563.7	41.6	38.54
Acetone	41.2573	1.2573	3 995	458.4	33.77	86.75

Table 4.14: Results of the analysis conducted at the Komati Power Station without a low-pressure turbine when implementing a simple BC cycle with regeneration (two FWHs) from a BC turbine under Scenario 1 assumptions

The second FWH also indicates an increase of 5.3 MW in useful. The second FWH increased the thermal efficiency of the cycle by 0.17% compared to the BC cycle with only one FWH.

4.4.1.2.2 A BC cycle without low-pressure turbine and regeneration (two FWHs) from the BC turbine – Scenario 2

Similarly, the theoretical configuration with the second FWH indicates an increase of 0.11% compared to the configuration with only one FWH tested under Scenario 2 conditions. An increase of 2% was achieved, compared to the original cycle.

Working fluid	$\eta_{th,\,BC}$	Efficiency increase	Gain in useful work (kW)	$\dot{m}_{BC}$ (kg/s)	$\dot{m}_{69}$ (kg/s)	P_{69} (kPa)
R718	42.07585	2.07585	6 599	96.46	3.333	14.59
Deuterium oxide	42.03483	2.03483	6 458	104.4	3.287	11.38
Ethanol	41.6687	1.6687	5 294	251.3	11.72	30.97
Isopropanol	41.41	1.41	3 995	303.9	2.783	13.12
Benzene	41.41	1.41	4 471	499.8	30.95	37.26
Acetone	41.3592	1.3592	4 319	426	29.37	86.98
Cyclopentane	41.1821	1.1821	3 755	525.2	39.62	112.7

Table 4.15: Results of the analysis conducted on the Komati Power Station with tap-off from the steam-side low-pressure turbine when implementing a simple BC cycle with regeneration (two FWHs) from a BC turbine

Table 4.15 indicates the maximum thermal efficiency obtained for the working fluids tested in this configuration, along with the tap-off pressure where the maximum thermal efficiency occurred.

4.4.1.3 A BC cycle without a low-pressure turbine and regeneration (three FWHs) from the BC turbine

The addition of a third FWH was also added to the configuration. The results are discussed below.

4.4.1.3.1 A BC cycle without a low-pressure turbine and regeneration (three FWHs) from the BC turbine – Scenario 1

The third FWH added to the cycle indicates a maximum increase of 1.84%, as indicated in Table 4.16, compared to the original cycle with an increase of 0.18% compared to the cycle with only two FWHs.

Working fluid	$\eta_{th,\,BC}$	Efficiency increase	Gain in useful work (kW)	$\dot{m}_{BC}$ (kg/s)	$\dot{m}_{6\,9}$ (kg/s)	P_{69} (kPa)
Ethanol	41.84785	1.84785	5 874	266.8	16.64	142.6
Isopropanol	41.55994	1.55994	4 957	350.3	28.77	106.3
Benzene	41.49704	1.49704	4 757	607.6	51.88	110.3
Acetone	41.50733	1.50733	4 790	493.8	41.75	233.1

Table 4.16: Results of the analysis conducted at the Komati Power Station without a low-pressure turbine when implementing a simple BC cycle with regeneration (three FWHs) from a BC turbine under Scenario 1 assumptions

The maximum thermal efficiency was obtained with ethanol as a working fluid at a tap-off pressure of 142.6 kPa with a corresponding mass flow rate of 16.64 kg/s. The increase in useful work amounted to 5.8 MW.

4.4.1.3.2 A BC cycle without a low-pressure turbine and regeneration (three FWHs) from the BC turbine – Scenario 2

Similarly, a third FWH indicates an increase of 0.11% in thermal efficiency compared to the cycle with two FWHs. The maximum thermal efficiency was achieved with a working fluid of R718. The total increase in thermal efficiency compared to the original cycle was 2.19%.

The maximum efficiency was obtained at a tap-off pressure of 72.61 kPa and corresponding mass flow rate of 3.7 kg/s. The configuration indicates an increase in useful work of 6.9 MW.

Working fluid	$\eta_{th,\ BC}$	Efficiency increase	Gain in useful work (kW)	$\dot{m}_{BC}$ (kg/s)	$\dot{m}_{72}$ (kg/s)	P_{72} (kPa)
R718	42.19059	2.19059	6 964	99.78	3.697	72.61
Deuterium oxide	42.15527	2.15527	6 852	108.3	4.309	66.91
Ethanol	41.84804	1.84804	5 874	265.7	16.52	142.8
Isopropanol	41.4747	1.4747	4 686	325	24.59	107.9
Benzene	41.63634	1.63634	5 201	535.3	41.47	114.9
Acetone	41.5958	1.5958	5 072	457.1	36.43	238.9
Cyclopentane	41.42228	1.42228	4 519	565.8	47.81	272.039

Table 4.17: Results of the analysis conducted at the Komati Power Station with tap-off from the steam-side low-pressure turbine when implementing a simple BC cycle with regeneration (three FWHs) from a BC turbine

4.5 A BC cycle with tap-off from a low-pressure turbine and FWHs

In this section, the results obtained from the theoretical configuration where steam is tapped off from the low-pressure turbine are discussed. The configuration indicated in Figure 4.16 was tested under the assumptions discussed in Section 3.3.5.4.1, namely scenarios 1 and 2. It should, however, be noted that the working fluids tested under scenarios 1 and 2 for a simple BC cycle indicating an increase in thermal efficiency above 40%, is considered for this configuration to ascertain whether an even further increase in thermal efficiency can be obtained.

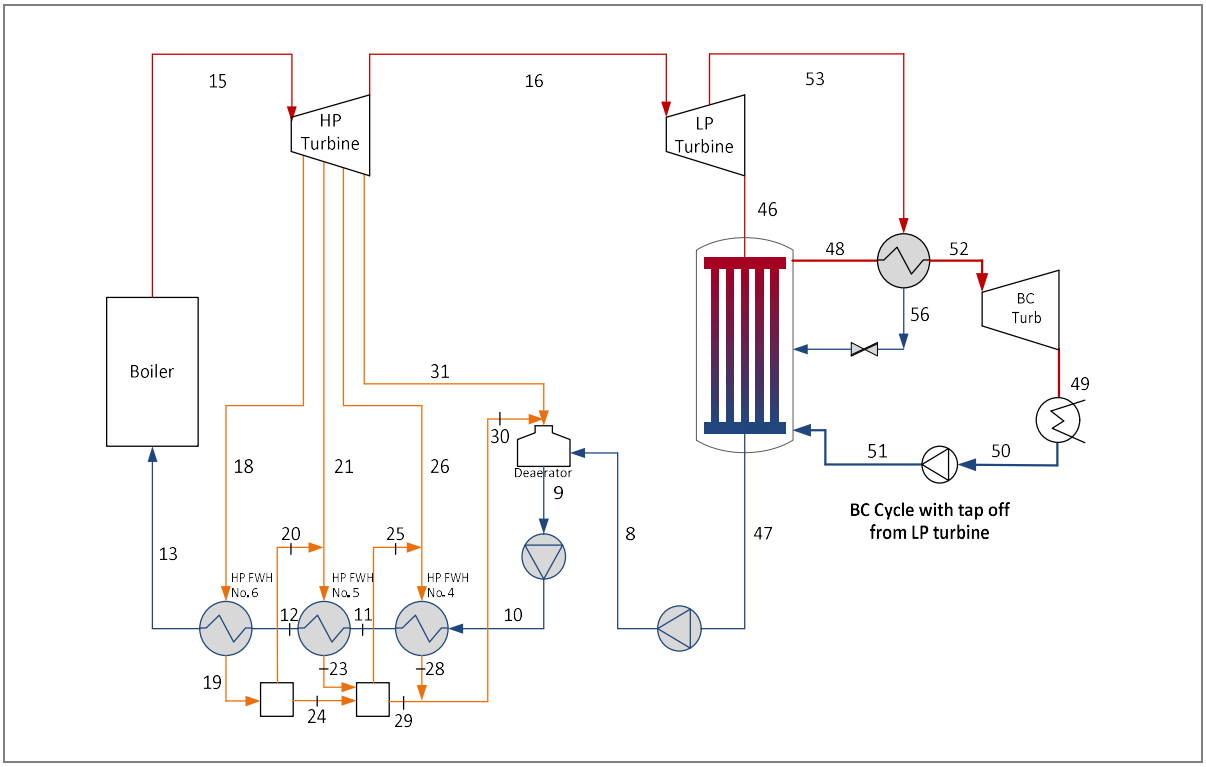

Figure 4.16: Component diagram of the Komati Power Station with tap-off from a low-pressure turbine into the BC cycle

4.5.1 A BC cycle with tap-off from a low-pressure turbine

The tested configuration is indicated in the Figure 4.16. This configuration was tested under the assumptions of scenarios 1 and 2. The working fluids that indicate an increase in thermal efficiency above 40% for scenarios 1 and 2, without the addition of a heat exchanger, are listed in Table 4.2. These working fluids will therefore be tested in the theoretical configuration where an additional heat exchanger is added and steam is tapped off from the low-pressure turbine to add additional heat to the system.

The results obtained for scenarios 1 and 2 are given below. It can be seen that the tap-off mass flow rate for each working fluid and both scenarios result in a maximum efficiency somewhere within the range.

The results obtained for each working fluid is indicated graphically for the tap-off mass flow rate range applicable to each working fluid. The maximum efficiency achieved for each working fluid tested in the configuration is indicated in a separate table.

It should be noted that Scenario 1 assumptions, with the working fluids ethanol and isopropanol, did not heed any useful results for this configuration. It is evident that all

configurations with heat exchangers did not indicate any useful results when tested under Scenario 1 conditions with the mentioned working fluids.

A maximum efficiency obtained for each working fluid within the tap-off mass flow rate range was determined and is indicated below in Table 4.18. R718 indicates the highest efficiency with an increase of 1.9% at a tap-off pressure of 129.7 kPa

Working fluid	$\eta_{th, BC}$	Efficiency increase	Gain in useful work (kW)	$\dot{m}_{BC}$ (kg/s)	$\dot{m}_{53}$ (kg/s)	P_{53} (kPa)
R718	41.9057	1.9057	6 058	87.02	0.09007	129.7
Deuterium oxide	41.8543	1.8543	5 894	93.79	0.101	129.7
Ethanol	41.516	1.516	4 816	220.5	0.5486	138
Isopropanol	41.2591	1.2591	4 000	261.8	1.439	154.6
Benzene	41.2301	1.2301	3 908	436.1	1.328	146.3
Acetone	41.1758	1.1758	3 735	362.4	2.22	158.7

Table 4.18: Results of the analysis conducted at the Komati Power Station with tap-off from the steam-side low-pressure turbine when implementing a simple BC cycle

The addition of a heat exchanger to this cycle indicates a clear increase in thermal efficiency and it would be beneficial to see what impact regeneration from the outlet of the BC turbine and from within the BC turbine will have.

4.5.2 Tap-off from a low-pressure turbine and FWHs

The configuration where the BC cycle included a heat exchanger with tap-off from the low-pressure steam turbine, along with regeneration from the BC turbine in the BC cycle is indicated below. Due to the fact that the configuration indicated in Figure 4.16 was tested under the assumptions of scenario 1 and did not heed any useful results, the configuration indicated in Figure 4.17 will only be tested under the assumptions discussed in Scenario 2 for the indicated working fluids.

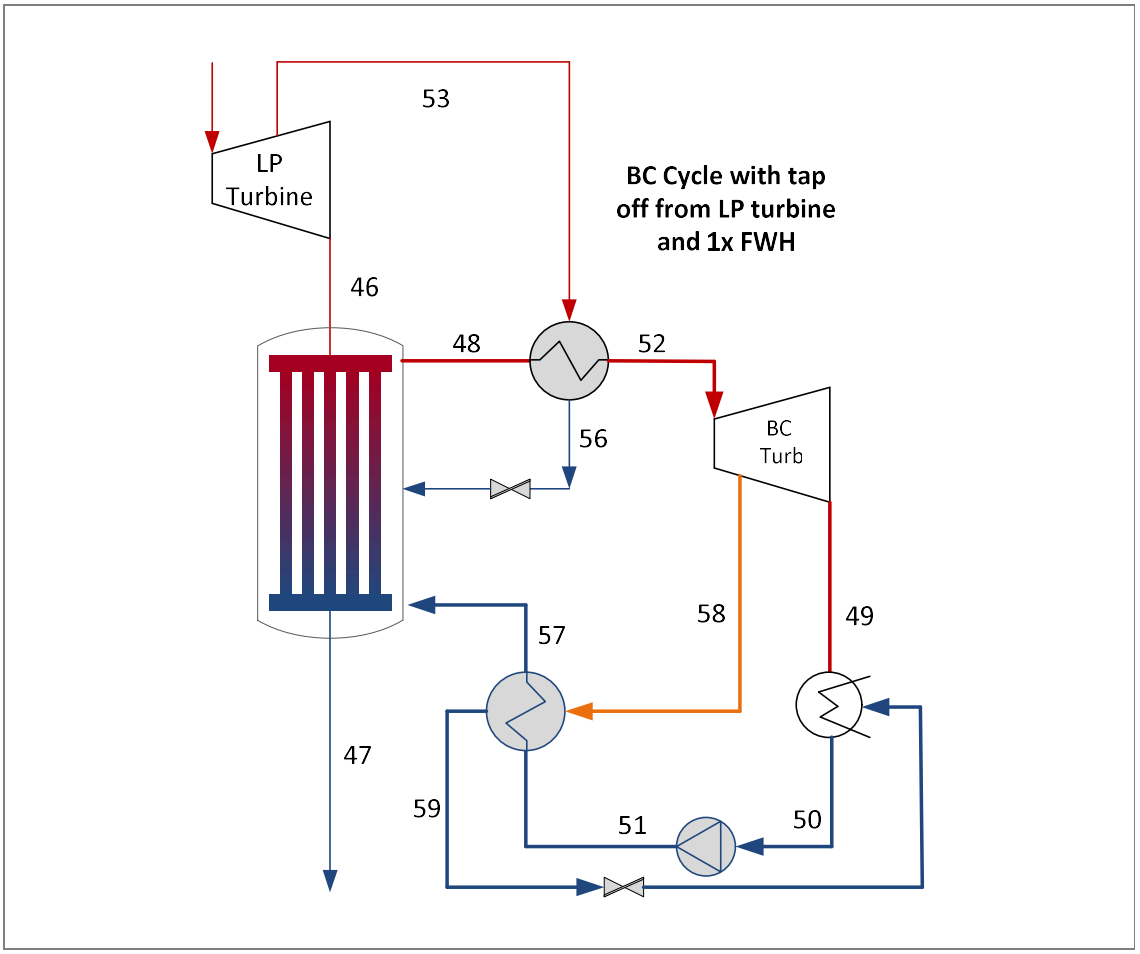

Figure 4.17: Component diagram of the Komati Power Station with tap-off from a low-pressure turbine into a BC cycle and BC cycle FWH

A maximum efficiency obtained for each working fluid within the tap-off mass flow rate range was determined and is shown below in Table 4.20. The maximum thermal efficiency was obtained with the working fluid R718 at a tap-off pressure of 24.42 kPa. The maximum thermal efficiency obtained for this configuration with the mentioned working fluid was 42.16%, which indicates an increase of 2.16% compared to the original cycle and an increase of 0.26% compared to the cycle without a FWH.

Working fluid	$\eta_{th,\,BC}$	Efficiency increase	Gain in useful work (kW)	$\dot{m}_{BC}$ (kg/s)	$\dot{m}_{58}$ (kg/s)	P_{58} (kPa)
R718	42.1561	2.1561	6 854	91.32	4.922	24.42
Deuterium oxide	42.1247	2.1247	6 754	98.8	5.763	22.13
Ethanol	41.8926	1.8926	6 016	238	20.56	55.04
Isopropanol	41.7266	1.7266	5 488	288.1	31.57	43.41
Benzene	41.7084	1.7084	5 430	480.8	53.86	56.12
Acetone	41.6598	1.6598	5 275	400.1	45.47	122.7

Table 4.19: Results of the analysis conducted at the Komati Power Station with tap-off from a steam-side low-pressure turbine into the BC cycle and regeneration (one FWH) from a BC turbine under Scenario 2 assumptions

4.6 A BC cycle with tap-off before the low-pressure turbine and FWHs

The results of the analysis conducted on the configuration where steam is tapped off before the low-pressure steam turbine and fed into a heat exchanger in the BC cycle are discussed below. It should be noted that Scenario 1 assumptions for all variations of the configuration did not heed any useful results. Consequently, only results for an analysis of Scenario 2 are indicated and discussed.

4.6.1 A BC cycle with tap-off before the low-pressure turbine

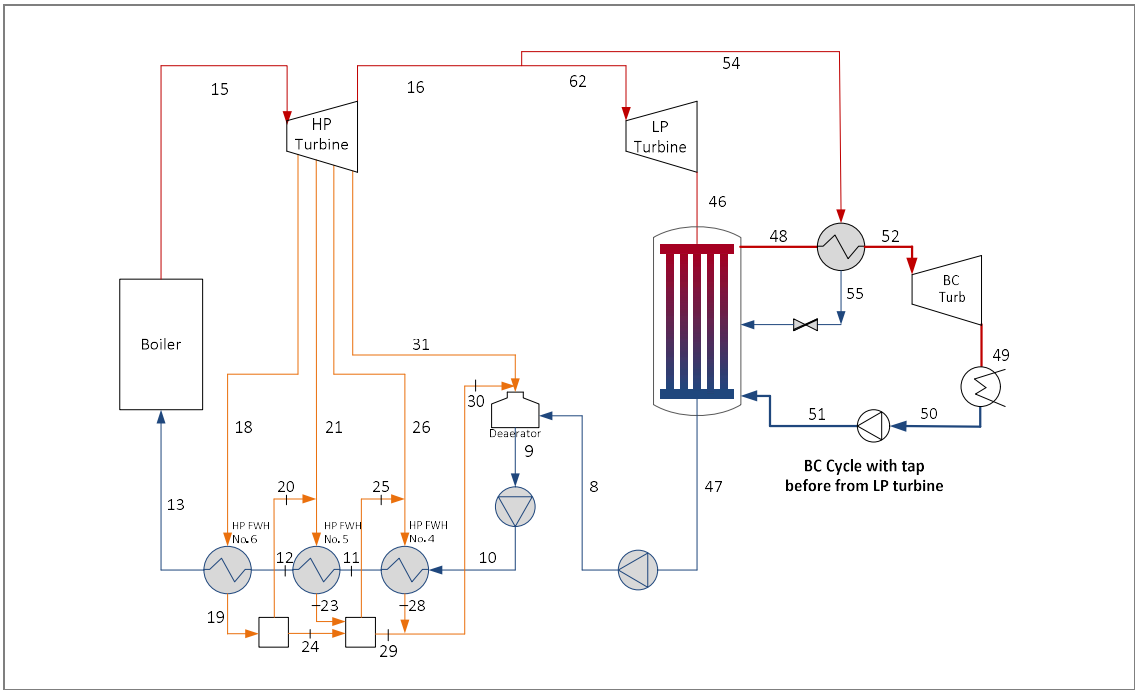

Figure 4.18: Component diagram of the Komati Power Station with tap-off before a low-pressure turbine into a BC cycle

The results obtained for this configuration under Scenario 2 assumptions are discussed below. It should be noted that only one tap-off mass flow rate was determined for this configuration, as steam is being tapped off at a fixed pressure before the low-pressure turbine. The results obtained for this configuration under Scenario 2 conditions are indicated below in Table 4.20.

An increase of 2.075% was obtained for this configuration with the working fluid R718. The tap-off mass flow rate, which was unique to the working fluid, was 1.675 kg/s.

Working fluid	$\eta_{th,\,BC}$	Efficiency increase	Gain in useful work (kW)	$\dot{m}_{BC}$ (kg/s)	$\dot{m}_{54}$ (kg/s)	P_{54} (kPa)
R718	42.07564	2.07564	6 598	84.54	1.675	245.7
Deuterium oxide	42.02672	2.02672	6 443	91.12	1.689	245.7
Ethanol	41.67621	1.67621	5 327	210.7	3.882	245.7
Acetone	41.31825	1.31825	4 188	344.2	6.152	245.7
Benzene	41.31663	1.31663	4 183	412.2	5.777	245.7
Cyclopentane	41.0452	1.0452	3 320	424.9	7.024	245.7

Table 4.20: Results of the analysis conducted on the Komati Power Station with tap-off before a steam-side low-pressure turbine into a BC cycle under Scenario 2 assumptions

4.6.2 Tap-off before the low-pressure turbine and FWHs

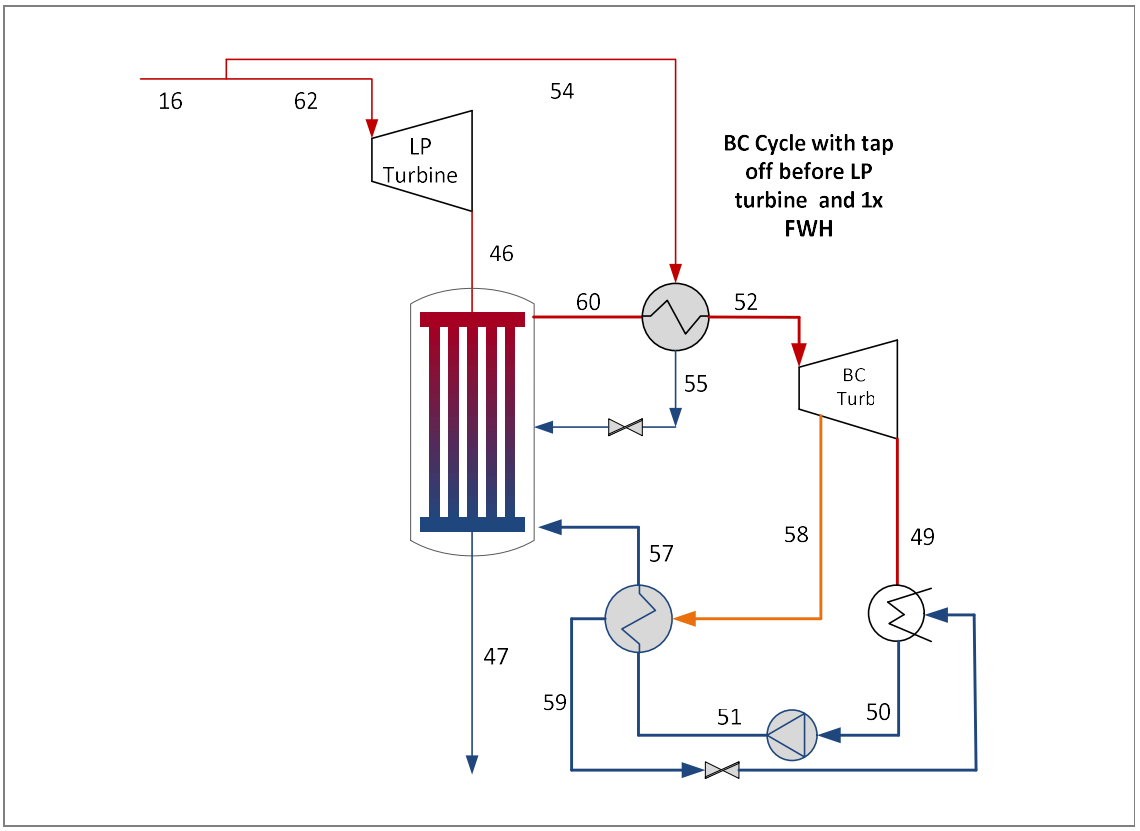

Figure 4.19: Component diagram of the Komati Power Station with tap-off before a low-pressure turbine into a BC cycle and BC cycle FWH

Figure 4.19 indicates the theoretical configuration where steam is tapped off before the inlet of the low-pressure steam turbine with the addition of a FWH. The method of analysis was followed as described in Chapter 3. The range of tap-off pressure, unique to each working fluid, would typically indicate a maximum thermal efficiency at a specific tap-off pressure. The maximum efficiency obtained for each working fluid within the tap-off mass flow rate range was determined and is indicated below in Table 4.21.

Working fluid	$\eta_{th,\,BC}$	Efficiency increase	Gain in useful work (kW)	$\dot{m}_{BC}$ (kg/s)	$\dot{m}_{58}$ (kg/s)	P_{58} (kPa)
R718	42.31793	2.31793	7 369	88.65	4.7	24.4
Deuterium oxide	42.28773	2.28773	7 273	95.9	5.489	22.12
Ethanol	42.03364	2.03364	6 465	226.8	18.88	54.86
Isopropanol	41.86568	1.86568	5 930	274.6	28.76	42.9
Benzene	41.75453	1.75453	5 577	451.9	47.47	55.41
Acetone	41.49446	1.49446	4 749	407.4	77.8	212.3

Table 4.21: Results of the analysis conducted on the Komati Power Station with tap-off from a steam-side low-pressure turbine into a BC cycle and regeneration (one FWH) from a BC turbine under Scenario 2 assumptions

A maximum increase of 2.32% was obtained for this theoretical configuration compared to the original steam cycle. The addition of a FWH added 0.24% to thermal efficiency compared to the configuration without a FWH. The increase in efficiency was achieved with the working fluid R718.

4.7 A BC cycle with tap-off in the high-pressure turbine and FWHs

Similar to the configurations discussed in sections 4.5 and 4.6, this section will indicate the results where steam is tapped off from the high-pressure turbine into a heat exchanger in the BC cycle. Again, Scenario 1 conditions did not heed any results. Consequently, only results for Scenario 2 are indicated. The configuration was tested with the addition of a FWH and with regeneration from the outlet of the BC turbine as well.

4.7.1 A BC cycle with tap-off in a high-pressure turbine

Figure 4.20 indicates the theoretical configuration that includes the heat exchanger, with steam tapped off from the high-pressure steam turbine, fed into the heat exchanger.

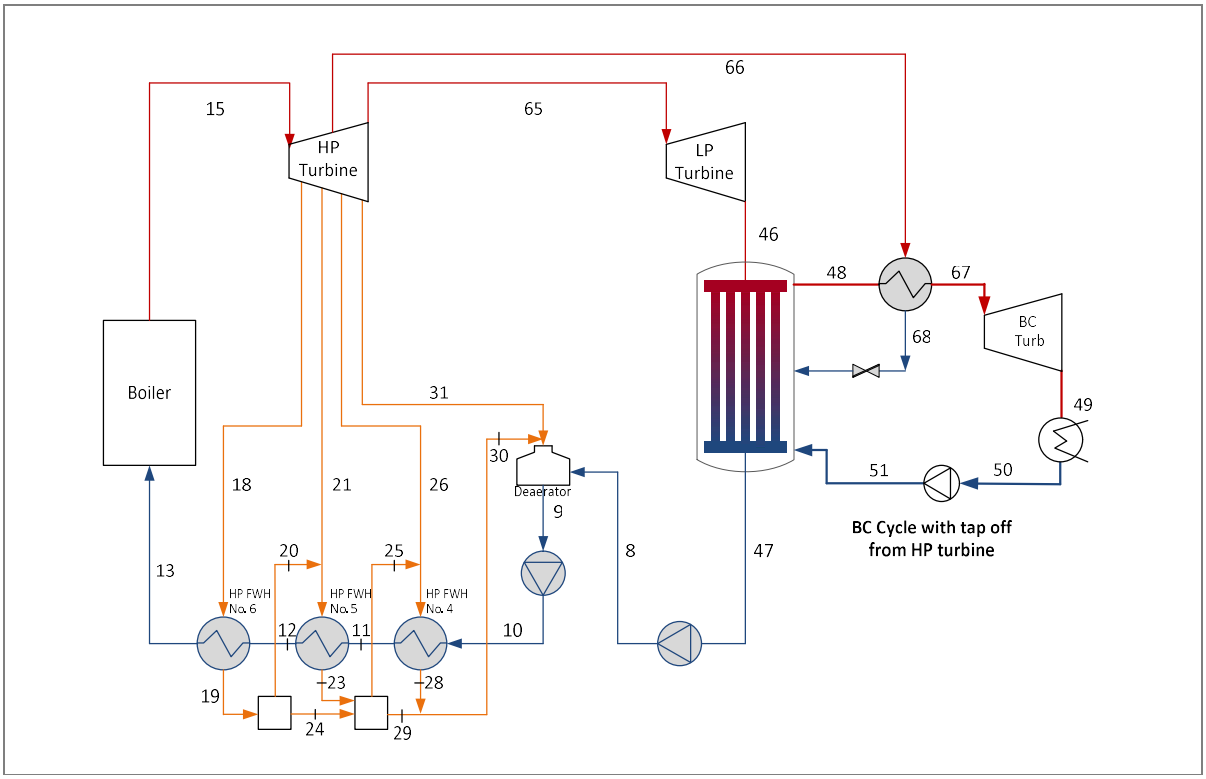

Figure 4.20: Component diagram of the Komati Power Station with tap-off from a high-pressure turbine into a BC cycle

The tap-off pressure range from the high-pressure turbine resulted in a unique range of tap-off mass flow rates for each working fluid. A maximum thermal efficiency was achieved within

this tap-off pressure range with a corresponding tap-off mass flow rate. The results obtained for this configuration is indicated in Table 4.22.

An increase of 1.798% was achieved with the working fluid R718. The characteristics of this configuration were different from the other configurations in that the maximum thermal efficiency of the cycle was achieved at the lowest tap-off pressure in the high-pressure turbine close to the outlet of the high-pressure turbine.

Working fluid	$\eta_{th,\ BC}$	Efficiency increase	Gain in useful work (kW)	$\dot{m}_{BC}$ (kg/s)	$\dot{m}_{66}$ (kg/s)	P_{66} (kPa)
R718	41.79771	1.79771	5 714	84.87	1.707	248.2
Deuterium oxide	41.74723	1.74723	5 553	91.46	1.722	248.2
Ethanol	41.39623	1.39623	4 436	211.4	3.958	248.2
Isopropanol	41.14357	1.14357	3 633	251.4	4.712	248.2
Benzene	41.0321	1.0321	3 278	413.6	5.89	248.2
Acetone	41.03547	1.03547	3 289	345.3	6.268	248.2

Table 4.22: Results of the analysis conducted on the Komati Power Station with tap-off from a steam-side high-pressure turbine when implementing a simple BC cycle

4.7.2 Tap-off from a high-pressure turbine and FWHs

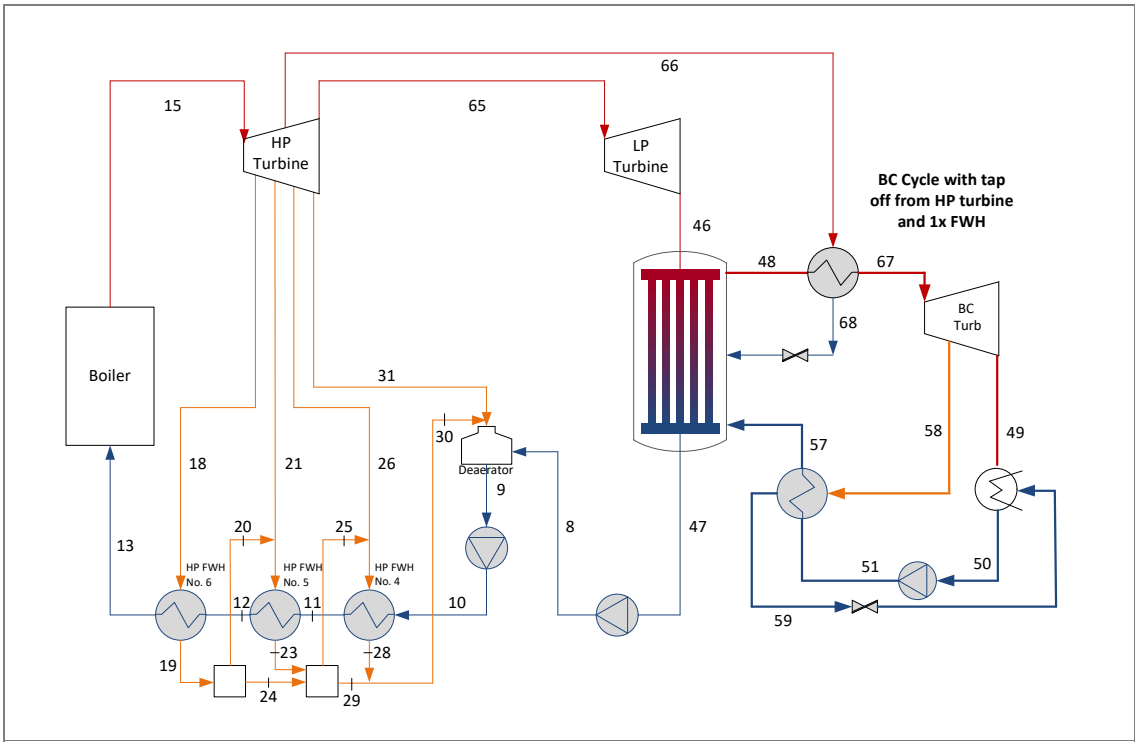

Figure 4.21: Component diagram of the Komati Power Station with tap-off from a high-pressure turbine into a BC cycle and BC cycle and one FWH

The configuration shown in Figure 4.21 indicates the theoretical situation where steam is tapped off from the high-pressure steam turbine to the BC cycle with the inclusion of a FWH.

The tap-off pressure range, ranging from the BC turbine inlet pressure to the BC turbine outlet pressure, is unique to each tested working fluid.

Working fluid	$\eta_{th,\,BC}$[49]	Efficiency increase	Gain in useful work (kW)	$\dot{m}_{BC}$ (kg/s)	$\dot{m}_{66}$ (kg/s)	P_{66} (kPa)
R718	42.04088	2.04088	6 488	88.99	4.716	24.4
Deuterium oxide	42.0098	2.0098	6 389	96.26	5.514	22.08
Ethanol	41.75469	1.75469	5 577	227.6	18.93	54.87
Isopropanol	41.58532	1.58532	5 038	275.5	28.82	42.88
Benzene	41.47078	1.47078	4 674	453.3	47.53	55.4
Acetone	41.48554	1.48554	4 721	379.2	40.63	121.3

Table 4.23: Results of the analysis conducted at the Komati Power Station with tap-off from a steam-side high-pressure turbine, when implementing a simple BC cycle with regeneration from a BC turbine under Scenario 2 assumptions

The maximum thermal efficiency obtained for each working fluid tested in the indicated configuration is shown in Table 4.23. It can be seen that the working fluid R718 has achieved the highest thermal efficiency, at a tap-off pressure of 24.4 kPa. The increase in thermal efficiency compared to the original steam cycle is 2.04%. Compared to the cycle that included tap-off from the high-pressure turbine to the BC cycle, an increase of 0.24% was achieved when implementing the FWH to the cycle.

4.8 BC cycle without a low-pressure turbine and tap-off from a high-pressure turbine and FWHs

The configurations discussed in this section are similar to the configuration discussed in Section 4.7. However, this theoretical configuration excludes the low-pressure turbine. Again, Scenario 1 assumptions did not heed any useful results for any of the configurations tested. Consequently, only the results of Scenario 2 are indicated below.

The working fluids tested in sections 4.4 that indicate an increase in efficiency higher than 40% are used in the configurations indicated below.

[49] Refer to the figure related to the discussed configuration to associate the thermal efficiency indicated to the specific tested configuration.

4.8.1 A BC cycle with tap-off in a high-pressure turbine and without the low-pressure turbine

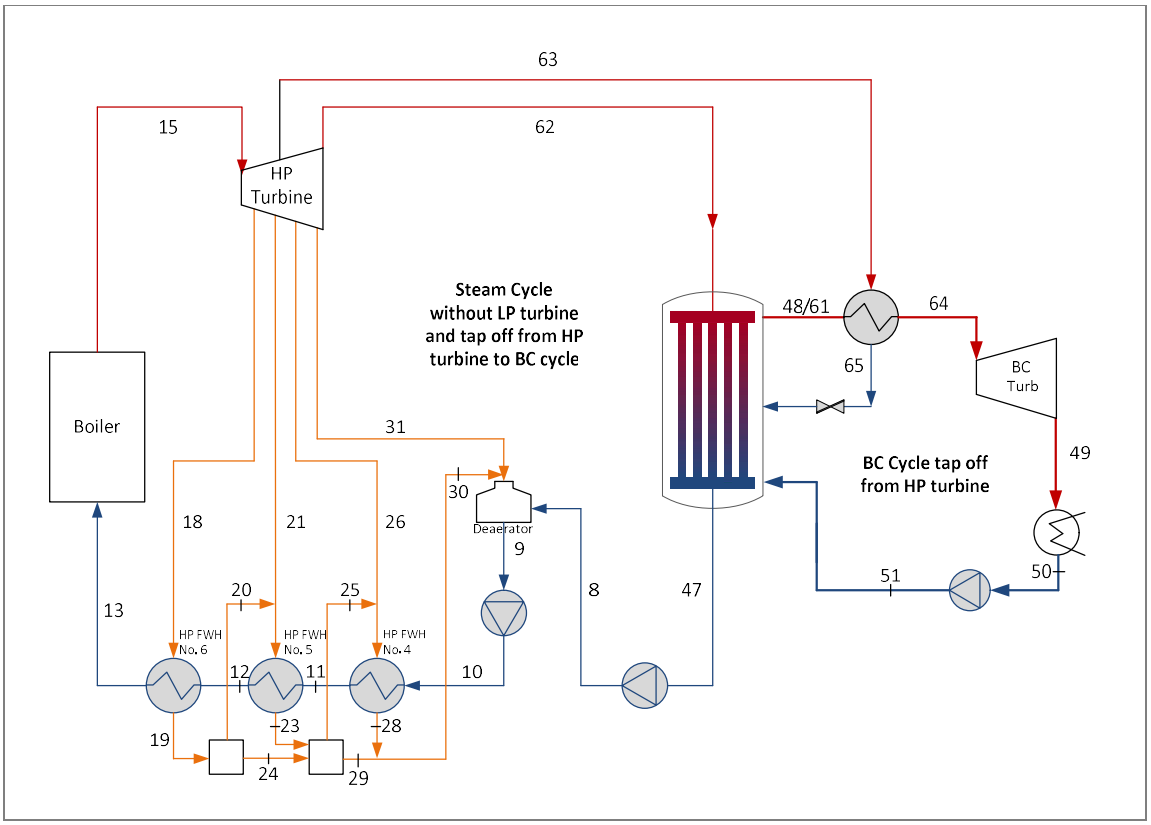

Figure 4.22: Component diagram of the Komati Power Station without a low-pressure turbine and with tap-off from a high-pressure turbine into a BC cycle

The theoretical configuration indicated in Figure 4.22 shows the implementation of the BC cycle as discussed in Section 3.3.5.7.1. The method explained in this section was implemented in this configuration. Similar to the configurations discussed above, a maximum thermal efficiency was obtained within the tap-off pressure range. The maximum thermal efficiency was obtained with R718 as a working fluid and indicates an increase in thermal efficiency of 1.14% compared to the original cycle at a tap-off pressure from the high-pressure turbine of 444.1 kPa.

Working fluid	$\eta_{th,\ BC}$	Efficiency increase	Gain in useful work (kW)	$\dot{m}_{BC}$ (kg/s)	$\dot{m}_{66}$ (kg/s)	P_{66} (kPa)
R718	41.14	1.14	3 615	88.72	1.928	444.1
DeuteriumOxide	41.05	1.05	3347	95.57	1.985	450.3
Ethanol	40.55	0.55	1754	216.4	5.407	490.5
Isopropanol	40.16	0.16	513	254.8	5.958	478
Benzene	40.104	0.104	326.2	425.7	4.048	350.4
Acetone	40.11	0.11	356.3	352.5	6.816	429.7

Table 4.24: Results of analysis conducted on Komati Power Station, without LP turbine and tap off from the steam side HP turbine, when implementing a simple BC cycle.

4.8.2 Tap off from HP turbine and feed water heaters

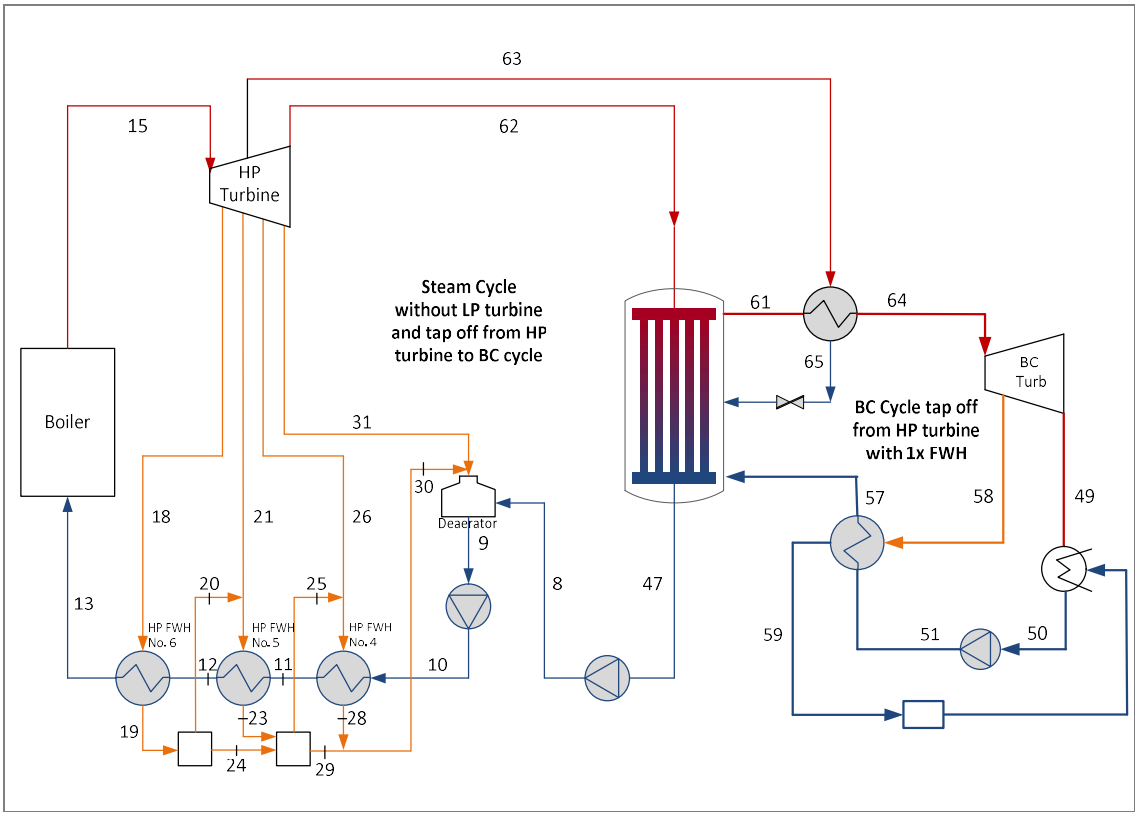

Figure 4.23: Component diagram of the Komati Power Station without a low-pressure turbine and tap-off from a high-pressure turbine into a BC cycle and BC cycle with one FWH

The theoretical configuration was also tested with the inclusion of a FWH as indicated in Figure 4.23. The tap-off pressure range from the BC turbine differed for each working fluid and reached a maximum within this range. The maximum thermal efficiency for this specific configuration was achieved for R718 as a working fluid and indicates an increase of 2.28%. The addition of a FWH increased the thermal efficiency of the cycle by 1.14% compared to the cycle without a FWH.

Working fluid	$\eta_{th, BC}$	Efficiency increase	Gain in useful work (kW)	$\dot{m}_{BC}$ (kg/s)	$\dot{m}_{66}$ (kg/s)	P_{66} (kPa)
R718	42.28	2.28	7 257	94.17	6.489	33.93
Deuterium oxide	42.22	2.22	7 073	101.9	7.561	30.84
Ethanol	41.86	1.86	5 902	237.1	25.35	74.08
Isopropanol	41.52	1.52	4 840	295.8	40.49	56.86
Benzene	41.52	1.52	4 828	476.9	64.44	69.12
Acetone	41.55	1.55	4 913	395.3	53.92	149

Table 4.25: Results of the analysis conducted on the Komati Power Station without a low-pressure turbine and tap-off from a steam-side high-pressure turbine when implementing a simple BC cycle with regeneration (one FWH) from the BC turbine

4.9 Summary of results

Each configuration discussed in this section indicated the results of several working fluids tested in each configuration. Table 4.26 indicates a summary of the maximum thermal efficiency achieved for each configuration discussed so far for the specific working fluid.

Section	Configuration	Working fluid	$\eta_{th, BC}$ (percentage)	Efficiency increase (percentage)	Gain in useful work (kW)	$\dot{m}_{BC}$ (kg/s)
	Original cycle	----	40	----	----	----
4.3	Simple BC cycle – Scenario 1	Ethanol	40.4	0.4	1 296	228.6
4.3	Simple BC cycle – Scenario 2	R718	40.83	0.83	2 621	87.86
4.3.1.1.1	Simple BC cycle with regeneration from BC turbine – Scenario 1	Ethanol	42.062	2.062	6 556	242.67
4.3.1.1.2	Simple BC cycle with regeneration (one FWH) from BC turbine – Scenario 2	R718	42.156	2.156	6 854	91.41
4.3.1.2.1	Simple BC cycle with regeneration (two FWHs) from BC turbine – Scenario 1	Ethanol	42.293	2.293	7 290	245.12
4.3.1.2.2	Simple BC cycle with regeneration (two FWHs) from BC turbine – Scenario 2	R718	42.224	2.224	7 070	91.41
4.3.1.3.1	**Simple BC cycle with regeneration (three FWHs) from BC turbine – Scenario 1**	**Ethanol**	**42.395**	**2.395**	**7 615**	**255.40**
4.3.1.3.2	Simple BC cycle with regeneration (three FWH) from BC turbine – Scenario 2	R718	42.293	2.293	7 290	93.848
4.4	BC cycle without a low-pressure turbine – Scenario 1	Ethanol	40.75	0.75	2 376	227.2

Section	Configuration	Working fluid	$\eta_{th, BC}$ (percentage)	Efficiency increase (percentage)	Gain in useful work (kW)	$\dot{m}_{BC}$ (kg/s)
4.4	BC cycle without low-pressure turbine – Scenario 2	R718	41.41	1.41	4 464	89.89
4.4.1.1.1	BC cycle without a low-pressure turbine and regeneration with tap-off from BC turbine – Scenario 1	Ethanol	41.49	1.49	4 748	252.3
4.4.1.1.2	BC cycle without a low-pressure turbine and regeneration with tap-off from BC turbine – Scenario 2	R718	41.96	1.96	6 246	96.46
4.4.1.2.1	BC cycle without a low-pressure turbine and regeneration (two FWHs) with tap-off from BC turbine – Scenario 1	Ethanol	41.665	1.665	5 291	252.3
4.4.1.2.2	BC cycle without a low-pressure turbine and regeneration (two FWHs) with tap-off from BC turbine – Scenario 2	R718	42.076	2.076	6 599	96.46
4.4.1.3.1	BC cycle without a low-pressure turbine and regeneration (three FWHs) with tap-off from BC turbine – Scenario 1	Ethanol	41.848	1.848	5 874	266.8
4.4.1.3.2	BC cycle without low-pressure turbine and regeneration (three FWHs) with tap-off from BC turbine – Scenario 2	R718	42.191	2.191	6 964	99.78
4.5.1	BC cycle with tap-off from low-pressure turbine – Scenario 2	R718	41.906	1.906	6 058	87.02
4.5.2	BC cycle with tap-off from low-pressure turbine with regeneration from BC turbine – Scenario 2	R718	42.156	2.156	6 854	91.32
4.6.1	BC cycle with tap-off before low-pressure turbine – Scenario 2	R718	42.076	2.076	6 598	84.54

Section	Configuration	Working fluid	$\eta_{th, BC}$ (percentage)	Efficiency increase (percentage)	Gain in useful work (kW)	$\dot{m}_{BC}$ (kg/s)
4.6.2	BC cycle with tap-off before low-pressure turbine with regeneration from BC turbine – Scenario 2	R718	42.318	2.318	7 369	88.65
4.7.1	BC cycle with tap-off in high-pressure turbine – Scenario 2	R718	41.798	1.798	5 714	84.87
4.7.2	BC cycle with tap-off in high-pressure turbine with regeneration from BC turbine – Scenario 2	R718	42.041	2.041	6 488	88.99
4.8.1	BC cycle without low-pressure turbine and with tap-off in high-pressure turbine – Scenario 2	R718	41.14	1.14	3 615	88.72
4.8.2	BC cycle without low-pressure turbine and with tap-off in high-pressure turbine with regeneration from BC turbine – Scenario 2	R718	42.28	2.28	7 257	94.17

Table 4.26: Summary of maximum results for all configurations

Out of the 30 theoretical configurations tested, the combination that indicates the highest increase in thermal efficiency was the configuration discussed in Section 4.3.1.3.1. The working fluid that indicates the highest increase in efficiency, which was tested in this theoretical configuration, was ethanol. Recent studies indicate that organic fluids with similar characteristics to ethane, such as isobutene and n-pentane, perform well in ORCs, specifically for geothermal application (Yekoladio, 2013).

The increase in thermal efficiency that results from this theoretical configuration with the working fluid ethanol was 2.395%. The configuration, which consists of three FWHs at tap-off pressures from the BC turbine of 29.46, 58.3 and 98.36 kPa each, resulted in corresponding tap-off mass flow rates of 10.678 kg/s, 22.95 kg/s and 11.38 kg/s respectively.

4.10 Conclusion of results

The configurations discussed in Chapter 3 and mapped out in Figure 3.46 were tested according to the method described in Chapter 3. The results obtained for each of the 31 configurations tested were discussed and summarised in Chapter 4.

The results obtained with a simple BC cycle, along with the different variations tested, were discussed. These results included regeneration from inside the BC turbine, from the outlet of the BC turbine and heat exchangers, with steam fed from the low-pressure turbine, high-pressure turbine and inlet of the low-pressure turbine.

The results obtained where the low-pressure turbine had been removed were also discussed, along with the different variations tested, which also included regeneration from inside the BC turbine and regeneration from the outlet of the BC turbine and heat exchangers with steam fed from the high-pressure turbine.

Several tested configurations included heat exchangers or FWHs that had a range of tap-off pressures with corresponding thermal efficiencies. A maximum thermal efficiency was obtained within the tap-off range for each working fluid tested in each configuration.

The maximum thermal efficiency obtained for each configuration, with the corresponding working fluid, is summarised in Table 4.26. The configuration that resulted in the highest increase in thermal efficiency was the simple BC cycle with three FWHs, which was tested under Scenario 1 conditions with the working fluid ethanol. The efficiency increase was 2.395%. The indicated increase in efficiency would be significant to an older power station. The benefits of the increase in thermal efficiency are discussed in Chapter 5.

5. ENVIRONMENTAL ANALYSIS AND BASIC ECONOMIC ANALYSIS

5.1 Introduction

An increase in the thermal efficiency of a coal-fired power plant has a direct impact on its generating cost and environmental impact. This chapter will discuss the high-level analysis of the impact of theoretically installing the BC cycle configuration that indicates the highest increase in thermal efficiency.

5.2 Basic economic analysis

The basic, high-level analysis of the cost saving due to an increase in thermal efficiency was based on Eskom's selling price of electricity (R/kWh) released in 2016, which includes the latest tariff increase approved by the National Energy Regulator of South Africa (NERSA).

5.2.1 Economic analysis methodology

There is a specified tariff for high- and low-demand seasons. There is also a tariff for a specific time of use (TOU)period, i.e. standard, peak and off-peak. Figure 5.1 indicates an example of the season and the TOU.

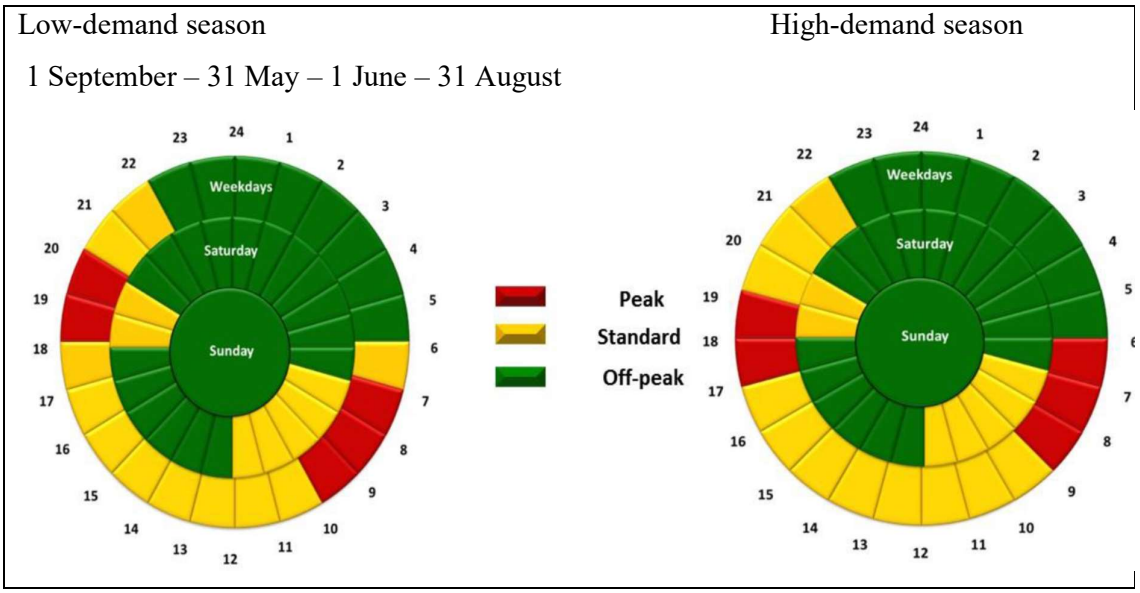

Figure 5.1: TOU periods for low- and high-demand seasons (Eskom, 2016)

The equation below indicates the basic principle used to determine the cost saved annually due to the theoretical implementation of the BC cycle that indicates the highest increase in thermal efficiency.

$$\boldsymbol{Annual\ saving = kW_{BC\ Cycle}\left(\sum_{Peak,Off\ peak}(R/kWh_{TOU} \times Hrs_{TOU})\right)} \quad \textbf{[R/annum]} \quad \textbf{(5.1)}$$

Equation 5.1 therefore works on the principle that the power plant will theoretically be generating additional power and, if Eskom, who with the theoretical implementation of the BC cycle, can sell the additional power generated, it can effectively be seen as the power station, saving a certain amount of money annually. It should also be noted that a rough assumption was made when using the indicated tariff. The indicated tariff is the tariff that Eskom uses to sell electricity to the municipality. The assumption in using this tariff is a rough assumption in the sense that it is assumed that the tariff includes all of the costs associated with generating a kWh of electricity, averaged out over Eskom's fleet of power stations. Seeing that this is a basic economic analysis, this assumption is valid.

The total hours per year for each specified season and TOU were calculated. The tariff applicable for each season and each TOU was then multiplied by the corresponding hours calculated annually and finally multiplied by the kW generated by the BC cycle.

5.2.2 Annual savings due to the implementation of the BC cycle discussed in Section 4.3.2.3.1

The BC cycle that indicates the highest increase in thermal efficiency is the cycle discussed in Section 4.3.1.3.1. The configuration that indicates the highest increase in thermal efficiency is indicated again below in Table 5.1 for ease of reference.

Section	Configuration	Working fluid	$\eta_{th,\ BC}$ (%)	Efficiency increase (%)	Gain in useful work (kW)	$\dot{m}_{BC}$ (kg/s)
4.3.2.3.1	**Simple BC cycle with regeneration (three FWHs) from BC turbine – Scenario 1**	Ethanol	42.395	2.395	7 615	255.4

Table 5.1: BC cycle with the highest increase in thermal efficiency

The method discussed in Section 5.2.1 was used to determine the annual saving when implementing the BC cycle mentioned in Table 5.1. The results are indicated in Table 5.2.

	High-demand season (June to August)			Low-demand season (September to May)		
	Peak	**Standard**	**Off-peak**	**Peak**	**Standard**	**Off-peak**
Total hours per year for TOU	325.0	806.0	1 053.0	975.0	2 418.0	3 159.0
Averaged tariff (R/kWh)[50]	2.71	0.82	0.45	0.89	0.61	0.39
Cost saved annually (R) for BC cycle (4.3.2.3.1)	R6 715 047.35	R5 046 485.40	R3 581 254.85	R6 573 113.27	R11 221 270.02	R9 303 424.43
Total annual saving (R/annum) for implementation of BC cycle (4.3.2.3.1)						**R42 440 595.31**

Table 5.2: Annual cost saved for the implementation of a BC cycle with regeneration from the BC turbine – Scenario 1 assumptions (Eskom, 2016)

[50] Tariffs indicated are averaged over certain sectors to which Eskom provides electricity.

A total annual saving of about R42.4 million was calculated for the theoretical implementation of the mentioned BC cycle. This translates to an annual saving of R17.7 million per increase in thermal efficiency for the Komati Power Station each year.

These figures could be used to determine a payback period for the proposed configuration once the detail design and method of installation for the proposed configuration have been determined.

5.3 Environmental analysis

The environmental study of the theoretical implementation of the indicated BC cycle configuration will cover direct and indirect environmental implications. The direct implication is the reduction in heat released into the atmosphere. The indirect influences on the environment, such as the reduction in CO_2/MW, will also be discussed.

5.3.1 Environmental analysis methodology

As mentioned, a direct and indirect environmental benefit can be gained by implementing the BC, specifically the cycle that indicates the highest increase in thermal efficiency.

5.3.1.1 Direct environmental benefit analysis methodology

Due to the increase in thermal efficiency, it can be deduced that the amount of heat rejected from the cycle will reduce. The amount of heat rejected was calculated during the analysis. The principle was that the heat rejected from the BC cycle's specific configuration was deducted from the heat rejected from the original cycle. The equation below illustrates the principle.

$$\dot{Q}_{Reduction} = \dot{Q}_{L,Original} - \dot{Q}_{L,BC\ cycle} \quad \text{[kW]} \quad (5.2)$$

The reduction in heat released was then related to the heat released per MW generated by the power plant, not considering the additional power generated by the BC cycle. This figure could then be related to the reduction in heat released into the atmosphere should the BC cycle theoretically be implemented on all coal-fired power plants in South Africa.

5.3.1.2 Indirect environmental benefit analysis methodology

The indirect environmental implications of implementing a BC cycle were also analysed by calculating the reduction in tons of CO_2/MW released with and without the BC cycle.

The analysis was conducted by considering the coal compilation of the Komati Power Station, specifically the percentage of carbon in the coal. Considering the normal combustion process,

along with the amount of coal burnt per day, the tons of CO_2 per MW can be calculated. The equations below illustrate this principle more clearly.

$$C + O_2 \rightarrow CO_2 \quad \textbf{(5.3)}$$

From Equation 5.3, the amount of CO_2 per MW was calculated, along with information given by Eskom.

5.3.2 Results from the environmental analysis

The reduction in direct heat released to the atmosphere by theoretically implementing the BC cycle indicated in Table 5.1, which resulted in the highest increase in thermal efficiency, is discussed below.

Table 5.3 indicates the results of the analysis discussed in Section 5.3.1.1. Theoretically implementing the BC cycle that indicates the highest increase in thermal efficiency at the Komati Power Station only resulted in the reduction of direct heat released into the atmosphere by 7.6 MW. If this amount of heat could be reduced at each coal-fired power plant in South Africa by implementing a form of the BC cycle, the theoretical reduction in direct heat released into the atmosphere could be around 2.1 GW.

Komati Power Station's capacity without the BC cycle	(MW)	125
Direct reduction in heat released with the BC cycle	(MW)	7.6
MW Reduction in heat rejected per MW generated	(MW heat reduction/ MW generated)	0.056
South Africa's installed coal-fired power plant capacity (Department of Energy, 2010)	(MW)	37 135
Reduction in direct heat released for all coal-fired power plants with the theoretical implementation of the BC cycle mentioned in Table 5.1	(MW)	2 092.22

Table 5.3: The reduction in direct heat released into the atmosphere with the theoretical implementation of the BC cycle that indicates the highest increase in thermal efficiency

The indirect environmental benefits related to theoretically implementing the BC cycle mentioned in Table 5.1 is also indicated below in Table 5.4.

With recent pressure on all countries to implement methods to mitigate CO_2 emissions and the possibility of introducing carbon tax in South Africa, it becomes clear that a cycle like the BC cycle not only proves to have economic benefits, but also proves to be useful in mitigating CO_2 emissions. The increase in thermal efficiency of a cycle also reduces the CO_2 released.

Several methods have been implemented and tested to increase the thermal efficiency of coal-fired power plants. A recent study by the Energy Information Administration (EIA) indicates a 6 –to 7% reduction in CO_2 emissions by only upgrading an existing plant to increase the thermal efficiency of the plant (Energy Information Administration, 2014b).

The Komati Power Station's upgrade increased its efficiency by 2 to 3% (Siemens, 2012). The BC cycle concept theoretically increases the thermal efficiency even further, which could lead to additional benefits in CO_2 mitigation. This concept is indicated below in Table 5.4. A 5.74% reduction in CO_2 emissions, quantified in t/MW annually, can be achieved.

CO_2 released with original cycle annually	1 075 378	t annually
CO_2 released per MW of generated power with original cycle	8 603.024	t/MW annually
CO_2 released per MW of generated power with implementation of the BC cycle	8109.022	t/MW annually
Difference in emissions between original cycle and BC cycle	494.0016	t/MW annually
Percentage reduction annually due to the BC cycle	5.74%	

Table 5.4: Reduction in CO_2 emissions due to the increase in thermal efficiency of the cycle by implementing the BC cycle

5.4 Conclusion of economic and environmental analysis

The theoretical implementation of the BC cycle with regeneration from the BC turbine (three FWHs) under Scenario 1 assumptions and ethanol as a working fluid could prove to be both economically and environmentally beneficial. An annual saving of R42 million could be achieved with the mentioned cycle implementation, along with an annual reduction of 5.74% in t/MW of CO_2 emissions.

6. CONCLUSION

6.1 Introduction

This chapter summarises all the chapters. The literature study is briefly discussed followed by a description of the theoretical configurations and the methodology used to analyse the theoretical configurations throughout the work. The results obtained from the tested configurations are also discussed, along with the possible benefits of implementing the proposed BC cycle.

6.2 Summary and conclusion on analysis

6.2.1 Summary of literature study

The energy demand is rising and the majority of energy is projected to still be generated from fossil fuel power plants. Coal-fired power plants in South Africa are and will remain the main source of electricity. However, the most common coal-fired power plants in South Africa, namely subcritical coal-fired power plants, generally have a thermal efficiency lower than 36%. This implies that a substantial amount of heat is lost or wasted throughout the cycle, with most of the losses occurring in the condenser.

The waste heat from a cycle can be categorised as high-, medium-, and low-grade waste heat. Several methods have been studied and implemented to recover high- and medium-grade waste heat. However, with most of the losses occurring in the condenser, it would be worthwhile to see if methods can be implemented to recover heat from this low-grade waste heat source.

Different cycles have been studied where heat can be recovered from low-grade waste heat sources, such as the ORC, regenerative ORC, supercritical ORC, trans critical CO_2 cycle, Kalina cycle, Goswami cycle and the trilateral flash cycle. Features and benefits of each of these cycles were discussed. The key issue around these cycles are the working fluids. When selecting a working fluid for an application, it is imperative to keep constraints and characteristics of the working fluid in mind.

A new method to recover waste heat in specifically steam Rankine cycles, namely the BC cycle, was also discussed. A study on the implementation of this cycle preliminarily indicated an increase in thermal efficiency in coal-fired power plants.

6.2.2 Summary of methodology

The methods used to theoretically analyse the proposed application of the BC at the Komati Power Station was then discussed along with the assumptions used for the analysis.

Some 30 configurations were theoretically tested where the BC was implemented. For each configuration, several different working fluids were tested. Some 103 working fluids were tested in the simple BC cycle and 71 of these indicated usable results. The 71 working fluids were tested in all other configurations.

The tested configurations included concepts such as regeneration, including heat exchangers in the BC cycle where steam is tapped off from the steam cycle and FWHs in the BC cycle with tap-off from the BC turbine. These configurations included the following configurations:

- A Configuration of simple BC cycle
- A Simple BC cycle without low-pressure turbine
- A BC cycle with Regeneration
- A BC cycle without a low-pressure turbine and with regeneration or feedwater heating
- A BC cycle with FWHs
- A BC cycle without low-pressure turbine and FWHs
- A BC cycle with tap-off from a low-pressure turbine
- A BC cycle with Tap-off from low-pressure turbine and FWHs
- A BC cycle with tap-off before low-pressure turbine
- A BC cycle with Tap-off before low-pressure turbine and FWHs
- A BC cycle with tap-off in high-pressure turbine
- BC cycle with tap-off in a high-pressure turbine and FWHs
- BC cycle with tap-off in a high-pressure turbine and without the low-pressure turbine
- BC cycle without a low-pressure turbine and tap-off from a high-pressure turbine and FWHs

6.2.3 Summary of results

The analyses of the theoretical implementation of the BC cycle, along with all the variations discussed were tested and the applicable results were discussed.

The discussion started off with a simple BC cycle that was theoretically tested under the assumptions described and scenarios 1 and 2. This served as a base to determine which working fluids can be used for all the proposed variations of the BC cycle. The working fluids tested in

the theoretical configuration under Scenario 1 and Scenario 2 assumptions, which indicated an increase in thermal efficiency above 40%, were discussed and were consequently used in the variations based on the simple BC cycle that included several different combinations, including heat exchangers, FWHs and regeneration from the outlet of the BC turbine.

The theoretical configuration and the working fluid in the theoretical configuration that indicated the highest increase in thermal efficiency was discussed and is indicated in the figure below. The increase in thermal efficiency was 2.395% compared to the original cycle. The working fluid that indicated this increase in thermal efficiency was ethanol.

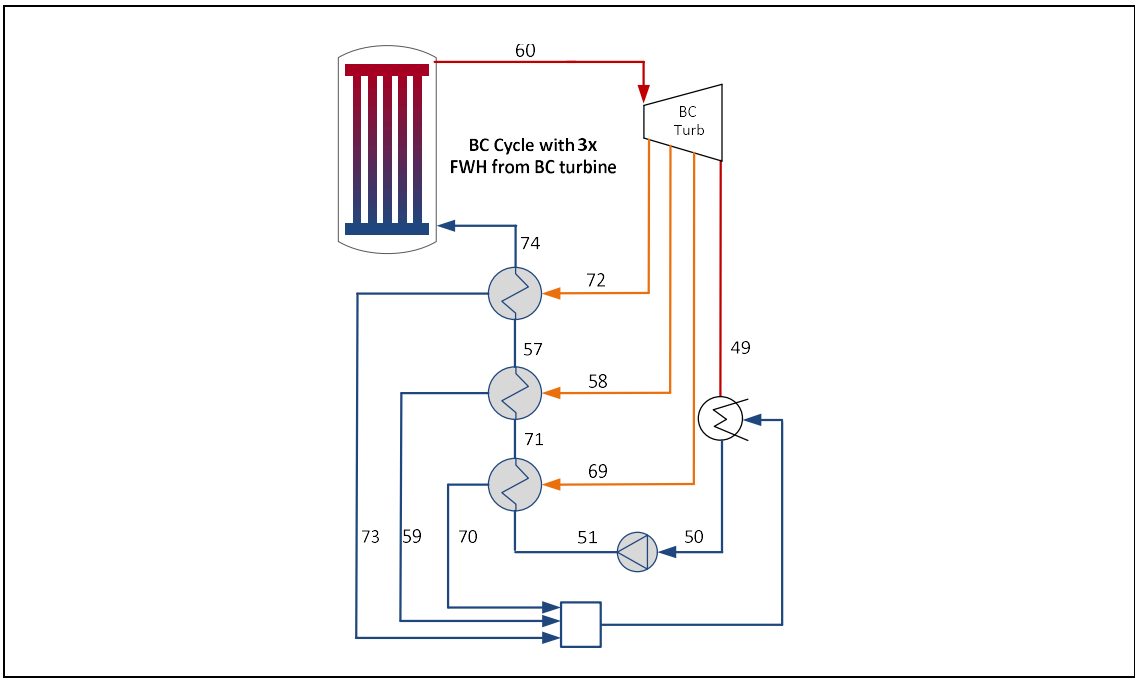

Figure 6.1: Theoretical configuration that resulted in the maximum increase in thermal efficiency

6.2.4 Summary of economic and environmental analysis

The theoretical implementation of the BC cycle, with regeneration from the BC turbine (three FWHs) under Scenario 1 assumptions and ethanol as a working fluid could prove to be both economically and environmentally beneficial. An annual saving of R42 million could be achieved with the mentioned cycle implementation, along with an annual reduction of 5.74% in t/MW of CO_2 emissions.

6.3 Final conclusion and recommendations

The theoretical implementation of the BC cycle on other power plants proved to be beneficial in the sense that it increases the thermal efficiency of the cycle, (Sharifpur, 2007). This study has shown that if the BC cycle were to be theoretically implemented at the Komati Power

Station, along with traditional methods used to increase the thermal efficiency of a power plant, like FWHs, it could result in a maximum increase in thermal efficiency of 2.4%. This increase in thermal efficiency is beneficial from both an economic and environmental point of view.

The increase of 2.4% in thermal efficiency when theoretically implementing the above cycle, though beneficial, did not prove to be as high as the increase in efficiency achieved when the simple BC cycle was tested on Catalagzi power plant. An increase of 7.5% was achieved with only a simple BC cycle (Sharifpur, 2007). A possible reason for the difference could be that the Catalagzi power plant's system presented a higher thermal source for the BC cycle. It can however be concluded that the theoretical implementation of the BC cycle proves to increase the thermal efficiency of a power plant.

A detail design of the recommended configuration, along with the plant layout and where it can be installed in the existing power plant, should be developed for a thorough economic analysis to be completed. With the economic analysis in hand, a recommendation can be made towards the feasibility of the proposed system's implementation at Komati Power Station.

7. REFERENCES

3M, 2003. *3M Novec engineered fluid HFE-7500.* [Online] Available at: http://www.bgrchem.com/specifications/A_SPEC_EN_8589.pdf [Accessed 20 December 2015].

Cengel, Y. A., 2006. *Heat and mass transfer: a practical approach.* 3rd ed. New York, NY: McGraw-Hill.

Cengel, Y. A. & Boles, M. A., 2006. *Thermodynamics an engineering approach.* New York, NY: McGraw-Hill.

Chen, H., Goswami, D. Y. & Stafanakos, E. K., 2010. A review of thermodynamic cycles and working fluids for the conversion of low-grade heat. *Renewable and Sustainable Energy Reviews,* Volume 14, pp. 3059–3067.

Chen, Y., Lundqvist, P., Johansson, A. & Platell, P., 2006. A comparative study of the carbon dioxide transcritical power cycle compared with an organic rankine cycle with R123 as working fluid in waste heat recovery. *Applied Thermal Engineering,* Volume 26, pp. 2142–2147.

Clark, R., 2013. Chief Engineer - Komati Power Station [Interview] (30 January 2013).

Coal Industry Advisory Board, 2010. Power generation from coal. [Online] Available at: https://www.iea.org/ciab/papers/power_generation_from_coal.pdf [Accessed 14 July 2015].

Cuda, P., 2012. *Exergoeconomic analysis and optimization of organic Rankine cycles,* Ontario: University of Ontario Institute of Technology.

Department of Energy, 2010. Integrated Resource Plan, Pretoria: Department of Energy.

Department of Energy, 2014. Basic electricity. [Online] Available at: http://www.energy.gov.za/files/electricity_frame.html [Accessed 13 July 2015].

Department of Energy, 2015. Cogeneration Independent Power Procurement Programme. [Online] Available at: https://www.ipp-cogen.co.za/ [Accessed 14 July 2015].

Drescher, U. & Bruggemann, D., 2006. Fluid selection for the Organic Rankine Cycle (ORC) in biomass power and heat plants. *Applied Thermal Engineering,* Volume 27, pp. 223–228.

Elliott, T., Chen, K. & Swanekamp, R., 1997. *Standard handbook of powerplant engineering.* New York, NY: McGraw-Hill.

El-Wakil, E. E., 1985. *Powerplant technology.* New York, NY: McGraw-Hill.

Energy Information Administration, 2011. International energy statistics - coal reserves. [Online] Available at: http://www.eia.gov/cfapps/ipdbproject/iedindex3.cfm?tid=1&pid=7&aid=6&cid=r6,&syid=2011&eyid=2011&unit=MST [Accessed 13 July 2015].

Energy Information Administration, 2012. EIA independent statistics and analysis. [Online] Available at: http://www.eia.gov/electricity/annual/html/epa_08_02.html [Accessed 22 December 2014].

Energy Information Administration, 2014. EIA independent statistis and analysis. [Online] Available at: www.eia.gov/tools/faqs [Accessed 22 December 2014].

Energy Information Administration, 2014. *Emissions reduction through upgrade of coal-fired power plants,* Paris: International Energy Agency.

Energy Information Administration, 2015. *Annual energy outlook 2013 with projections to 2040.* [Online] Available at: http://www.eia.gov/ [Accessed 10 October 2016].

Engineering Edge, 2006. Power plant components - thermodynamics. [Online] Available at: http://www.engineersedge.com/thermodynamics/power_plant_components.htm [Accessed 2 July 2014].

Engineering Equation Solver, 2015. *Engineering Equation Solver.* New York, NY: McGraw-Hill.

Eskom, 2010. Komati Power Station. [Online] Available at: www.eskom.co.za [Accessed 27 March 2014].

Eskom, 2012. Practical considerations in the implementation of emissions reduction solutions at Eskom's coal-fired power plants. [Online] Available at: http://www.energy.gov.za/files/4thEUSouthAfricaCleanCoalWorkingGroup/Practical%20Considerations%20in%20the%20Implementation%20of%20Emissions%20Reduction%20Solutions%20in%20SA%20Coal%20Fired%20Power%20Plant%20Final.pdf [Accessed 12 July 2015].

Eskom, 2013. Coal in South Africa. [Online] Available at: http://www.eskom.co.za/AboutElectricity [Accessed 17 March 2014].

Eskom, 2013. Facts and figures. [Online] Available at: http://www.eskom.co.za/AboutElectricity [Accessed April 2013].

Eskom, 2014. Power station. [Online] Available at: http://www.eskom.co.za/Whatweredoing/ElectricityGeneration/PowerStations/Pages/Arnot_Power_Station.aspx [Accessed 13 July 2015].

Eskom, 2016. Eskom - Schedule of standard prices for Eskom tariffs. [Online] Available at: http://www.eskom.co.za/CustomerCare/TariffsAndCharges/Pages/Tariffs_And_Charges.aspx [Accessed 31 March 2016].

Habib, M. A. & Zubair, S. M., 1992. Second-law-based thermodynamic analysis of regeneratibe-reheat Rankine cycle power plants. *Energy,* Volume 17(3), pp. 295–301.

Hettiarachchi, H. D. M., Golubovic, M., Worek, W. M. & Ikegami, Y., 2007. Optimum design criteria for an Organic Rankine Cycle using low-temperature geothermal heat sources. *Energy ,* Volume 32, pp. 1698–1706.

Hettiarachchi, H. D. M., Golubovic, M., Worek, W. M. & Ikegami, Y., 2007. The performance of the Kalina Cycle System 11 (KCS-11) with low-temperature heat sources. *Journal of Energy Resources Technology,* Volume 129, pp. 243–247.

Kacludis, A., Lyons, S., Nadav, D. & Zdankiewicz, E., 2012. *Waste heat to power (WH2P) applications using a supercritical CO_2-based power cycle.* Orlando, FL, s.n.

Kiameh, P., 2002. *Power generation handbook: selection, applications, operation, maintenance.* New York, NY: McGraw-Hill.

Larjola, J., 1995. Electricity from industrial waste heat using high-speed Organic Rankine Cycle (ORC). *International Journal Production Economics,* Volume 41, pp. 227–235.

Lui, B., Chien, K. & Wand, C., 2004. Effect of working fluids on Organic Rankine Cycle for waste heat recovery. *Energy,* Volume 29, pp. 1207–1217.

Moran, M. J. & Shapiro, H. N., 2004. *Fundamentals of engineering thermodynamics.* Hoboken, NJ: Wiley.

Nag, P. K. & Gupta, A. V. S. S. K. S., 1998. Energy analysis of the Kalina cycle. *Applied Thermal Engineering,* Volume 18(6), pp. 427–439.

Paanu, T., Niemi, S. & Rantanen, P., 2012. *Waste heat recovery - bottoming cycle alternatives,* Vaasa: University of Vaasa.

Padilla, R. V. et al., 2012. Performance analysis of a Rankine cycle integrated with the Goswami combined power and cooling cycle. *Journal of Energy Resources Technology,* Volume 134, pp. 032001-1 to 032001-8.

Petchers, N., 2003. *Combined heating, cooling and power handbook: technologies and applications.* 1st ed. New York, NY: The Fairmont Press.

Saleh, B., Koglbauer, G., Wandland, M. & Fischer, J., 2007. Working fluids for low-temperature organic Rankine cycles. *Energy ,* Volume 32, pp. 1210–1221.

Sharifpur, M., 2007. *Designing boiling condenser for more efficiency in power plants and less environmental defects.* San Antonio, TX, ASME, pp. 2007–22201.

Siemens, 2012. Komati coal-fired power plant in South Africa back on the grid with new Siemens control technology. [Online] Available at: www.siemens.com [Accessed 27 March 2014].

Sloss, L., 2011. *Efficiency and emissions monitoring and reporting,* Paris: IEA Clean Cloal Centre.

Smith, I., Stosic, N. & Aldis, C., 1995. Trilateral flash cycle system - a high efficiency power plant for liquid resources. *Geothermal Energy,* pp. 2109–2114.

Sonntag, R. E., Brognakke, C. & Van Wylen, G. J., 2002. *Fundemantals of thermodynamics.* New York NY: McGraw-Hill.

Stewart, J., 2003. *Calculus,* 5th ed. Belmont: Thomson Learning.

Tchanche, B. F., Petrissans, M. & Papadakis, G., 2014. Heat resources and organic Rankine Cycle machines. *Renwable and Sustainable Energy Reviews,* Volume 39, pp. 1186–1198.

The Carbon Report, 2014. When will South Africa introduce carbon tax? [Online] Available at: http://www.thecarbonreport.co.za/carbon-tax/ [Accessed 13 July 2015].

Thunmann, A., 1984. *Fundamentals of energy engineering.* Upper Saddle River, NJ: Prentice-Hall.

U.S. Department of Energy, 2014. Waste heat recovery technology assessment. [Online] Available at: http://energy.gov/sites/prod/files/2015/02/f19/QTR%20Ch8%20-%20Waste%20Heat%20Recovery%20TA%20Feb-13-2015.pdf [Accessed 14 July 2015].

United Nations Environmental Program, 2015. Sustainable Innovation Forum - find our more about COP21. [Online] Available at: http://www.cop21paris.org/about/cop21 [Accessed 13 July 2015].

Vijayaraghavan, S. & Goswami, D., 2005. Organic working fluids for a combined power and cooling cycle. *Journal of Energy Resources Technology,* Volume 127, pp. 125–130.

World Coal Association, 2006. Improving efficiencies. [Online] Available at: www.worldcoal.org [Accessed 27 March 2014].

World Coal Association, 2012. Coal statistics. [Online] Available at: http://www.worldcoal.org/ [Accessed 17 March 2014].

World Coal Association, 2014. *A global platform for accelerating coal efficiency.* [Online] Available at: file:///C:/Users/Elmie/Downloads/pace_concept_paper(09_01_2015).pdf [Accessed 13 July 2015].

Yekoladio, P., 2013. *Thermodynamic optimisation of sustainable energy system: application to the optimal design of heat exchangers for geothermal power systems,* Pretoria: University of Pretoria.

Index

Appendix list of figures

Appendix list of tables

APPENDIX A: CHART OF TESTED CONFIGURATIONS

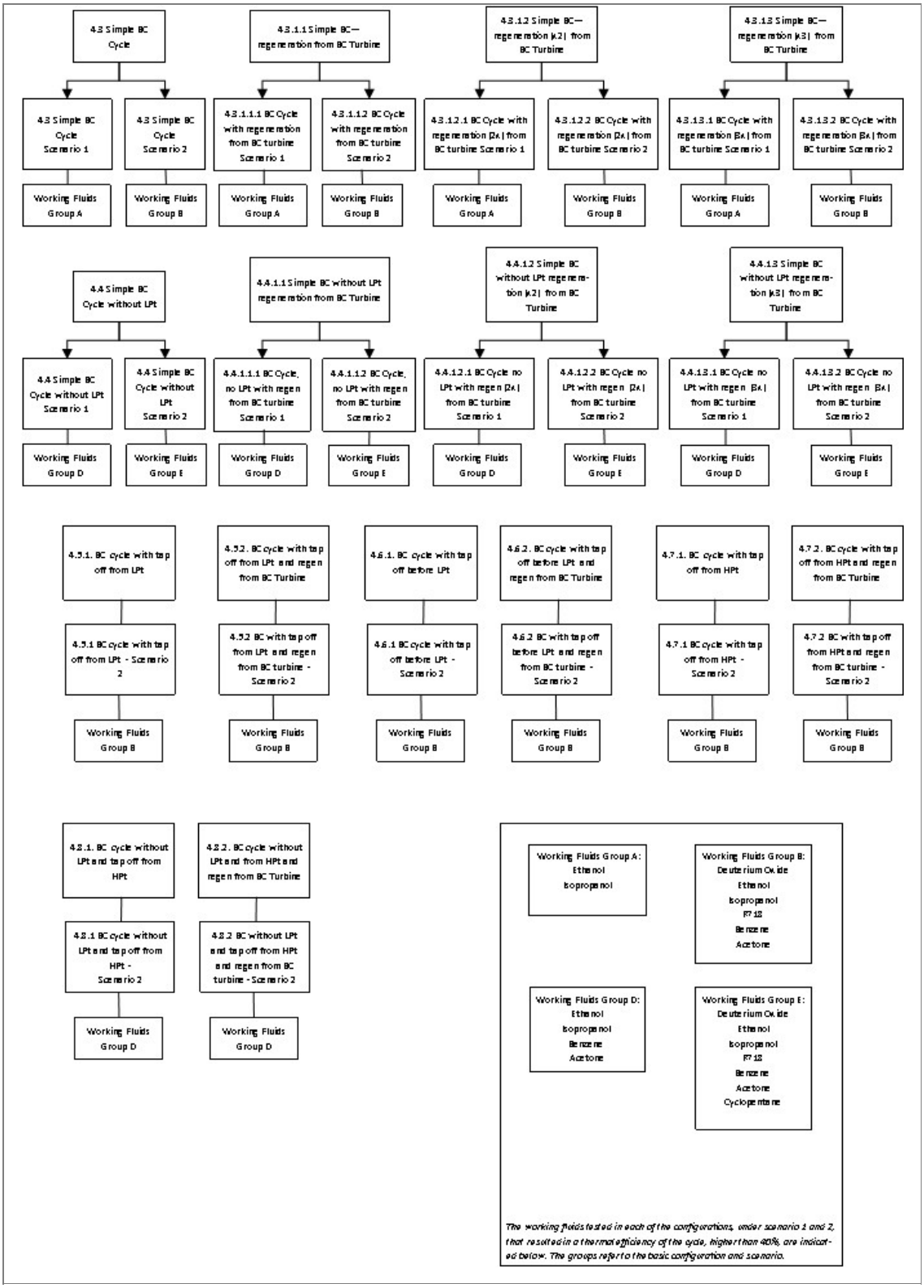

Figure A.1: A chart of tested configurations

APPENDIX B: RESULTS OF CONFIGURATIONS AND WORKING FLUIDS TESTED

B.1 Introduction

The results of the implementation of the boiling condenser (BC) in the different configurations discussed in Chapter 3 will be indicated in Appendix B. The configurations that indicated an increase in thermal efficiency above 40% are discussed in Chapter 4. The configurations and working fluids tested in each configuration that did not result in an increase in thermal efficiency above 40% were not mentioned in Chapter 4. These configurations and working fluids will be indicated here.

B.2 Configuration of a simple BC cycle

The theoretical configuration where the BC was implemented at Komati Power Station is again indicated in **Error! Reference source not found.**2

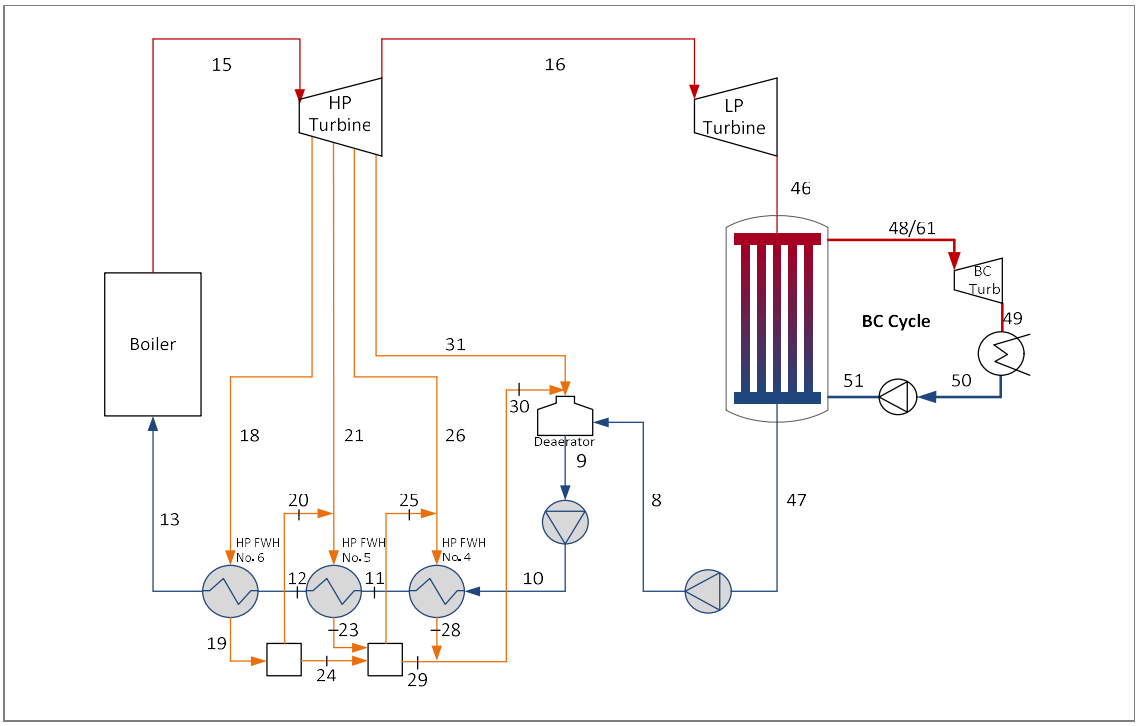

Figure B.2: Component diagram of the Komati Power Station with the BC cycle

The working fluids tested for this configuration, along with the thermal efficiency obtained for each working fluid tested in this configuration, are indicated in Table B.1. The results that indicated an increase in efficiency above 40% are indicated in Chapter 4 and are highlighted in the table below.

Working fluids tested	Scenario 1: With outlet of BC turbine assumed. Note: 25.11.2015: Coding changed to have an efficiency of pump and turbine in the BC cycle = 0.9	η,th,bc	ṁbc (kg/s)	Scenario 2: With inlet of BC turbine assumed. Note: Fixed turbine inlet at T = 100 °C and saturated vapour. Note x_49 as the quality of the outlet of the BC turbine should be above 0.86 to protect the turbine.	η,th,bc	ṁbc (kg/s)	x_49
R11		9.75	1 197		39.88	1 085	0.9905
R113		39.3	1 432		39.54	1 186	1
R114		38.5	1 735		38.81	1 396	1
R12		38.04	1 634		38.15	1 624	0.909
R 123		39.4	1 267		39.6	1 086	1
R1233zd(E)		39.1	1 145		39.41	982.2	1
R1234yf		37.5	1 593		P_61>Pcrit		
R1234ze(E)		38.2	1 370		38.39	1 276	0.9616
R1234ze(Z)		39.3	1 066		39.48	977.9	0.9779
R124		38.5	1 536		38.81	1 357	1
R1243zf		38.2	1 263		38.19	1 286	0.8829
R 125		36.4	2 283		P_61>Pcrit		
R134a		38.2	1 292		37.87	1 446	0.8065
R141b		39.6	951.9		39.76	841.4	1
R142b		39	1 095		39.26	103.2	0.9937
R143a		37	1 534		P_61>Pcrit		
R143m		38.2	1 286		38.22	1 269	0.9099
R152a		38.8	807.2		38.84	826.5	0.8772
R161		38.4	673.1		38.23	816.2	0.742
R218		35.6	3 287		P_61>Pcrit		
R227ea		37.2	2 083		37.64	1 859	0.9992
R22		38.1	1 264		P_61>Pcrit		
R236ea		38.4	1 437		38.87	1 172	1
R236fa		38.2	1 555		38.68	1 295	1
R245fa		38.9	1 162		39.24	980.7	1
R290		38	688.4		P_61>Pcrit		
R32		37.4	886.3		P_61>Pcrit		
R365mfc		38.9	1 122		39.17	893.1	1
R40		39.2	589.8		39.76	607.8	0.8641
R 41		36.4	1 306		P_61>Pcrit		
R500		38.5	1 374		37.53	1 452	0.8614
R 502		37.4	1 884		P_61>Pcrit		
R 600		38.9	610.9		39.23	513.2	1
R600a		38.6	678.1		38.98	571.6	1
R717		38.5	192.3		39.72	209.8	0.8062
R718		39.3	87.71		**40.83**	87.86	0.8749
RC318		37.3	2 212		38.03	1 681	1
Acetone		40	400.5		**40.08**	373.4	0.9636
Ammonia		38.5	192.3		39.72	209.8	0.8062

Working fluids tested	η,th,bc	ṁbc (kg/s)	η,th,bc	ṁbc (kg/s)	x_49
Benzene	40	491.8	**40.14**	445.5	0.9911
Butene	38.8	614.5	39.11	534.4	1
C6 fluoroketone	37.2	2 419	37.68	1 545	1
Carbonyl sulphide	38.3	928	38.74	1 120	0.7372
Cis-2-butene	39.3	557.2	39.51	497.8	1
Cyclohexane	39.7	545.8	39.89	467	1
Cyclopentane	39.8	527.5	39.98	464.9	1
Deuterium oxide	39.3	94.53	**40.76**	94.71	0.8757
Diethyl ether	39.1	595.8	39.41	491.9	1
Dimethyl carbonate	39.9	507	39.52	453.6	1
Dimethyl ether	39.1	554.1	39.17	536.2	0.9278
Ethanol	**40.4**	228.6	**40.43**	223.6	0.9197
FC72	37.1	2 426	37.64	1 562	1
FC87	37	2 408	37.59	1 584	1
HFE7000	38.5	1 627	38.75	1 212	1
HFE7100	38.2	1 817	38.43	1 279	1
HFE7500	38.2	2016	38.33	1 326	1
Isobutane	38.6	678.1	38.98	571.6	1
Isobutene	39	615.1	39.3	533	1
Isopropanol	**40.1**	286	**40.16**	267.7	0.96
MM	38.3	956.4	38.55	688.3	1
n-Butane	38.9	610.9	39.23	513.2	1
n-Dodecane	39.3	596.5	39.41	470.2	1
Neopentane	38.6	729.7	38.92	570.6	1
n-Heptane	39.2	592.3	39.42	471.4	1
n-Hexane	39.1	593.4	39.32	475	1
Nitrous oxide	20	6 622	P_61>Pcrit		
n-Octane	39.3	592.4	39.44	469.4	1
n-Pentane	39.1	595	39.33	103.1	1
n-undecane	39.3	589.1	39.35	471.4	1
Propane	38	688.4	P_61>Pcrit		
SES36	38.4	1 367	38.76	1 176	1
Sulphur dioxide	39.3	616.3	39.97	630.8	0.868
Trans-2-butene	39.2	577.6	39.48	507.7	1

Table B.1: Results from all the working fluids tested in the BC cycle

B.2.1 A simple BC cycle with regeneration

The theoretical configuration where the BC was implemented at the Komati Power Station, which included regeneration from the outlet of the BC turbine, is again indicated in Figure B.33.

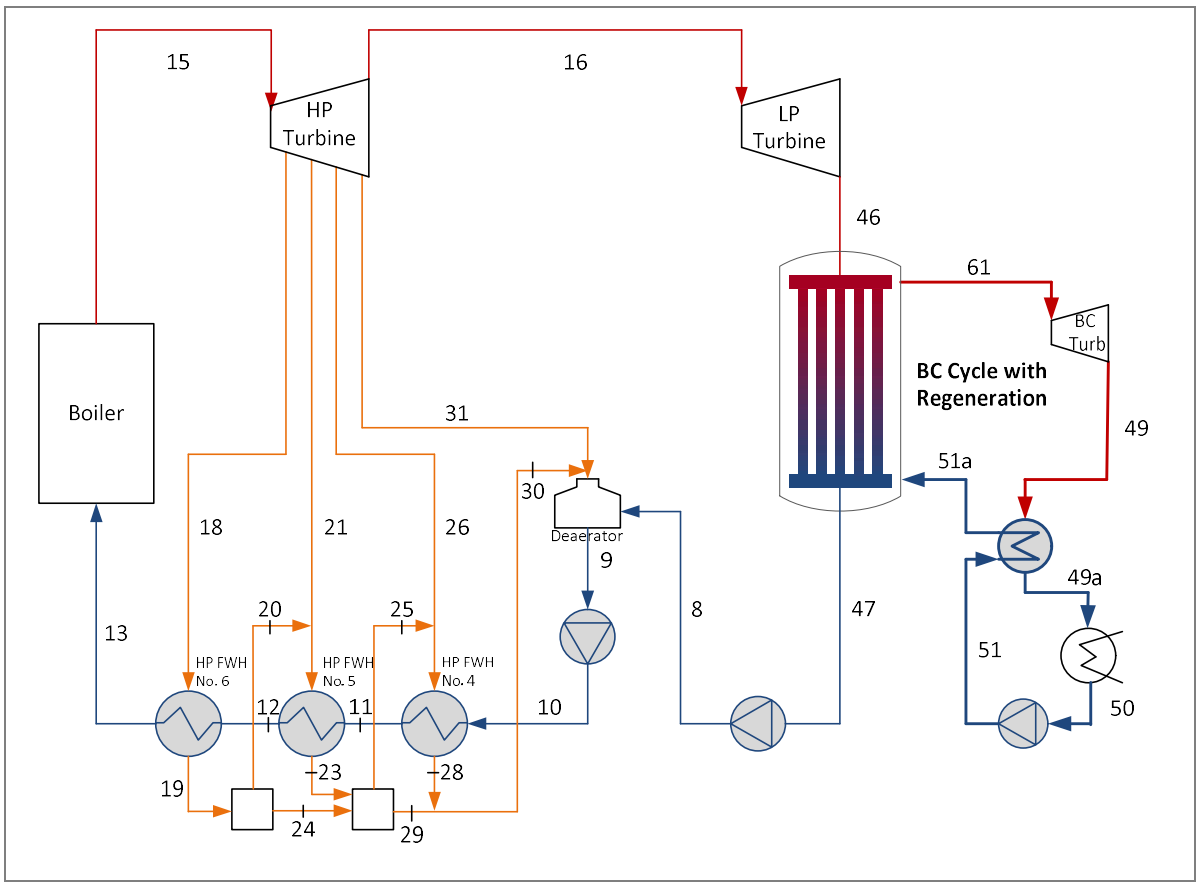

Figure B.3: Component diagram of the Komati Power Station with the BC cycle and regeneration

Table B.1, Scenario 2 indicates the quality at the outlet of the BC turbine. If the quality at the outlet of the BC turbine was 1, the working fluid was tested in the above configuration.

The working fluids tested for this configuration, along with the thermal efficiency obtained for each working fluid tested in this configuration, are indicated in Table B.1. The results that indicated an increase in efficiency above 40% are indicated in Chapter 4 and are highlighted below.

Working Fluids tested for the following 3 scenarios	η,th,bc	ṁbc [kg/s]	Regeneration η gain
R 11			
R 113	39.69	1206	-0.31
R 114	38.99	1425	-1.01
R12			
R 123	39.61	1086	-0.39
R1233zd(E)	BC turbine Outlet temp is too low to allow for a DT of 10degC between T49a and T51a		
R1234yf	P_61>Pcrit		
R1234ze(E)	Not suitable for regeneration, x_49<1		
R1234ze(Z)	Not suitable for regeneration, x_49<1		
R124	BC turbine Outlet temp is too low to allow for a DT of 10degC between T49a and T51a		
R1243zf	Not suitable for regeneration, x_49<1		
R 125	P_61>Pcrit		
R134a	Not suitable for regeneration, x_49<1		
R141b	BC turbine Outlet temp is too low to allow for a DT of 10degC between T49a and T51a		
R142b	Not suitable for regeneration, x_49<1		
R143a	P_61>Pcrit		
R143m	Not suitable for regeneration, x_49<1		
R152a	Not suitable for regeneration, x_49<1		
R161	Not suitable for regeneration, x_49<1		
R218	P_61>Pcrit		
R227ea	Not suitable for regeneration, x_49<1		
R22	P_61>Pcrit		
R236ea	38.99	1188	-1.01
R236fa	BC turbine Outlet temp is too low to allow for a DT of 10degC between T49a and T51a		
R245fa	39.26	982.3	-0.74
R290	P_61>Pcrit		
R32	P_61>Pcrit		
R365mfc	39.46	921.2	-0.54
R40	Not suitable for regeneration, x_49<1		
R 41	P_61>Pcrit		
R500	Not suitable for regeneration, x_49<1		
R 502	P_61>Pcrit		

R 600	39.26	514.8	-0.74
R600a	BC turbine Outlet temp is too low to allow for a DT of 10degC between T49a and T51a		
R717	Not suitable for regeneration, x_49<1		
R718	Not suitable for regeneration, x_49<1		
RC318	38.29	1736	-1.71
Other working fluids			
Acetone	Not suitable for regeneration, x_49<1		
Ammonia	Not suitable for regeneration, x_49<1		
Benzene	Not suitable for regeneration, x_49<1		
Butene	BC turbine Outlet temp is too low to allow for a DT of 10degC between T49a and T51a		
C6 Fluoroketone	38.56	1722	-1.44
Carbonyl Sulfide	Not suitable for regeneration, x_49<1		
cis-2-butene	Not suitable for regeneration, x_49<1		
cyclohexane	39.95	469.9	-0.05
cyclopentane	BC turbine Outlet temp is too low to allow for a DT of 10degC between T49a and T51a		
DeuteriumOxide	Not suitable for regeneration, x_49<1		
DiethylEther	39.55	499.6	-0.45
dimethylcarbonate	BC turbine Outlet temp is too low to allow for a DT of 10degC between T49a and T51a		
DimethylEther	Not suitable for regeneration, x_49<1		
Ethanol	Not suitable for regeneration, x_49<1		
FC72	38.52	1749	-1.48
FC87	38.4	1754	-1.6
HFE7000	EES doesn't have this working fluid's properties anymore		
HFE7100	39.12	1383	-0.88
HFE7500	39.15	1692	-0.85
ISOBUTANE	BC turbine Outlet temp is too low to allow for a DT of 10degC between T49a and T51a		
Isobutene	BC turbine Outlet temp is too low to allow for a DT of 10degC between T49a and T51a		
isopropanol	Not suitable for regeneration, x_49<1		
MM	39.19	740.3	-0.81
n-Butane	39.26	514.8	-0.74
n-Dodecane	39.8	489.3	-0.2
Neopentane	39.22	590.2	-0.78
n-Heptane	39.75	488	-0.25
n-Hexane	39.61	490.2	-0.39
NitrousOxide	P_61>Pcrit		
n-Octane	39.79	487	-0.21
n-Pentane	39.55	494.7	-0.45
n-undecane	39.72	490.4	-0.28
Propane	P_61>Pcrit		

SES36	BC turbine Outlet temp is too low to allow for a DT of 10degC between T49a and T51a
Sulfurdioxide	Not suitable for regeneration, x_49<1
trans-2-butene	Not suitable for regeneration, x_49<1

Table B.2: Results from all working fluids tested in the BC cycle with regeneration from the outlet of the BC turbine

B.2 A simple BC cycle without a steam-cycle low-pressure turbine

The theoretical configuration where the BC was implemented at the Komati Power Station and the low-pressure turbine was removed is indicated again in Figure B.44.

All the results obtained for this tested configuration, along with the tested working fluids, are indicated in Table B.3.

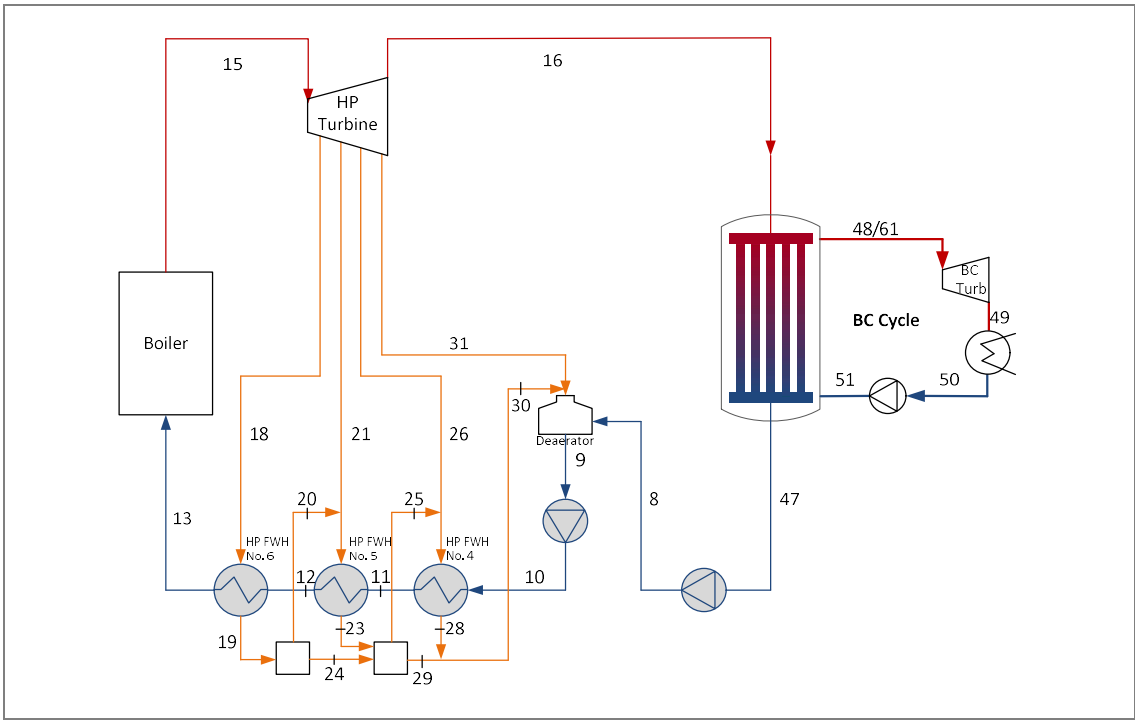

Figure B.4: Component diagram of the Komati Power Station without a low-pressure turbine with the BC cycle

Working fluids tested		η,th,bc	ṁbc (kg/s)		η,th,bc	ṁbc (kg/s)
R11	Scenario 1: No low-pressure turbine with the outlet of the	39.69	1 198	Scenario 2: No low-pressure turbine with the inlet of the	39.88	1 084
R113		38.93	1 441		39.38	1 157
R114		37.6	1 762		38.18	1 383
R12		37.68	1 659		P_61>Pcrit	
R123		39.04	1 275		39.46	1 071
R1233zd(E)		38.64	1 154		39.15	976.5

Working fluids tested	η,th,bc	ṁbc (kg/s)	η,th,bc	ṁbc (kg/s)
R1234yf	36.17	1 627	P_61>Pcrit	
R1234ze(E)	36.99	1 397	P_61>Pcrit	
R1234ze(Z)	38.95	1 073	39.17	1 000
R124	37.55	1 560	37.72	1 499
R1243zf	37.12	1 287	P_61>Pcrit	
R125	35.35	2 316	P_61>Pcrit	
R134a	37.07	1 316	P_61>Pcrit	
R141b	39.38	955.1	39.7	834.6
R142b	38.42	1 106	38.74	1 012
R143a	36.04	1 556	P_61>Pcrit	
R143m	37	1 312	P_61>Pcrit	
R152a	37.95	819.2	P_61>Pcrit	
R161	P51>Pcrit		P_61>Pcrit	
R218	P51>Pcrit		P_61>Pcrit	
R227ea	35.78	2 130	P_61>Pcrit	
R22	37.34	1 280	P_61>Pcrit	
R236ea	37.49	1 460	38.29	1 173
R236fa	37.1	1 584	37.79	1 370
R245fa	38.34	1 175	38.85	973.8
R290	36.91	700.5	P_61>Pcrit	
R32	36.82	894.6	P_61>Pcrit	
R365mfc	38.23	1 134	38.82	865.3
R40	38.69	595.9	39.52	648.6
R41	35.52	1 321	P_61>Pcrit	
R500	37.46	1 397	P_61>Pcrit	
R502	36.42	1913	P_61>Pcrit	
R600	38.24	617.8	38.85	509.4
R600a	37.73	688.1	38.39	580.2
R717	37.88	194.3	39.27	237.9
R718	38.19	89.48	**41.41**	89.89
RC318	35.77	2 267	P_61>Pcrit	
Acetone	40.11	399.6	**40.25**	373.7
Ammonia	37.88	194.3	39.72	237.9
Benzene	40.09	491.1	**40.32**	440
Butene	38.29	620.1	38.78	538.7
C6 fluoroketone	35.33	2 494	36.68	1 444
Carbonyl sulphide	37.63	937.9	P_61>Pcrit	
Cis-2-butene	38.9	561	39.29	495.2
Cyclohexane	39.58	547	39.91	454.4

Working fluids tested	η,th,bc	ṁbc (kg/s)	η,th,bc	ṁbc (kg/s)
Cyclopentane	39.73	528.1	**40.04**	456.9
Deuterium oxide	38.18	96.43	**41.32**	96.88
Diethyl ether	38.65	600.8	39.18	480.2
Dimethyl carbonate	39.91	506.7	39.71	446.4
Dimethyl ether	38.44	560.4	38.38	590.3
Ethanol	**40.75**	227.2	**40.75**	226.3
FC72	35.42	2 497	36.69	1 459
FC87	35.13	2 485	36.41	1 481
HFE7000	37.49	1 655	38.15	1 161
HFE7100	37.03	1 852	37.74	1 204
HFE7500	36.95	2 059	37.54	1 230
Isobutane	37.73	688.1	38.39	580.2
Isobutene	38.35	621.8	38.89	535.3
Isopropanol	**40.2**	285.4	**40.33**	267.8
MM	37.39	971.7	37.98	649.4
n-Butane	38.24	617.8	38.85	509.4
n-Dodecane	38.87	600.7	39.17	448.9
Neopentane	37.66	741	38.42	553.7
n-Heptane	38.81	596.8	39.18	452.5
n-Hexane	38.69	597.9	39.09	457.4
Nitrous oxide	P51>Pcrit		P_61>Pcrit	
n-Octane	38.86	596.7	39.21	449.5
n-Pentane	38.57	600.2	39.08	469.1
n-undecane	38.86	602.3	39.35	471.4
Propane	36.91	700.5	P_61>Pcrit	
SES36	37.9	1 379	38.45	1 174
Sulphur dioxide	38.66	622.9	39.91	665.1
Trans-2-butene	38.76	582.3	39.21	505.2

Table B.3: A BC cycle without steam-side low-pressure turbine working fluids tested and results

B.2.1 A BC cycle without a low-pressure turbine and with regeneration from the BC turbine outlet

The theoretical configuration where the BC was implemented at the Komati Power Station and where the low-pressure turbine was removed, with regeneration in the BC cycle, is indicated again in Figure B.55.

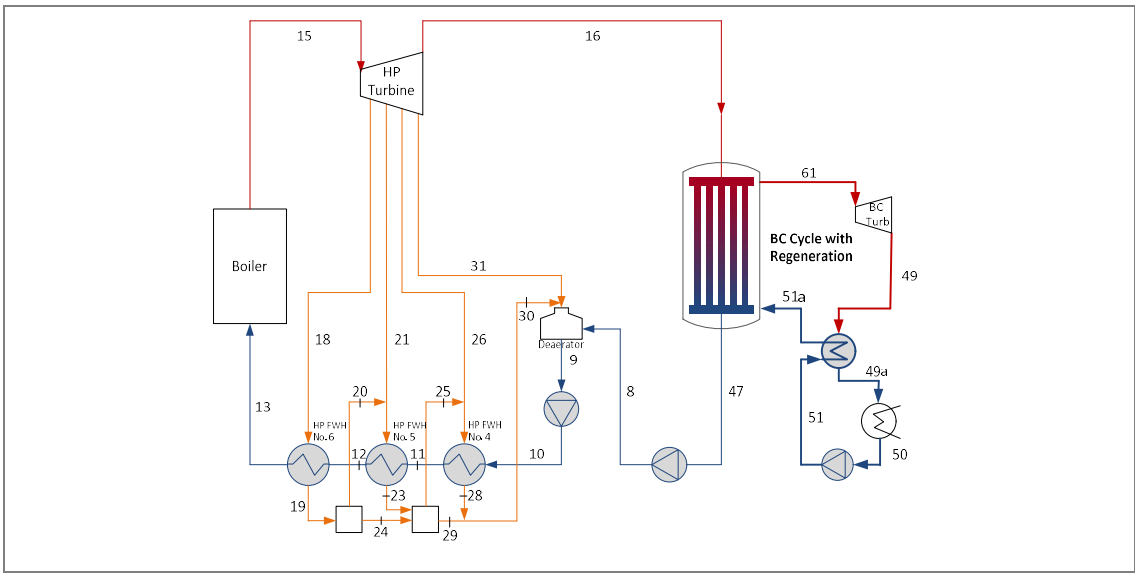

Figure B.5: Component diagram of the Komati Power Station without a low-pressure turbine, including the BC cycle with regeneration

All the results obtained for this tested configuration, along with the tested working fluids, are indicated in Table B.34.

Working Fluids tested for the following 3 scenarios		η,th,bc	ṁbc [kg/s]	Regeneration η gain
R 11	Scenario 3. NO LP turbine. Simple BC with fixed turbine inlet and regeneration on working fluids with super heater vapor @	Not suitable for regeneration, x_49<1		
R 113		**39.72**	1190	-0.28
R 114		**38.47**	1422	-1.53
R12		P_61>Pcrit		
R 123		**39.56**	1079	-0.44
R1233zd(E)		**39.17**	978.5	-0.83
R1234yf		P_61>Pcrit		
R1234ze(E)		Not suitable for regeneration, x_49<1		
R1234ze(Z)		Not suitable for regeneration, x_49<1		
R124		Not suitable for regeneration, x_49<1		
R1243zf		Not suitable for regeneration, x_49<1		

R 125		P_61>Pcrit		
R134a		Not suitable for regeneration, x_49<1		
R141b		Not suitable for regeneration - BCt outlet temp is too low		
R142b		Not suitable for regeneration, x_49<1		
R143a		P_61>Pcrit		
R143m		Not suitable for regeneration, x_49<1		
R152a		Not suitable for regeneration, x_49<1		
R161		Not suitable for regeneration, x_49<1		
R218		P_61>Pcrit		
R227ea		Not suitable for regeneration, x_49<1		
R22		P_61>Pcrit		
R236ea		**38.47**	1193	-1.53
R236fa		Not suitable for regeneration - BCt outlet temp is too low		
R245fa		**38.93**	981	-1.07
R290		P_61>Pcrit		
R32		P_61>Pcrit		
R365mfc		**39.36**	906.9	-0.64
R40		Not suitable for regeneration, x_49<1		
R 41		P_61>Pcrit		
R500		Not suitable for regeneration, x_49<1		
R 502		P_61>Pcrit		
R 600		**38.95**	513.8	-1.05
R600a		Not suitable for regeneration - BCt outlet temp is too low		
R717		Not suitable for regeneration, x_49<1		
R718		Not suitable for regeneration, x_49<1		
RC318		P_61>Pcrit		
Other working fluids				
Acetone		Not suitable for regeneration, x_49<1		
Ammonia		Not suitable for regeneration, x_49<1		
Benzene		Not suitable for regeneration, x_49<1		
Butene		Not suitable for regeneration - BCt outlet temp is too low		
C6 Fluoroketone		**38.04**	1661	-1.96
Carbonyl Sulfide		Not suitable for regeneration, x_49<1		
cis-2-butene		Not suitable for regeneration - BCt outlet temp is too low		
cyclohexane		**40.14**	462.9	0.14
cyclopentane		Not suitable for regeneration - BCt outlet temp is too low		
DeuteriumOxide		Not suitable for regeneration, x_49<1		
DiethylEther		**39.5**	493.8	-0.5
dimethylcarbonate		Not suitable for regeneration - BCt outlet temp is too low		
DimethylEther		Not suitable for regeneration, x_49<1		
Ethanol		Not suitable for regeneration, x_49<1		

FC72		**38.11**	1689	-1.89
FC87		**37.69**	1698	-2.31
HFE7000		Not suitable for regeneration - BCt outlet temp is too low		
HFE7100		**38.88**	1340	-1.12
HFE7500		**38.87**	1395	-1.13
ISOBUTANE		Not suitable for regeneration - BCt outlet temp is too low		
Isobutene		Not suitable for regeneration - BCt outlet temp is too low		
isopropanol		Not suitable for regeneration, x_49<1		
MM		**39.06**	717.4	-0.94
n-Butane		**38.95**	513.8	-1.05
n-Dodecane		**39.9**	477.2	-0.1
Neopentane		**38.96**	581.8	-1.04
n-Heptane		**39.82**	477.3	-0.18
n-Hexane		**39.66**	480.5	-0.34
NitrousOxide		P_61>Pcrit		
n-Octane		**39.88**	475.7	-0.12
n-Pentane		**39.52**	487.2	-0.48
n-undecane		**39.83**	478.2	-0.17
Propane		P_61>Pcrit		
SES36		Not suitable for regeneration - BCt outlet temp is too low		
Sulfurdioxide		Not suitable for regeneration, x_49<1		
trans-2-butene		Not suitable for regeneration, x_49<1		

Table B.4: Results from all working fluids tested in the BC cycle without a low-pressure steam turbine and with regeneration from the outlet of the BC turbine

B2.2 A BC cycle without a low-pressure turbine and FWHs with tap off from the BC turbine

The results obtained for the captioned theoretical configurations will be discussed below. The configurations with one, two and three feed water heaters (FWHs) are indicated for Scenario 1 and Scenario 2.

Each configuration's theoretical component diagram will be indicated, followed by the results obtained for the working fluids tested under Scenario 1 and Scenario 2 conditions.

B2.2.1 A BC cycle without a low-pressure turbine and one FWH with tap off from BC turbine

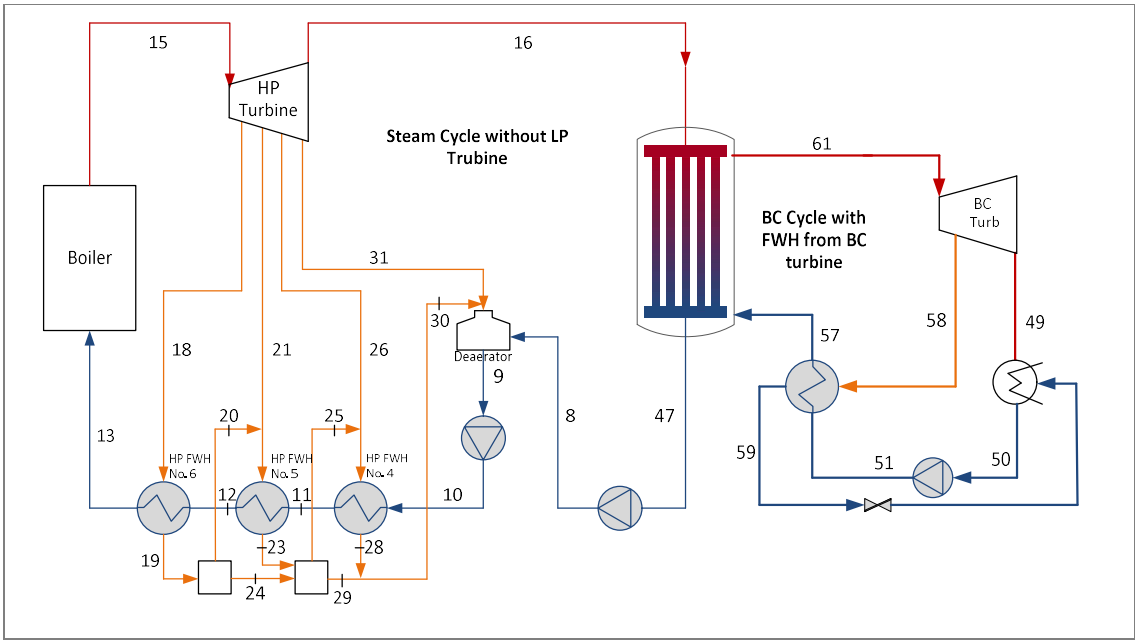

Figure B.6: Component diagram of the Komati Power Station without a low-pressure turbine, including the BC cycle with one FWH

B2.2.1.1 A BC cycle without a low-pressure turbine and one FWH with tap off from the BC turbine – Scenario 1

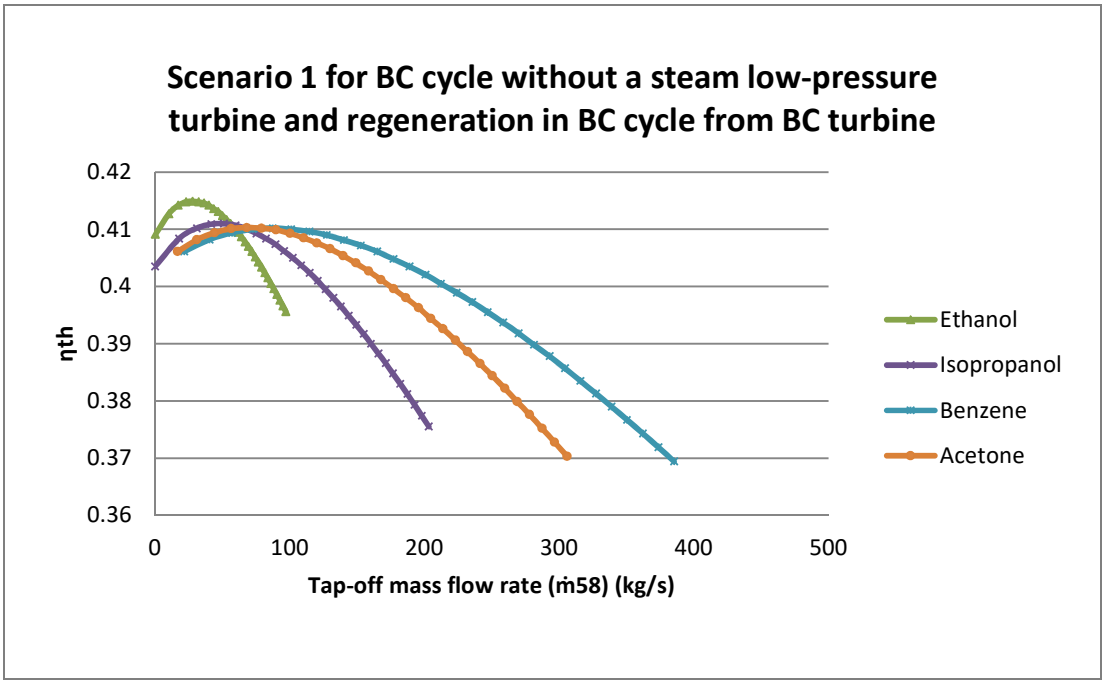

Figure B.7: The thermal efficiency for the tap-off mass flow rate range for analysis conducted at the Komati Power Station without a low-pressure turbine and regeneration (one FWH) in the BC cycle from the BC turbine under Scenario 1 assumptions

B2.2.1.2 A BC cycle without a low-pressure turbine and one FWH with tap off from the BC turbine – Scenario 2

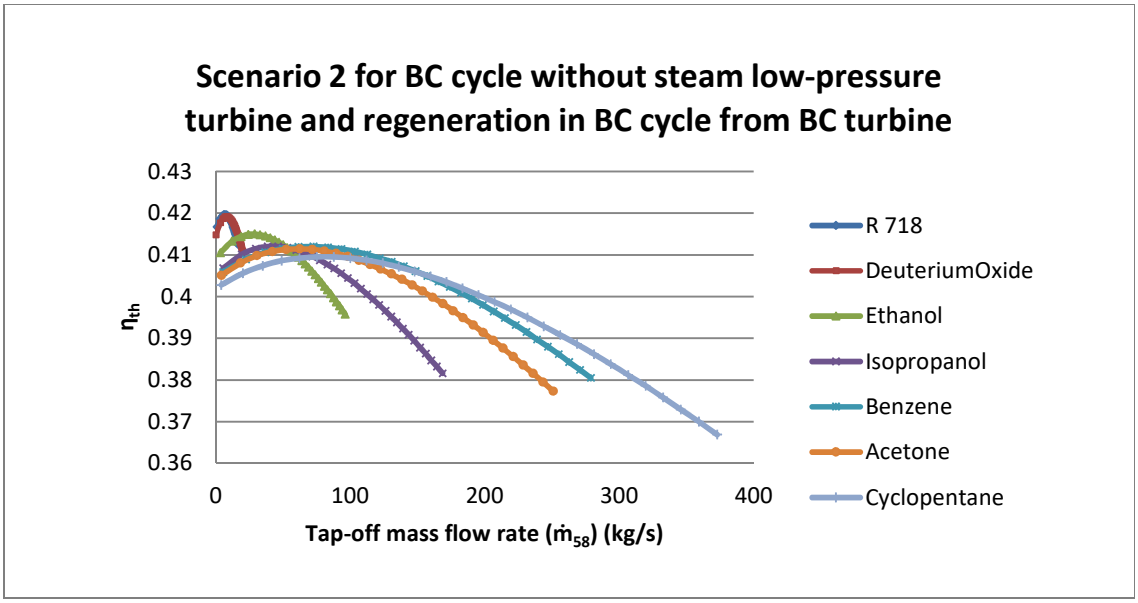

Figure B.8: The thermal efficiency for the tap-off mass flow rate range for analysis conducted at the Komati Power Station without a low-pressure turbine and regeneration (one FWH) in the BC cycle from the BC turbine under Scenario 2 assumptions

B2.2.2 A BC cycle without a low-pressure turbine and two FWHs with tap off from a BC turbine

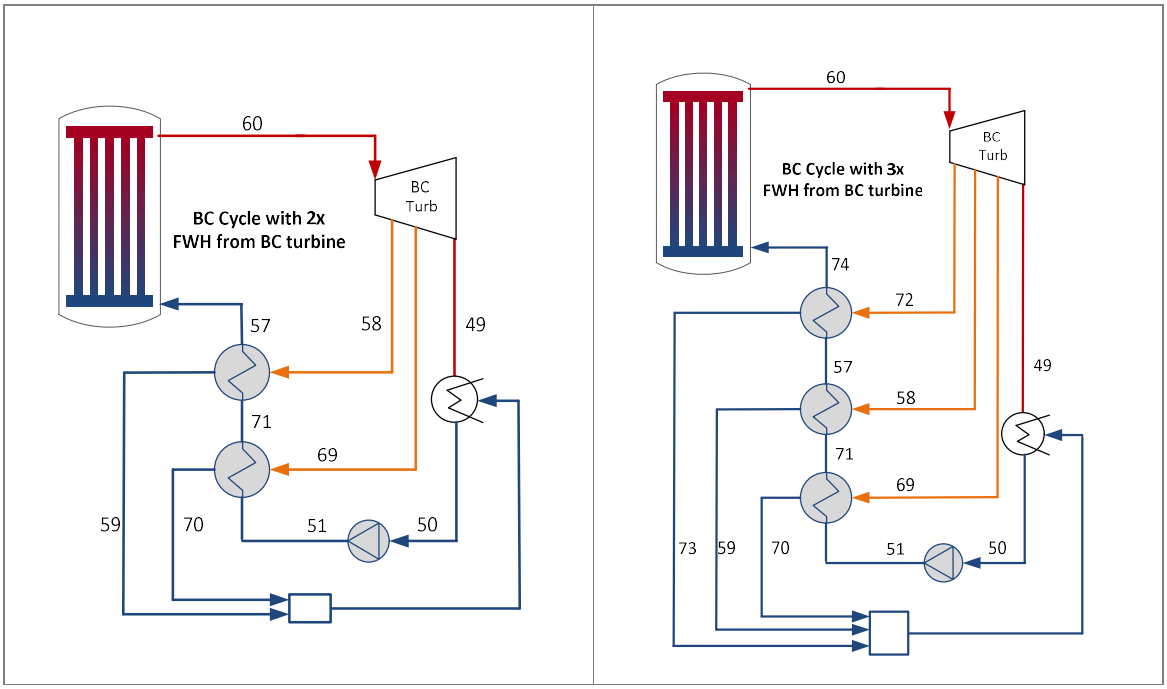

Figure B.9: A BC cycle with two and three FWHs

B2.2.2.1 A BC cycle without a low-pressure turbine and two FWHs with tap off from the BC turbine – Scenario 1

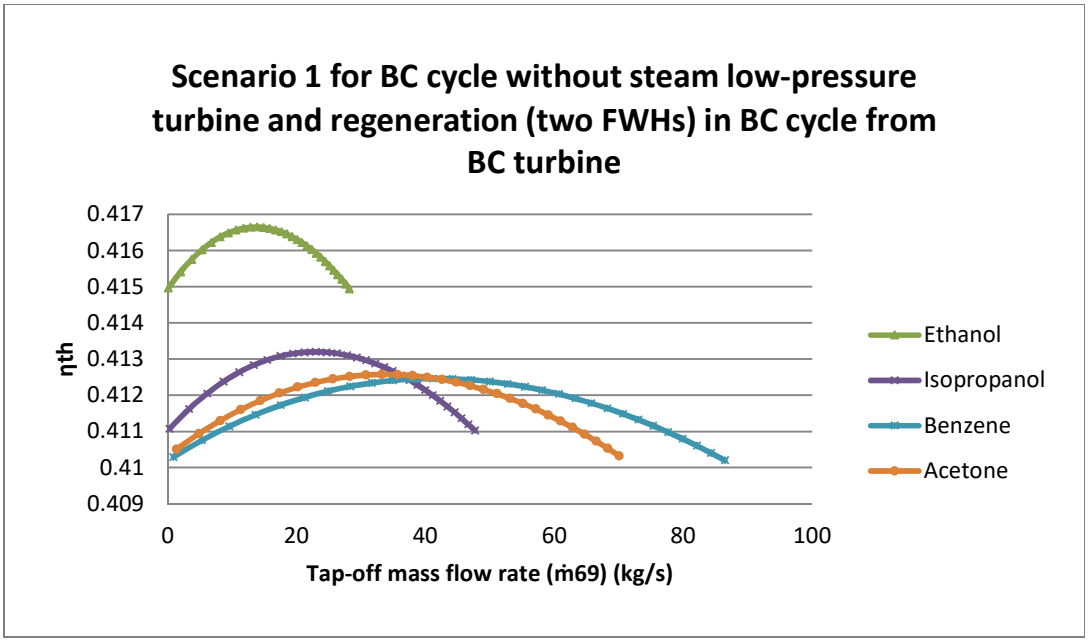

Figure B.10: The thermal efficiency for the tap-off mass flow rate range for analysis conducted at the Komati Power Station, without a low-pressure turbine and regeneration (two FWHs) in the BC cycle from the BC turbine under Scenario 1 assumptions

B2.2.2.2 A BC cycle without a low-pressure turbine and two FWHs with tap off from the BC turbine – Scenario 1

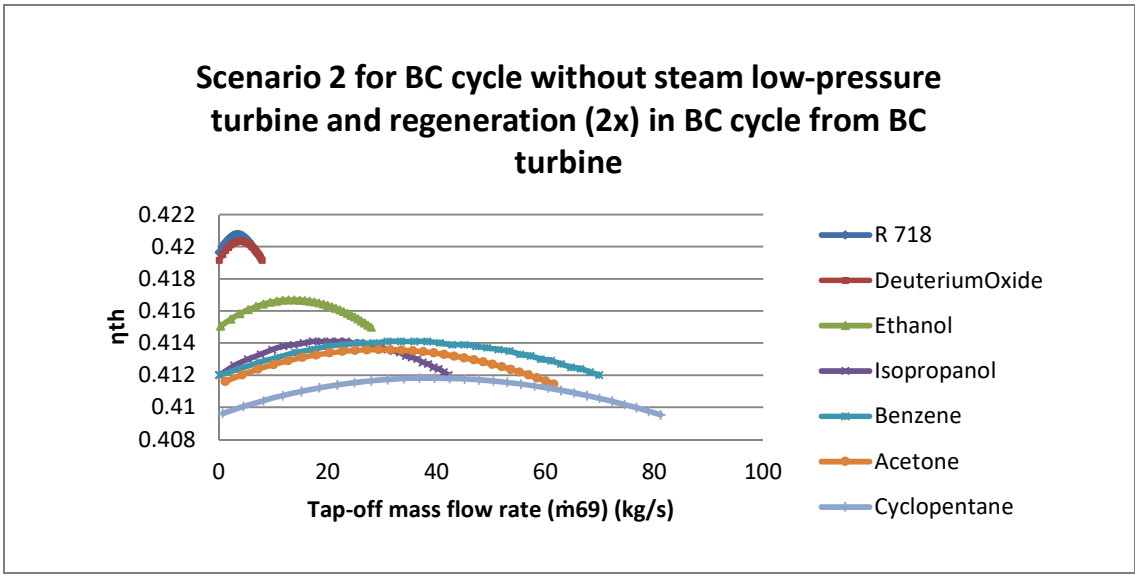

Figure B.11: The thermal efficiency for the tap-off mass flow rate range for analysis conducted at the Komati Power Station, without a low-pressure turbine and regeneration (two FWHs) in the BC cycle from the BC turbine

B2.2.3 A BC cycle without a low-pressure turbine and three FWHs with tap off from the BC turbine

B2.2.3.1 A BC cycle without a low-pressure turbine and three FWHs with tap off from the BC turbine – Scenario 1

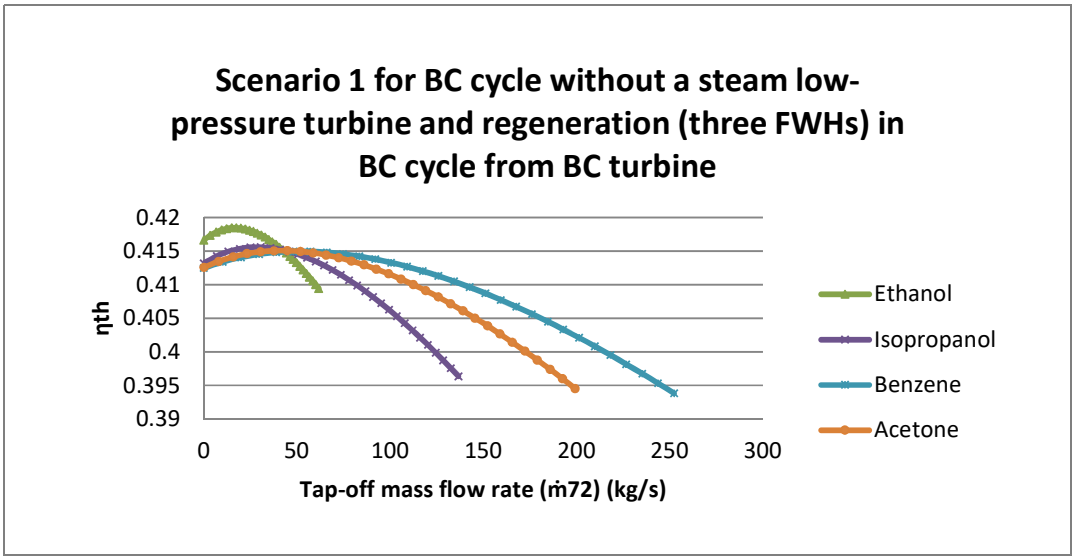

Figure B.12: The thermal efficiency for the tap-off mass flow rate range for analysis conducted at the Komati Power Station, without a low-pressure turbine and regeneration (three FWHs) in the BC cycle from the BC turbine under Scenario 1 assumptions

B2.2.3.2 A BC cycle without a low-pressure turbine and three FWHs with tap off from the BC turbine – Scenario 2

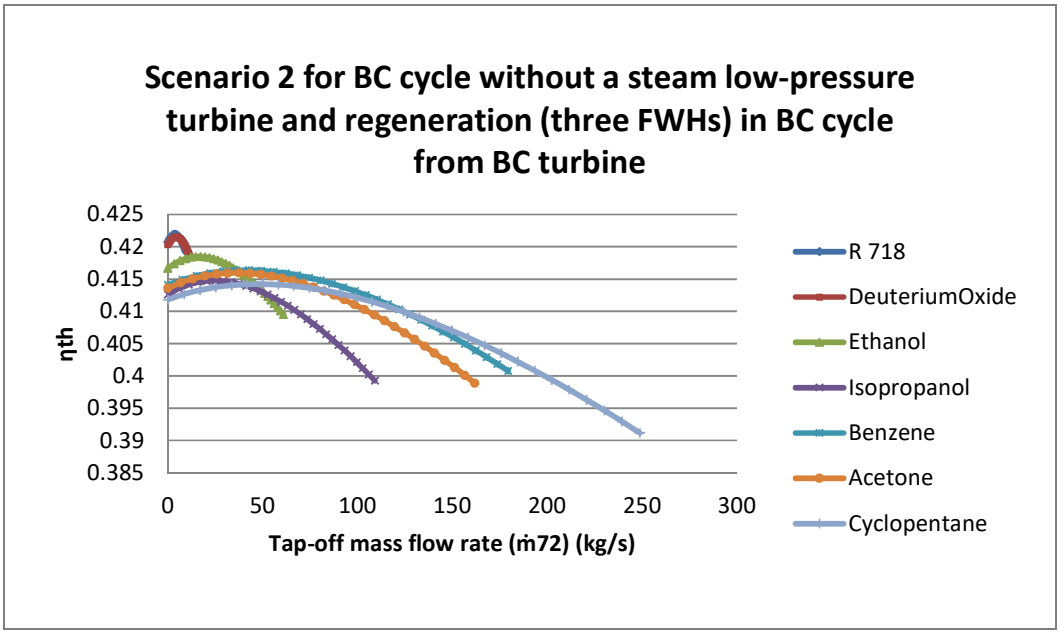

Figure B.13: The thermal efficiency for the tap-off mass flow rate range for analysis conducted at the Komati Power Station without a low-pressure turbine and regeneration (three FWHs) in the BC cycle from the BC turbine

B.3 A BC cycle with tap off in a low-pressure turbine and FWHs

The results for the configuration indicated in Figure B.144 will be discussed below.

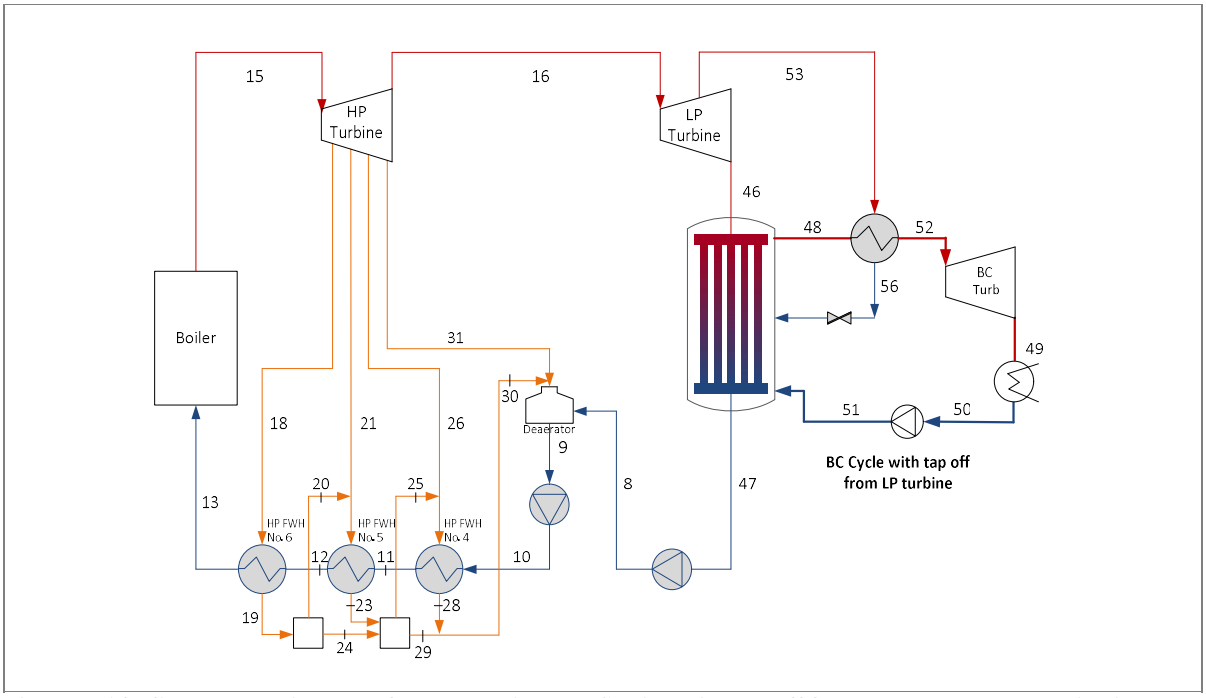

Figure B.14: Component diagram of the Komati Power Station with tap off from a low-pressure turbine in the BC cycle

Only Scenario 2 assumptions indicated useful results. These assumptions are shown below.

B.3.1 A BC cycle with tap off in a low-pressure turbine

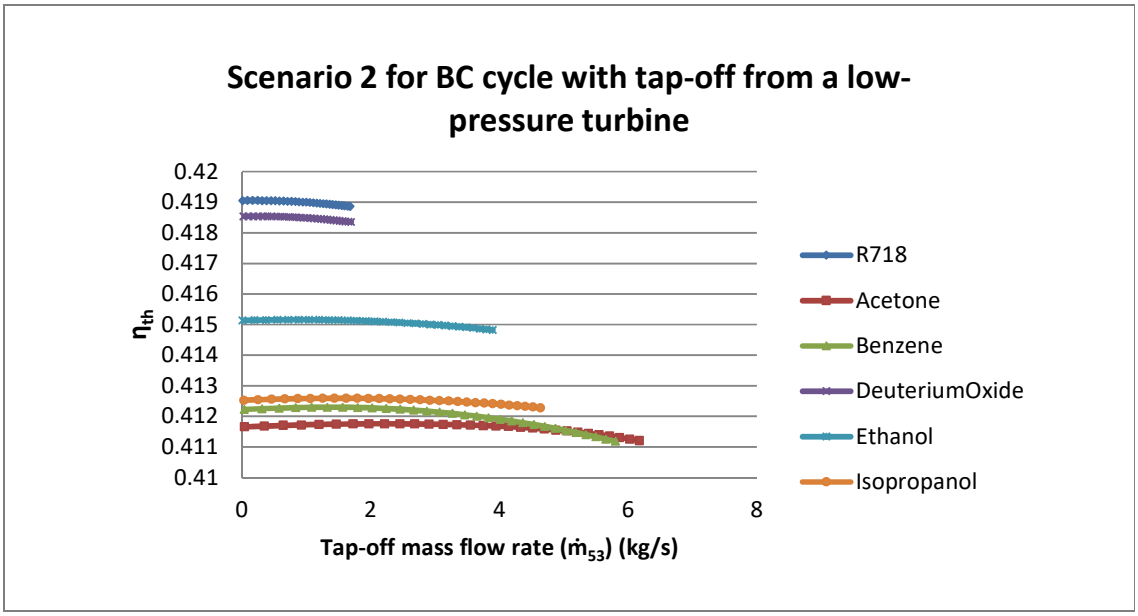

Figure B.15: The thermal efficiency for the tap-off mass flow rate range for analysis conducted at the Komati Power Station, with tap off from the steam-side low-pressure turbine when implementing a simple BC cycle

B.3.2 Tap off in a low-pressure turbine and FWHs

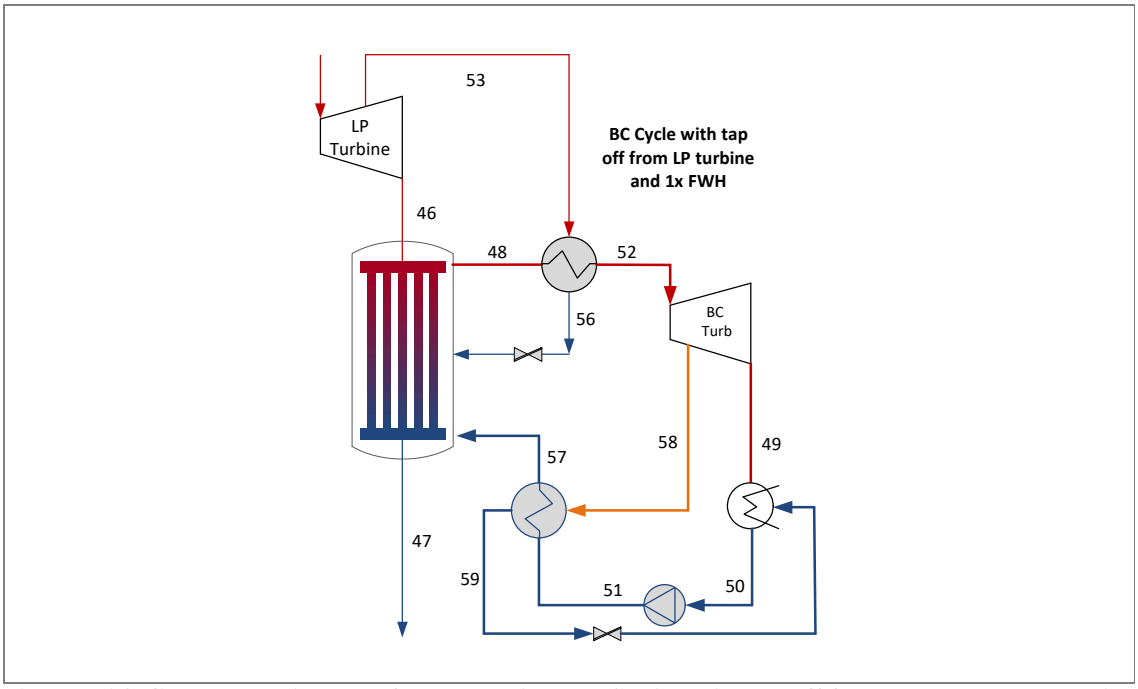

Figure B.16: Component diagram of the Komati Power Station with tap off from a low-pressure turbine into the BC cycle and FWHs

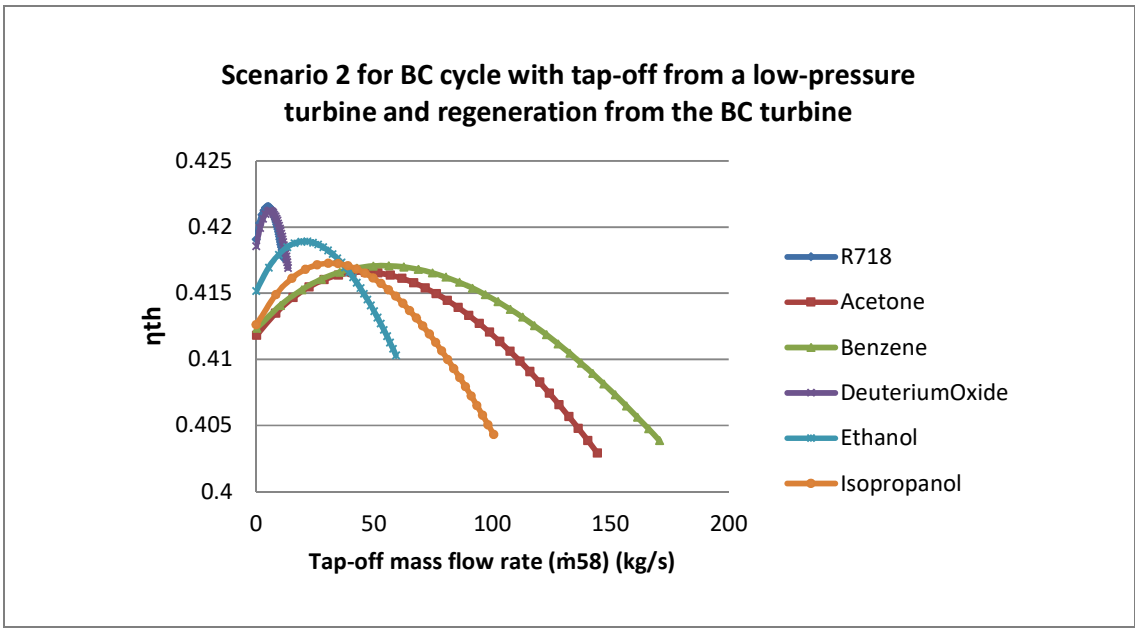

Figure B.17: The thermal efficiency for the tap-off mass flow rate range from the BC turbine for analysis conducted at the Komati Power Station, with tap off from a steam-side low-pressure turbine into the BC cycle and regeneration (one FWH) from the BC turbine under Scenario 2 assumptions

B3.3 Tap off from a low-pressure turbine with regeneration from the outlet of the BC turbine

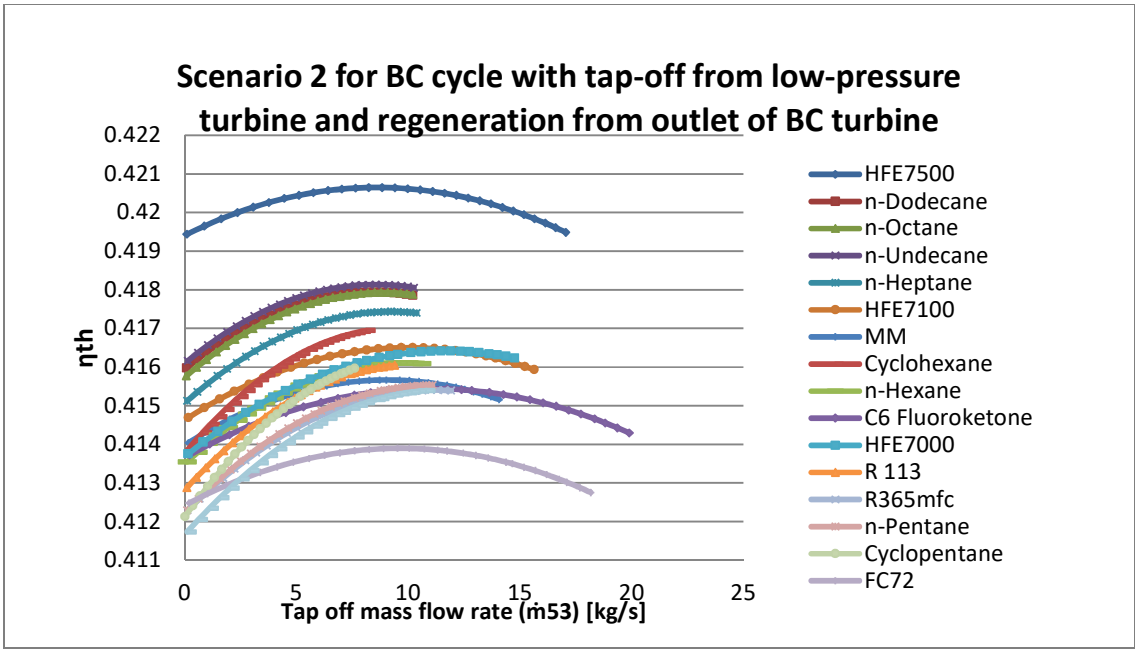

Figure B.18: The thermal efficiency for the tap-off mass flow rate range from the BC turbine for analysis conducted at the Komati Power Station with tap off from the steam-side low-pressure turbine into the BC cycle and regeneration from the outlet of the BC turbine under Scenario 2 assumptions

B.4 A BC cycle with tap off before a low-pressure turbine and FWHs

The configuration indicated in Figure B.199 only had one tap-off pressure. Consequently, the results are tabulated in Chapter 4. The configuration with a FWH and regeneration will be indicated.

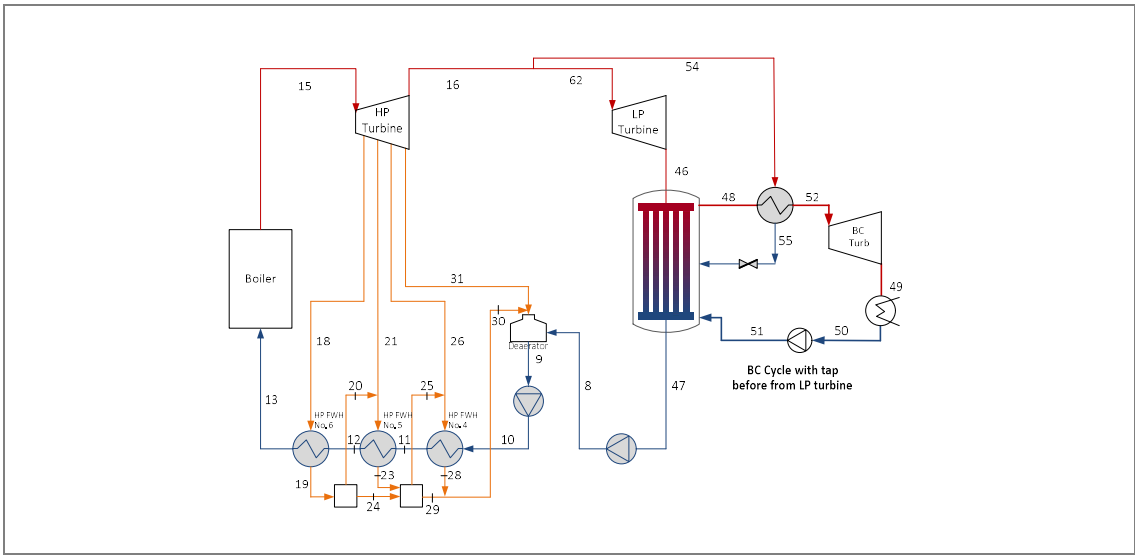

Figure B.19: Component diagram of the Komati Power Station with tap off before a low-pressure turbine into the BC cycle

B.4.1 A BC cycle with tap off before a low-pressure turbine and FWHs

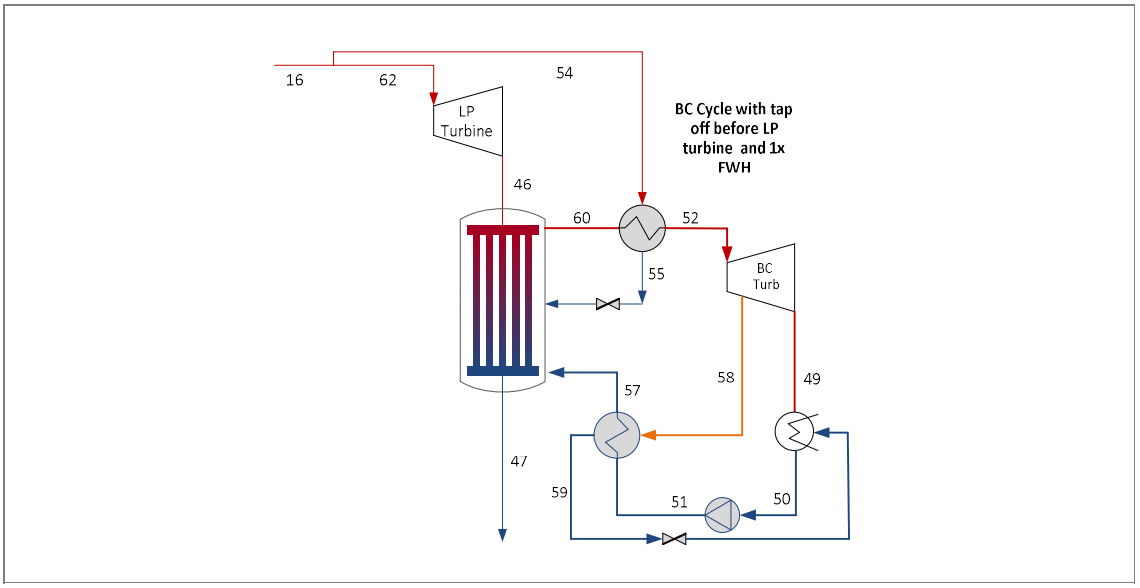

Figure B.20: Component diagram of the Komati Power Station with tap off before a low-pressure turbine into the BC cycle with a FWH

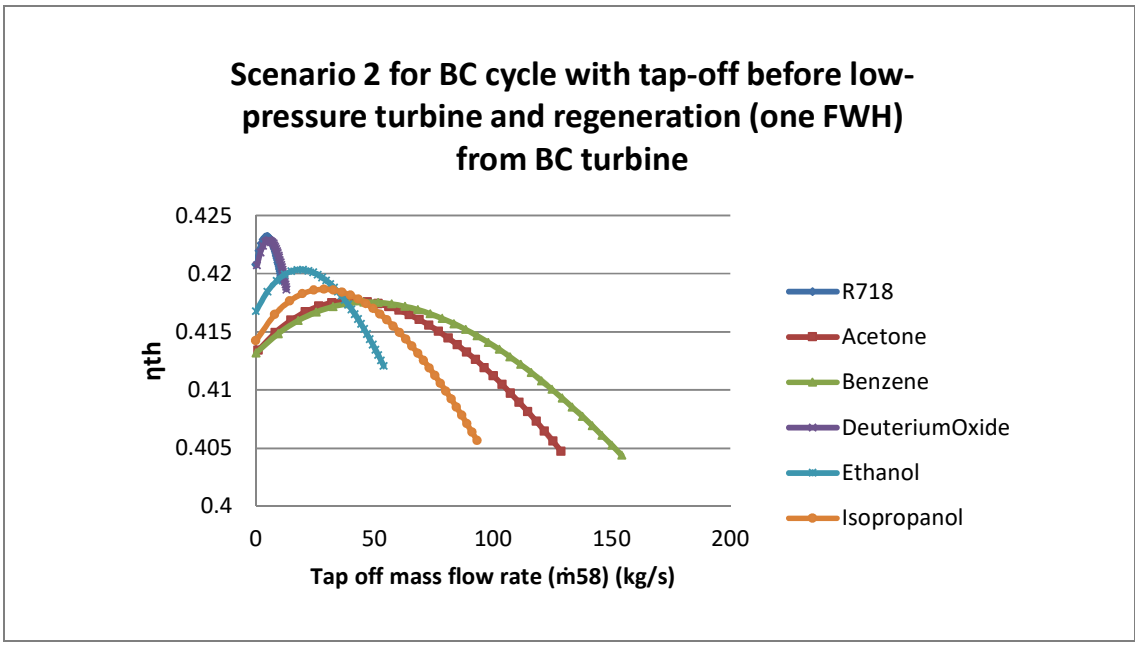

Figure B.21: The thermal efficiency for the tap-off mass flow rate range from the BC turbine for analysis conducted at the Komati Power Station with tap off before the steam-side low-pressure turbine into the BC cycle and regeneration (one FWH) from the BC turbine under Scenario 2 assumptions

B.5 A BC cycle with tap off in a high-pressure turbine and FWHs

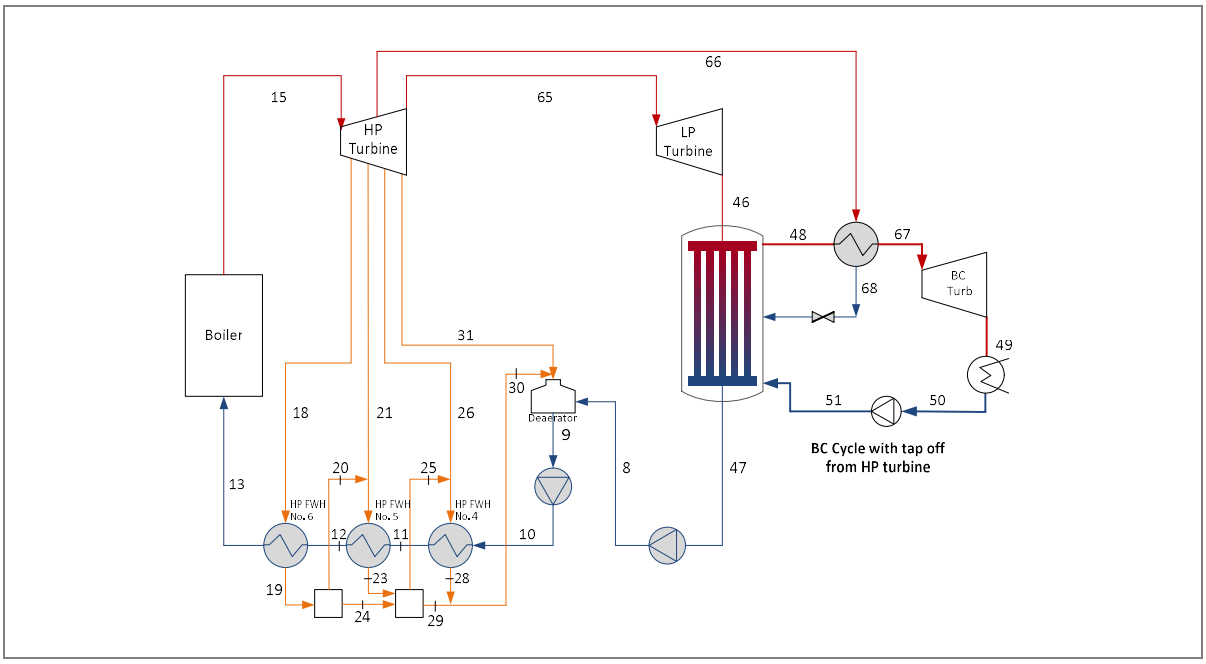

Figure B.22: Component diagram of the Komati Power Station with tap off from a high-pressure turbine into the BC cycle

B.5.1 A BC cycle with tap off in a high-pressure turbine

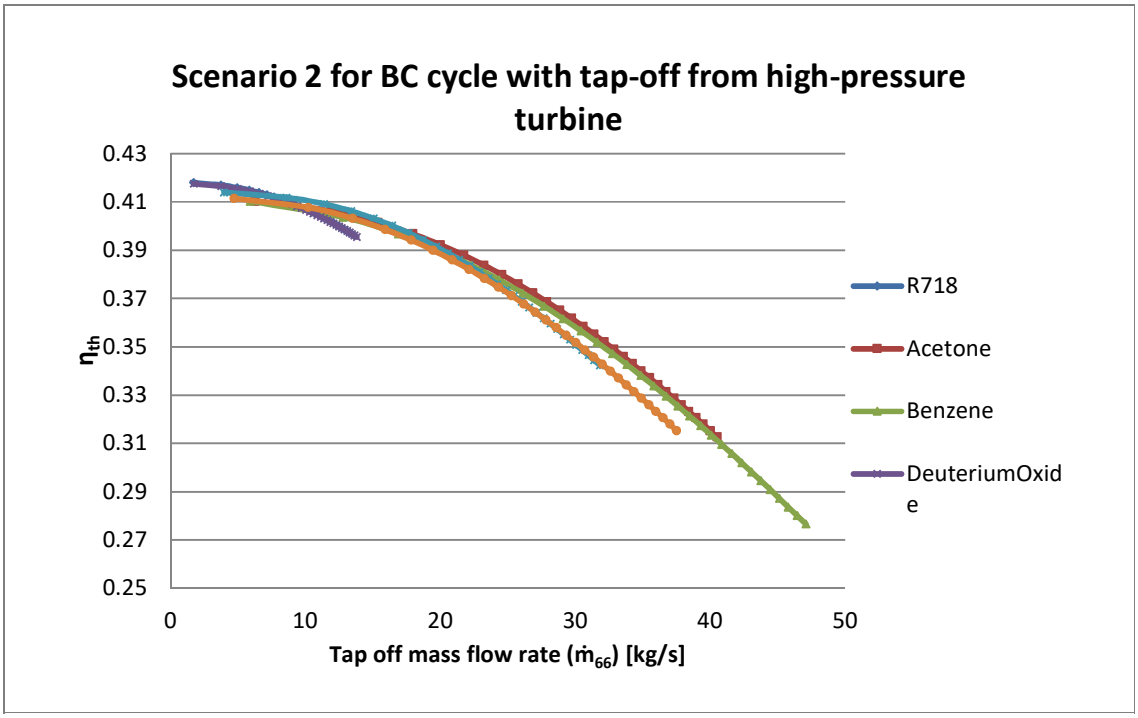

Figure B.23: The thermal efficiency for the tap-off mass flow rate range for analysis conducted at the Komati Power Station with tap off from the steam-side high-pressure turbine when implementing a simple BC cycle

B.5.2 Tap off from a high-pressure turbine and FWHs

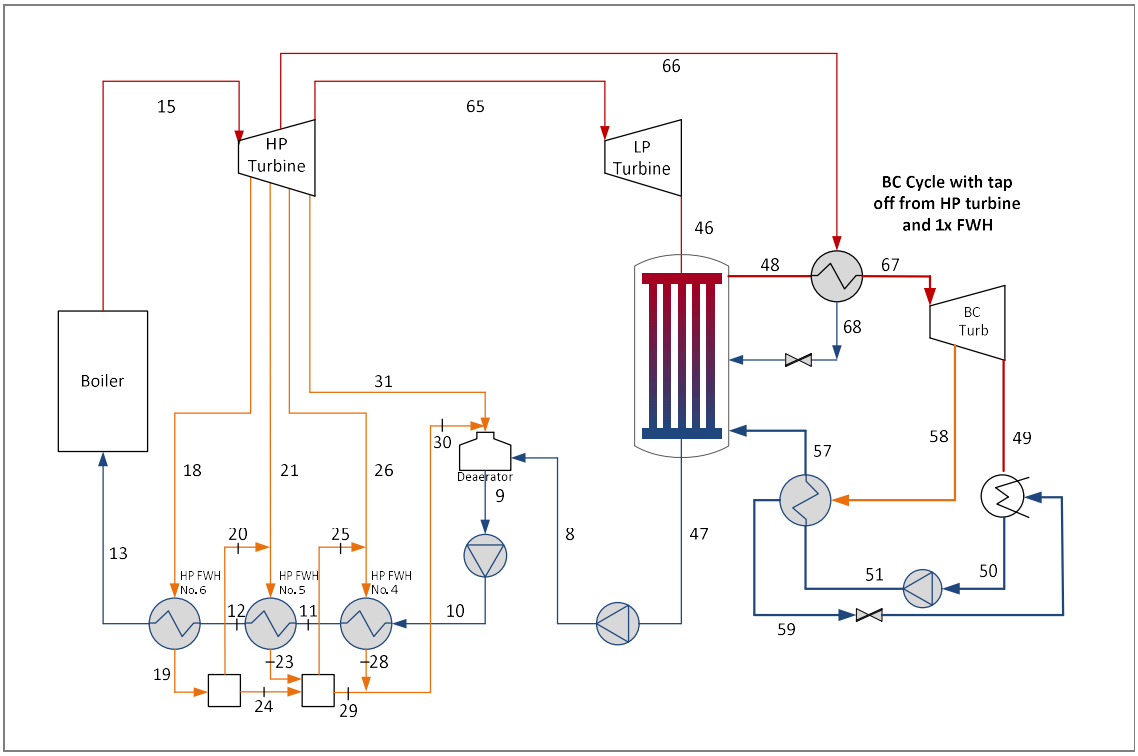

Figure B.24: Component diagram of the Komati Power Station with tap off from a high-pressure turbine into the BC cycle and BC cycle with one FWH

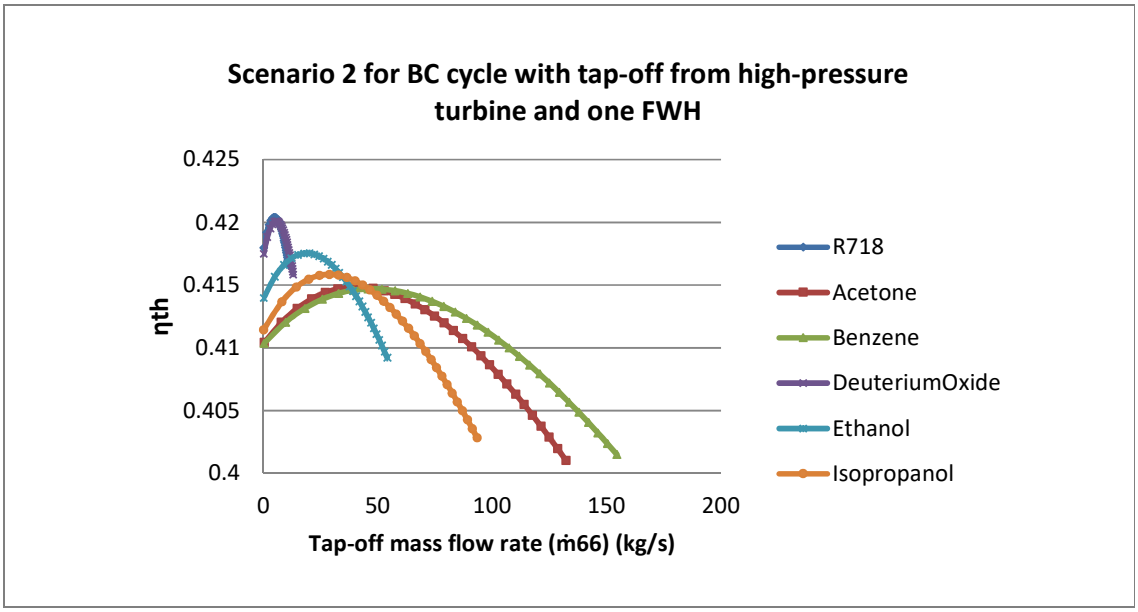

Figure B.25: The thermal efficiency for the tap-off mass flow rate range for analysis conducted at the Komati Power Station with tap off from the steam-side high-pressure turbine when implementing a simple BC cycle with regeneration from the BC turbine under Scenario 2 assumptions

B.6 A BC cycle without a low-pressure turbine and tap off from a high-pressure turbine and FWHs

The results for the indicated configuration, with its variations, will be shown below.

B.6.1 A BC cycle with tap off in a high-pressure turbine and without a low-pressure turbine

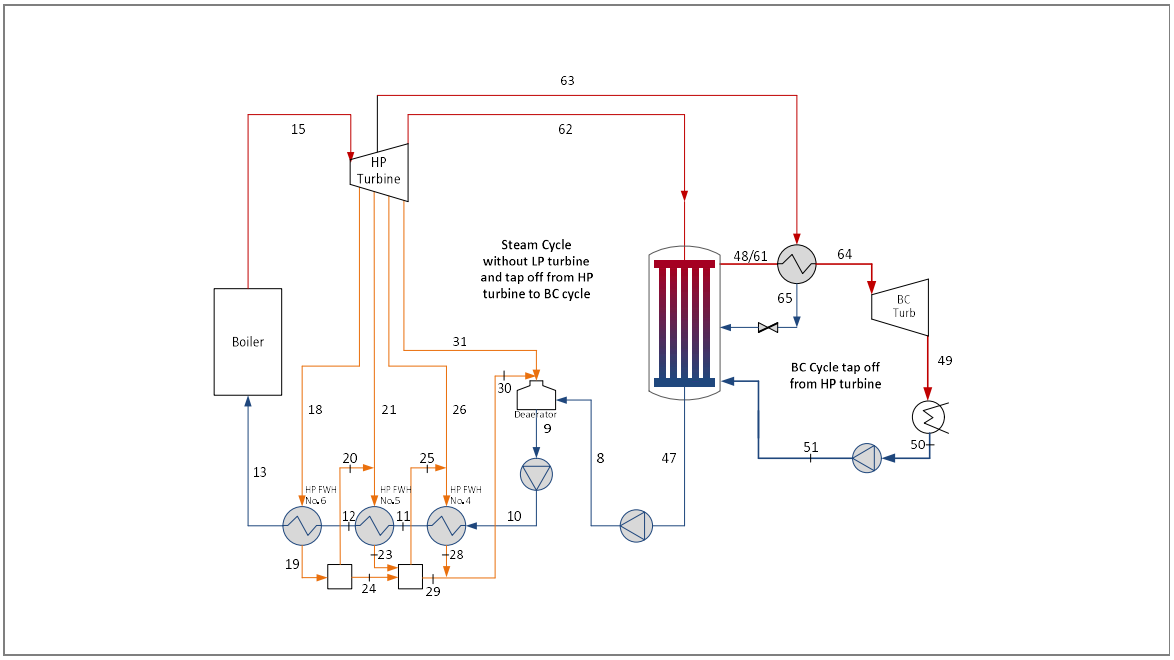

Figure B.26: Component diagram of the Komati Power Station without a low-pressure turbine and with tap off from a high-pressure turbine into the BC cycle

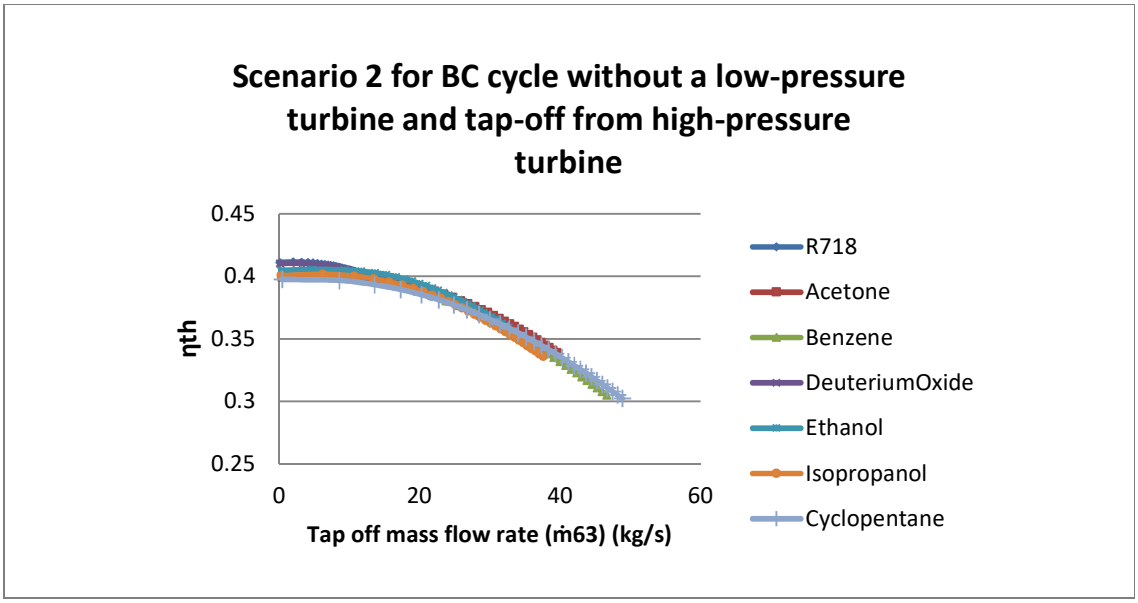

Figure B.27: The thermal efficiency for the tap-off mass flow rate range for analysis conducted at the Komati Power Station without a low-pressure turbine and tap off from the steam-side high-pressure turbine when implementing a simple BC cycle

B.6.2 Tap off from a high-pressure turbine without a low-pressure turbine and FWHs

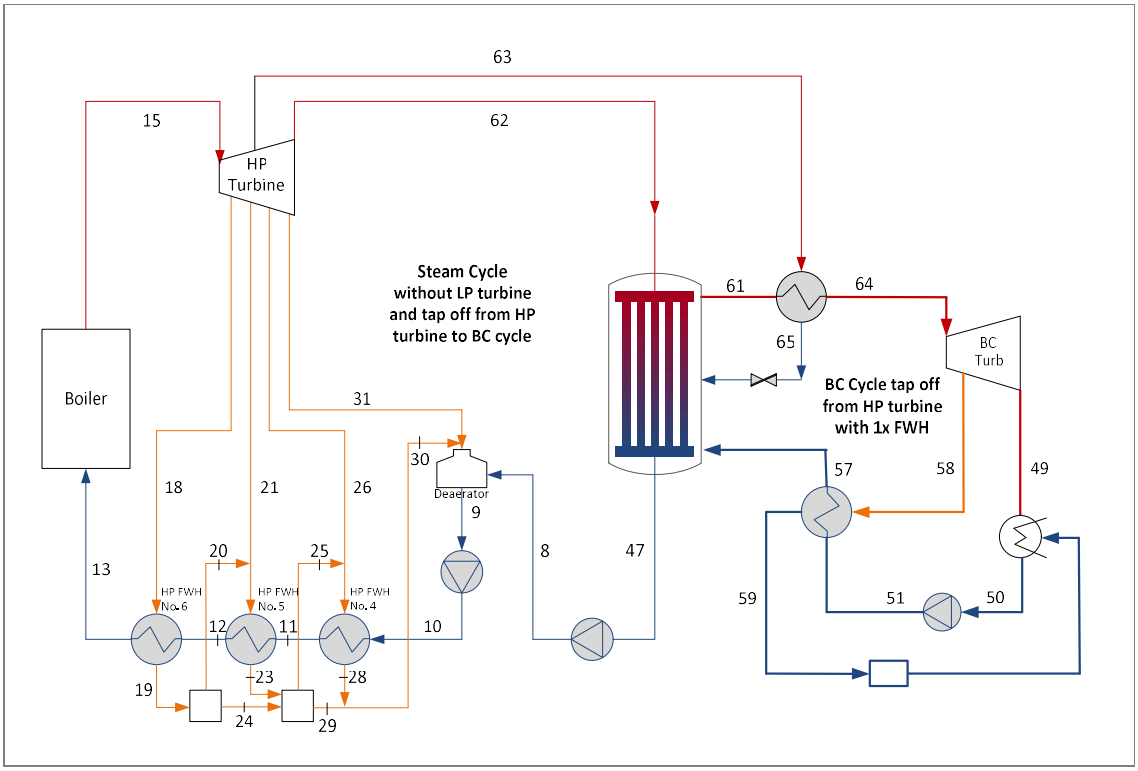

Figure B.28: Component diagram of the Komati Power Station without a low-pressure turbine and tap off from a high-pressure turbine into the BC cycle and a BC cycle with one FWH

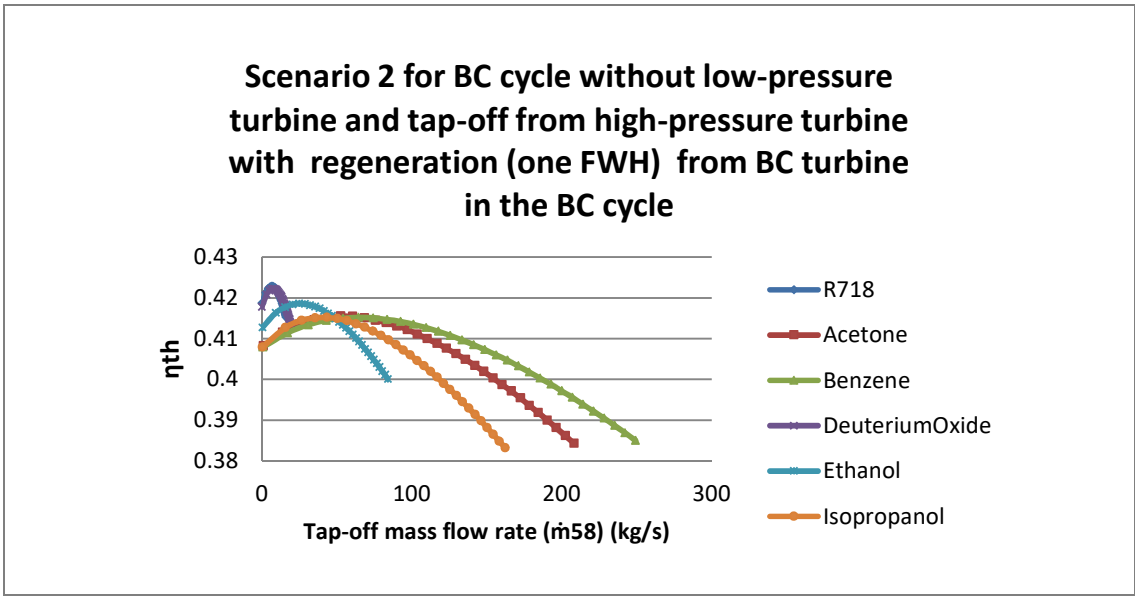

Figure B.29: The thermal efficiency for the tap-off mass flow rate range for analysis conducted at the Komati Power Station without a low-pressure turbine and tap off from the steam-side high-pressure turbine when implementing a simple BC cycle with regeneration (one FWH) from a BC turbine